Title
High Recovery Desalination of Brackish Water by Chemically-Enhanced Seeded Precipitation

Author
McCool, Brian Carey

Publication Date
2012

Peer reviewed|Thesis/dissertation

UNIVERSITY OF CALIFORNIA

Los Angeles

High Recovery Desalination of Brackish Water by Chemically-Enhanced Seeded Precipitation

A dissertation submitted in partial satisfaction of the requirements for the degree Doctor of Philosophy in Chemical Engineering

by

Brian Carey McCool

2012

ABSTRACT OF THE DISSERTATION

High Recovery Desalination of Brackish Water

by Chemically-Enhanced Seeded Precipitation

by

Brian Carey McCool

Doctor of Philosophy in Chemical Engineering

University of California, Los Angeles, 2012

Professor Yoram Cohen, Chair

Various regions around the world are confronted with dwindling water supplies and thus the need for exploiting non-traditional inland brackish water resource, as well as reclamation and reuse of municipal wastewater and agricultural drainage (AD) water. Reverse osmosis (RO) membrane desalination is the primary technology for inland brackish water desalting. However, successful implementation of RO technology requires operation at high product water recovery (>85%) in order to minimize the volume of generated concentrate (i.e., brine). Brine management is a key factor governing the economics of inland water desalination. Therefore, brine volume reduction is critical to enabling various brine residual management options. At high water recovery, dissolved mineral salts (e.g., $CaSO_4$, $BaSO_4$, $CaCO_3$) may become concentrated above their solubility limits and may crystallize in the bulk and onto the surface of the RO membranes. Mineral crystallization leads to membrane scaling and hence leads to flux decline,

increased process costs, and shortening of membrane life. Therefore, the attainable desalination water recovery is limited by mineral scaling. Many inland brackish water sources contain high concentrations of sparingly soluble mineral salts. In certain areas, such as in California's San Joaquin Valley (SJV), brackish water is near saturation with respect to calcium sulfate and barium sulfate. Based on the current work, single-stage RO desalination in SJV would generally be limited to ~50-70%.

In order to desalt brackish water of high mineral scaling propensity at a high recovery level (>85%), the feasibility of intermediate concentrate demineralization (ICD) of primary RO (PRO) concentrate, as a means of enabling secondary RO (SRO) desalting, was investigated with a focus on brackish water having high concentrations of gypsum salt precursor ions (i.e., calcium and sulfate). Accordingly, a two-step chemically-enhanced seeded precipitation (CESP) ICD process was developed in which the PRO concentrate is treated prior to further SRO desalting. The first step is lime precipitation softening (PS) which serves to induce sufficient $CaCO_3$ crystallization in order to remove residual antiscalant (AS), a PRO feed treatment additive (generally polymeric) used for scale control, that would otherwise inhibit precipitation (in the ICD) of the target mineral salt scalants. Subsequently, gypsum seeded precipitation (GSP) is carried out to reduce the level of calcium sulfate saturation.

The CESP process was evaluated experimentally, in a batch crystallizer, using synthetic PRO concentrate and also PRO concentrate generated in the field, from AD water, using a spiral-wound RO pilot plant. The effect of residual AS (from the PRO stage) on retardation of mineral salt precipitation (in the ICD) was evaluated using both a generic (polyacrylic acid) and a commercial AS. Laboratory batch CESP studies were carried out in which the CESP process conditions were first optimized with respect to the required lime and gypsum seed doses. For raw

brackish water that was about 98% saturated with respect to gypsum, PRO desalination at 52%-62% recovery yielded a brine stream 70-150% above saturation. CESP treatment, at lime doses of 0.25-0.35 mg/L and gypsum seeding of 4-5 g/L, enabled reduction of gypsum concentration to only 10-15% above its saturation. In general, the sequential processes of lime treatment for 10-20 minutes followed by ~1 hr of GSP were sufficient to achieve the above level of gypsum desupersaturation. GSP alone reduced gypsum saturation by only ~5%. PRO brine desupersaturation via CESP was feasible due to the effectiveness of AS removal (up to 90% for AS content of up to 10 mg/L in the PRO brine). Analysis of AS removal using a fundamental AS adsorption model, along with measurements of the size distribution of precipitating $CaCO_3$ crystals, indicated that the area for AS adsorption provided by lime-induced nucleation of $CaCO_3$ crystals is the key factor governing AS removal. In order to establish the feasibility of deploying CESP as a continuous process, a numerical model was developed for a fluidized bed reactor for the GSP stage. Model simulations indicated that the required level of calcium sulfate desupersaturation could be maintained by solids recycling leading to a steady-state particle size distribution.

Process simulations and economic analysis were carried out for the integrated process of PRO, CESP and SRO (PRO-CESP-SRO) demonstrating the existence of an optimal recovery (with respect to product water treatment cost). For the evaluated SJV brackish AD water source, the optimal recovery was about 93%. Overall brackish water treatment cost, when considering the disposal cost of high salinity AD water, was lower for PRO-CESP-SRO relative to a similar process based on conventional PS or utilizing a single stage RO which would be of limited recovery (≤62%). The current work suggests that, at inland areas with limited options for management of high salinity water, high recovery desalination can be economically attractive

when considering the reduction in brine disposal cost and the value of the product water produced by the PRO-CESP-SRO process.

The dissertation of Brian Carey McCool is approved.

_____

Panagiotis Christofides

_____

Jennifer A. Jay

_____

Gerassimos Orkoulas

_____

Yoram Cohen, Committee Chair

University of California Los Angeles

2012

To my wife Fawn.

TABLE OF CONTENTS

LIST OF TABLES ix

LIST OF FIGURES xi

NOMENCLATURE xix

ACKNOWLEDGEMENTS xxi

VITA xxii

PUBLICATIONS AND PRESENTATIONS xxii

ABSTRACT OF THE DISSERTATION xxiv

Chapter 1: Introduction 1

1.1 Background 1

1.2 Problem Statement 6

1.3 Objectives of the dissertation 7

1.4 Approach 9

Chapter 2. Literature Review 16

2.1.1 RO desalination 16

2.1.2 RO membranes 19

2.1.3 Concentration polarization 20

2.1.4 Water quality measurements 21

2.1.5 Recovery limitations 23

2.2 High recovery RO desalination via intermediate concentrate demineralization 26

2.2.1 Demineralization via alkaline induced calcium precipitation 31

2.2.2 Demineralization via seeded precipitation 32

2.2.3 Chemically-enhanced seeded precipitation 34

Chapter 3. Recovery limit estimation and the feasibility of RO desalination in the San Joaquin Valley 40

3.1 Overview 40

3.2 Analysis 42

3.3 Experimental 48

3.3.1 Materials and Reagents 48

3.3.2. PFRO system & mineral scaling tests 49

3.3.3. Water quality data 51

3.4 Results and Discussion 52

3.4.1 Water quality variability 52

3.4.2 Recovery limits for the 1999–2004 and 2006–2007 monitoring data 57

3.4.3 Experimental RO desalting tests 60

3.5 Conclusions and Recommendations 67

Chapter 4. Antiscalant removal in accelerated desupersaturation of RO concentrate via chemically-enhanced seeded precipitation (CESP) 71

4.1 Overview 71

4.2 Experimental 75

4.2.1 Model solutions 75

4.2.2 Chemical demineralization experiments 76

4.2.3 Analytical measurements 78

4.3 Results and Discussion 79

4.3.1 Antiscalant removal by calcium carbonate precipitation via lime treatment 79

4.3.2 Calcium carbonate precipitation in the presence of PAA 80

4.3.3 Impact of antiscalant concentration on calcium carbonate precipitation 84

4.3.4 Impact of initial supersaturation level on calcium carbonate precipitation 87

4.3.5 Lime dosing procedure 90

4.3.6 Residual AS inhibition of seeded gypsum precipitation 91

4.3.7 Filterability of CESP-treated RO concentrate 95

4.4 Conclusions and Recommendations 96

Chapter 5**.** Field validation and economic feasibility of RO concentrate demineralization via chemically-enhanced seeded precipitation 101

5.1 Overview 101

5.2 Experimental 105

5.2.1 Materials 105

5.2.2 RO desalination pilot and crystallizer 105

5.2.3 Field test site and generation of RO concentrate 106

5.2.4 Chemically-enhanced seeded precipitation experiments 109

5.2.5 Estimation of AS removal 110

5.3 Economic analysis 111

5.4 Results and Discussion 113

5.4.1 RO concentrate desupersaturation by CESP 113

5.4.2 CESP performance 116

5.4.3 Recovery limit 119

5.5 Economic feasibility of high recovery RO via CESP 120

5.6 Conclusions and Recommendations 128

Chapter 6. Recycling of gypsum solids in multi-cycle CESP 133

6.1 Overview 133

6.2 Experimental 135

6.2.1. Model solutions and chemicals 135

6.2.2. CESP experiments 136

6.3 Results and Discussion 137

6.3.1. CESP with multiple cycles of solids recycling 137

6.3.2. Gypsum precipitation rate constant during multi-cycle CESP 140

6.3.3. Reactor simulation model 143

6.3.4. Reactor sizing 147

6.3.5. Reactor simulation results 150

6.4 Conclusions and Recommendations 152

Appendix A. Water quality analytical reports 155

A.1 CNR, 7/31/06 156

A.2 ERR, 1/29/07 157

A.3 LNW, 2/15/06 158

A.4 OAS, 4/10/06 159

A.5 VGD, 11/13/06 160

A.6 DP-25, 4/28/09 161

A.7 DP-25 5/19/2009: RO feed 162

A.8 DP-25 5/19/2009: RO concentrate (52.3% recovery) 163

A.9 DP-25 5/19/2009: Treated RO concentrate 1 164

A.10 DP-25 5/19/2009: Treated RO concentrate 2 165

A.11 San Joaquin Valley Historic water quality 166

A.12 DP-25: Historic water quality data collected by CA DWR 168

Appendix B. Detailed experimental procedures 170

Appendix C. Calcium ion selective electrode (ISE) calibration 187

Appendix D. Estimation of ion concentrations from calcium activity pH data 189

Appendix E. Gypsum solids recycling and GSP reactor simulation validation 191

E.1 Gypsum seeded precipitation mixing rate optimization 191

E.2 Reactor simulation validation 194

E.3 Summary of reactor simulation results 197

E.2 Simulation code 203

LIST OF TABLES

Table 2-1. Relevant work in high recovery RO desalination via precipitation of scaling mineral salt precursors. Note: an asterisk (*) after the citation indicates that high recovery desalting was demonstrated by integration of demineralization with RO. 27

Table 3-1. Summary of average water quality and saturation indices for the most recent 12-month period of available data from the DWR database (2003–2004) 53

Table 3-2. Variability of water quality measurements and saturation indices for the OAS location 53

Table 3-3. Summary of water quality and saturation indices for the collected field water samples (2006–2007) † 54

Table 3-4. Detailed water quality analyses for five location in the SJV sampled during 2006–2007 57

Table 3-5. Recovery limits for water samples having the maximum and minimum TDS observed during the most recent 12-month period of reported data. 58

Table 3-6. Recovery limits estimated based on water quality analysis of field water samples 59

Table 3-7. Diagnostic flux decline experimental conditions and 24-hour flux decline 61

Table 5-1. Summary of water quality data from the field demonstration of CESP for high recovery desalination of AD water*. 109

Table 5-2. Itemized costs used in the analysis of brackish water management costs. 113

Table 5-3. Impact of varying AD source water salinity on the cost of water management (desalination and brine disposal) at the optimal recovery (**Fig. 5-8**) 124

Table C-1. Calcium calibration standard solution compositions 188

Table E-1. Continuous reactor simulation input and outputs 199

LIST OF FIGURES

Figure 1-1. High recovery RO process utilizing intermediate concentrate demineralization (ICD) 3

Figure 1-2. Research flowchart; bold hexagons indicate major results. Abbreviations: AS, antiscalant; CESP, chemically-enhanced seeded precipitation. 7

Figure 2-1. Schematic of cross-flow plate-and-frame RO system 18

Figure 2-2. Cut-away of spiral wound RO membrane module [12] 18

Figure 2-3. Schematic of typical two stage (2:1) RO desalination 18

Figure 2-5. Cross section of a typical RO membrane showing layered structure [13] 19

Figure 2-4. Schematic of cross-flow plate-and-frame RO system showing the formation of a concentration boundary layer. Block arrow represent solute fluxes. J is the water flux, C_m and C_p are the respective concentrations at the membrane surface and in the permeate, D is the solute diffusivity, and dC/dy is the solute concentration gradient in the y-direction. 21

Figure 3-1. San Joaquin Valley (SJV) field water sampling locations: OAS (1), VGD (2), ERR (3), LNW (4), & CNR (5). 41

Figure 3-2. Saturation indices as a function of recovery for OAS water field water (11020 mg/L TDS, sampled on 4/10/2006, calculated based on 98% salt rejection) 44

Figure 3-3. Saturation indices as a function of pH for OAS field water (11020 mg/L TDS, sampled on 4/10/2006) 44

Figure 3-4. Gypsum saturation index at the membrane surface as a function of recovery for OAS field water (sampled on 4/10/2006) illustrating the effect of concentration polarization (i.e., increasing with α value) 47

Figure 3-5. Illustration of water quality variations for the 2003–2004 period in the DWR

database [4] and for the 2006 field samples: (a) at the OAS site, (b) at the CNR site, and (c) at the LNW site 56

Figure 3-6. Permeate flux (ratio of the flux at time *t*, J_t, to the initial flux, J_0, respectively) for 24-hr scaling tests at the natural pH of the field water and at an acidic pH for: (a) OAS, (b) CNR, and (c) LNW; and at an acidic pH with AS addition (0.2 ppm PC-504) for (a) OAS, and (b) CNR 62

Figure 3-7. Examples of membrane coupons images after 24-hour scaling tests on field water samples from: (a) OAS at the natural pH=7.42, (b) OAS at an acidic pH=5.47, (c) LNW at the natural pH=7.43, and (d) LNW at an acidic pH=6.48. 63

Figure 3-8. Images of the membrane coupon exit regions after 24-hr scaling tests (see Table 7). 64

Figure 4-1. High recovery RO process utilizing intermediate concentrate demineralization (ICD) between primary RO (PRO) and secondary RO (SRO) desalination stages. 72

Figure 4-2. Fraction of antiscalant removed from solution A (**Table 4-1**), initially containing 10 mg/L PAA, 30 minutes after single lime doses. The values in parentheses above and below the data points correspond to the *SIc* and mass concentration (mg/L) of precipitated $CaCO_3$, respectively, 30 minutes after lime addition. 80

Figure 4-3. (a)Time varying saturation indices (*SIg* and *SIc*) during lime-induced (2.70 mM) precipitation of $CaCO_3$ in AS-containing (3 mg/L PAA) solution B (**Table 4-1**); (b) SEM of $CaCO_3$ precipitate. Initial conditions after alkaline dosing: SIc_0= 374, SIg_0 = 2.57. The shaded area indicates the rapid mixing period (G = 1000 s^{-1}), which was subsequently reduced (G = 200 s^{-1}). 82

Figure 4-4. Time varying number (a) and volume (b) during lime-induced (2.70 mM)

precipitation of $CaCO_3$ in AS-containing (3 mg/L PAA) solution B (**Table 4-1**). Initial conditions after alkaline dosing: SIc_0= 374, SIg_0 = 2.57. 83

Figure 4-5. Impact of initial AS concentration (3–12 mg/L PAA) on time varying extents of reaction during lime-induced (3.37mM) precipitation of $CaCO_3$ in AS-containing solution B (**Table 4-1**). Initial conditions after alkaline dosing: SIc_0= 468, SIg_0 = 2.58. The shaded area indicates the rapid mixing period (G = 1000 s^{-1}), which was subsequently reduced (G = 200 s^{-1}). 85

Figure 4-6. Impact of initial AS concentration (3–12 mg/L PAA) on particle number distribution during lime-induced (3.37 mM) precipitation of $CaCO_3$ in AS-containing solution B (**Table 4-1**). Initial conditions after alkaline dosing: SIc_0= 468, SIg_0 = 2.58. 86

Figure 4-7. Impact of initial calcite saturation index (SIc_0) on time varying extents of reaction during lime-induced precipitation of $CaCO_3$ in AS-containing (3 mg/L PAA) solution B (**Table 4-1**) using 1.35, 2.02, 2.36, 2.70, or 3.37 mM of lime with corresponding SIc_0 of 187, 280, 327, 374, or 468 upon lime addition, respectively. SIg_0 changed little upon lime addition varying only between 2.55–2.58. 88

Figure 4-8. Impact of initial calcite saturation index (SIc_0) on particle number distribution during lime-induced precipitation of $CaCO_3$ in AS-containing (3 mg/L PAA) solution B (**Table 4-1**) using 1.35, 2.36, 2.70, or 3.37 mM of lime with corresponding SIc_0 of 187, 327, 374, or 468 upon lime addition, respectively. SIg_0 changed little upon lime addition varying only between 2.55–2.58. 89

Figure 4-9. Impact of initial calcite saturation index (SIc_0) on the number concentration of particles above 5.6 μm ($N_{5.6}$) and modal number diameter (d_{mode}) during lime-induced precipitation of $CaCO_3$ in AS-containing (3 mg/L PAA) solution B (**Table 4-1**), using 1.35,

2.02, 2.36, 2.70, or 3.37 mM of lime with corresponding SIc_0 of 187, 280, 327, 374, or 468 upon lime addition, respectively. SIg_0 changed little upon lime addition varying only between 2.55–2.58. 89

Figure 4-10. Calcite saturation index, *SIc*, after 0.10 g/L lime addition: single dose at t = 0 min (◊); staged dosing with three equal fractions added t = 0, 5.4, and 10.4 min (●). 91

Figure 4-11. Gypsum saturation index (▲) and sulfate extent of reaction $\alpha_{sulfate}$ (●) after 85 min, ratio of AS (PAA) concentration after to before lime treatment (♦), and concentration of precipitated $CaCO_3$ solids after lime treatment (■) in solution B (**Table 4-1**) with 3 mg/L PAA, initially. 95

Figure 4-12. Turbidity of solution B (**Table 4-1**) after lime dose treatment (2.7 mM) and subsequent microfiltration. 96

Figure 5-1. High recovery RO process utilizing intermediate concentrate demineralization (ICD) treatment of primary RO (PRO) prior to secondary RO (SRO) desalination. 103

Figure 5-2. DP-25 field test site in Central California's San Joaquin Valley. Adapted from [9]. 107

Figure 5-3. (a) Calcite saturation index, (b) gypsum saturation index, and (c) carbonate and sulfate extents of reaction during CESP treatment of DP-25 RO concentrate of initial *SIg* was ~1.7 (generated from RO desalting at recovery of 52.3% and containing 6.3 mg/L AS equivalent to 3.3 mg/L on a solids basis) in with 0.25 g/L lime addition followed by 5 g/L gypsum seeding. 116

Figure 5-5. Sulfate extent of reaction during CESP treatment of DP-25 RO concentrate (initial SIg was ~1.7; concentrate generated by RO desalting at 52.3% recovery and containing, 6.3 mg/L AS) with 5 g/L gypsum seeding without prior lime treatment (■), and

with lime treatment of either 0.25 g/L (♦) or 0.35 g/L (▲). 118

Figure 5-6. Removal fraction of major scale precursors after CESP treatment DP-25 RO concentrate (**Table 5-1**) in using 0.25 or 0.35 g/L lime and 5.0 g/L gypsum seeds. 119

Figure 5-8. Total brackish water management cost ($/m3–product) for PRO-ICD-SRO treatment methods as a function of overall recovery (PRO at 62% Y) assuming a brine disposal cost of 1.10 $/m3. The dashed line indicates the concentrate osmotic pressure limit (1000 psi) at 93% Y. 122

Figure 5-9. Total brackish water management cost ($/m3–feed) for various treatment methods assuming a brine disposal cost of 1.10 $/m3. The costs for the RO and PRO-ICD-SRO processes are calculated at their corresponding recovery limits—62% and 93%, respectively. Note that these costs do not account for the potential costs savings that may be realized from the value of the product water and that 1.0 $/m3 = 1230 $/A.F. 123

Figure 5-10. Total water management cost ($/m3–feed) for various treatment methods as a function of brine disposal cost. The costs for the RO and PRO-ICD-SRO processes are calculated at their corresponding recovery limits—62% and 93%, respectively. 126

Figure 5-11. Total water management cost ($/m3–feed) for various treatment methods as a function of product selling price assuming an average brine disposal cost of 1.10 $/m3. The costs for the RO and PRO-ICD-SRO processes are calculated at their corresponding recovery limits—62% and 93%, respectively. Note that negative net costs represent net revenue for the plant. 127

Figure 6-1. Schematic of a proposed continuous CESP process illustrating pretreatment via lime-induced $CaCO_3$ precipitation for AS removal prior to gypsum desupersaturation via gypsum seeded precipitation with recycling of gypsum solids. 135

Figure 6-2. Sulfate extent of reaction (a) and gypsum solids mass (b) in model PRO concentrate (*SIg* = 2.5) subsequent to 0.25 g/L lime treatment (not shown) during five cycles of CESP with 5 g/L gypsum seeds to induce gypsum precipitation in the 1st cycle followed by recycled solids in the remaining cycles. 138

Figure 6-3. Sulfate extent of reaction, $\alpha_{sulfate}$, during the 1st (a) and 5th (b) cycles of seeded precipitation using 5 g/L gypsum seeds to induce gypsum precipitation for the 1st cycle followed by recycled solids in the remaining cycles. Gypsum seeding was tested in model PRO concentrate (*SIg* = 2.5) with and without the presence of 3 mg/L AS and at two different lime pretreatment doses (0.25 or 0.15 g/L) for AS removal. 140

Figure 6-4. Initial gypsum precipitation rate constants (a) and average residual AS concentration (b) for five cycles of seeded precipitation using 5 g/L gypsum seeds to induce gypsum precipitation for the 1st cycle followed by recycled solids in the remaining cycles. Gypsum seeding was tested in model PRO concentrate (*SIg* = 2.5) with and without the presence of 3 mg/L AS and at two different lime pretreatment doses (0.25 or 0.15 g/L) for AS removal. 143

Figure 6-5. Detail of the GSP step of the continuous CESP process indicating gypsum recycle and simulation parameters. 144

Figure 6-6. Reactor simulation flowchart 145

Figure 6-7. Gypsum seeded precipitation PFR reactor (crystallizer) sizing flowchart. The desired reactor state (α, ϕ, d_p) is the input and the reactor size (H, D, n) and seed makeup requirement ($\dot{m}_s$) are the outputs. 149

Figure 6-8. Crystallizer residence time, τ, and height, H (a), solids purge rate, $\dot{m}_p$ (b), and seed makeup rate, $\dot{m}_s$ (c) as a function of extent of reaction, α_{sulfate}, and *SIg* for solids

fraction, ϕ = 0.1–0.5, all using 65-μm seeds. 152

Figure B-1. Photo of Simple SDI test kit taken from www.simplesdi.com. 170

Figure B-2. Picture of the HACH model AL-DT alkalinity test kit taken from www.hach.com. 172

Figure B-3. (a) PFRO system diagram, (b) picture of two PFRO cells in parallel. 173

Figure B-4. Diagram of field-deployed M3 pilot RO system providing RO concentrate for CESP precipitation studies (§2.2). Adapted from [2]. 177

Figure B-4. General procedure for CESP demineralization experiments. 179

Figure B-5. Lab-scale 1-L crystallizer with 4 rectangular jar testers. 179

Figure B-6. Bench-scale 20-L brine demineralization crystallizer: (a) overhead view during brine demineralization with inset close-up view of radial-flow mixing impeller and (b) close-up of calcium ion, pH, and temperature probes and support platform with the stirring impeller shaft in the foreground. 180

Figure B-7. Beckman Coulter Multisizer 3 particle size analyzer and data acquisition computer. 183

Figure B-8. Beckman coulter Multisizer 3 particle size analyzer. 184

Figure C-1. Calcium ISE master calibration curve of potential difference as a function of $p(Ca^{2+})$, i.e., the negative logarithm of calcium ion activity (mol/kg-water). 188

Figure E-1. Calcium removal as a function of time during seeded precipitation of PRO concentrate model solution (SIg = 2.5) with 5.0 g/L gypsum seed dose (45–μm diameter) and mixing rates ranging from 75 to 275 rpm in a 1-L rectangular crystallizer with a radial--flow impeller (see **§4.2.2**). 191

Figure E-2. Particle size distribution during seeded precipitation of PRO concentrate model

solution (*SIg* = 2.5, see **§4.2.2**) with 5.0 g/L gypsum at mixing rates of 75 rpm and 200 rpm, respectively. 193

Figure E-3. Particle number concentration and modal diameter during seeded precipitation of PRO concentrate model solution (*SIg* = 2.5, see **§4.2.2**) with 5.0 g/L gypsum seed dose and mixing rates ranging from 75 to 275 rpm. 194

Figure E-4. Representative concentration profile and sulfate extent of reaction for an ideal PFR (solid lines) and for the simulated GSP crystallizer with 40 bins (circles) at the following conditions: τ = 10 min, ϕ = 0.5, d_p = 65 μm, A = 5.27 m^2/L, and $\alpha_{sulfate}$ = 0.914. The feed was PRO concentrate model solution (*SIg* = 2.5, see **§4.2.2**). 195

Figure E-5. Representative steady-state particle size distribution and surface area distribution from the simulation of the GSP crystallizer at the following conditions: τ = 10 min, ϕ = 0.5, d_p = 65 μm, $\alpha_{sulfate}$ = 0.914. The feed was PRO concentrate model solution (*SIg* = 2.5, see **§4.2.2**). 196

Figure E-6. Independence of model results with respect to the number of reactor bins. The sulfate extent of reaction, $\alpha_{sulfate}$, was calculated over a range of number of reactor bins simulated, n (10–360). 197

NOMENCLATURE

α	concentration polarization allowance factor
$\alpha_{\text{carbonate}}$	carbonate extent of reaction
α_{sulfate}	sulfate extent of reaction
ACP	Accelerated Chemical Precipitation
AD	Agricultural Drainage
AS	Antiscalant
C_0	initial concentration
C_b	bulk concentration
C_m	concentration at membrane surface
C_p	permeate concentration
C_S	saturation concentration
CESP	Chemically-Enhanced Seeded Precipitation
CF	Concentration Factor
CND	Crystal Number Density
CP	Concentration Polarization
CR	Colorado River
CSD	Crystal Size Distribution
d_p	particle diameter
d_{mode}	modal particle diameter
DLS	Dynamic Light Scattering
EC	Electrical Conductivity
γ	ion activity coefficient
ϕ	membrane scale coverage fraction; reactor solids fraction
G	sheer rate
IAP	Ion Activity Product
ICD	Intermediate Concentrate Demineralization
J	permeate flux
k	reaction rate constant
K_{SP}	solubility product
L_P	membrane permeability
LSI	Langlier Saturation Index
$\dot{m}_s$	gypsum seed makeup rate
MF	Microfiltration
NF	Nanofiltration
NOM	Natural Organic Matter
NTU	Nephelometric Turbidity Units
π	osmotic pressure
PAA	Poly(Acrylic Acid)
PFRO	Plate-and-Frame Reverse Osmosis
PRO	Primary Reverse Osmosis
PSD	Particle Size Distribution
PS	Precipitation Softening
PVD	Particle Volume Distribution
Q_C	concentrate volumetric flow rate
Q_F	feed volumetric flow rate
Q_P	permeate volumetric flow rate
Q_R	retentate volumetric flow rate
R_0	observed salt rejection
RO	Reverse Osmosis
RPM	Revolutions Per Minute
S_A	surface area
SCR	Solids-Contact Reactor

SDI	Silt Density Index
SEM	Scanning Electron Micrograph/Microscope
SGP	Seeded Gypsum Precipitation
SI_B	barite saturation index
SIc	calcite saturation index
SIg	gypsum saturation index
SIs	silica saturation index
SJV	San Joaquin Valley
SRO	Secondary Reverse Osmosis
τ	reactor residence time
TDS	Total Dissolved Solids
TOC	Total Organic Carbon
$\bar{u}$	average cross-flow velocity
Y	recovery

ACKNOWLEDGEMENTS

Chapter 3 is a version of Brian C. McCool, Anditya Rahardianto, Jose Faria, David Lara, and Yoram Cohen, Feasibility of RO Desalination of Brackish Water in the San Joaquin Valley, *Desalination* **261** (2010) 240-250.

Chapter 4 is a version of Brian C. McCool, Anditya Rahardianto, and Yoram Cohen, Antiscalant removal in accelerated desupersaturation of RO concentrate via chemically-enhanced seeded precipitation, *Water Research* **46** (2012) pp. 4261-4271.

Chapter 5 is a version of Brian C. McCool, Anditya Rahardianto, and Yoram Cohen, Field validation and economic feasibility of RO concentrate demineralization via chemically-enhanced seeded precipitation (CESP), *Desalination*, **Submitted**.

VITA

1979	Born, Corpus Christi, Texas
2002	BS, Chemical Engineering University of Texas at Austin
2003-04	Environmental Consultant Environmental Resources Management Houston, Texas
2005-08	Teaching Assistant Department of Chemical and Biomolecular Engineering, University of California, Los Angeles
2008	MS, Chemical Engineering University of California, Los Angeles
2008-11	Teaching Fellow Department of Chemical and Biomolecular Engineering, University of California, Los Angeles

PUBLICATIONS AND PRESENTATIONS

Rahardianto, A, B. McCool and Y. Cohen, "Reverse Osmosis Desalting of Inland Brackish Water of High Gypsum Scaling Propensity: Kinetics and Mitigation of Membrane Mineral Scaling," Env. Sci. Technol. 42, 4292-4297 (2008).

McCool, B.C., A. Rahardianto, J. Faria, K. Kovac, D. Lara, Y. Cohen, "Feasibility of Reverse Osmosis Desalination of Brackish Agricultural Drainage Water in the San Joaquin Valley, Desalination, 261, 240-250 (2010).

Rahardianto, A., B.C. McCool, Y. Cohen, "Accelerated Desupersaturation of Reverse Osmosis Concentrate by Chemically-Enhanced Seeded Precipitation," Desalination, 264, 256-267 (2010).

McCool, B.C., A. Rahardianto, J. Faria, D. Lara, and Y. Cohen, *Field evaluation of brine demineralization for high recovery RO desalination*, AMTA Membrane Residuals Solutions Newsletter, Fall 2010.

McCool, B.C., A. Rahardianto and Y. Cohen, "Antiscalant removal in accelerated desupersaturation of RO concentrate via chemically-enhanced seeded precipitation (CESP)," Water Research, 46, 4261–4271 (2012).

Cohen, Y., B.C. McCool, A. Rahardianto and E.M. Lyster, "Integration of Accelerated Seeded Crystallization Precipitation for Enhanced Water Recovery in Low-pressure Membrane Desalination of Brackish Water," Final Report prepared for Metropolitan Water District of Southern California, under the "Desalination Research and Innovation Partnership IV", USEPA, Federal Grant Assistance no. XP-96992301, January 7, 2011.

Cohen, Y., J. Glater, B. McCool, A. Rahardianto and M. Kim, "Membrane Desalination of Agricultural Drainage Water," Review paper, in preparation

McCool, B.C., A. Rahardianto, Y. Cohen, "Field validation and economic feasibility of RO concentrate demineralization via chemically-enhanced seeded precipitation," Desalination, in preparation

Rahardianto, A., B. C. McCool, S. Rezvani and Y. Cohen, "High Recovery Desalination of Agricultural Drainage Water: Integration of Accelerated Seeded Precipitation with RO Membrane Desalination," California/Nevada Section American Water Works Association (CA/NV AWWA) 2006 Spring Conference, Burlingame, CA April 24-28, 2006.

Rahardianto, A., B. McCool, M. Uchymiak and Y. Cohen, "Impact of Mixed Mineral Salt Scaling and Its Mitigation in Brackish Water RO Desalination," CA/NV AWWA 2006 Fall Conference, Long Beach, CA, October 2-5, 2006.

McCool, B. C., A. Rahardianto, S. Rezvani and Y. Cohen, "Technical and Economic Feasibility of Reverse Osmosis Reclamation of Agricultural Drainage Water in the San Joaquin Valley," Session: Novel Membranes and Membrane Processes for Water Treatment and Production, Annual AIChE Meeting, November 12-17, 2006, San Francisco, California.

Rahardianto, A., B. McCool, M. Uchymiak and Y. Cohen, "RO Membrane Desalination of Inland Brackish Water: Scaling by Gypsum in the Presence of Bicarbonate," paper presented at the "Characterization and prediction of fouling" Session, 2007 North American Membrane Society Meeting, Orlando, FL May 12-16 (2007. (This work was also presented in a Poster Session in the same meeting).

Rahardianto, A., B. McCool, Y. Cohen, High recovery inland water desalination via RO integrated with accelerated chemical demineralization – Laboratory and Pilot studies, presented in the RO Membrane Process Development and Novel Membranes Session, 2008 CA-NV AWWA Spring Conference, Hollywood, CA, April 21-24 (2008).

Rahardianto, A., B. C. McCool, and Y. Cohen, "Accelerated Demineralization of Reverse Osmosis Concentrate of High Gypsum Scaling Propensity," (paper 551a), in session on "Novel Membranes and Processes for Water Treatment and Purification," Annual AIChE Meeting, November 16-21, 2008, Philadelphia, PA.

McCool, C. B., A. Rahardianto and Y. Cohen, "Kinetics of Mineral Precipitation and Organics Removal In Brackish Water Desalination," Paper 624d, in Session on Water Desalination and Purification, Annual AIChE Meeting, November 16-21, 2008, Philadelphia, PA.

Bartman, A., J. Thompson, A. Rahardianto, H. Gu, B. C. McCool, A. Zhu, M. Uchymiak, Y. Lam, P. D. Christofides, W. J. Kaiser and Y. Cohen, Cohen, Y., "A Novel Approach and System for Rapid Field Evaluation of Water Desalination ," Paper (412a) in session," in Session "Hybrid and Emerging Membrane-Based Separations Technologies," 2009 Annual AIChE Meeting, Nashville, TN, November 8-13 (2009).

McCool, B. C., A. Rahardianto and Y. Cohen, "Field Demonstration of Brine Demineralization for High Recovery RO Desalination," paper 579g in session Novel Membranes and Processes for Water Treatment, Desalination and Purification II, 2009 Annual AIChE Meeting, Nashville, TN, November 8-13 (2009).

McCool, B.C., A. Rahardianto and Y. Cohen, "Field Demonstration of Brine Demineralization for High Recovery Desalination," AMTA (American Membrane Technol. Association) Annual Conference & Exposition, July 12-15, 2010, San Diego, CA.

Rahardianto, R., B. C. McCool and Y. Cohen, "The Role Of Brine Management in the Optimization of Brackish Water Desalinating with High Permeability RO Membranes," AMTA, Annual Conf. & Expo. July 12-15, 2010, San Diego, CA.

Eric Lyster, Alex Bartman, Brian McCool, and Yoram Cohen, "A Direct Method for Evaluating the Effectiveness of Antiscalant Retardation of Crystal Nucleation and Growth on RO Membranes," in session on "Recent Research Advances in RO Desalination II," AWWA Spring Meeting, Long Beach, California, March 28-31, 2011.

Bartman, A., E. Lyster, H. Gu, B. McCool, R. Rallo, P. Christofides and Y. Cohen, "Real time monitoring of mineral scaling in RO membrane desalination – fundamentals of surface crystallization, process optimization and RO plant control," Session: Desalination 2, Int. Cong. Memb. & Membrane Processes, Amsterdam, The Netherlands, July 23-29, 2011.

Zhu, A., A. Bartman, A. Rahardianto, B. McCool, P. Christofides and Y. Cohen, Strategies for reducing the cost of RO water desalination via process integration and optimization," Session: Modeling, International Congress on Membranes and Membrane Processes, Amsterdam, The Netherlands, July 23-29, 2011.

Bartman, A., E. Lyster, H. Gu, B. McCool, R. Rallo, P. Christofides and Y. Cohen, "Real-time monitoring of mineral scaling in RO membrane desalination – fundamentals of surface crystallization, process optimization and RO plant control," in Session on Desalination, Int. Congress on Membranes and Membrane Processes, July 23-29, 2011, Amsterdam, The Netherlands.

Zhu, A., A. Bartman, A. Rahardianto, B. McCool, P. Christofides and Y. Cohen, "Strategies for reducing the cost of RO water desalination via process integration and optimization," in Session on Modeling, Int. Congress on Membranes and Membrane Processes, July 23-29, 2011, Amsterdam, The Netherlands.

Brian McCool, Eric Lyster, Alex Bartman, and Yoram Cohen, *A direct method for evaluating the effectiveness of antiscalant retardation of crystal nucleation and growth on RO membranes*, 2011 AWWA Membrane Technology Conference & Expo, Long Beach, CA.

Alex Bartman, Eric Lyster, Han Gu, Brian McCool, Robert Rallo, Panagiotis Christofides, and Yoram Cohen, *Real-time monitoring of mineral scaling in RO membrane desalination—fundamentals of surface crystallization, process optimization and RO plant control*, ICOM 2011, Amsterdam.

Aihua Zhu, Alex Bartman, Anditya Rahardianto, Brian McCool, Panagiotis Christofides, and Yoram Cohen, *Strategies for reducing the cost of RO water desalination via process integration and optimization*, ICOM 2011, Amsterdam.

Brian C. McCool, Anditya Rahardianto, and Yoram Cohen, *High recovery RO desalination of brackish water: a systematic approach to process development*, AWWA, California-Nevada Section, 2009 Annual Spring Conference, Santa Clara, CA.

Brian C. McCool, Anditya Rahardianto, and Yoram Cohen, *Economic analysis of high recovery brackish water desalination*, AWWA, California-Nevada Section, 2009 Annual Spring Conference, Santa Clara, CA.

Anditya Rahardianto, Brian C. McCool, and Yoram Cohen, *High Recovery Inland water desalination via RO integrated with accelerated chemical demineralization—laboratory and pilot studies*, AWWA, California-Nevada Section, 2008 Annual Spring Conference, Hollywood.

Brian C. McCool, Anditya Rahardianto, and Yoram Cohen, *High recovery RO desalination of inland brackish water: antiscalant removal via partial lime softening*, AIChE 2008 Annual Meeting, Philadelphia.

Chapter 1

Introduction

1.1 Background

In recent years there has been a renewed interest in the use of reverse osmosis (RO) and nanofiltration (NF) membrane desalination of SJV brackish groundwater as a potentially viable approach for reclamation of AD water for agricultural reuse and possibly potable water consumption [1], while also reducing the challenge of concentrate (brine) management. As the percentage recovery of permeate product of the RO process is increased the volume of brine discharge is decreased. However, the achievable RO recovery may be limited because SJV brackish water is often near or above saturation with respect to various sparingly water soluble mineral salts such as gypsum ($CaSO_4 \cdot 2H_2O$), calcium carbonate ($CaCO_3$), and silica (SiO_2). Upon RO desalting, the concentration of such salts on the feed-side and near the RO membrane surface can increase to levels exceeding their solubility limits which can then lead to surface crystallization of these mineral salts and/or the deposition of their bulk-formed crystals onto the membrane surface. The resulting mineral surface scale leads to water permeate flux decline and potential damage to the membrane [2-7]. Consequently, the feasible recovery limit and process efficiency are reduced and water production costs increase. Given that the composition of SJV brackish water varies with location and time (e.g., with respect to salinity and the composition of sparingly soluble mineral salts) the mineral scaling propensity of such water is also location and time-dependent.

While RO is considered a mature technology, its application for desalination of brackish water remains challenging due to the high costs of managing and disposing residual RO concentrate, especially at inland locations [8-10]. High product water recovery is desirable in

these locations in order to minimize concentrate management costs, however, the recovery levels achievable by RO desalination are typically limited by mineral scaling (e.g. gypsum, silica, calcium carbonate). For example, brackish agricultural drainage waters in the San Joaquin Valley (SJV; 2000–30,000 mg/L TDS) are generally limited to recoveries of 50–75% using traditional RO desalting methods [6, 11, 12] due to a number of factors including, most importantly, mineral salt scaling as described in previous work [13]. Several processes have been proposed to achieve high recovery levels by treating the RO concentrate to allow further water extraction including solar evaporation ponds, vacuum membrane distillation, electrodialysis, ion exchange columns, forward osmosis, and induced precipitation [14]. With the exception of induced precipitation, all of the above methods are impractical for large-scale inland desalination processes.

However, high recovery RO desalination via two-stage RO with intermediate concentrate demineralization (ICD; **Fig. 1-1**) has been shown to be a promising method for concentrate minimization for brackish water desalination [3, 6, 15-18]. The ICD process reduces the concentration of scale precursors (e.g. calcium) in the primary RO concentrate to below their scaling thresholds, allowing the treated concentrate to be further desalted in a secondary RO process in order to enhance the overall recovery in brackish water desalination to >85% and thus to minimize the residual RO concentrate [3, 6, 19].

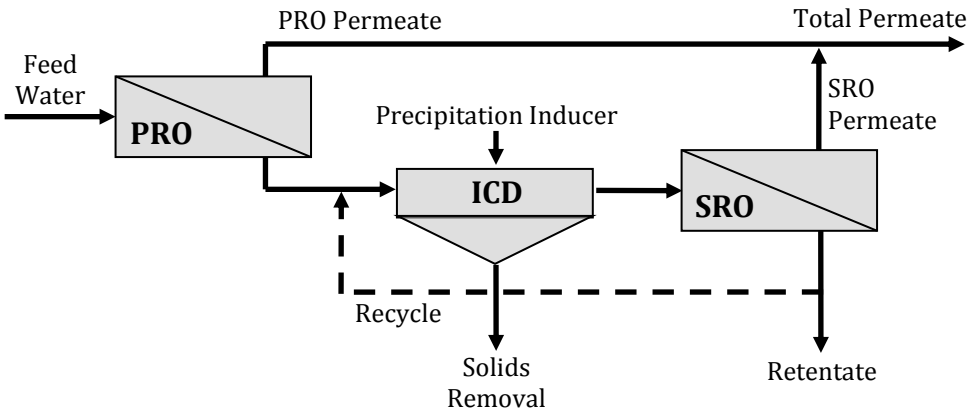

Figure 1-1. High recovery RO process utilizing intermediate concentrate demineralization (ICD)

One promising ICD method for reducing the mineral scale precursor concentrations is through accelerated precipitation softening in which the pH is increased by addition of an alkaline chemical (e.g. sodium hydroxide, calcium hydroxide, sodium bicarbonate, or sodium carbonate) and crystal seeds are added to induce precipitation of calcium carbonate [3, 6, 20]. Accelerated precipitation softening has been shown to be effective at significantly reducing calcium, magnesium, barium, and silica concentrations [3]. Once the scale precursor concentrations are reduced below scaling thresholds, RO desalting can be carried out to higher recoveries (>90%). Chemical precipitation softening has been shown in previous studies as an effective ICD method, targeting calcium ion removal achieved via alkaline-induced $CaCO_3$ precipitation. The approach primarily reduces RO concentrate supersaturation with respect to calcium-bearing mineral scalants (e.g., gypsum, calcite) [3, 6], but also leads to the removal of other trace constituents via co-precipitation processes [3, 6]. While effective, precipitation softening is chemically intensive as it requires at least stoichiometric amounts of an alkaline chemical (e.g. sodium hydroxide, calcium hydroxide, sodium bicarbonate, or sodium carbonate) to induce precipitation of calcium carbonate [3, 6, 20]. Precipitation softening of water lean in bicarbonate (e.g. San Joaquin Valley agricultural drainage water) requires alkaline dosing with

chemicals containing carbonate (e.g. Na_2CO_3), which are generally more expensive than other alkaline sources (e.g. $Ca(OH)_2$) [21], and may cause ICD via the softening process to be economically unattractive compared to ICD via seeded precipitation.

Seeded gypsum precipitation (SGP) is a more promising method for achieving high recovery desalination of bicarbonate-lean (i.e., ratio of bicarbonate to calcium ions less than unity) brackish waters of high gypsum scaling propensity. This approach takes advantage of the fact that PRO concentrate is typically already supersaturated with respect to the gypsum, stabilized by the antisclant carry-over from the PRO desalting step. In this approach the primary RO (PRO) retentate, supersaturated with respect to gypsum, is seeded to enable desupersaturation by precipitative crystal growth prior to the secondary RO (SRO) [16, 22, 23]. While many types of seeds may be used, gypsum seeds are most effective because of the inherent crystal matrix compatibility providing a preferential surface for heterogeneous gypsum precipitation [24]. SGP is less chemically intensive than chemical precipitation in that it requires only seeding for precipitation rather than alkaline dosing of at least stoichiometric amounts relative to the desired amount of calcium removal. Therefore, an SGP process may potentially be cheaper than a softening process for high recovery processes, especially considering the potential ability to recycle seed crystals. However, antiscalant (AS) carry-over often present in PRO concentrate (typically ~3 ppm on a total dissolved solids basis) can interfere with the crystallization process in SGP by stabilizing the supersaturated PRO concentrate [1, 16, 17, 19, 22, 23, 25-34] and by poisoning the gypsum seeds reducing their growth rate which is detrimental to the SGP process. Electrochemical oxidation, polymeric coagulant additives, and surfactants have been investigated as methods to disrupt AS action by AS scavenging or degradation prior to ICD by seeded precipitation [23-25, 32-37]. However, these treatment

strategies may be detrimental to downstream processes where the presence of additives may be undesirable and may lead to membrane fouling [38-41] or where the destruction of AS and other natural organic matter (NOM) present in natural waters may produce hazardous disinfection by-products [42-44]. The increased chemical and storage costs of these methods may increase the costs of desalination compared to SGP.

Previous work [19] has demonstrated that the sequential combination of partial chemical softening and seeded precipitation can balance chemical use with favorable precipitation kinetics in the demineralization of AS-containing PRO concentrate (i.e. gypsum desupersaturation proceeds at the same rate during SGP in the absence of AS as it does in the presence of AS if the AS-containing concentrate is alkaline-treated prior to SGP)—an approach referred to as chemically-enhanced seeded precipitation (CESP). The feasibility of the CESP approach was explored by focusing on the challenge of high recovery desalting of agricultural drainage (AD) water in California's San Joaquin Valley for a specific location (OAS) [13] where the gypsum saturation index is nearly saturated (SIg = 0.99). It was postulated that lime-precipitated $CaCO_3$ particles were able to scavenge generic and commercial polycarboxylic-acid antiscalants, thereby facilitating subsequent $CaSO_4$ precipitation with minimal retardation due to AS-action. The study also demonstrated, via a series of batch CESP cycles, that gypsum particle recycling can sustain $CaSO_4$ precipitation, suggesting that a continuous CESP process could be feasible while enhancing overall water recovery from 63% up to 87% for the case of gypsum-saturated RO feed water.

While high recovery desalination via integration of ICD with RO has been proposed in the literature in various configurations [3, 6, 11, 16, 17, 19, 22, 24-26, 28, 32, 45-53], in general, the processes have not yet been fully developed into a mature technology. Although high

recovery via integration of RO with precipitation softening has been performed in pilot-scale demonstrations with promising results [3, 6, 11, 17, 24-26, 28, 45-51, 53], the processes may not be attractive for water sources lean in bicarbonate as the required carbonate-containing alkaline chemicals (e.g., Na_2CO_3) are typically more expensive than other alkaline chemicals (e.g., $Ca(OH_2)$). On the other hand, high recovery via integration of RO with seeded precipitation of pH-insensitive mineral salts (e.g., gypsum, barite) has been investigated with mixed results [16, 19, 22, 32, 52, 54] but the problem of precipitation inhibition due to seed poisoning by AS has not been satisfactorily solved.

1.2 Problem Statement

In order to design a high recovery RO process for inland brackish water desalination, a rigorous method for estimating the RO recovery limits based on feed water thermodynamic properties must first be developed. Given a frame-work for estimating RO recovery limits in brackish water RO desalination, a high recovery RO process can be designed in order to reduce the substantial brine management costs. Moreover, the AS removal process (i.e., alkaline-induced $CaCO_3$ precipitation) utilized in CESP must be further quantified to enable consistently effective AS removal and thus prevent gypsum seed poisoning during subsequent seeded precipitation. Successful AS removal prevents gypsum seed poisoning which substantially reduces costs by allowing reduced seed loadings, reduced contact times (i.e., smaller crystallizer vessels), and solids recycling in the CESP process. In order for the CESP process to be deployed successfully, it must be demonstrated with field water. Moreover, both the AS removal process and the subsequent gypsum precipitation process must be quantified in order to develop or arrive

at design parameters for a continuous process. A flowchart of the dissertation work is presented in **Fig. 1-2**.

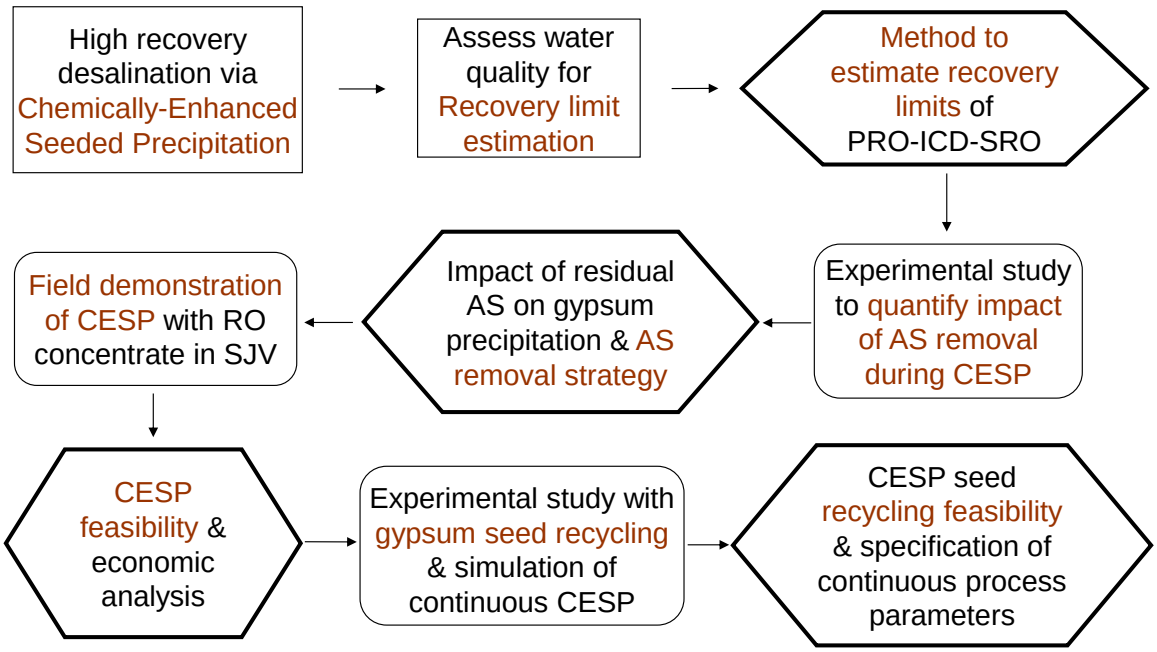

Figure 1-2. Research flowchart; bold hexagons indicate areas of major contributions. Abbreviations: AS, antiscalant; CESP, chemically-enhanced seeded precipitation.

1.3 Objectives of the Dissertation

The major goals of the dissertation were to: (a) develop a method for estimating RO desalination recovery limits, and (b) develop a sustainable high recovery desalination process utilizing chemically-enhanced seeded precipitation (CESP) with integrated antiscalant (AS) removal and gypsum precipitation. First, a method was introduced for RO recovery limit estimation based on water quality analysis. Enhancement of RO recovery making use of intermediate concentrate demineralization (ICD) was then investigated with the specific goal of overcoming the retardation of mineral precipitation by residual AS from the primary RO (PRO) desalination step. The inhibition of ICD by AS-action was then explored and alkaline-induced $CaCO_3$ precipitation is investigated as a means of AS removal prior to further secondary RO (SRO) desalting. Additionally, the technical and economic feasibility of the CESP process for

demineralization of PRO concentrate generated in a pilot RO system in the San Joaquin Valley was demonstrated in a field study. Furthermore, the potential for solids recycling was demonstrated in a series of batch CESP tests for model RO concentrate solutions. Finally, the process requirements for continuous CESP were estimated from simulations of the continuous process. The main objectives of the research were to:

1. Develop an experimental method for estimating RO desalination recovery limits imposed by scaling and operating pressure based on thermodynamic properties (mineral salt solubility and osmotic pressure) of feed water; Develop a diagnostic method for verifying the estimated recovery limits based on bench-scale RO studies of brackish water samples from the San Joaquin Valley in order to determine the feasibility of RO desalination.
2. Develop a method to enhance RO desalination recovery limits via ICD followed by secondary RO desalting with the following specific objectives:
    a. Develop a process for removal of AS carryover (from the primary RO concentrate stream) in order to overcome the AS inhibition of mineral salt precipitation during ICD.
    b. Investigate the mechanism of AS removal during alkaline-induced $CaCO_3$ precipitation via direct measurements of AS concentration and quantification of the impact of initial AS concentration, supersaturation level (lime dose), and staged alkaline dosing.
    c. Quantify the effectiveness of AS removal in enabling subsequent seeded gypsum precipitation via an antiscalant Langmuir adsorption model to account for gypsum seed “poisoning”.

3. Demonstrate the feasibility of the CESP process in a field study making use of RO concentrate generated from agricultural drainage water via a spiral-wound RO system.
4. Investigate and experimentally demonstrate the feasibility of solids recycling, considering gypsum precipitation kinetics in the CESP process, in addition to determining the required crystallizer (i.e., reactor) operating conditions for continuous CESP for high recovery RO desalination.

1.4 Approach

The previously stated objectives were achieved through a combination of theoretical analysis and experimental investigations. Thermodynamic properties, including mineral salt solubility and osmotic pressure, were calculated using rigorous multi-electrolyte analysis in order to design desalination process and to determine process parameters. Laboratory RO desalination studies were performed in both a plate-and-frame RO desalination system and in a batch crystallizer ICD system in order to: (a) evaluate and optimize different process conditions, and (b) verify the results of theoretical analysis. Field studies provided proof-of-concept verification for the developed high recovery desalination process.

The framework developed for estimating recovery limits based on water quality analysis of field water samples from the SJV is described in **Ch. 3**. Thermodynamic solubility analysis was utilized to estimate limits imposed by both membrane mineral scaling and concentrate osmotic pressure. A method to account for concentration polarization in the RO feed channel was also developed enabling the estimation of more realistic recovery limits encountered in an RO plant. Laboratory diagnostic assays were performed with field samples of brackish agricultural drainage water from the SJV using a plate-and-frame RO desalination system in

order to verify the estimated recovery limits by direct observation of the presence or absence of membrane scaling at various conditions. The equivalent recovery of the PFRO system was estimated based on equating conditions at the membrane surface in the PFRO system to the expected conditions in the exit of the tail element of a traditional RO process.

The approach to antiscalant removal during CESP is described in **Ch. 4** for model RO concentrate solutions based on a central San Joaquin Valley water source (OAS). The feasibility of AS removal from RO concentrate via lime treatment was experimentally demonstrated and quantified. The efficiency of AS removal with respect to lime dosage was explored and the effectiveness of subsequent seeded gypsum precipitation to reduce the level of gypsum supersaturation was established. In addition, the filterability of the treated RO concentrate was evaluated by quantifying the size of the formed precipitate particles and measuring the turbidity of treated RO concentrate before and after microfiltration.

In **Ch. 5**, results from a limited field study are described and serve as a proof-of-concept of the high recovery RO process developed in the present work. The potential for high recovery RO desalination, via interstage demineralization, was demonstrated for a brackish agricultural drainage water source in the central San Joaquin Valley (DP-25 location) utilizing the concentrate generated by a pilot spiral-wound RO system. The concentrate was collected at ~52% recovery and was used for batch demineralization experiments in both a small one-liter and a larger 20-liter crystallizer. The field-study was carried out in order to confirm the effectiveness of the CESP process using field water. Additionally, an economic analysis was performed to demonstrate the attractiveness of the CESP process relative to precipitation softening for high recovery desalination.

Chapter 6 reports on the study of multi-cycle seeded gypsum precipitation batch experiments with solids recycling. These studies were performed in order to assess the feasibility of a continuous CESP process for high recovery desalination. The requirements for AS removal, which is needed in order to avoid gypsum seed poisoning during CESP, were evaluated over multiple cycles. These experiments served to determine the feasibility of maintaining the rate of calcium removal. Subsequently, the required gypsum seed makeup rate was estimated from direct simulations of the continuous CESP process.

References

1. Rahardianto, A., B.C. McCool, and Y. Cohen, *Reverse osmosis desalting of inland brackish water of high gypsum scaling propensity: Kinetics and mitigation of membrane mineral scaling.* Environmental Science & Technology, 2008. **42**(12): p. 4292-4297.
2. Boerlage, S.F.E., M.D. Kennedy, I. Bremere, G.J. Witkamp, J.P. Van der Hoek, and J.C. Schippers, *The scaling potential of barium sulphate in reverse osmosis systems.* Journal of Membrane Science, 2002. **197**(1-2): p. 251-268.
3. Gabelich, C.J., M.D. Williams, A. Rahardianto, J.C. Franklin, and Y. Cohen, *High-recovery reverse osmosis desalination using intermediate chemical demineralization.* Journal of Membrane Science, 2007. **301**(1-2): p. 131-141.
4. Hasson, D., A. Drak, and R. Semiat, *Inception of CaSO4 scaling on RO membranes at various water recovery levels.* Desalination, 2001. **139**(1-3): p. 73-81.
5. McCool, B.C., A. Rahardianto, and Y. Cohen. *Technical and Economic Feasibility of Reverse Osmosis Reclamation of Agricultural Drainage Water in the San Joaquin Valley*. in *Proceedings of the AIChE Annual Conference*. 2006. San Francisco, CA.
6. Rahardianto, A., J. Gao, C.J. Gabelich, M.D. Williams, and Y. Cohen, *High recovery membrane desalting of low-salinity brackish water: Integration of accelerated precipitation softening with membrane RO.* Journal of Membrane Science, 2007. **289**(1-2): p. 123-137.
7. Uchymiak, M., A. Rahardianto, E. Lyster, J. Glater, and Y. Cohen, *A novel RO ex situ scale observation detector (EXSOD) for mineral scale characterization and early detection.* Journal of Membrane Science, 2007. **291**(1-2): p. 86-95.
8. Committee on Advancing Desalination Technology, Water Science and Technology Board, and National Research Council, *Desalination: A National Perspective*. 2008, Washington, DC: National Academies Press.
9. Bond, R. and S. Veerapaneni, *Zero Liquid Discharge for Inland Desalination*. 2007, Denver, CO: AWWA Research Foundation, AWWA, & IWA Publishing.
10. Mickley, M.C., *Membrane concentrate disposal: practice and regulation*. 2006, Mickley & Associates, US Bureau of Reclamation: Denver, CO.
11. Rahardianto, A., B.C. McCool, S. Rezvani, and Y. Cohen. *High recovery desalination of agricultural drainage water: integration of accelerated chemical precipitaion with RO membrane desalination*. in *Procedings of the AIChE Annual Conference*. 2005. Cincinnati, OH.
12. Lee, R.-W., J. Glater, Y. Cohen, C. Martin, K. Kovac, M.N. Milobar, and D.W. Bartel, *Low-pressure RO membrane desalination of agricultural drainage water.* Desalination, 2003. **155**(2): p. 109-120.
13. McCool, B.C., A. Rahardianto, J. Faria, K. Kovac, D. Lara, and Y. Cohen, *Feasibility of reverse osmosis desalination of brackish agricultural drainage water in the San Joaquin Valley.* Desalination, 2010. **261**(3): p. 240-250.
14. Pérez-González, A., A.M. Urtiaga, R. Ibáñez, and I. Ortiz, *State of the art and review on the treatment technologies of water reverse osmosis concentrates.* Water Research, 2012. **46**(2): p. 267-283.

15. Almulla, A., M. Eid, P. Côté, and J. Coburn, *Developments in high recovery brackish water desalination plants as part of the solution to water quantity problems.* Desalination, 2003. **153**(1-3): p. 237-243.
16. Bremere, I., M.D. Kennedy, A. Johnson, R. van Emmerik, G.J. Witkamp, and J.C. Schippers, *Increasing conversion in membrane filtration systems using a desupersaturation unit to prevent scaling.* Desalination, 1998. **119**(1-3): p. 199-204.
17. Sanciolo, P., L. Zou, S. Gray, G. Leslie, and D. Stevens, *Accelerated seeded precipitation pre-treatment of municipal wastewater to reduce scaling.* Chemosphere, 2008. **72**(2): p. 243-249.
18. Ning, R.Y., A. Tarquin, M. Trzcinski, and G. Patwardhan, *Recovery optimization of RO concentrate from desert wells.* Desalination, 2006. **201**(1-3): p. 315-322.
19. Rahardianto, A., B.C. McCool, and Y. Cohen, *Accelerated Desupersaturation of Reverse Osmosis Concentrate by Chemically-Enhanced Seeded Precipitation.* Desalination, 2010. **264**(3).
20. Kedem, O. and G. Zalmon, *Compact accelerated precipitation softening (CAPS) as a pretreatment for membrane desalination I. Softening by NaOH.* Desalination, 1997. **113**(1): p. 65-71.
21. U.S. Geological Survey, Mineral commodity summaries 2011: U.S. Geological Survey, 198 p.
22. Bremere, I., M. Kennedy, P. Michel, R. van Emmerik, G.J. Witkamp, and J. Schippers, *Controlling scaling in membrane filtration systems using a desupersaturation unit.* Desalination, 1999. **124**(1-3): p. 51-62.
23. Yang, Q.F., Y.Q. Liu, H. David, and R. Semiat, *Scaling salt removal by addition of inorganic particles.* J. Chem. Eng. Japan, 2008. **41**(1): p. 6-12.
24. Yang, Q., Y. Liu, D. Hasson, and R. Semiat, *Removal of CaCO3 Scaling Salt from RO Concentrates by Air-Blow and Inorganic Inducers.* Journal of Chemical Engineering of Japan, 2008. **41**(1): p. 13-20.
25. Greenlee, L.F., F. Testa, D.F. Lawler, B.D. Freeman, and P. Moulin, *The effect of antiscalant addition on calcium carbonate precipitation for a simplified synthetic brackish water reverse osmosis concentrate.* Water Research, 2010. **44**(9): p. 2957-2969.
26. Greenlee, L.F., F. Testa, D.F. Lawler, B.D. Freeman, and P. Moulin, *Effect of antiscalant degradation on salt precipitation and solid/liquid separation of RO concentrate.* Journal of Membrane Science, 2011. **366**(1-2): p. 48-61.
27. Hasson, D., A. Drak, and R. Semiat, *Induction times induced in an RO system by antiscalants delaying CaSO4 precipitation.* Desalination, 2003. **157**: p. 193-207.
28. Hasson, D., R. Segev, D. Lisitsin, B. Liberman, and R. Semiat, *High recovery brackish water desalination process devoid of precipitation chemicals.* Desalination, 2011. **283**: p. 80-88.
29. Lyster, E., M.-m. Kim, J. Au, and Y. Cohen, *A method for evaluating antiscalant retardation of crystal nucleation and growth on RO membranes.* Journal of Membrane Science, 2010. **364**(1-2): p. 122-131.
30. Oner, M., O. Dogan, and G. Oner, *The influence of polyelectrolytes architecture on calcium sulfate dihydrate growth retardation.* Journal of Crystal Growth, 1998. **186**(3): p. 427-437.

31. Xiao, J.J., A.T. Kan, and M.B. Tomson, *Prediction of BaSO4 precipitation in the presence and absence of a polymeric inhibitor: Phosphino-polycarboxylic acid.* Langmuir, 2001. **17**(15): p. 4668-4673.
32. Yang, Q., D. Lisitsin, Y. Liu, D. Hasson, and R. Semiat, *Desupersaturation of RO Concentrates by Addition of Coagulant and Surfactant.* Journal of Chemical Engineering of Japan, 2007. **40**(9): p. 730-735.
33. Yang, Q., Z. Ma, D. Hasson, and R. Semiat, *Destruction of anti-scalants in RO concentrates by electrochemical oxidation.* J. Chem. Ind. Eng. (China), 2004. **55**(2): p. 339-340.
34. Yang, Q.-F., Z.-F. Ma, D. Hasson, and R. Semiat, *Destruction of Anti-Scalants in RO Concentrates by Electrochemical Oxidation.* Journal of Chemical Industry and Engineering (China), 2004. **55**(2): p. 339-340.
35. Barthrope, R.T., *Removal of scale-forming inorganic salts form a produced brine*, US Patent, Editor. 1994: United States.
36. Yang, Q.F., D. Lisitsin, Y.Q. Liu, H. David, and R. Semiat, *Desupersaturation of RO concentrates by addition of coagulant and surfactant.* J. Chem. Eng. Japan, 2007. **40**(9): p. 730-735.
37. Yasunaga, N., S. Furukawa, Y. Kawaai, and J. Hirotsuji, *Investigation of radical reactions for efficiency improvement in ozone-hydrogen peroxide treatment.* Water Science and Technology, 2001. **43**(2): p. 205-2112.
38. Gabelich, C.J., W.R. Chen, T.I. Yun, B.M. Coffey, and I.H. Suffet, *The Role of Dissolved Aluminum in Silica Chemistry for Membrane Processes.* Desalination, 2005. **180**: p. 307-319.
39. Gabelich, C.J., K.P. Ishida, F.W. Gerringer, R. Evangelista, M. Kalyan, and I.H. Suffet, *Control of residual aluminum from conventional treatment to improve reverse osmosis performance.* Desalination, 2006. **190**(1-3): p. 147-160.
40. Kim, M.M., J. Au, A. Rahardianto, J. Glater, Y. Cohen, F.W. Gerringer, and C.J. Gabelich, *Impact of Conventional Water Treatment Coagulants on Mineral Scaling in RO Desalting of Brackish Water.* Industrial & Engineering Chemistry Research, 2009. **48**(6): p. 3126-3135.
41. Shih, W.-Y., J. Gao, A. Rahardianto, J. Glater, Y. Cohen, and C.J. Gabelich, *Ranking of antiscalant performance for gypsum scale suppression in the presence of residual aluminum.* Desalination, 2006. **196**(1-3): p. 280-292.
42. Hua, G. and D.A. Reckhow, *Comparison of disinfection byproduct formation from chlorine and alternative disinfectants.* Water Research, 2007. **41**(8): p. 1667-1678.
43. Krasner, S.W., *The formation and control of emerging disinfection by-products of health concern.* Philosophical Transactions of the Royal Society a-Mathematical Physical and Engineering Sciences, 2009. **367**(1904): p. 4077-4095.
44. Wert, E.C., F.L. Rosario-Ortiz, D.D. Drury, and S.A. Snyder, *Formation of oxidation byproducts from ozonation of wastewater.* Water Research, 2007. **41**(7): p. 1481-1490.
45. Gabelich, C.J., A. Rahardianto, R.C. Northrup, and Y. Cohen, *Process evaluation of intermediate concentrate demineralization for water recovery enhancement in production-scale brackish water desalting.* Desalination, 2011. **272** (1-3): p. 36-45.
46. Gilron, J., D. Chaikin, and N. Daltrophe, *Demonstration of CAPS pretreatment of surface water for RO.* Desalination, 2000. **127**(3): p. 271-282.

47. Gilron, J., N. Daltrophe, M. Waissman, and Y. Oren, *Comparison between compact accelerated precipitation softening (CAPS) and conventional pretreatment in operation of brackish water reverse osmosis (BWRO).* Industrial & Engineering Chemistry Research, 2005. **44**(15): p. 5465-5471.
48. Lisitsin, D., D. Hasson, and R. Semiat, *The potential of CO2 stripping for pretreating brackish and wastewater desalination feeds.* Desalination, 2008. **222**(1-3): p. 50-58.
49. Nason, J.A. and D.F. Lawler, *Particle size distribution dynamics during precipitative softening: Declining solution composition.* Water Research, 2009. **43**(2): p. 303-312.
50. Oren, Y., V. Katz, and N.C. Daltrophe, *Improved compact accelerated precipitation softening (CAPS).* Desalination, 2001. **139**(1-3): p. 155-159.
51. Sanciolo, P., E. Ostarcevic, G. Atherton, T. Fane, Y. Cohen, M. Payne, and S. Gray, *Enhancement of Reverse Osmosis Water Recovery Using Interstage Calcium Precipitation.* Desalination, 2012. **495**: p. 43-52.
52. Seewoo, S., R. Van Hille, and A. Lewis, *Aspects of gypsum precipitation in scaling waters.* Hydrometallurgy, 2004. **75**(1-4): p. 135-146.
53. Segev, R., D. Hasson, and R. Semiat, *Improved high recovery brackish water desalination process based on fluidized bed air stripping.* Desalination, 2011. **281**: p. 75-79.
54. Rahardianto, A., *High recovery desalting of brackish water, doctoral dissertation*. 2009, University of California Los Angeles.

Chapter 2

Literature Review

2.1.1 RO Desalination

Reverse osmosis (RO) is the process by which pressure is applied to a feed solution across a semipermeable membrane that allows water passage, but largely rejects solute passage resulting in a solute lean stream (permeate or product) and a solute rich stream (retentate or concentrate) [1-4]. The applied pressure must be greater than the osmotic pressure of the solution for separation to occur (i.e. non-zero permeate flux) [5]. An RO membrane can be characterized by its permeability, L_P, and its salt rejection, R_0. The permeability is a measure of how easily water passes through the membrane and is proportional to the inverse of the membrane's resistance to water passage and salt rejection is a measure of the degree to which dissolved ions are rejected from passing through the membrane. The flux through the membrane is equal to the permeability times the net driving pressure as shown below [5]:

$$J_W = L_P(\Delta p - \sigma \cdot \Delta \pi) \tag{2-1}$$

where J_W is the water flux through the membrane, L_P is the membrane water permeability, $\Delta p = p_f - p_m$, where p_f and p_m are the feed and permeate pressures, respectively, σ is the salt reflection coefficient, and $\Delta\pi$ is the osmotic pressure difference between the feed and permeate sides. The osmotic pressure of saline water increases with solute concentration and for dilute solutions can be calculated with **Eqn. (2-2**) [6]:

$$\pi = iC_S RT \tag{2-2}$$

where π is the osmotic pressure (atm), i is the van't Hoff factor for a given solute, C_S is the solute concentration (mol/L), R is the ideal gas constant (0.08206 $L \cdot atm \cdot mol^{-1} \cdot K^{-1}$), and T is temperature (K) [6]. For non-dilute solutions the osmotic pressure is a more complex function of

salt concentrations and its calculation must take into account non-idealities associated with mixed salt systems [7, 8].

RO desalination is typically carried out in a cross-flow scheme in which the saline feed water enters the membrane channel and flows tangentially across the membrane surface under high pressure. The feed stream exits the membrane channel as a concentrate stream. In plate-and-frame type modules, the membrane is supported by a rigid, porous layer as shown in **Fig. 2-1**. When treating large volumes of feed water, spiral-wound membrane modules (see **Fig. 2-2**) are often used because they provide a large membrane surface area to volume ratio and most state-of-the-art RO membranes are manufactured in this arrangement [9-11]. A spiral-wound module consists of alternating layers of RO membrane sheets and mesh spacer sheets wrapped around a central channel, all encased within a plastic shell. The spacers provide the channels (i.e. space) through which feed and permeate water can flow.

Most large scale RO desalination plants use a multistage arrangement of spiral-wound modules connected in series with each stage containing modules in parallel as needed based on the expected flows. As the permeate is separated from the feed the volume of the retentate decreases, often necessitating fewer modules in parallel in the second stage (and subsequent stages if present) as illustrated in **Fig. 2-3**. However, as most natural feed waters contain suspended particles, pretreatment is required prior to desalting to remove particulates and debris that could damage or plug the RO membranes.

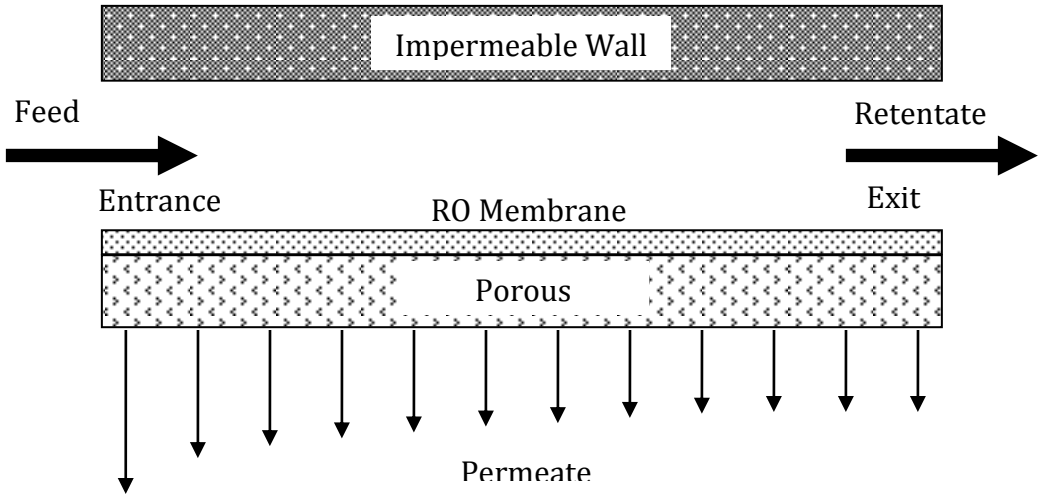

Figure 2-1. Schematic of cross-flow in a rectangular channel

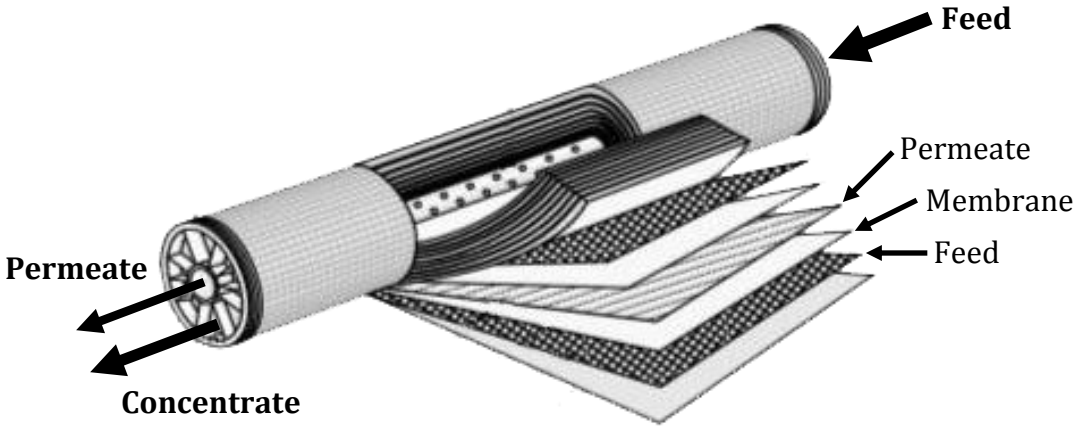

Figure 2-2. Cut-away of spiral wound RO membrane module [12]

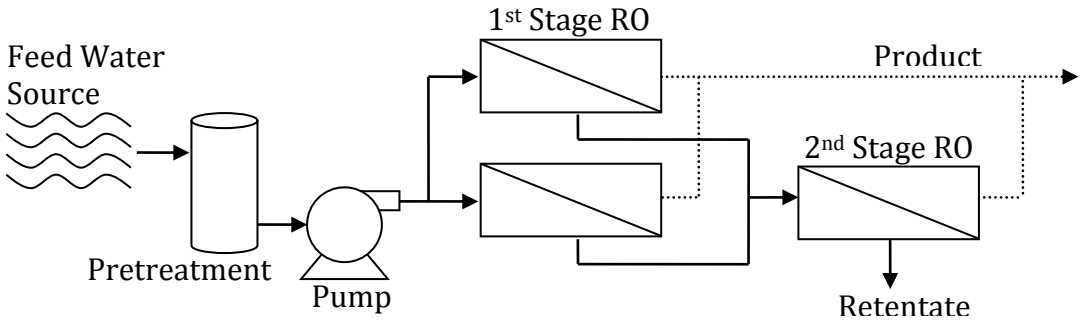

Figure 2-3. Schematic of typical two stage (2:1) RO desalination process

2.1.2 RO Membranes

RO membranes are thin film composites of an aromatic polyamide active layer (~200 nm thick) supported by a porous polysulfone layer (~60 μm) which is itself supported by an underlying non-woven fabric (~150 μm) as shown in **Fig. 2-5**. The active layer is where the separation occurs while the polysulfone and non-woven fabric provide structural support without impeding the flow of water through the membrane.

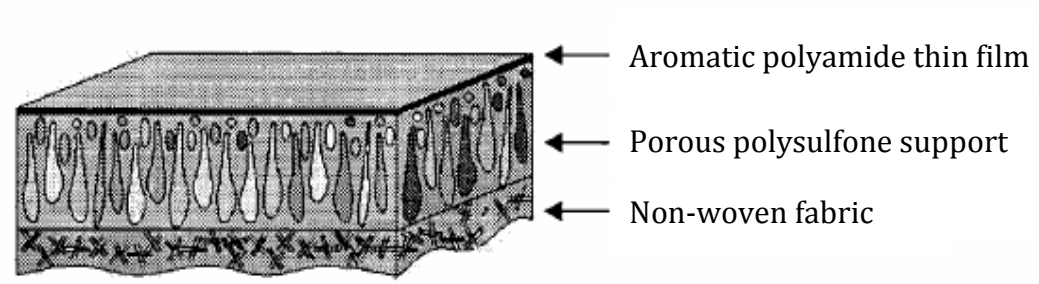

Figure 2-5. Cross section of a typical RO membrane showing layered structure [13].

Salt rejection is a measure of the membrane's ability to block salt passage—the more salt that passes through the membrane the lower the salt rejection. The observed salt rejection of an RO membrane, R_0, is defined as:

$$R_0 = 1 - \frac{C_P}{C_B} \tag{2-3}$$

where C_P and C_B are the concentrations of the permeate and bulk streams, respectively. In typical operation at low recovery per membrane module, the bulk concentration is equal to the feed concentration, C_F. Permeate productivity is measured in terms of the fractional recovery, Y, defined as:

$$Y = \frac{Q_P}{Q_F} = 1 - \frac{Q_R}{Q_F} \tag{2-4}$$

where Q_P, Q_F, and Q_R are the permeate, feed, and retentate volumetric flow rates, respectively. As an RO process achieves overall higher recoveries, the retentate stream becomes more

concentrated and the level of concentration in the retentate is typically expressed in terms of a concentration factor, $CF = C_C/C_F$, where C_C and C_F are the respective concentrate and feed concentrations. The concentration factor can be related to the recovery level, Y, of an RO process by performing a salt balance over the membrane channel and by utilizing **Eqns. (2-3)** & **(2-4)** as below:

$$CF = \frac{C_C}{C_F} = \frac{1 - Y(1 - R_0)}{1 - Y} \tag{2-5}$$

Eqn. (2-5) can be rearranged such that the recovery can be found as a function of the concentration factor and the salt rejection:

$$Y = \frac{CF - 1}{CF - 1 + R_0} \tag{2-6}$$

where Y is the fractional product water recovery, CF is the concentration factor, and R_0 is the observed fractional salt rejection.

2.1.3 Concentration Polarization

As water permeates across an RO membrane, rejected salt ions accumulate near and at the membrane surface resulting in an increased local concentration. The solute concentration at the membrane surface is always higher than that found in the bulk solution (for non-zero recoveries) due to the formation of a concentration boundary layer. The concentration polarization (CP) modulus [14] which expresses the level of concentration increase at the membrane surface relative to the bulk, is often quantified by the simple film model given as:

$$CP = \frac{C_m}{C_b} = 1 - R_0 + R_0 \exp\left(\frac{J}{k}\right) \tag{2-7}$$

where C_m and C_b are the concentrations of the solute at the membrane surface and in the bulk, respectively, R_0 is the observed salt rejection, and J is the permeate flux and k is the solute feed-side mass transfer coefficient. It is important to quantify the CP modulus at the operating conditions of the RO system because salts that are below their solubility limit (or saturation) in the bulk may be supersaturated at the membrane surface and can potentially precipitate or crystallize onto the membrane even if undersaturated in the bulk. The degree of concentration polarization gradually increases as the feed flows along the membrane channel towards the exit region as described by the boundary layer model [15]. As the concentration and osmotic pressure at the membrane surface gradually increase from the entrance to the exit as the feed-side salinity increases, the effective net driving force for permeation decreases, thus, the permeate flux decreases towards the exit region as illustrated in **Fig. 2-4**. Typically, the degree of concentration polarization is expected to be ~10–20% (i.e., CP = 1.1 –1.2) [16].

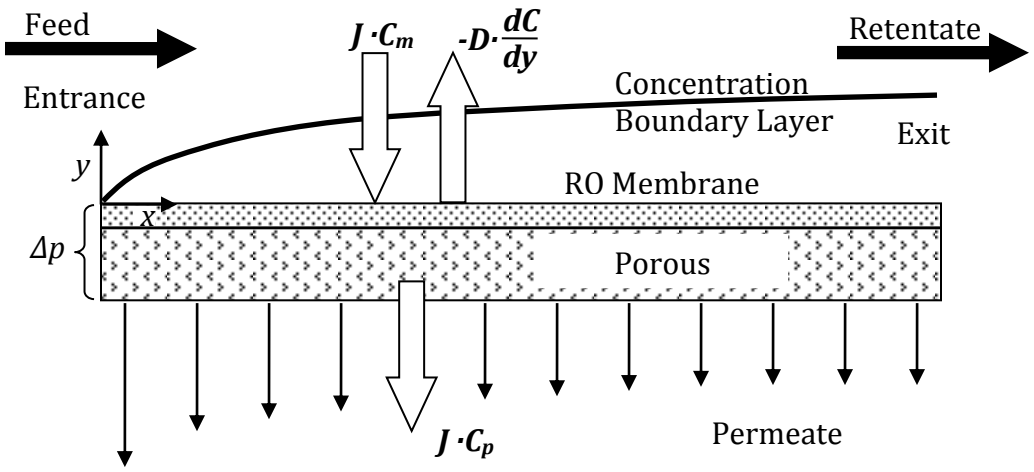

Figure 2-4. Schematic of rectangular RO channel showing the formation of a concentration boundary layer. Block arrow represent solute fluxes. J is the water flux, C_m and C_p are the respective concentrations at the membrane surface and in the permeate, D is the solute diffusivity, and dC/dy is the solute concentration gradient in the y-direction.

2.1.4 Water quality measurements

There are various practical measurements of water quality, several of those relevant to the present work are described in this section. Total Dissolved Solids (TDS) is a measure of all ionic species present and is typically reported in milligrams per liter (mg/L). The TDS is usually determined on the basis of an equivalent salt concentration for a measured electrical conductivity of the solution. Natural waters can typically be classified into four different categories by their salinity: fresh water (<1000 mg/L), low salinity brackish water (1000–3000 mg/L), high salinity brackish water (3000–35,000 mg/L), and seawater (35,000 mg/L).

Electrical conductivity (EC) measures the ability of a solution to conduct electricity and is an indirect measure of the salinity of the solution. By comparing the EC of the feed in an RO system to that of the permeate, the EC-based salt rejection can be calculated:

$$R_S = 1 - \frac{EC_P}{EC_F} \tag{2-8}$$

where EC_P and EC_F denote the permeate and feed conductivities, respectively.

Total alkalinity is a measure of water's ability to neutralize acid and is usually measured in mg/L as calcium carbonate ($CaCO_3$). Carbonate (CO_3^{2-}) and bicarbonate (HCO_3^-) ions are in equilibrium with carbonic acid (H_2CO_3) and dissolved carbon dioxide (CO_2) according to the following reactions:

$H_2CO_3 \leftrightarrow HCO_3^- + H^+$, $\quad pK_{a1} = 3.60$ (25 ºC)

$HCO_3^- \leftrightarrow CO_3^{2-} + H^+$, $\quad pK_{a2} = 10.25$ (25 ºC)

$CO_2 + H_2O \leftrightarrow HCO_3^- + H^+$, $\quad pK_a = 6.36$ (25ºC)

The relative equilibrium concentrations of the above species depend primarily on pH, temperature, and carbon dioxide partial pressure. The alkalinity of seawater is between 200 and 250 mg/L as $CaCO_3$, while that of brackish water in the SJV typically is highly variable and is in

the range of 100 to 700 mg/L as $CaCO_3$ [17]. The bicarbonate ion typically has the greatest contribution to total alkalinity in natural waters, although other species can also contribute including phosphate, nitrate, silicates, borate, ammonia, sulfide, carbonate, hydroxide, and conjugate bases of organic acids. The bicarbonate concentration can be estimated where analytical data are unavailable by assuming that all other contributors to total alkalinity are negligible. The total alkalinity is measured by titration to a pH endpoint of 4.5 using sulfuric acid (see **Appendix B**).

The silt density index (SDI) is a measure of the particulates present in natural waters that are rejected by a 0.45 μm filter. The SDI is calculated by comparing the length of time required to collect a 500 mL of permeate initially and after a certain length of time in dead-end filtration. The SDI is defined by the ASTM Standard Test Method D4189-07 [18]:

$$SDI_T = \frac{\%P_{30}}{T} = \frac{\left[1 - \frac{t_i}{t_f}\right]100}{T} \tag{2-9}$$

where $\%P_{30}$ is the plugging factor at a trans-membrane pressure of 30 psi, T is the time between sample collections (min), and t_i and t_f are the elapsed times (min) to collect initial and final permeate samples, respectively. Prefiltration is generally recommended for water having an SDI_{15} greater than 5.0 to prevent particulates from plugging the RO membrane [19].

Turbidity measures the amount light back-scattered from suspended solids in water samples and is a function of the concentration, size, shape, and optical characteristics of the particulates. The turbidity, measured in nephelometric turbidity units (NTU), of feed water for RO desalination is generally recommended to be <1.0 NTU [20] to prevent premature fouling of the RO membranes and can be reduced by adequate prefiltration.

2.1.5 Recovery Limitations

Mineral salt scaling and osmotic pressure are the two fundamental factors that can limit product water recovery in RO desalination [21-33]. Mineral salt scaling is the process by which sparingly soluble salts exceed their saturation concentrations and precipitate in bulk or crystallize on RO membrane surfaces obstructing permeate flow through the membrane reducing the productivity of the process. Consequently, RO desalination processes must be operated such that the concentrations of mineral scaling salts at the membrane surface remain below their scaling thresholds. The corresponding scaling imposed recovery limits can be estimated by **Eqn. (2-6)** by establishing the *CF* at which the retentate concentrations reach the mineral salt scaling thresholds. The above approach provides an upper limit estimate of the feasible recovery since it does not consider the impact of concentration polarization [14] (see **Ch. 3**). The corresponding scaling thresholds of mineral salts of concern (e.g. gypsum, silica, calcite) are typically expressed in terms of the saturation index which is the ratio of the ion activity product (*IAP*) to the solubility product (K_{SP}):

$$SI = \frac{IAP}{K_{SP}} \tag{2-10}$$

For example, the SIs for gypsum, SI_G, calcite, SI_C, and barite, SI_B, are defined as:

$$SI_G = \frac{(Ca^{2+})(SO_4^{2-})}{K_{SP,G}}, \quad SI_C = \frac{(Ca^{2+})(CO_3^{2-})}{K_{SP,C}}, \quad SI_B = \frac{(Ba^{2+})(SO_4^{2+})}{K_{SP,B}} \tag{2-11}$$

where (Ca^{2+}), (Ba^{2+}), (SO_4^{2-}), and (CO_3^{2-}) are the calcium, barium, sulfate, and carbonate ion activities, respectively, and $K_{SP,G}$, $K_{SP,C}$, and $K_{SP,B}$ are the gypsum, calcite, and barite solubility products, respectfully. The RO feed is often dosed with antiscalant (AS) additives which reduce the kinetics of crystallization and enable RO operation at or above saturation (i.e. $SI_i \geq 1$). Therefore, the scaling threshold is typically taken to be the *SI* above which membrane scaling is

likely to occur even in the presence antiscalant. For example, recommended scaling thresholds, with the appropriate antiscalant use, for gypsum, barite, and silica are SI_G = 2.3–4.0, SI_B = 60–80, and SI_S = 1.0–3.0 respectively [34].

Another measure of scaling threshold is the Langelier saturation index (LSI) which is commonly used for predicting calcite scale solubility. It is defined as the difference between the measured pH of the solution and the pH at which the solution would be saturation with respect to calcite:

$$\mathrm{LSI} = \mathrm{pH} - \mathrm{pH_S} \tag{2-12}$$

where pH and $\mathrm{pH_S}$ are the measured pH and the saturation pH, respectively. Solutions with a negative LSI are undersaturated and thus dissolve calcite, solutions with a positive LSI are oversaturated and thus calcite may precipitate, and solutions with LSI near zero are close to calcite saturation and small changes in temperature or pH may lead to under- or over-saturated solutions [35].

The osmotic pressure of the retentate limits RO recovery by reducing the effective pressure driving force available for permeate production (**Eqn. (2-1)**). The retentate concentration increases with increasing recovery which in turn increases the osmotic pressure; eventually the permeate flux will vanish when the osmotic pressure reaches the applied pressure. In general, for non-scaling water, recovery is ultimately limited by the available pumping power and/or maximum operating pressure (600–1000 psi) of the membrane pressure vessels.

Biofouling is the process by which bacteria or other microorganisms adhere to and grow on the membrane surface reducing water permeation through the membrane and increasing downtime of the RO process. Biofouling leads to flux decline and has also been shown to enhance mineral scaling [36]. Often the microbes form a biofilm which can be difficult and

costly to remove. In general, feed pretreatment required to retard biofouling for source water rich in microbes [37, 38].

2.2 High Recovery RO Desalination via intermediate concentrate demineralization

In order to exceed the mineral scaling imposed recovery limits that are encountered in traditional RO the concentration of mineral scale forming ions must be reduced below the scaling threshold. A two-stage process that integrates RO desalting with intermediate concentrate demineralization (ICD) is one of the technically viable solutions for achieving this goal [28]. In one configuration of this process, primary RO (PRO) desalting is carried out up to a product recovery level just below the membrane scaling threshold. The scaling threshold is dictated by the source water quality, operating pH, and the antiscalant type and dose. The PRO concentrate stream is then demineralized or desupersaturated during ICD to reduce the concentration of scale precursor ions (e.g. calcium, sulfate, and carbonate ions), followed by a secondary RO (SRO) or NF desalting of the treated PRO concentrate (i.e. PRO-ICD-SRO approach). For example, brackish agricultural drainage waters in the San Joaquin Valley (2000–30,000 mg/L TDS) are generally limited to recoveries of 50–75% using traditional RO desalting methods [28, 29, 39], however recoveries in excess of 85% may be achieved via ICD [40-42]. Various methods have been proposed for high recovery RO desalination via incorporation of demineralization of the RO feed or concentrate by induced precipitation of scale precursors (e.g., calcium, barium, sulfate, carbonate, and phosphate ions). These demineralization processes can be classified into two categories: 1) alkaline induced calcium precipitation, and 2) seeded precipitation as described in the following sections. A summary of the relevant prior work on high recovery RO desalination via precipitation of scaling mineral salt precursors is provided in **Table 2-1**.

Table 2-1. Relevant prior work on high recovery RO desalination via precipitation of scaling mineral salt precursors. Note: an asterisk (*) after the citation indicates that high recovery desalting was demonstrated by integration of demineralization with RO.

Citation	Demineralization Process	Feed Water Conditions	Findings & Limitations
Gilron, Chaikin, Daltrophe, Desalination, 2000* **[43]**	$CaCO_3$ via NaOH (pH→8.3–9) and calcite seeds (CAPS); RO pretreatment, continuous reactor, treated water desalinated in RO unit	Nahal Tahinim brook, Israel (filtered & unfiltered); 140–150 ppm Ca^{2+}, 200–220 ppm SO_4^{2-}, 300 ppm HCO_3^-	**F:** 67–87% calcium removal; decrease in RO flux decline "overnight" (batch total-recycle) after calcium removal: 80% & 90% *Y* demonstrated after CAPS treatment with 0% & 10–15% F.D., respectively; 80% *Y* demonstrated w/o CAPS treatment with 60% F.D. **L:** requires carbonate-rich source water and expensive caustic (NaOH)
Gilron, Daltrophe, Waissman, Oren, Ind. Eng. Chem. Res., 2005* **[44]**	$CaCO_3$ via NaOH & $Ca(OH)_2$ (pH→9–9.5) and calcite seeds (CAPS); RO pretreatment, batch16-L reactor	brackish groundwater, Negev, Israel: 188–274 ppm Ca^{2+}, 420–520 ppm SO_4^{2-}, 218–324 ppm HCO_3^-; LSI 0.79	**F:** decrease in RO flux decline "overnight" for "about a week" (batch total-recycle) after calcium removal: 90% *Y* demonstrated with & w/o CAPS treatment with 0% 70% F.D., respectively; **L:** caustic consumption ~2x stoichiometric amount required to remove calcium hardness due to CO_2 re-uptake
Greenlee, Testa, Lawler, Freeman, Moulin, Water Research, 2010 **[45]**	$CaCO_3$ via NaOH & $NaHCO_3$ (pH→8–11); PRO concentrate treatment, batch "jar test" apparatus	synthetic brackish groundwater concentrate (80% Y): 1325 ppm Ca^{2+}, 0 ppm SO_4^{2-}, 2570 ppm HCO_3^-; 0–10.5 mg/L (DOC) AS (DQ2066, DQ2006, DQ2054, Coatex)	**F:** $CaCO_3$ ppt occurs at pH>8 with/without AS; AS reduces amount of $CaCO_3$ ppt; AS alters morphology & decreases particle size & causing denser MF filter cake; **L:** uses expensive caustics: NaOH & Na_2HCO_3; potential recovery enhancement not quantified

Citation	Demineralization Process	Feed Water Conditions	Findings & Limitations
Greenlee, Testa, Lawler, Freeman, Moulin, JMS, 2011 **[46]**	$CaCO_3$ via NaOH & $NaHCO_3$ (pH→10.5); AS disruption via ozone, hydrogen peroxide; PRO concentrate treatment, batch 1-L "jar test" square beakers	model brackish groundwater concentrate (80% Y): "complete": 1030 ppm Ca^{2+}, 2 ppm Ba^{2+}, 515 ppm Mg^{2+}, 991 ppm SO_4^{2-}, 780 ppm alk (as $CaCO_3$), SIc = 64; "simplified" 1030 ppm Ca^{2+}, 0 ppm Ba^{2+}, 0 ppm Mg^{2+}, 0 ppm SO_4^{2-}, 780 ppm alk (as $CaCO_3$), SIc = 64; 0–85 ppm AS (DQ2066, DQ2006, DQ2054, Coatex)	**F:** could increase recovery from 80% to 90% or 94%; oxidation deactivated AS; AS reduces amount of $CaCO_3$ ppt; AS alters morphology; **L:** uses expensive caustics: NaOH & Na_2HCO_3; formation of oxidation byproducts
Hasson, Segev, Lisitsin, Liberman, Semiat, Desalination, 2011* **[47]**	$CaCO_3$ via air stripping of CO_2 (pH→8.9) in PRO conc.; PRO-ICD-SRO, continuous 20-L crystallizer (model) and batch/continuous one to three 1-m^3 crystallizers in series (field)	model concentrate: 615–690 ppm Ca^{2+}, 1350–2500 ppm alk as $CaCO_3$., 10–25 ppm AS (SHMP or Permatreat 191); field concentrate (78% Y): side-stream from 1.5 MCM/day desal. plant near Atlit:1300 ppm Ca^{2+}, 1460 ppm alk. as $CaCO_3$.	**F:** 52–56% $CaCO_3$ ppt conversion; >95% *Y* anticipated; 78% → 90% *Y* demonstrated over 30 hr (no mention of F.D.); **L:** large crystallizer residence times required: 1–4 hr; scaling of aeration nozzles; inadequate settling device; cartridge filter plugging prior to SRO
Lisitsin, Hasson, Semiat, Desalination, 2008 **[48]**	$CaCO_3$ via air stripping of CO_2 (pH→9) in alkaline water; RO pretreatment, batch/continuous 21-L crystallizer	"typical" model concentrate: 680 ppm Ca^{2+}, 2450 ppm as $CaCO_3$ alk., 0 ppm SO_4^{2-}, 25 ppm AS (Permatreat 191); LSI 0.1–2.1	**F:** CO_2 mass transfer coef. increases with increasing air flow rate and mixing rate; 84% reduction in Ca^{2+} conc.; **L:** proof-of-concept only; over-simplified model solution
Nason, Lawler, Water Research, 2009 **[49]**	$CaCO_3$ via lime, NaOH, and/or $NaHCO_3$ (pH→10–11) and calcite seeds; ICD treatment, bench-scale rectangular jar tester	solution composition emulating "actual" softening process: 1.9–10.12 mM HCO_3^-, 0.99–6.23 mM Ca^{2+}, 0 ppm SO_4^{2-}, *SIc* = 36–576	**F:** Greater *SIc* enhances both precipitative growth and "flocculation"; calcite seeding increases precipitation rate, particle size, flocculation, and decreases nucleation; High mixing intensities hinders aggregation; **L:** model solution is bicarbonate rich; expensive alkaline chemicals used
Oren, Katz, Daltrophe, Desalination, 2001 **[50]**	$CaCO_3$ via NaOH (pH→8–10.5) and calcite seeds (CAPS); RO pretreatment, continuous 25-L vessel	tap water: 65–80 ppm Ca^{2+}, 35–40 ppm Mg^{2+}, 210–260 ppm HCO_3^-	**F:** 80–90% calcium removal; **L:** experiments performed with tap water; requires bicarbonate-rich water

Citation	Demineralization Process	Feed Water Conditions	Findings & Limitations
Sanciolo, Zou, Gray, Leslie, Stevens, Chemosphere, 2008 **[51]**	$CaCO_3$ via NaOH and Na_2CO_3 (pH→9.5) and calcite seeds; pretreatment or RO concentrate treatment, batch 1-L beaker	treated municipal wastewater (spiked): 75–81 ppm Ca^{2+}, 159–165 ppm HCO_3^-, 81–85 ppm SO_4^{2-}	**F:** 91–94% calcium removal; **L:** expensive caustics required to increase SIc, long pretreatment period (1 hr) at pH 9.5 required prior to calcite seeding to remove more than 34% calcium; 2 seed additions required in some cases; high seed dose required (10–20 g/L)
Segev, Hasson, Semiat, Desalination, 2011 **[52]**	$CaCO_3$ via air stripping of CO_2 (to increase pH) in PRO conc. and quartz seeds; PRO concentrate treatment, fluidized bed crystallizer (19–35 cm high)	"typical" carbonate-rich model concentrate: 1442 ppm Ca^{2+}, 460 ppm Mg^{2+}, 1910 ppm alk as $CaCO_3$, 790 ppm SO_4^{2-}, 18 ppm AS (Spectra Guard); LSI 1.5	**F:** 90% calcium conversion enabling recovery enhancement from 70% to 95%; mass transfer coef. Increased with temperature and varied with seed type; **L:** requires carbonate-rich source water
Yang, Liu, Hasson, Semiat, J. Chem. Engr. Japan, 2008 **[53]**	$CaCO_3$ via air stripping of CO_2 (pH→8.2) and calcite, kaoline, alumina, dolomite, magnesia, or diatomite seeds; PRO concentrate treatment & recycling to feed, 1-L beaker	"simulated" model concentrate: 532–1107 ppm Ca^{2+}, 107–202 ppm SO_4^{2-}, 654–1554 ppm HCO_3^-, 10–22 ppm AS (LB0100, LB2000, or LB3000); LSI 1.6–2.5	**F:** $CaCO_3$ ppt accompanied by adsorption ppt of AS; 30–80% reduction in Ca^{2+} conc.; **L:** high seed dose: 20–50 g/L,
Sanciolo, Ostarcevic, Atherton, Leslie, Fane, Cohen, Payne, Gray, Desalination, 2012* **[54]**	$CaHPO_4$ via NaOH, $NaHCO_3$ (pH→7.5–10.5) and KH_2PO_4, and seeds ($CaCO_3$, $CaSO_4$, $CaHPO_4$); PRO concentrate treatment prior to ceramic ultrafiltration, 0.1-L lab-scale (batch) and 500-L pilot scale flocculation tank (continuous)	RO concentrate (70% Y) from desalination of wastewater from Donald, Victoria, Australia: 96–220 ppm Ca^{2+}, 140–360 ppm Mg^{2+}, 370–410 ppm alk as $CaCO_3$, 170–970 ppm SO_4^{2-}, 3 ppm AS (in feed) (Flocon 135), pH 7.0–8.8	**F:** Recoveries of 70–90% demonstrated over 2 days with 8% flux decline; optimum pH = 9.5, Recycle of $CaHPO_4$ seeds possible, lab/pilot ICD cost 2.6/21 $\$/m^3$; **L:** Ceramic UF permeate heating may require heat exchanger to control temperature, high $CaHPO_4$ seed dose (20 g/L), KH_2PO_4 dosing required in addition to NaOH

Citation	Demineralization Process	Feed Water Conditions	Findings & Limitations
Seewoo, Van Hille, Lewis, Hydrometallurgy, 2004 **[55]**	$CaSO_4$ via gypsum seeding (SPARRO); RO pretreatment w. concentrate recycle, 5-L batch reactor	"typical" mine water: 30 mM Ca^{2+}, 30–300 mM SO_4^{2-}	**F:** desupersaturation (i.e equilibrium) reached in 48–152 min for 7–1% (vol) solids; needle morphology of gypsum formed at low supersaturation levels (*SIg* = 2.27) can damage RO membrane; **L:** high level of seeding required; effect of AS not addressed; possible membrane scouring due to direct contact with seeds
Yang, Lisitsin, Liu, David, Semiat, J. Chem. Engr. Japan, 2007 **[56]**	$CaSO_4$ via gypsum seeding after AS disruption by coagulant and surfactant addition (polyaluminum chloride coagulant, polyacrylamide AP410C flocculant, sodium dodecyl sulfate surfactant); PRO concentrate treatment & recycling to feed, 1-L beaker	"simulated" model concentrate: 3250 ppm Ca^{2+}, 6300 ppm SO_4^{2-}, 0 ppm HCO_3^-, 10–34 ppm AS (LB0100, LB2000, LB3000, or SHMP); SIg=4.4	**F:** SIg reduced to 1; CaCO3 ppt after coagulant and surfactant addition accompanied by removal of AS; **L:** surfactant dosing may be expensive; SDS not effective for all AS tested; residual aluminum could be detrimental to RO process; SIg higher than practical in RO concentrate; SIg estimated from ROPRO7 (Koch); high seed dose: 20 g/L
Bremere, Kennedy, Johnson, Emmerik, Witkamp, Schippers, Desalination, 1998 **[57]**	$BaSO_4$ via fixed bed reactor (barite seeds); PRO concentrate treatment, 1 of 3 continuous cylindrical packed beds (0.34–2.9 L)	field concentrate (80–85% Y) side-stream from surface water pilot plant: 0.19–0.44 ppm Ba^{2+}, 290–650 ppm SO_4^{2-}; SIb=3.1–3.2	**F:** decreased SIb to 1.2–1.6, NOM may be used as a "natural antiscalant"; **L:** NOM poisoning of packed bed reduces desupersaturation efficiency

Citation	Demineralization Process	Feed Water Conditions	Findings & Limitations
Bremere, Kennedy, Michel, Emmerik, Witkamp, Schippers, Desalination, 1999 **[58]**	$BaSO_4$ via fixed bed reactor (barite seeds), "acidified" water (pH 2–3) for bed regeneration; PRO concentrate treatment, 1 of 2 continuous cylindrical packed beds (0.09–0.37 L)	synthetic RO concentrate; field concentrate (80–85% Y) from "pilot-scale" RO unit; filed concentrate (70% Y) from ground water NF pilot plant: 0.13–0.45 ppm Ba^{2+}, 156–680 ppm SO_4^{2-}; SIb=2.0–3.2	**F:** initially, up to 70% or 80% reduction in Ba^{2+} conc. for field conc. and synthetic NOM-free water, respectively, followed by rapid barite poisoning; ozonation increases fraction of low molar-mass acid NOM and increases poisoning of barite seeds, reversibility of barite seed poisoning varies with NOM source; **L:** severe NOM poisoning of packed bed reduced desupersaturation efficiency, irreversible poisoning of barite seeds with certain water sources

2.2.1 Demineralization via alkaline induced calcium precipitation

Chemical precipitation softening has been shown in previous studies [43-53] as an effective ICD method. Such approaches typically target calcium ion removal, achieved via alkaline-induced $CaCO_3$ precipitation, often with the addition of seeds to induce precipitation in order to increase precipitation kinetics, and hence reduce the time required for precipitation. Various seed types have been tested including calcite, kaoline, alumina, dolomite, magnesia, and diatomite. However, calcite seeds have been found to be most effective [43, 44, 49-53] as the most stable precipitating phase (calcite) is compatible with the calcite seed crystal lattice. The precipitation softening approach primarily reduces RO concentrate supersaturation with respect to calcium-bearing mineral scalants (e.g., gypsum, calcite) [25, 28].It also leads to removal of other trace constituents via co-precipitation [25, 28]. Precipitation softening in combination with RO desalting has been shown to be effective for enhancing water recoveries in excess of 90% [28, 44, 46, 47, 49-52, 54]. Precipitation softening, however, is chemically intensive as it requires at least stoichiometric amounts of an alkaline chemical (e.g. sodium hydroxide, calcium

hydroxide, sodium bicarbonate, or sodium carbonate) to induce precipitation of calcium carbonate [25, 28, 59] and [43-46, 49-51]. Alternatively, it is possible to employ air stripping of CO_2 instead of alkaline chemical dosing in order to increase the pH of the PRO concentrate and induce $CaCO_3$ precipitation [47, 48, 52, 53]. However, air stripping was found to be limited by scaling of aeration nozzles and requires a bicarbonate-rich feed water. Precipitation softening of water lean in bicarbonate (e.g. San Joaquin Valley agricultural drainage water) requires alkaline dosing with chemicals containing carbonate (e.g. Na_2CO_3), which are generally more expensive than other alkaline sources (e.g. $Ca(OH)_2$) [60]. Therefore, ICD via softening is more costly relative to ICD via seeded precipitation. However, an attractive benefit of softening is that demineralization is feasible even in presence of antiscalants that are normally present in the PRO concentrate with little impact of the effectiveness of precipitation [45, 61]. An approach similar to softening has been applied by [54] for calcium removal via alkaline induced $CaHPO_4$ precipitation as its solubility decreases with pH. While effective, this method of calcium removal is only applicable to phosphate-rich source waters and also requires an expensive alkaline (NaOH) and a high $CaHPO_4$ seed dose (20 g/L) to enhance $CaHPO_4$ removal.

2.2.2. Demineralization via seeded precipitation

Seeded precipitation is the process by which precipitation is induced in a metastable supersaturated solution by adding crystal seeds in order to supply a preferential surface area for heterogeneous crystal growth. Seeded precipitation is a more promising method than softening for achieving high recovery desalination of bicarbonate-lean (or phosphate lean) brackish waters. This process takes advantage of the fact that PRO concentrate is typically already supersaturated with respect to the mineral scalants of concern, stabilized by the antisclant carry-over from the

PRO desalting step. In this approach the primary RO (PRO) retentate, supersaturated with respect to gypsum, is seeded to enable desupersaturation by precipitative crystal growth prior to the secondary RO (SRO) [57, 58, 62]. The seeded precipitation process has been applied primarily for mineral salts with solubilities insensitive to pH adjustment (e.g. calcium sulfate, barium sulfate) [55-58]. It is less chemically intensive than chemical precipitation softening in that it requires only seeding for precipitation. In contrast, alkaline dosing requires at least stoichiometric amounts for the desired amount of calcium removal. Therefore, seeding may potentially be cheaper than softening for high recovery desalination especially considering the potential benefit of recycling of seed crystals. Seeded precipitation processes have several potential limitations, however, including seed poisoning by natural organic matter and antiscalants [41, 56-58, 61], the requirement of large crystal seed doses at low initial supersaturation levels [56], and, in one process [55], RO/NF membrane damage by needle-like seeds scouring the membrane surface. In most cases seed poisoning is the primary limitation encountered in seeded precipitation processes [41, 56-58, 61].

Antiscalant (AS) carry-over often present in PRO concentrate (typically ~3–10 ppm on a total dissolved solids basis [63]) and natural organic matter (NOM) can interfere with the crystallization process in seeded precipitation by stabilizing the supersaturated PRO concentrate and by poisoning the crystal seeds reducing their growth rate [62]. Electrochemical oxidation, polymeric coagulant additives, and surfactants have been investigated as methods to disrupt antiscalant action by antiscalant scavenging or degradation prior to ICD by seeded precipitation [45, 53, 56, 62, 64-68]. These methods were successfully demonstrated to disrupt antiscalant action for all antiscalants tested with the exception of the SDS surfactant which was ineffective in disrupting three out of four antiscalants tested [56]. However, these treatment strategies may

be detrimental to downstream processes where the presence of additives may be undesirable and may lead to membrane fouling [63, 69-71] or where the destruction of AS and other NOM present in natural waters may produce hazardous disinfection by-products [72-74]. The increased chemical and storage costs of these methods may increase the costs of desalination and offset the potential savings compared to softening. In order for a high recovery RO process that utilizes seeded precipitation to compete with softening, a low cost and effective method must be developed to prevent seed poisoning by NOM and/or AS in the PRO concentrate.

2.2.3 Chemically-Enhanced Seeded Precepitation

A novel, two-step, chemically-enhanced seeded precipitation (CESP) process [41] was developed in the present work combining softening and seeded precipitation. The first step of CESP utilizes partial lime-softening (i.e. incomplete lime-softening) to remove AS carry-over from PRO concentrate by precipitation with $CaCO_3$. After sufficient AS removal from the PRO concentrate has been achieved, gypsum seeds are added for demineralization prior to SRO. The CESP process is described in more detail in **Ch. 4**.

References

1. Alghoul, M.A., P. Poovanaesvaran, K. Sopian, and M.Y. Sulaiman, *Review of brackish water reverse osmosis (BWRO) system designs.* Renewable and Sustainable Energy Reviews, 2009. **13**(9): p. 2661-2667.
2. Fritzmann, C., J. Löwenberg, T. Wintgens, and T. Melin, *State-of-the-art of reverse osmosis desalination.* Desalination, 2007. **216**(1–3): p. 1-76.
3. Li, D. and H. Wang, *Recent developments in reverse osmosis desalination membranes.* Journal of Materials Chemistry, 2010. **20**(22): p. 4551-4566.
4. Malaeb, L. and G.M. Ayoub, *Reverse osmosis technology for water treatment: State of the art review.* Desalination, 2011. **267**(1): p. 1-8.
5. Zhu, A.Z., P.D. Christofides, and Y. Cohen, *Effect of Thermodynamic Restriction on Energy Cost Optimization of RO Membrane Water Desalination.* Industrial & Engineering Chemistry Research, 2009. **48**(13): p. 6010-6021.
6. Cussler, E.L., *Diffusion: Mass Transfer in Fluid Systems*. Second ed. 1997, New York: Cambridge University Press.
7. Kumar, A. and V.S. Patwardhan, *Aqueous solutions of single electrolytes: thermodynamic properties at high temperature and concentration.* Chemical Engineering Science, 1992. **47**(15-16): p. 4039-4047.
8. Yokozeki, A., *Osmotic pressures studied using a simple equation-of-state and its applications.* Applied Energy, 2006. **83**(1): p. 15-41.
9. Gorenflo, A., J.A. Redondo, and F. Reverberi, *Basic options and two case studies for retrofitting hollow fiber elements by spiral-wound RO technology.* Desalination, 2005. **178**(1-3): p. 247-260.
10. Al-Mobayed, A.S., F.M. Mubeen, and S. Balaji, *Comparison of the performance of hollow fine fiber and spiral-wound membranes in the Al-Jubail SWRO desalination plant.* Desalination, 2005. **178**(1-3): p. 273-286.
11. Polasek, V., S. Talo, and T. Sharif, *Conversion from hollow fiber to spiral technology in large seawater RO systems -- process design and economics.* Desalination, 2003. **156**(1-3): p. 239-247.
12. *Agritech Smartwater: Wellington Dam Water Recovery Project*. 2006 [cited 2007 October 15, 2007]; Available from: http://www.agritechsmartwater.com.au/agritech_smartwater_reverse_osmosis_process.htm.
13. Shih, W.-Y., *Formation and Control of Calcium Sulfate Dihydrate (Gypsum) Crystallization on RO Membranes and Surrogate Polymeric Surfaces*, in *Chemical and Biomolecular Engineering*. 2007, University of California Los Angeles.
14. Lyster, E. and Y. Cohen, *Numerical study of concentration polarization in a rectangular reverse osmosis membrane channel: Permeate flux variation and hydrodynamic end effects.* Journal of Membrane Science, 2007. **303**(1-2): p. 140-153.
15. Zydney, A.L., *Stagnant film model for concentration polarization in membrane systems.* Journal of Membrane Science, 1997. **130**(1-2): p. 275-281.
16. McCool, B.C., A. Rahardianto, J. Faria, K. Kovac, D. Lara, and Y. Cohen, *Feasibility of reverse osmosis desalination of brackish agricultural drainage water in the San Joaquin Valley.* Desalination, 2010. **261**(3): p. 240-250.

17. *Selection of Candidate Sumps to Determine Critical Membrane Desalination Process Requirements*. 2004, California Department of Water Resources.
18. ASTM-International, *ASTM D4189-07 Standard Test Method for Silt Density Index (SDI) of Water*. 2007. **11.01**.
19. Hydranautics, *LFC1 Membrane Element Spec Sheet*. 2003.
20. Hydranautics, *Element Spec Sheet LFC3-LD*. 2011.
21. Abbas, A., *On the performance limitation of reverse osmosis water desalination systems.* International Journal of Nuclear Desalination, 2007. **2**(3): p. 205-218218.
22. Boerlage, S.F.E., M.D. Kennedy, I. Bremere, G.J. Witkamp, J.P. Van der Hoek, and J.C. Schippers, *The scaling potential of barium sulphate in reverse osmosis systems.* Journal of Membrane Science, 2002. **197**(1-2): p. 251-268.
23. McCool, B.C., A. Rahardianto, S. Rezvani, and Y. Cohen. *Technical and Economic Feasibility of Reverse Osmosis Reclamation of Agricultural Drainage Water in the San Joaquin Valley*. in *Procedings of the AIChE Annual Conference*. 2006. San Francisco, CA.
24. Calabro, V. and E. Drioli, *Polarization phenomena in integrated reverse osmosis and membrane distillation for seawater desalination and waste water treatment.* Desalination, 1997. **108**(1-3): p. 81-82.
25. Gabelich, C.J., M.D. Williams, A. Rahardianto, J.C. Franklin, and Y. Cohen, *High-recovery reverse osmosis desalination using intermediate chemical demineralization.* Journal of Membrane Science, 2007. **301**(1-2): p. 131-141.
26. Hasson, D., A. Drak, and R. Semiat, *Inception of CaSO4 scaling on RO membranes at various water recovery levels.* Desalination, 2001. **139**(1-3): p. 73-81.
27. Hydranautics, *Chemical Pretreatment of RO and NF, Technical Application Bulletin No. 111 Rev. C*. 2008, Nitto Denko: Oceanside, CA. p. 10.
28. Rahardianto, A., J. Gao, C.J. Gabelich, M.D. Williams, and Y. Cohen, *High recovery membrane desalting of low-salinity brackish water: Integration of accelerated precipitation softening with membrane RO.* Journal of Membrane Science, 2007. **289**(1-2): p. 123-137.
29. Rahardianto, A., B.C. McCool, S. Rezvani, and Y. Cohen. *High recovery desalination of agricultural drainage water: integration of accelerated chemical precipitaion with RO membrane desalination*. in *Procedings of the AIChE Annual Conference*. 2005. Cincinnati, OH.
30. Rautenbach, R. and K. Vossenkaul, *Pressure driven membrane processes - the answer to the need of a growing world population for quality water supply and waste water disposal.* Separation and Purification Technology, 2001. **22-3**(1-3): p. 193-208.
31. Romero-Ternero, V., L. Garcia-Rodriguez, and C. Gomez-Camacho, *Thermoeconomic analysis of a seawater reverse osmosis plant.* Desalination, 2005. **181**(1-3): p. 43-59.
32. Semiat, R., *Energy Issues in Desalination Processes.* Environmental Science & Technology, 2008. **42**(22): p. 8193-8201.
33. Uchymiak, M., A. Rahardianto, E. Lyster, J. Glater, and Y. Cohen, *A novel RO ex situ scale observation detector (EXSOD) for mineral scale characterization and early detection.* Journal of Membrane Science, 2007. **291**(1-2): p. 86-95.
34. Hydranautics, *Chemical Pretreatment of RO/NF, Technical Application Bulletin No. 111 Rev. C*. 2008.

35. Patzay, G., G. Stahl, F.H. Karman, and E. Kalman, *Modeling of scale formation and corrosion from geothermal water.* Electrochimica Acta, 1998. **43**(1-2): p. 137-147.
36. Thompson, J., N. Lin, E. Lyster, R. Arbel, T. Knoell, J. Gilron, and Y. Cohen, *RO membrane scaling in the presence of a biofilm.* Journal of Membrane Science, 2012. **Submitted**.
37. Flemming, H.C., G. Schaule, T. Griebe, J. Schmitt, and A. Tamachkiarowa, *Biofouling--the Achilles heel of membrane processes.* Desalination, 1997. **113**(2-3): p. 215-225.
38. Herzberg, M. and M. Elimelech, *Biofouling of reverse osmosis membranes: Role of biofilm-enhanced osmotic pressure.* Journal of Membrane Science, 2007. **295**(1-2): p. 11-20.
39. Lee, R.-W., J. Glater, Y. Cohen, C. Martin, K. Kovac, M.N. Milobar, and D.W. Bartel, *Low-pressure RO membrane desalination of agricultural drainage water.* Desalination, 2003. **155**(2): p. 109-120.
40. Rahardianto, A., *High recovery desalting of brackish water, doctoral dissertation*. 2009, University of California Los Angeles.
41. Rahardianto, A., B.C. McCool, and Y. Cohen, *Accelerated Desupersaturation of Reverse Osmosis Concentrate by Chemically-Enhanced Seeded Precipitation.* Desalination, 2010. **264**(3).
42. Zhu, A., A. Rahardianto, P.D. Christofides, and Y. Cohen, *Reverse osmosis desalination with high permeability membranes—Cost optimization and research needs.* Desalination and Water Treatment, 2010. **15** p. 256-266.
43. Gilron, J., D. Chaikin, and N. Daltrophe, *Demonstration of CAPS pretreatment of surface water for RO*. Desalination, 2000. **127**(3): p. 271-282.
44. Gilron, J., N. Daltrophe, M. Waissman, and Y. Oren, *Comparison between compact accelerated precipitation softening (CAPS) and conventional pretreatment in operation of brackish water reverse osmosis (BWRO).* Industrial & Engineering Chemistry Research, 2005. **44**(15): p. 5465-5471.
45. Greenlee, L.F., F. Testa, D.F. Lawler, B.D. Freeman, and P. Moulin, *The effect of antiscalant addition on calcium carbonate precipitation for a simplified synthetic brackish water reverse osmosis concentrate.* Water Research, 2010. **44**(9): p. 2957-2969.
46. Greenlee, L.F., F. Testa, D.F. Lawler, B.D. Freeman, and P. Moulin, *Effect of antiscalant degradation on salt precipitation and solid/liquid separation of RO concentrate.* Journal of Membrane Science, 2011. **366**(1-2): p. 48-61.
47. Hasson, D., R. Segev, D. Lisitsin, B. Liberman, and R. Semiat, *High recovery brackish water desalination process devoid of precipitation chemicals.* Desalination, 2011. **283**: p. 80-88.
48. Lisitsin, D., D. Hasson, and R. Semiat, *The potential of CO2 stripping for pretreating brackish and wastewater desalination feeds.* Desalination, 2008. **222**(1-3): p. 50-58.
49. Nason, J.A. and D.F. Lawler, *Particle size distribution dynamics during precipitative softening: Declining solution composition.* Water Research, 2009. **43**(2): p. 303-312.
50. Oren, Y., V. Katz, and N.C. Daltrophe, *Improved compact accelerated precipitation softening (CAPS).* Desalination, 2001. **139**(1-3): p. 155-159.
51. Sanciolo, P., L. Zou, S. Gray, G. Leslie, and D. Stevens, *Accelerated seeded precipitation pre-treatment of municipal wastewater to reduce scaling.* Chemosphere, 2008. **72**(2): p. 243-249.

52. Segev, R., D. Hasson, and R. Semiat, *Improved high recovery brackish water desalination process based on fluidized bed air stripping.* Desalination, 2011. **281**: p. 75-79.
53. Yang, Q., Y. Liu, D. Hasson, and R. Semiat, *Removal of CaCO3 Scaling Salt from RO Concentrates by Air-Blow and Inorganic Inducers.* Journal of Chemical Engineering of Japan, 2008. **41**(1): p. 13-20.
54. Sanciolo, P., E. Ostarcevic, G. Atherton, T. Fane, Y. Cohen, M. Payne, and S. Gray, *Enhancement of Reverse Osmosis Water Recovery Using Interstage Calcium Precipitation.* Desalination, 2012. **495**: p. 43-52.
55. Seewoo, S., R. Van Hille, and A. Lewis, *Aspects of gypsum precipitation in scaling waters.* Hydrometallurgy, 2004. **75**(1-4): p. 135-146.
56. Yang, Q., D. Lisitsin, Y. Liu, D. Hasson, and R. Semiat, *Desupersaturation of RO Concentrates by Addition of Coagulant and Surfactant.* Journal of Chemical Engineering of Japan, 2007. **40**(9): p. 730-735.
57. Bremere, I., M.D. Kennedy, A. Johnson, R. van Emmerik, G.J. Witkamp, and J.C. Schippers, *Increasing conversion in membrane filtration systems using a desupersaturation unit to prevent scaling.* Desalination, 1998. **119**(1-3): p. 199-204.
58. Bremere, I., M. Kennedy, P. Michel, R. van Emmerik, G.J. Witkamp, and J. Schippers, *Controlling scaling in membrane filtration systems using a desupersaturation unit.* Desalination, 1999. **124**(1-3): p. 51-62.
59. Kedem, O. and G. Zalmon, *Compact accelerated precipitation softening (CAPS) as a pretreatment for membrane desalination I. Softening by NaOH.* Desalination, 1997. **113**(1): p. 65-71.
60. U.S. Geological Survey, Mineral commodity summaries 2011: U.S. Geological Survey, 198 p.
61. Rahardianto, A., B.C. McCool, and Y. Cohen, *Reverse osmosis desalting of inland brackish water of high gypsum scaling propensity: Kinetics and mitigation of membrane mineral scaling.* Environmental Science & Technology, 2008. **42**(12): p. 4292-4297.
62. Yang, Q.F., Y.Q. Liu, H. David, and R. Semiat, *Scaling salt removal by addition of inorganic particles.* J. Chem. Eng. Japan, 2008. **41**(1): p. 6-12.
63. Kim, M.M., J. Au, A. Rahardianto, J. Glater, Y. Cohen, F.W. Gerringer, and C.J. Gabelich, *Impact of Conventional Water Treatment Coagulants on Mineral Scaling in RO Desalting of Brackish Water.* Industrial & Engineering Chemistry Research, 2009. **48**(6): p. 3126-3135.
64. Barthrope, R.T., *Removal of scale-forming inorganic salts form a produced brine*, US Patent, Editor. 1994: United States.
65. Yang, Q., Z. Ma, D. Hasson, and R. Semiat, *Destruction of anti-scalants in RO concentrates by electrochemical oxidation.* J. Chem. Ind. Eng. (China), 2004. **55**(2): p. 339-340.
66. Yang, Q.F., D. Lisitsin, Y.Q. Liu, H. David, and R. Semiat, *Desupersaturation of RO concentrates by addition of coagulant and surfactant.* J. Chem. Eng. Japan, 2007. **40**(9): p. 730-735.
67. Yang, Q.-F., Z.-F. Ma, D. Hasson, and R. Semiat, *Destruction of Anti-Scalants in RO Concentrates by Electrochemical Oxidation.* Journal of Chemical Industry and Engineering (China), 2004. **55**(2): p. 339-340.

68. Yasunaga, N., S. Furukawa, Y. Kawaai, and J. Hirotsuji, *Investigation of radical reactions for efficiency improvement in ozone-hydrogen peroxide treatment.* Water Science and Technology, 2001. **43**(2): p. 205-2112.
69. Gabelich, C.J., W.R. Chen, T.I. Yun, B.M. Coffey, and I.H. Suffet, *The Role of Dissolved Aluminum in Silica Chemistry for Membrane Processes.* Desalination, 2005. **180**: p. 307-319.
70. Gabelich, C.J., K.P. Ishida, F.W. Gerringer, R. Evangelista, M. Kalyan, and I.H. Suffet, *Control of residual aluminum from conventional treatment to improve reverse osmosis performance.* Desalination, 2006. **190**(1-3): p. 147-160.
71. Shih, W.-Y., J. Gao, A. Rahardianto, J. Glater, Y. Cohen, and C.J. Gabelich, *Ranking of antiscalant performance for gypsum scale suppression in the presence of residual aluminum.* Desalination, 2006. **196**(1-3): p. 280-292.
72. Hua, G. and D.A. Reckhow, *Comparison of disinfection byproduct formation from chlorine and alternative disinfectants.* Water Research, 2007. **41**(8): p. 1667-1678.
73. Krasner, S.W., *The formation and control of emerging disinfection by-products of health concern.* Philosophical Transactions of the Royal Society a-Mathematical Physical and Engineering Sciences, 2009. **367**(1904): p. 4077-4095.
74. Wert, E.C., F.L. Rosario-Ortiz, D.D. Drury, and S.A. Snyder, *Formation of oxidation byproducts from ozonation of wastewater.* Water Research, 2007. **41**(7): p. 1481-1490.

Chapter 3

Recovery limit estimation and the feasibility of RO desalination in the San Joaquin Valley

3.1 Overview

The San Joaquin Valley (SJV) in central California (see **Fig. 3-1**) is one of the United States' most productive agricultural regions [1, 2]. Decades of irrigation and evapotranspiration combined with a shallow water table and naturally saline soil have led to the rise in groundwater salinity in the SJV. As the brackish water table intrudes into the root-zone increasing the soil salinity, many crops are adversely affected. When the salinity tolerances of the crops are exceeded the land is often retired, progressively diminishing the productivity of the SJV [3-6]. The rising groundwater salinity level in the SJV, now in the range of about 3,000–30,000 mg/L total dissolved solids (TDS), is a problem of major concern [5-7]. In order to reduce further buildup of salt in the soil, beginning in the late 1940s, surface and subsurface drains were installed throughout the valley to collect the brackish agricultural drainage (AD) water and then convey it to evaporation ponds or other discharge sites; by 1965 more than 1000 miles of drains had been built [4]. Construction of a master drain discharging to the Sacramento-San Joaquin River Delta was stopped in 1983 after the drainage from a preliminary portion of the drain that had been discharging into the Kesterson Reservoir was found to contain high levels of selenium [4, 6, 8]. It is noted that, where natural drainage does not exist, the use of evaporation ponds or other discharge sites for high salinity drainage water has become infeasible due to concern regarding bioaccumulation of selenium [4, 6, 8].

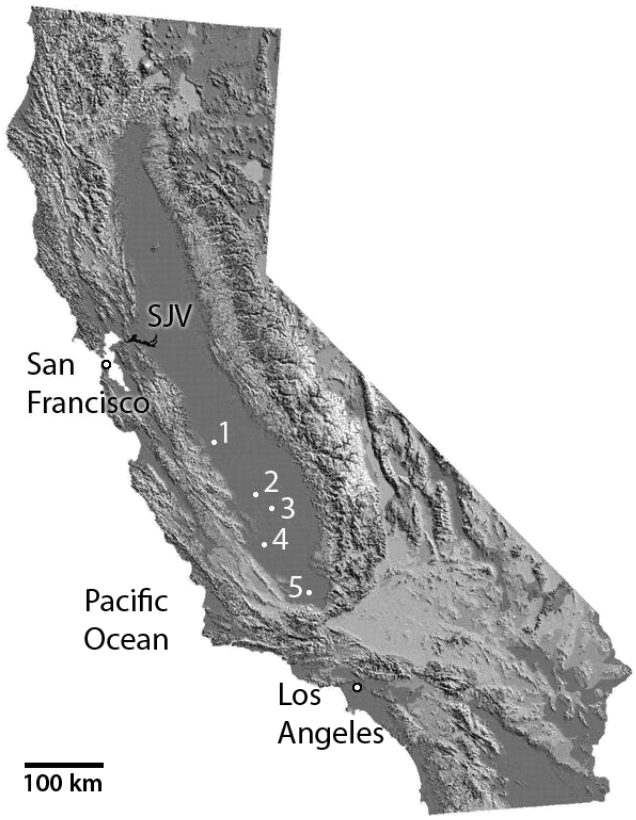

Figure 3-1. San Joaquin Valley (SJV) field water sampling locations: OAS (1), VGD (2), ERR (3), LNW (4), & CNR (5) [9].

In recent years there has been a renewed interest in the use of reverse osmosis (RO) and nanofiltration (NF) membrane desalination of SJV brackish groundwater as a potentially viable approach for reclamation of AD water for agricultural reuse and possibly potable water consumption [7], while also reducing the challenge of concentrate (brine) management. As the percentage recovery of permeate product of the RO process is increased the volume of brine discharge is decreased. However, the achievable RO recovery may be limited because SJV brackish water is often near or above saturation with respect to various sparingly water soluble mineral salts such as gypsum ($CaSO_4 \cdot 2H_2O$), calcium carbonate ($CaCO_3$), and silica (SiO_2). Upon RO desalting, the concentration of such salts on the feed-side and near the RO membrane surface can increase to levels exceeding their solubility limits which can then lead to surface

crystallization of these mineral salts and/or the deposition of their bulk-formed crystals onto the membrane surface. The resulting mineral surface scale leads to water permeate flux decline and potential damage to the membrane [10-15]. Consequently, the feasible recovery limit and process efficiency are reduced and water production costs increase. Given that the composition of SJV brackish water varies with location and time (e.g., with respect to salinity and the composition of sparingly soluble mineral salts) the mineral scaling propensity of such water is also location and time-dependent.

In order to assess the technical feasibility of RO desalination of SJV brackish water, there is a need to evaluate the product water recovery limits that are imposed by mineral salt scaling. Accordingly, in the present study, SJV AD water from a number of representative geographical locations was first characterized using available monitoring data for the 1999–2004 period with respect to composition, mineral salt saturation levels, and temporal variability. Based on RO process considerations, the upper limits on water recoveries were first estimated based on thermodynamic solubility analysis. Subsequently, laboratory bench-scale plate-and-frame RO (PFRO) mineral scaling tests were performed using water samples from five different representative locations to confirm the scaling propensity of SJV AD water and establish the expected range for the upper level of RO recoveries.

3.2 Analysis

Product water recovery limits governed by mineral salt scaling can be estimated given knowledge of the water feed chemistry in order to establish the threshold for mineral scaling. In brackish water desalination the maximum allowable pressure for the membrane modules (typically 4,140 kPa or 600 psi) may also dictate a practical limit on recovery that may be above

or below the limit dictated by mineral scaling. Increased product water recovery, *Y*, of an RO desalination process (defined as $Y = Q_P/Q_F$ where Q_P and Q_F are the permeate and feed flow rates, respectively) increases the average mixed-cup concentration of the retentate (or brine) stream, C_R, by a factor *CF* relative to the feed concentration, C_F (i.e., $CF = C_R/C_F$). This concentration factor is related to the recovery and salt rejection, R_S ($R_S = 1 - C_P/C_F$, where C_P is the permeate concentration) via a material balance:

$$CF = \frac{1 - Y(1 - R_S)}{1 - Y} \tag{3-1}$$

As recovery increases, the retentate concentration in the membrane channel can increase to levels such that sparingly soluble mineral salts can exceed their saturation concentrations (**Fig. 3-2**), and precipitate in the bulk or crystallize onto the membrane surface [16, 17], thereby resulting in membrane scaling, which reduces permeate flux and can also shorten the membrane life [18-20]. Mineral salt scalants that are of particular concern in brackish water desalination include gypsum ($CaSO_4 \cdot 2H_2O$), calcium carbonate ($CaCO_3$), and barite ($BaSO_4$) in addition to scaling by colloidal silica [18-21]. The recovery limits for a given feed water source can be estimated using **Eq. (3-1)** by establishing the *CF* at which the retentate concentrations reach the mineral salt scaling thresholds. The above approach provides an upper limit estimate of the feasible recovery since it does not consider the impact of concentration polarization [22].

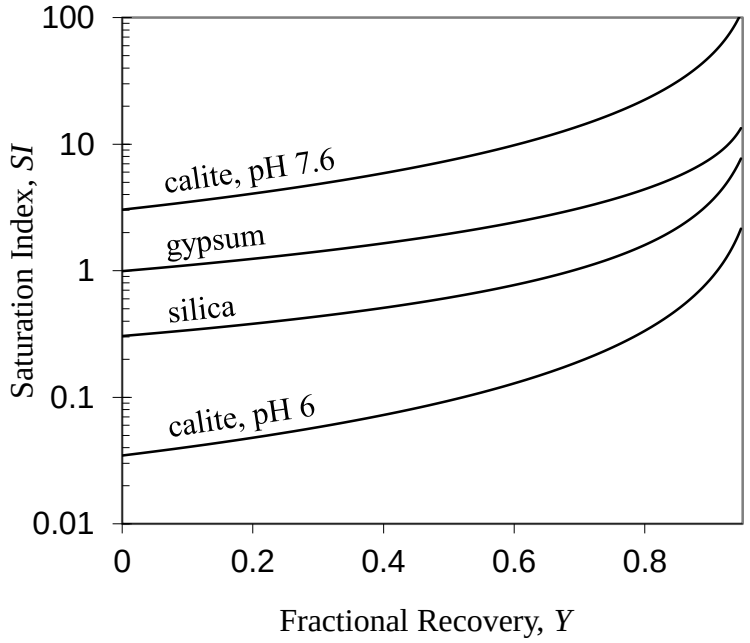

Figure 3-2. Saturation indices as a function of recovery for OAS water field water (11020 mg/L TDS, sampled on 4/10/2006, calculated based on 98% salt rejection)

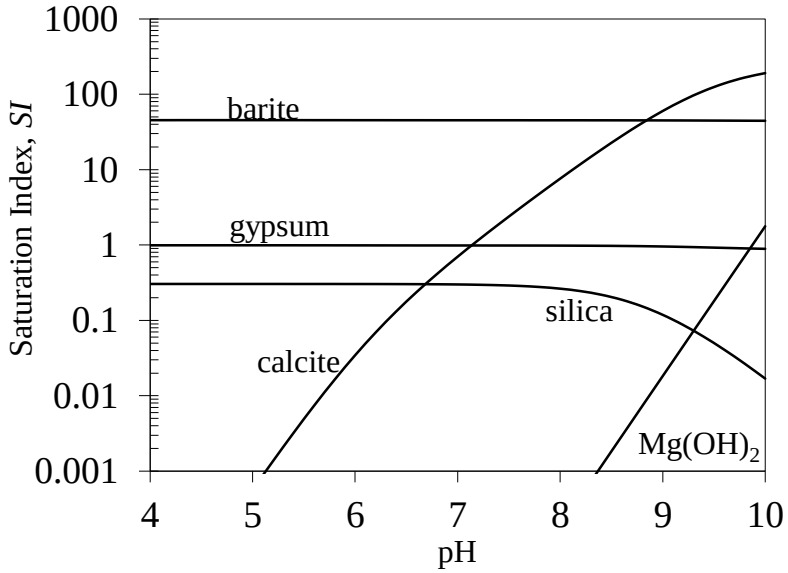

Figure 3-3. Saturation indices as a function of pH for OAS field water (11020 mg/L TDS, sampled on 4/10/2006)

Concentration polarization results in higher salt concentrations at the membrane surface relative to the bulk solution; thus, a lower recovery limit would result relative to the estimate from **Eq. (3-1)** which is based on the on a mixed-cup average retentate concentration. Membrane

manufacturers typically specify that the concentration polarization modulus, *CP* (=C_M/C_B, where C_M and C_B are the salt concentrations at the membrane surface and in the bulk of the membrane channel, respectively) in a given spiral-wound element be no greater than about 1.20 [23]. In order to estimate recovery limits while considering the additional impact of concentration polarization, one can define a concentration polarization modulus allowance [23, 24] at the exit region of the tail element as $C_M = \alpha C_R$, where α is a concentration polarization allowance factor.

In order to estimate RO permeate recovery, based on information from an overall salt mass balance or desalting tests in small plate-and-frame RO systems with negligible recovery, a simple approach is proposed to provide a reasonable estimate of the equivalent recovery expected in RO plants. Accordingly, when a *CF* threshold is established based, for example, on the maximum allowable mixed-cup retentate concentration (e.g., due to solubility or pressure constraints) one must correct the estimate from **Eq. (3-1)** to account for concentration polarization. Accordingly, *CF* can be adjusted by introducing a concentration polarization allowance factor ($\alpha = C_M / C_R$, where C_R is the mixed-cup retentate salt concentration) such that CF / α replaces *CF* in **Eq. (3-1)**.

The mineral scaling threshold dictates the maximum allowable recovery and is expressed in terms of the saturation index, SI_i, for the limiting mineral salt *i*, defined as

$$SI_i = \frac{IAP_i}{K_{SP,i}} \tag{3-2}$$

where IAP_i is the ion activity product of the constituent ions and $K_{SP,i}$ is the solubility product. The RO feed is often dosed with antiscalant (AS) additives to enable RO operation at or above saturation (i.e. $SI_i \geq 1$). Therefore, the scaling threshold is typically taken to be the *SI* above which membrane scaling is likely to occur even in the presence antiscalant. For example,

recommended scaling thresholds, with the appropriate antiscalant use, for gypsum, barite, and silica are SI_G = 2.3–4.0, SI_B = 60–80, and SI_S = 1.0–3.0 respectively [25]. The pH dependence of the saturation indices for calcite, gypsum, barite, and magnesium hydroxide are shown in (**Fig. 3-3**) for a representative water sample from a specific site (OAS, Table 3) in the SJV (**Fig. 3-1**). The saturation indices for gypsum and barite are pH insensitive while calcite and magnesium hydroxide saturation indices are highly dependent on pH. Therefore, the SI_C can be adjusted to desired levels by pH adjustment of the feed. Magnesium hydroxide, however, is well below saturation (SI < 0.001) over the expected range of operating pH for RO processes (pH 6–8) and therefore, it is not likely to impact the recovery limits. The saturation indices for barite are upper limits, given that barium concentrations for the above water source were reported at or below the detection limit (i.e., 0.25 mg/L). It is noted that although thermodynamic solubility analysis suggests that SI_C can be reduced by acid dosing, recent work [7] has shown that operating at reduced pH in waters of high gypsum scaling propensity but low in carbonate may be counterproductive; for such a water source, the rate of gypsum precipitation may increase due to the decreased bicarbonate concentration, thereby leading to a reduction in bicarbonate's tendency to retard gypsum precipitation.

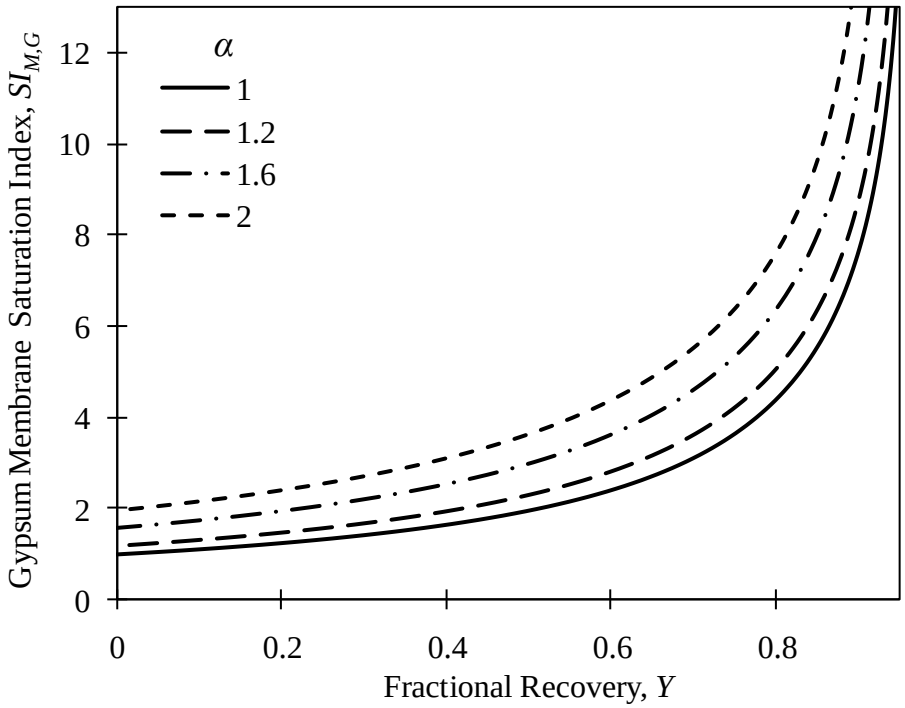

Figure 3-4. Gypsum saturation index at the membrane surface as a function of recovery for OAS field water (sampled on 4/10/2006) illustrating the effect of concentration polarization (i.e., increasing with α value)

Estimates of recovery from experimental studies with a traditional plate-and-frame RO (PFRO) system are also feasible to obtain, despite the typically low recovery in such units (≤ 1–2%), since a relatively high level of concentration polarization may be achieved even in such small systems [14, 15, 20, 26]. The equivalent recovery in a full-scale RO system can be estimated from PFRO data as the recovery at which a full-scale RO system would experience a concentration at the membrane surface at the exit region equivalent to the average membrane surface concentration in the PFRO system. The average surface concentration for the PFRO cell is calculated based on the average concentration polarization modulus, $\overline{CP}$, (defined as $\overline{CP} = \bar{C}_M / C_B$ where $\bar{C}_M$ is the average membrane concentration) using the numerical procedure developed specifically for the present RO cell geometry [22]. The equivalent recoveries are then calculated using Eq. (1), replacing *CF* with $\overline{CP}$, with α = 1.0 or 1.2 (i.e.,

without and with concentration polarization allowance to yield reasonable upper and lower limit recovery estimates, respectively, **Fig. 3-4**). In order to determine if mineral scaling should be expected at the operating conditions in the PFRO, the saturation indices at the membrane surface, $\overline{SI}_i$, for the mineral salts of concern may be calculated accounting for $\overline{CP}$ as below:

$$\overline{SI}_{M,i} = \frac{IAP_{M,i}}{K_{SP,i}} = \frac{\overline{CP}^{n}}{K_{SP,i}} \prod_{j} C_{B,j} \gamma_j \qquad (3\text{-}3)$$

where $IAP_{M,i}$ is the ion activity product at the membrane surface for mineral salt *i*, $C_{B,j}$ is the bulk concentration of mineral salt's constituent ion *j*, γ_j is the ion activity coefficient at the membrane surface, and *n* is the number of ions contained in mineral salt *i*. The above approach assumes that the level of concentration polarization is the same for all ions, a simplification that is reasonable for estimation purposes. Finally, it is noted that the saturation indices and osmotic pressures were calculated using a multi-electrolyte thermodynamic simulation software [27].

3.3 Experimental

3.3.1 Materials & Reagents

Stock solutions of hydrochloric acid (1.0 M) and sodium hydroxide (0.1 M) were prepared from concentrated hydrochloric acid (22^{o} Bé, technical, Fisher Scientific) and sodium hydroxide pellets (A.C.S. reagent, Sigma Aldrich), respectively, in DI water for pH adjustment of field water samples. The antiscalant PC-504 (Nalco Company, Naperville, IL) was used in some of the scaling tests at a low dose of 0.2 ppm to demonstrate the impact on scale inhibition. Agricultural drainage water field samples from five selected San Joaquin Valley locations were provided by the California Department of Water Resources (DWR) [28] and were refrigerated and maintained at 5ºC prior to use. Analyses of metals, anions, alkalinity, total organic carbon

(TOC), and silica were performed using methods published in Standard Methods for the Examination of Water and Wastewater [29] or using USEPA analytical methods for drinking water [30]. All water quality data were reconciled to ensure ion charge balance and pH consistency [27].

All RO desalting tests were carried out using the LFC-1 (Hydranautics, Oceanside, CA) brackish water RO membrane because of its low biofouling potential, high permeability, and high salt rejection [18]. This membrane has a reported permeability of $9.8 \pm 0.3 \times 10^{7}$ $m \cdot bar^{-1}s^{-1}$, a salt rejection of ~98% (based on electrical conductivity measurements for desalting of field water samples), and a root-mean-square (RMS) surface roughness of 67.4 nm [26, 31]. Membrane compaction/conditioning was accomplished using solutions of sodium sulfate (certified A.C.S anhydrous, Fisher Scientific, Pittsburgh, PA) in de-ionized water following previously established procedures [7, 20, 26].

3.3.2 PFRO System & Mineral Scaling Tests

The laboratory plate-and-frame RO (PFRO) membrane system consisted of two reverse osmosis cells arranged in parallel. Details of the system are described elsewhere [7, 20, 26] (see **App. B**). Briefly, each of the RO cells had an effective membrane surface area of 19.8 cm^2 (2.6 cm x 7.6 cm) with a channel height of 2.6 mm. The feed was pressurized by a ¾ hp positive displacement pump (Dayton Electric Mfg. Co., Niles, IL). A bypass valve allowed regulation of the feed flow rate to the reverse osmosis cells. Pressure in the cells was regulated by a backpressure valve in place following the recombination of the two parallel retentate streams. The feed reservoir was continuously stirred and temperature controlled (±0.5 °C) using a refrigerated recirculator (Fisher Scientific, Pittsburg, PA). All RO experiments were carried out

in a total recycle mode with the permeate and retentate flow rates monitored using a digital flow meter and a rotameter, respectively. The retentate from the PFRO cells was filtered using a 0.2 µm Nylon filter cartridge prior to being diverted to the feed tank. This was done as a precautionary measure in order to remove any mineral scale crystals that may have formed in the bulk (on the feed-side of the membrane) or dislodged from the membrane surface. Feed pH was measured with a pH electrode (Cole Parmer Instrument Company, Vernon Hill, IL) and conductivities (of the permeate and feed) were measured using a conductivity meter (model WD-35607-30, Oakton Research, Vernon Hills, IL). Optical images of the dried membranes were obtained using a high-resolution digital camera (Nikon model D100, Nikon Corp., Japan) with a 28–105 mm lens and a 4+ macro lens attachment, and high contrast imaging of the scaled surface was achieved using a low angle dark-field illuminator as described in previous work [26].

RO desalting tests with the field water sources (**Table 3-7**) were carried out at the natural field water pH and at acidic conditions (pH range ~5.3–6.5, $SI_C \leq 0.37$), both with and without a low dose of antiscalant (0.2 ppm). Prior to each RO test each field water sample was pre-filtered successively through a 5-µm gradient-density polypropylene filter cartridge and then a 0.2 µm pleated Nylon filter cartridge (Cole-Parmer Instrument Company, Vernon Hills, IL) to remove suspended particles. In order to reduce pH drift (during the experiments performed at a reduced pH) air was bubbled through the water feed reservoir during pH adjustment to reduce the time to reach equilibrium with respect to carbon dioxide. Membranes used in the PFRO cells were cut from a commercial stock membrane roll. The membrane coupons were rinsed with ~500 mL of DI water and then soaked in DI water for at least two hours prior to placement in the RO cells. Prior to each desalting run, the membrane coupons were placed in the RO cells and conditioned with a sodium sulfate solution having approximately the same osmotic pressure as the field water

solution. Membrane compaction was carried out at a retentate flow rate of about 4.5 L/min (average cross-flow velocity, $\bar{u}$, of 110 cm/s) for an hour and then for three hours at retentate and permeate flow rates necessary to produce the desired equivalent recovery in the subsequent RO desalting tests (see **Eq. (3-1)**). After membrane conditioning, each RO test was initiated to attain an average concentration polarization level $\overline{CP}$, in the range of 1.6–2.1 for each feed water source. The series of RO desalting tests for each given water source were carried out at the same initial flux and cross flow velocity in order to ensure flux decline comparisons at the same initial level of concentration polarization and, thus, the same initial saturation index with respect to gypsum (which was not influenced by pH adjustment). The initial average saturation indices for calcite, gypsum, and silica, at the membrane surface ($\overline{SI}_{M,C}$, $\overline{SI}_{M,G}$, $\overline{SI}_{M,S}$, respectively) were estimated based on the average concentration at the membrane surface (see **Eq. (3-3)**). The percent flux decline as a function of time, $FD_t = (1 - J_t/J_0)\cdot 100$ (where J_0 and J_t are the initial flux and the flux at time t, respectively) was determined for each RO desalting test in order to assess the impact of scaling and membrane compaction. The percent of the membrane covered by scale after the 24-hr test period, ϕ_{24}, was also determined based on image analysis of the scaled membranes. The experimental conditions are provided in **Table 3-7**.

3.3.3. Water Quality Data

Two data sets were utilized to assess brackish water quality at different locations in the SJV: (a) California Department of Water Resources (DWR) monitoring data from 1999–2004 from which four representative sites were identified [28, 32], and (b) field water sampling data collected during 2006–2007 from five sites (four were the same sites identified in (a)) specifically for the present study (**Fig. 3-1**) (see **App. A**). The DWR monitoring data were

reviewed to evaluate temporal and geographic variability of water quality and the implications for RO recovery limits, specifically for the latest 12-month period for the representative sites identified from the DWR drainage monitoring data. These four sites were selected as being representative of the diversity of water compositions with respect to salinity (i.e. TDS), gypsum saturation index, and calcite saturation index. However, because the monitoring database [4] lacked information on the concentrations of bicarbonate, carbonate, hydroxides, and silica, and given the temporal variability of water quality, experimental RO desalting tests were carried out for field samples collected in the SJV during the testing period (2006–2007).

3.4 Results and Discussion

3.4.1 Water Quality Variability

Brackish groundwater monitoring data for four representative monitoring sites in the SJV were analyzed with respect temporal and spatial variations in water quality and to assess the potential range of RO recovery limits. These sites designated by DWR as CNR 0801, LNW 6467, OAS 2548, and VGD 4406, hereafter referred to as CNR, LNW, OAS and VGD, respectively, are shown in **Fig. 3-1** (see **Appendix A**). Thermodynamic solubility analysis was performed for the latest 12-month period of the 1999–2004 data and for the 2006–2007 field samples which included, in addition to the above sites, a water source sample from site ERR 8429 [4], referred to as ERR (**Fig. 3-1**).

AD water quality for the 1999-2004 period exhibited significant spatial variability among the monitoring sites (**Table 3-1**). Analysis of the latest 12-month period of data (for each site) revealed that average salinity from the selected sites ranged from 6,987 to 23,480 mg/L TDS for the CNR and VGD sites, respectively, with corresponding average osmotic pressures ranging

from 315–1,000 kPa (45.7–145 psi). All water sources were oversaturated with respect to calcite with the average SI_C ranging from 2.3 to 5.3 (**Table 3-1**) and near saturation with respect to gypsum with the average SI_G in the range of 0.75–0.99 (OAS and LNW sites, respectively). The above spatial variations are significant in both osmotic pressure and saturation indices suggesting that RO operating conditions (which will impact the cost of water desalination) must be tailored for each specific location within the SJV.

Table 3-1. Summary of average water quality and saturation indices for the most recent 12-month period of available data from the DWR database (2003–2004)

Name	**Location**	**TDS, mg/L**	**pH**	**π_0†, kPa**	**SI_C†**	**SI_G†**
OAS	Central Area	7,999	7.7	408	3.9	0.75
LNW	Southern Area, Lost Hills	11,944	7.5	834	2.3	0.99
CNR	Southern Area, Kern Lake Bed	6,987	7.7	315	5.1	0.76
VGD	Southern Area, Lemoore	23,480	7.9	1000	5.3	0.84

† π_0, SI_C, and SI_G were calculated at 20 °C.

Table 3-2. Variability of water quality measurements and saturation indices for the OAS location

Date	7/14/2003	9/9/2003	11/12/2003	1/12/2004	3/22/2004	5/10/2004	Average
TDS, mg/L	5,864	3,828	9,344	11,100	9,576	8,284	7,999
$[Ca^{2+}]$, mg/L	283	224	385	430	454	358	356
$[SO_4^{2-}]$, mg/L	3,990	2,340	5,550	6,460	5,630	4,890	4,810
Total Alkalinity, mg/L as $CaCO_3$	271	239	160	173	146	217	201
pH	7.6	7.1	7.9	7.9	7.9	7.9	7.7
π_0†, kPa	371	231	466	534	443	407	409
SI_C†	3.2	0.86	4.3	4.7	4.5	5.8	3.9
SI_G†	0.57	0.41	0.83	0.93	0.98	0.76	0.75

† π_0, SI_C, and SI_G were calculated at 20 °C.

Table 3-3. Summary of water quality and saturation indices for the collected field water samples (2006–2007) †

Name	Location	Sample Date	TDS, mg/L	pH	π_0†, kPa	SI_C†	SI_G†	SI_S†
OAS	Central Area	4/10/2006	11020	7.6	515	3.0	0.99	0.29
LNW	Southern Area, Lost Hills	2/15/2006	11270	7.6	723	2.7	1.03	0.35
CNR	Southern Area, Kern Lakebed	7/31/2006	6372	7.5	286	2.7	0.70	0.22
VGD	Southern Area, Lemoore	11/13/2006	28780	7.6	1320	2.2	0.95	0.38
ERR	Southern Area, Corcoran	1/29/2007	4115	8.0	265	9.5	0.12	0.34

† π_0, SI_C, and SI_G were calculated at 20 °C.

Water quality also varies temporally as illustrated in **Fig. 3-5** where the percent deviation from the 12-month average values is shown for the selected field. As an example, detailed water quality data for one of the sites, OAS, for the latest 12-month period of available data (from the DWR monitoring database), is provided in **Table 3-2**. Water salinity exhibited maximum absolute deviations from the 12-month averages ranging from 12% to 52% for LNW and OAS, respectively, and the maximum osmotic pressure deviations were in the range of 10%–44%. Both calcite and gypsum saturation indices varied substantially over the 12 month periods for the selected sites. The maximum absolute deviation of SI_C relative to the average ranged from 54% to 92% for VGD and CNR, respectively, while the maximum absolute deviation of SI_G from the 12-month average was in the range of 3.3%–45% for CNR and OAS, respectively. SI_C variations were primarily due to pH fluctuations, while SI_G variations were primarily due to fluctuations in calcium and sulfate ion concentrations. These large temporal variations in water quality (e.g., salinity and saturation indices) would prove challenging to traditional RO plants that are typically designed to process water of a relatively narrow range of salinity and mineral scaling propensity. As water quality changes, the osmotic pressure and saturation indices vary and will affect the energy consumption (proportional to the feed osmotic pressure and desired recovery), required chemical doses, and scaling recovery limits. Analysis of the 2006–2007 sampling data

revealed that the water quality of the more recent samples was largely within the ranges established for the earlier DWR database (**Table 3-3**, **Fig. 3-5**). Detailed water quality analysis for each of the five locations in the SJV is provided in **Table 3-4** (see **Appendix A**).

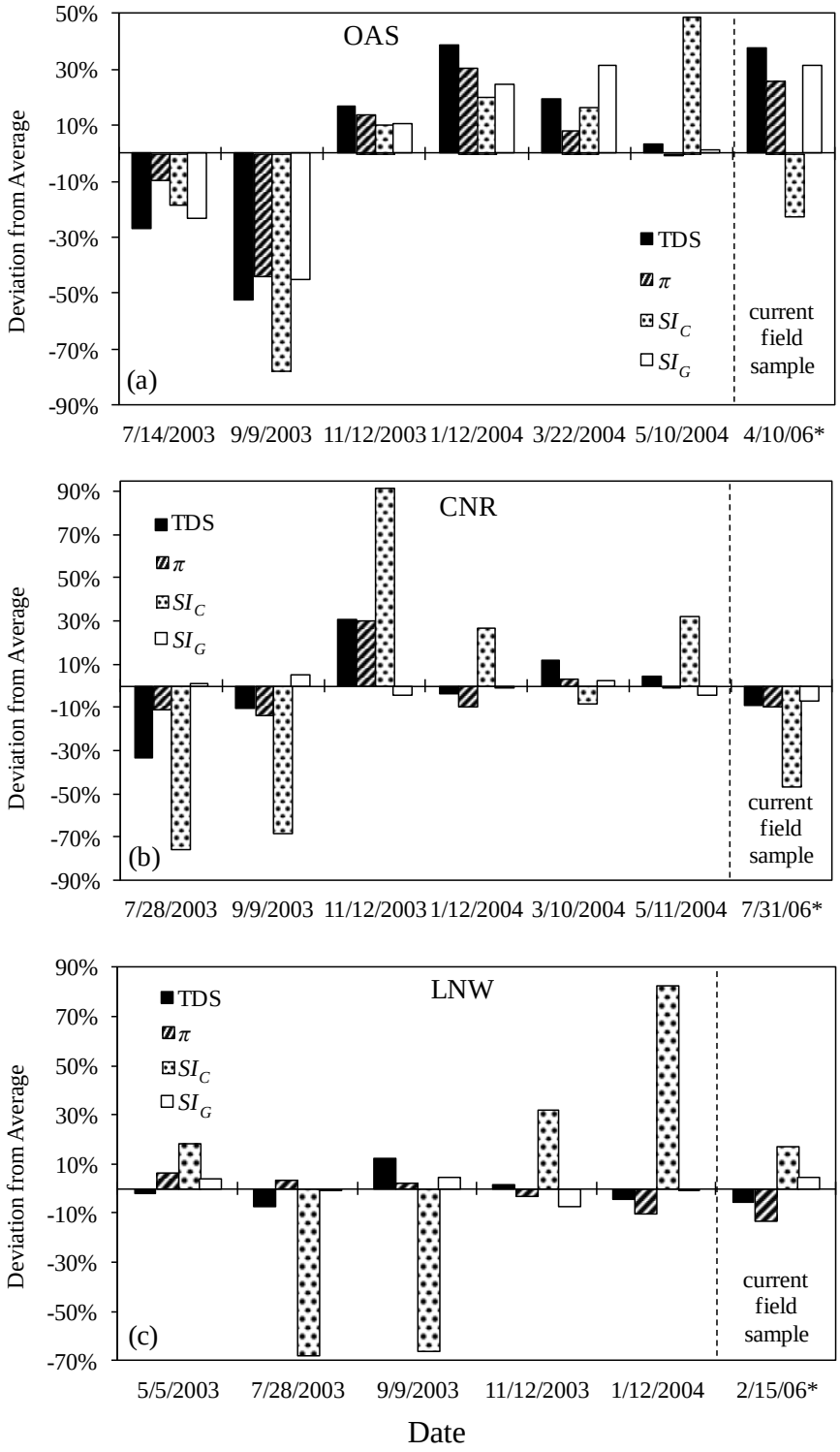

Figure 3-5. Illustration of water quality variations for the 2003–2004 period in the DWR database [4] and for the 2006 field samples: (a) at the OAS site, (b) at the CNR site, and (c) at the LNW site

Table 3-4. Detailed water quality analyses for five location in the SJV sampled during 2006–2007

Measurement	Units	Location				
		OAS	LNW	CNR	VGD	ERR
Conductance	µS/cm	12620	14430	7111	26070	5580
pH	pH units	7.6	7.6	7.5	7.6	8
UV Absorbance (254 nm)	absorbance/cm	0.13	0.09	0.13	0.18	0.59
Dissolved Analytes						
Bicarbonate	mg/L as $CaCO_3$	212	128	229	367	699
Boron	mg/L	23.5	17.5	13.5	43.4	2.6
Calcium	mg/L	462	625	350	422	88
Carbonate	mg/L as $CaCO_3$	1 [a]	1 [a]	1 [a]	1 [a]	7
Chloride	mg/L	1060	3020	324	1910	632
Fluoride	mg/L	10 [a]	10 [a]	5 [a]	5 [a]	5 [a]
Hydroxide	mg/L as $CaCO_3$	1 [a]	1 [a]	1 [a]	1 [a]	1 [a]
Magnesium	mg/L	284	198	236	962	59
Nitrate	mg/L	47	155	344	52	51
DOC	mg/L as C	5.1	4.6	4.2	6.2	15.8
Potassium	mg/L	5 [a]	5 [a]	46.7	7.8	3.5
Selenium	mg/L	0.18	0.22	0.03	0.05 [a]	0.01
Silica	mg/L	31	38	24	43	38
Sodium	mg/L	2780	2820	1250	9270	1250
Sulfate	mg/L	6360	4520	3700	21400	1570
Total Analytes						
Total Alkalinity	mg/L as $CaCO_3$	213	128	230	368	706
Aluminum	mg/L	0.05 [a]	0.1 [a]	0.1 [a]	0.5 [a]	0.102
Arsenic	mg/L	0.006	0.014	0.01 [a]	0.05 [a]	0.089
Barium	mg/L	0.25 [a]	0.5 [a]	0.5 [a]	2.5 [a]	0.5 [a]
TDS	mg/L	11020	11270	6372	28780	4115
Iron	mg/L	0.05	0.15	0.17	1.4	0.28
Manganese	mg/L	0.025 [a]	0.05 [a]	0.05 [a]	1.55	0.60
TOC	mg/L as C	5.1	3.4	4.5	6.2	16.7
Phosphorus	mg/L	0.08	0.03	0.01 [a]	0.12	1.96
Selenium	mg/L	0.195	0.235	0.034	0.05 [a]	0.013
Strontium	mg/L	5.5	10.0	17.2	9.6	0.9
TSS	mg/L	4	4	1 [a]	2	4

[a] Measured value is at or below reporting limit.

3.4.2 Recovery Limits for the 1999–2004 and 2006–2007 Monitoring Data

RO recovery limits based on the highest and lowest reported salinity for each field location (**Fig. 3-1**) over the latest 12-month period for the DWR 1999–2004 monitoring data set are summarized in **Table 3-5**. The recovery limits based on scaling thresholds for gypsum were computed for SI_G =1 (without AS use) and SI_G = 2.3 (with AS use) and for calcite at SI_C = 1.0 (assumed to be achievable via pH adjustment). Recovery limits were calculated at both the field water pH = 7.5 and at a reduced pH = 6.0 to illustrate the effect of pH adjustment. At the natural

pH, calcite is the limiting mineral scalant. However, at pH = 6.0 gypsum becomes the limiting scalant with desalting being either infeasible (e.g., LNW feed $SI_G \approx 1$) or limited to low recoveries (**Table 3-5**) with the highest recovery being 44%–53% (for α = 1.2 and 1, respectively, **§3.2**) for OAS. When the gypsum scaling threshold is set at the level allowable with antiscalant treatment (i.e., SI_G = 2.3), the recovery limits increase to the range of 43%–76% or 53%–80% with and without allowance for concentration polarization, respectively. It is noted that the osmotic pressures at the scaling recovery limits for each of the sites are well below 4140 kPa (600 psi), the typical pressure limit for brackish water RO modules. The above analysis indicates that variability in water quality (temporally and geographically) would require site-specific plant design, in addition to effective feed-back process control to handle variability in feed water quality.

Table 3-5. Recovery limits for water samples having the maximum and minimum TDS observed during the most recent 12-month period of reported data.

Site	Sample Date	TDS, mg/L	Recovery Limits				
			Pressure	calcite (pH 7.5)	calcite (pH 6.0)	gypsum (pH 6.0)	gypsum (pH 6.0)
			π = 60800 kPa	SI = 1	SI = 1	SI = 1	SI = 2.3
OAS	1/12/2004	11100	86–88%	0* %	92–93%	0* %	47–56%
OAS	9/9/2003	3828	94–95%	0* %	88–90%	44–53%	76–80%
LNW	9/9/2003	13400	76–80%	0* %	84–86%	0* %	43–53%
LNW	7/28/2003	11030	75–80%	0* %	85–87%	0*–0.002%	46–55%
CNR	11/12/2003	9136	90–91%	0* %	83–86%	8.6–24%	62–68%
CNR	7/28/2003	4660	93–94%	0* %	86–88%	3.7–19%	57–64%
VGD	1/13/2004	29760	68–73%	0* %	89–91%	0*–7.6%	61–68%
VGD	7/29/2003	14110	77–80%	0* %	90–92%	3.6–18%	65–71%

Note: The given ranges indicate the minimum and maximum expected recoveries (i.e. for α=1.2 or 1.0, respectively). (*) indicates that the feed is oversaturated at the membrane surface.

Table 3-6. Recovery limits estimated based on water quality analysis of field water samples

Site	TDS, mg/L	Nat pH	Recovery Limits: Pressure (nat. pH)	calcite (nat. pH)	calcite (pH 6)	gypsum (pH 6)	gypsum (pH 6)	silica (pH 6)
			π = 60800 kPa	SI_c = 1	SI_c = 1	SI_g = 1	SI_g = 2.3	SI_s = 1
OAS	11,020	7.6	87–89%	0* %	89–91%	0*–0.7%	49–58%	63–69%
LNW	11,270	7.6	80–83%	0* %	88–90%	oversat.	44–54%	54–62%
CNR	6,372	7.5	93–94%	0* %	89–91%	13–27%	62–68%	72–77%
VGD	28,780	7.6	64–70%	0* %	89–91%	0*–6.2%	60–67%	46–55%
ERR	4,116	8.0	93–94%	0* %	86–88%	82–85%	93–94%	56–63%

Note: The given ranges indicate the minimum and maximum expected recoveries (i.e. for α=1.2 or 1.0, respectively). (*) indicates that the feed is oversaturated at the membrane surface.

In order to further assess the impact of changes in water quality on RO recovery limits, the five locations in the SJV (**Fig. 3-1**) were sampled over the 2006–2007 season with the water quality data provided in **Table 3-4**. Recovery limits were estimated based on gypsum scaling thresholds of SI_G = 1 (without AS use) and SI_G = 2.3 (with AS use), silica scaling threshold of SI_S = 1, and calcite scaling threshold of SI_C = 1.0. Product water recoveries were calculated at both the natural source water pH, which ranged from 7.5 to 8.0 among the five selected sites, and at an acidic pH of 6.0. Each of the brackish water sites was oversaturated with respect to calcite at the natural field water pH (**Table 3-6**) implying that feed acidification would be required to lower the saturation index with respect to calcite. However, even if calcite scaling were inhibited, gypsum would remain the limiting scalant with estimated lower and upper recovery ranges of 44%–62% and 54%–68% with and without CP allowance (**§3.2**), respectively, except for the ERR site for which silica was the limiting scalant (**Table 3-6**) even with gypsum scale mitigation with antiscalants (allowing operation up to ~ SI_G=2.3). Estimated product water recovery limits due to gypsum scaling range from being infeasible for LNW (SI_G = 1.03; **Table 3-3**) to as high as 63% for ERR. However, even at the higher gypsum scaling threshold (SI_G = 2.3 with AS treatment) gypsum remained the limiting scalant for CNR, OAS, and LNW, while silica was the limiting scalant for both the ERR and VGD samples. The overall recovery limits when considering both gypsum and silica scaling are between 46% and 77% and are consistent

with the estimated recovery limits determined using on the 1999–2004 DWR monitoring data. It should be noted that in all cases (**Table 3-6**), if the operating pressure is limited by the typical rating of the brackish water RO vessels (4,140 kPa or 600 psi), the recovery limit would be higher than that which would be imposed by mineral scaling. Water quality data obtained over the 2006–2007 period of the current study confirmed that geographic variability of brackish water quality in the SJV is significant as was determined for the 1999–2004 data set with recovery limits (53–80%) imposed by gypsum and silica scaling.

3.4.3 Experimental RO Desalting Tests

In order to confirm the estimated range of water recovery feasible for the SJV (**§3.2**), RO desalting tests were performed with field water samples (**Table 3-3**) at the natural source water pH, and at a reduced pH with and without a low dosage of antiscalant over the range of operating conditions indicated in **Table 3-7**. These tests targeted equivalent recoveries in the range of about 38%–53% for which the average saturation index for gypsum at the membrane surface was in the range of 1.4–2.1. Desalting tests at the reduced pH along with AS dosing of the feed revealed a flux decline of 7%–9% after 24 hours (FD_{24}) and no observed mineral scaling (**Table 3-7**) despite the level of supersaturation of the solution at the membrane surface (e.g., up to $\overline{SI}_{M,G}$ = 2.1 for ERR, CNR and OAS). Previous work with the LFC1 membrane has shown that typically up to about 5–7% flux decline could be the result of membrane compaction [26]. Therefore, it is likely that a major contribution to flux decline for the above desalting tests (and other tests for which no scaling was visually observed; **Table 3-7**) was from compaction with possibly low levels of colloidal or organic fouling (7–9%). In contrast, significant flux decline (>10%; **Table 3-7**, **Fig. 3-6**) and membrane scaling were observed (**Figs. 3-7** & **3-8**) for the tests

performed without AS feed treatment when $\overline{SI}_{M,G} \geq 1.9$ at the natural source water pH (for which $\overline{SI}_{M,C} \geq 4.2$) or when $\overline{SI}_{M,G} \geq 1.5$ at the reduced pH (for which $\overline{SI}_{M,C} \leq 0.37$). The greater extent of scaling and flux decline at the lower $\overline{SI}_{M,G}$ (< 2), observed at the reduced pH, is consistent with recent work on a similar water source [7]. It was shown in previous work [7] that the above behavior is associated with the reduction of the bicarbonate concentration (by at least an order of magnitude for the pH range of ~7.5–6.5 in the present study), thereby reducing the ability of bicarbonate to inhibit gypsum scaling.

Table 3-7. Diagnostic flux decline experimental conditions and 24-hour flux decline

Site	Condition	pH	P, kPa	u, cm/s	$J_0 \cdot 10^3$, cm/s	$SI_{M,C}$	$SI_{M,G}$	$SI_{M,S}$	FD_{24}	ϕ_{24}	Y_{eqv} α=1.2–1
OAS	Nat. pH	7.42	2500	19.1	2.45	5.4	2.1	0.61	11 %	12%	43–53%
OAS	Low pH	5.47	2580	19.1	2.45	0.014	2.1	0.66	47 %	65%	43–53%
OAS	Low pH & AS	5.94	2410	19.1	2.44	0.86	2.1	0.66	7.9 %	0%	44–53%
CNR	Nat. pH	7.50	1920	19.1	2.44	7.4	1.53	0.46	6.4 %	2.5%	44–53%
CNR	Low pH	5.27	1860	19.1	2.44	0.01	1.55	0.49	11 %	3.8%	44–53%
CNR	Low pH & AS	6.00	2010	19.1	2.44	0.11	1.55	0.49	6.7 %	0%	44–53%
ERR	Nat. pH	8.02	2080	19.1	2.446	29	0.28	0.68	12 %	0%	44–53%
ERR	Low pH	5.37	2110	19.1	2.44	0.01	0.31	0.79	12 %	0%	44–53%
ERR	Low pH & AS	6.00	1900	19.1	2.44	0.13	0.30	0.79	7.5 %	0%	44–53%
LNW	Nat. pH	7.43	1930	25.1	1.91	4.2	1.9	0.64	11 %	5.7%	34–45%
LNW	Low pH	6.48	1950	25.1	1.89	0.37	1.9	0.68	14 %	7.6%	34–45%
VGD	Nat. pH	7.53	3120	19.1	1.36	3.2	1.4	0.61	8.0 %	1.8%	26–38%
VGD	Low pH	5.56	2980	19.1	1.35	0.01	1.4	0.71	8.9 %	0.5%	25–38%
VGD	Low pH+AS	5.93	3140	19.1	1.36	0.05	1.4	0.72	9.4 %	0%	26–38%

Note: $SI_{M,C}$, $SI_{M,G}$, and $SI_{M,S}$ are the initial average saturation indices for calcite, gypsum and silica at the membrane surface; u is the cross-flow velocity of the feed; P is the applied pressure; Y_{eqv} is the equivalent recovery in for an RO plant with the given ranges indicating the minimum and maximum expected recoveries (i.e. for α=1.2 or 1.0, respectively; see Eq. 1).

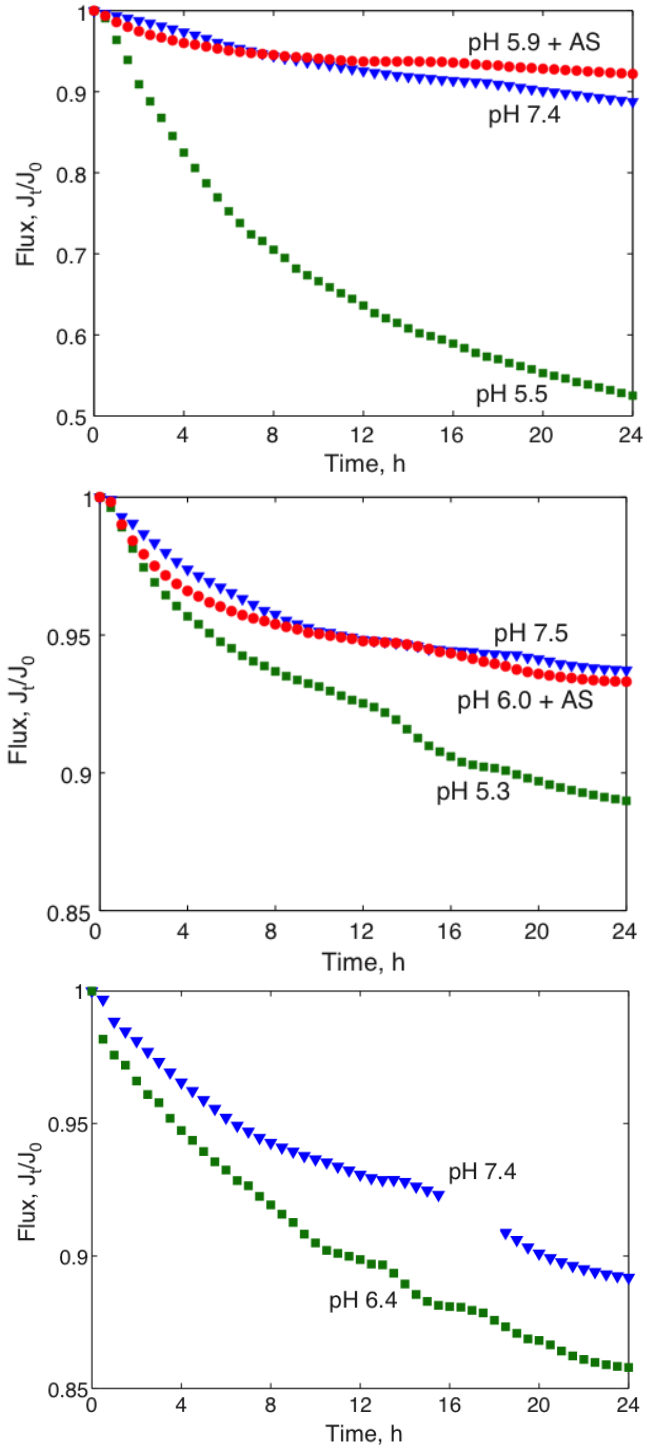

Figure 3-6. Normalized permeate flux (ratio of the flux at time *t*, J_t, to the initial flux, J_0, respectively) for 24-hr scaling tests at the natural pH of the field water and at an acidic pH for: (a) OAS, (b) CNR, and (c) LNW; and at an acidic pH with AS addition (0.2 ppm PC-504) for (a) OAS, and (b) CNR

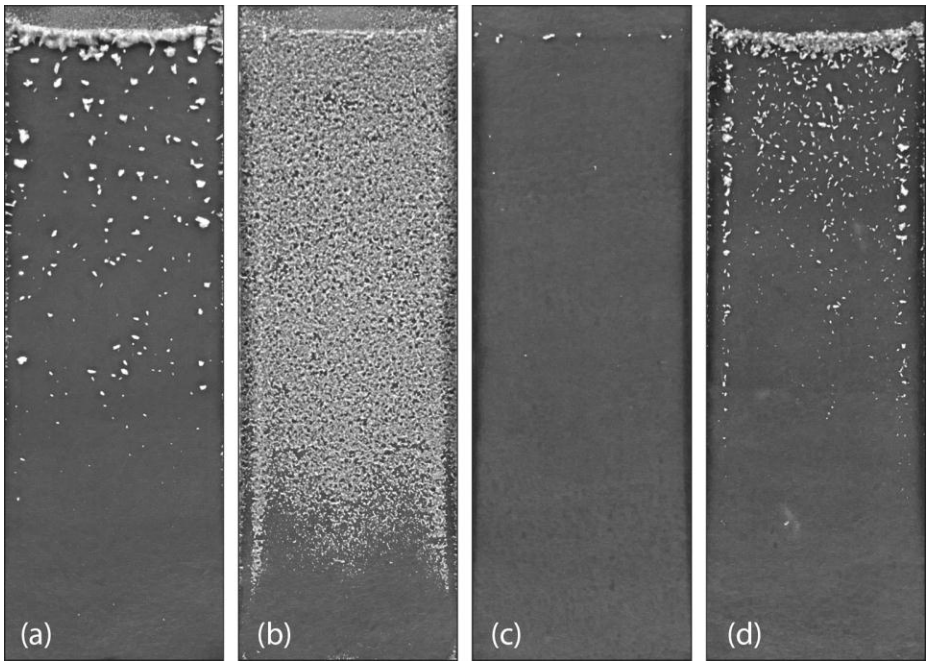

Figure 3-7. Examples of membrane coupons images after 24-hour scaling tests on field water samples from: (a) OAS at the natural pH=7.42, (b) OAS at an acidic pH=5.47, (c) LNW at the natural pH=7.43, and (d) LNW at an acidic pH=6.48.

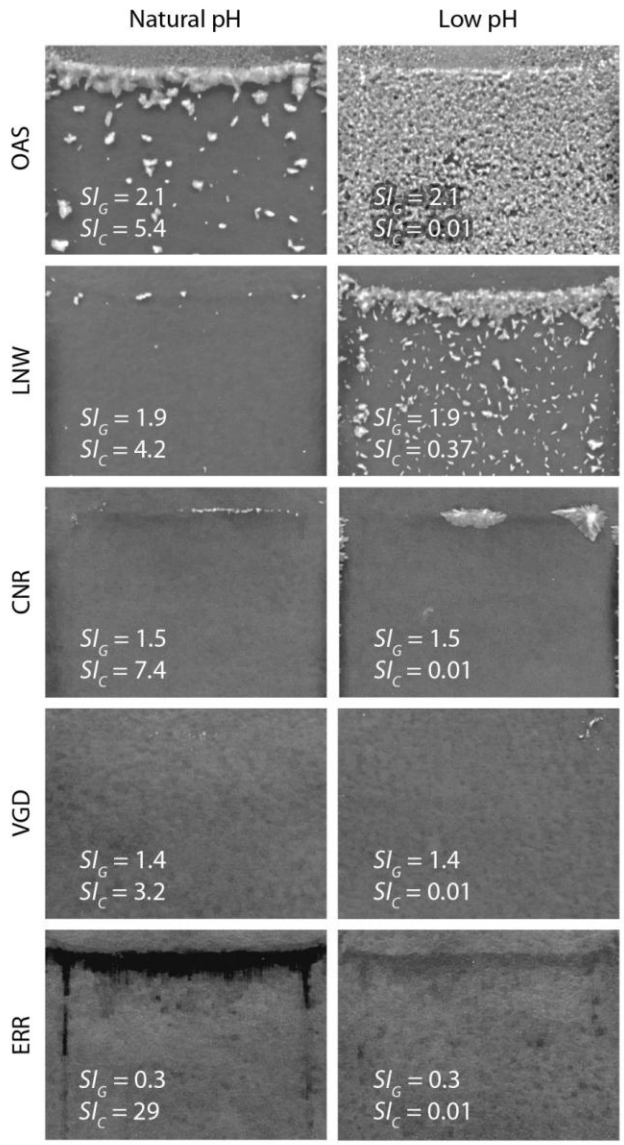

Figure 3-8. Images of the membrane coupon exit regions after 24-hr scaling tests (see Table 7).

For the RO tests performed for the three field source water samples having $SI_G \approx 1.0$ (VGD, LNW, and OAS) the percent flux decline and surface scale coverage (**Table 3-7**, **Figs. 3-7** & **3-8**) increased with increasing level of solution saturation at the membrane surface (or equivalent recovery, **Table 3-7**). Scale formation is more severe toward the downstream (or exit) region of the membrane channel (**Fig. 3-8**), which is consistent with the increasing concentration along the membrane channel [22]. Comparison of the severity of mineral scaling in the RO

channel exit region (**Fig. 3-8**) was consistent with the degree of flux decline (**Table 3-7**). The results for the ERR water source were anomalous, having a significant flux decline (12% after 24 hr) without visible surface scaling. However, the ERR test resulted in a darkened membrane surface, suggesting the possibility of organic fouling. The ERR water source also had the highest TOC (total organic carbon) of the five selected sites (3–6 mg/L, **Table 3-4**) and thus the highest organic fouling potential. The PFRO desalting tests demonstrated that, for SJV water sources evaluated in the present study, RO operation at the natural alkaline pH of the source water (where the solution is oversaturated with respect to calcite) would be preferable to operating at lower acidic pH (i.e., conditions of undersaturation with respect to calcite). Although one could operate at acidic pH, this would require higher antiscalant dosing (and thus higher desalination cost) to suppress gypsum scaling.

It should be recognized that even though the recovery level in the PFRO system is small (< 2%), the equivalent recovery in an actual RO plant can be estimated by assuming that the same level of concentration polarization level in the PFRO cell can be sustained in a full-scale RO plant (for the tail-end elements). Accordingly, **Eq. (3-1)** can be used to estimate the equivalent recovery whereby *CF* is replaced by CP/α with $\alpha = 1.2$; when α is set to unity the assumption is that the plant operates such that the salt concentration is uniform across the membrane channel (a condition that would exist when the plant operates up to the thermodynamic limit [33]. The estimated equivalent recoveries (assuming $\alpha = 1$) were 38% and 45% for sites VGD and LNW, respectively, and 53% for sites ERR, CNR and OAS. Scale-free operation would be feasible without antiscalant use when operating at the natural source water pH for the CNR, VGD, and ERR sites at the above equivalent recoveries. Given that the LNW water source had a salinity (11,270 mg/L TDS) almost equal to that of the OAS water (11,020

mg/L TDS), a series of RO tests were performed with the LNW water at a slightly lower equivalent recovery (45%) for which a significant decrease in scaling was observed at both at the natural source water pH and at pH ~6.5. In addition, from a practical viewpoint, it is apparent that for the VGD water source (salinity of 28,780 mg/L TDS) achieving recovery approaching 70% would require an applied pressure approaching or exceeding the rated pressure for the brackish RO elements (~ 4140 kPa or 600 psi).

The PFRO tests indicated that a low level of antiscalant dosing should make it possible to achieve scale-free desalting operation at the indicated recovery levels (**Table 3-7)** for the five water sources at either the natural source water pH or at an acidic pH. One is cautioned, however, that within the context of the present rapid PFRO diagnostic approach, acceptable operating conditions for full-scale plant operation should be established based on a criterion of no-flux decline (after accounting for the effect of membrane compaction) and verification of the absence of mineral scaling on the membrane surface. It is noted that the expected recovery levels for the five tested water sources are relatively low for inland water desalting. In order to minimize the brine management challenge and decrease overall water desalination cost, a higher recovery level operation would be required. Indeed, recent studies indicate that higher recovery operation is feasible [11, 14, 34, 35]. In such a process, it is suggested that high recovery can be achieved by chemical demineralization of the primary RO (PRO) in an interstage crystallizer to reduce the concentration of mineral scale precursors, followed by filtration and subsequent desalting of the treated PRO in a secondary RO stage to increase the overall recovery.

3.5 Conclusions and Recommendations

The recovery limits of RO desalting of brackish agricultural drainage water in the San Joaquin Valley were evaluated based on field water quality monitoring data from various locations in the SJV, in addition to laboratory RO tests using field water samples. Analysis of DWR monitoring data revealed salinity in the different locations being in the range of 7,000–23,000 mg/L TDS, with significant salinity variations of 12–52% relative to the 12-month averages. SJV brackish water was found to have a high mineral scaling propensity with the saturation indices for gypsum and calcite reaching levels as high as 0.99 and 5.3, respectively, with corresponding 12-month variations in the ranges of 5%–45% and 54%–92% (relative to the 12-month average for the different locations studied).

Analysis of the RO recovery limits, based on historical water quality data (for five representative geographical locations) and experimental RO scaling tests with field data suggested expected RO product water recovery range of 44–68% across the SJV. Thermodynamic solubility analysis suggested lowering the feed pH would reduce calcite supersaturation. In contrast, laboratory RO desalting tests in a diagnostic PFRO cell indicated that operation at the natural source water pH (~7.5–8) was preferable since it resulted in lower degree of membrane mineral scaling. The above behavior was consistent with previous work [7] with the above water sources that demonstrated antagonistic calcite and gypsum crystallization kinetics resulting in reduced mineral scaling at alkaline pH.

Implementation of RO technology for desalination of SJV AD water would require site-specific RO process optimization because of the geographical variability in water quality. Field evaluation of RO desalting with advanced mobile RO pilot plants [36] can provide the means for rapid optimization of RO operating conditions. Future developments of RO technology for

operation, under conditions of significant temporal variability of brackish water quality and desalting near the mineral scaling threshold (i.e., near the maximum allowable recovery in order to minimize brine generation), would require effective real-time methods of mineral scale detection [15, 37] and a plant operation that can be adjusted to mitigate mineral scaling (e.g., adjusting recovery and/or antiscalant dose or initiating membrane cleaning).

References

1. *California Agricultural Resource Directory 2006*. 2006, USDA, National Agricultural Statistics Service, California Department of Food and Agriculture.
2. *Assessing the Region Via Indicators: The Economy*, in *The State of the Great Central Valley of California*

2005, Great Valley Center: Modesto.

3. *Evaluation of the 1990 Drainage Management Plan for the Westside San Joaquin Valley, California*. 2000, San Jaoquin Valley Drainage Implementation Program and University of California Ad Hoc Coordination Committee.
4. Gabelich, C., et al., *Pilot-scale testing of reverse osmosis using conventional treatment and microfiltration.* Desalination, 2003. **154**(3): p. 207-223.
5. *Desalination Demonstration Report for Buena Vista Water Storage District.* 2003.
6. Clinton Williams, M.A., *Agricultural Drainage in the San Joaquin Valley: A Gap Analysis*. 2002, San Joaquin Valley Drainage Implementation Program.
7. Rahardianto, A., B.C. McCool, and Y. Cohen, *Reverse osmosis desalting of inland brackish water of high gypsum scaling propensity: Kinetics and mitigation of membrane mineral scaling.* Environmental Science & Technology, 2008. **42**(12): p. 4292-4297.
8. Gao, S., et al., *Chemical status of selenium in evaporation basins for disposal of agricultural drainage.* Chemosphere, 2007. **69**(4): p. 585-594.
9. *San Joaquin Valley Drainage Monitoring Program 2000*. 2003, State of California, Department of Water Resources.
10. Boerlage, S.F.E., et al., *The scaling potential of barium sulphate in reverse osmosis systems.* Journal of Membrane Science, 2002. **197**(1-2): p. 251-268.
11. Gabelich, C.J., et al., *High-recovery reverse osmosis desalination using intermediate chemical demineralization.* Journal of Membrane Science, 2007. **301**(1-2): p. 131-141.
12. Hasson, D., A. Drak, and R. Semiat, *Inception of CaSO4 scaling on RO membranes at various water recovery levels.* Desalination, 2001. **139**(1-3): p. 73-81.
13. McCool, B.C., A. Rahardianto, and Y. Cohen. *Technical and Economic Feasibility of Reverse Osmosis Reclamation of Agricultural Drainage Water in the San Joaquin Valley*. in *Proceedings of the AIChE Annual Conference*. 2006. San Francisco, CA.
14. Rahardianto, A., et al., *High recovery membrane desalting of low-salinity brackish water: Integration of accelerated precipitation softening with membrane RO.* Journal of Membrane Science, 2007. **289**(1-2): p. 123-137.
15. Uchymiak, M., et al., *A novel RO ex situ scale observation detector (EXSOD) for mineral scale characterization and early detection.* Journal of Membrane Science, 2007. **291**(1-2): p. 86-95.
16. Brusilovsky, M., J. Borden, and D. Hasson, *Flux decline due to gypsum precipitation on RO membranes.* Desalination, 1992. **86**(2): p. 187-222.
17. Lee, S. and C.-H. Lee, *Effect of operating conditions on CaSO4 scale formation mechanism in nanofiltration for water softening.* Water Research, 2000. **34**(15): p. 3854-3866.
18. Lee, R.-W., et al., *Low-pressure RO membrane desalination of agricultural drainage water.* Desalination, 2003. **155**(2): p. 109-120.

19. Shih, W.-Y., et al., *A dual-probe approach for evaluation of gypsum crystallization in response to antiscalant treatment.* Desalination, 2004. **169**(3): p. 213-221.
20. Shih, W.-Y., et al., *Morphometric characterization of calcium sulfate dihydrate (gypsum) scale on reverse osmosis membranes.* Journal of Membrane Science, 2005. **252**(1-2): p. 253-263.
21. Ning, R.Y., *Discussion of silica speciation, fouling, control and maximum reduction.* Desalination, 2002. **151**: p. 67-73.
22. Lyster, E. and Y. Cohen, *Numerical study of concentration polarization in a rectangular reverse osmosis membrane channel: Permeate flux variation and hydrodynamic end effects.* Journal of Membrane Science, 2007. **303**(1-2): p. 140-153.
23. Hydranautics, *Terms and Equations of Reverse Osmosis.* 2001.
24. Koch Membrane Systems, I., *ROPRO*. 2008.
25. Hydranautics, *Chemical Pretreatment of RO/NF, Technical Application Bulletin No. 111 Rev. C*. 2008.
26. Rahardianto, A., et al., *Diagnostic characterization of gypsum scale formation and control in RO membrane desalination of brackish water.* Journal of Membrane Science, 2006. **279**(1-2): p. 655-668.
27. OLI, *OLI Analyzer 2.0*. 2005, OLI Systems, Morris Plains, NJ.
28. Kurt Kovac, et al., *Drainage water samples and laboratory reports*, Brian C McCool and Y. Cohen, Editors. 2006-2007: Los Angeles, CA.
29. AWWA, *Standard Methods for the Examination of Water and Wastewater*. 20th ed. 1998, Washington, DC: American Public Health Association.
30. USEPA. *Clean Water Act Analytical Methods: Approved General-Purpose Methods*. 2010 [cited 2010; Available from: http://www.epa.gov/waterscience/methods/method/.
31. Norberg, D., et al., *Surface characterization and performance evaluation of commercial fouling resistant low-pressure RO membranes.* Desalination, 2007. **202**(1-3): p. 45-52.
32. *Selection of Candidate Sumps to Determine Critical Membrane Desalination Process Requirements*. 2004, California Department of Water Resources.
33. Zhu, A., P.D. Christofides, and Y. Cohen, *On RO membrane and energy costs and associated incentives for future enhancements of membrane permeability.* Journal of Membrane Science, 2009. **344**(1-2): p. 1-5.
34. Rahardianto, A., B.C. McCool, and Y. Cohen, *Accelerated Desupersaturation of Reverse Osmosis Concentrate by Chemically-Enhanced Seeded Precipitation (in Press).* Desalination, 2010.
35. Zhu, A., et al., *Reverse Osmosis Desalination with High Permeability Membranes - Cost Optimization and Research Needs (in Press).* Desalination and Water Treatment, 2010.
36. Uchymiak, M., et al., *Brackish water reverse osmosis (BWRO) operation in feed flow reversal mode using an ex situ scale observation detector (EXSOD).* Journal of Membrane Science, 2009. **341**(1-2): p. 60-66.
37. Bartman, A.R., et al., *Model-predictive control of feed flow reversal in a reverse osmosis desalination process.* Journal of Process Control, 2009. **19**(3): p. 433-442.

Chapter 4

Antiscalant removal in accelerated desupersaturation of RO concentrate via chemically-enhanced seeded precipitation (CESP)

4.1 Overview

Reverse osmosis (RO) has received increased attention due to dwindling fresh water supplies and increasing future water demands [1]. While RO is considered a mature technology, its application for desalination of brackish water remains challenging due to the high costs of managing and disposing residual RO concentrate, especially at inland locations [1-3]. High product water recovery is desirable in inland locations in order to minimize concentrate management costs; however, the recovery levels achievable by RO desalination are typically limited by mineral scaling (e.g., gypsum, barite, silica, calcium carbonate) even with the use of antiscalants. For example, desalination of brackish agricultural drainage waters in California's San Joaquin Valley (SJV; 2000–30,000 mg/L TDS) is generally limited to recoveries of 50–75% using traditional RO desalting methods primarily due to mineral salt scaling (see **Ch. 3**) [4-6]. Because inland desalination of brackish water at low recoveries (<85%) has been shown to be infeasible due to high brine disposal costs [7], two-stage RO with intermediate concentrate demineralization (ICD; **Fig. 4-1**) has been proposed as a promising method to overcome the scaling-imposed recovery limits in desalting brackish water with high potential for membrane mineral scaling [8-13]. The ICD process reduces the concentration of scale precursors (e.g. calcium, carbonate, and/or sulfate ions) in the primary RO (PRO) concentrate to below the effective solubility limit of the mineral scalants of concern (e.g., gypsum and calcite), allowing the treated concentrate to be further desalted in a subsequent secondary RO (SRO) process. Recent studies have shown that the above approach coupling RO with ICD can enhance the

overall recovery in brackish water desalination to >85% and thus minimize the residual volume of generated RO concentrate [10, 11, 14].

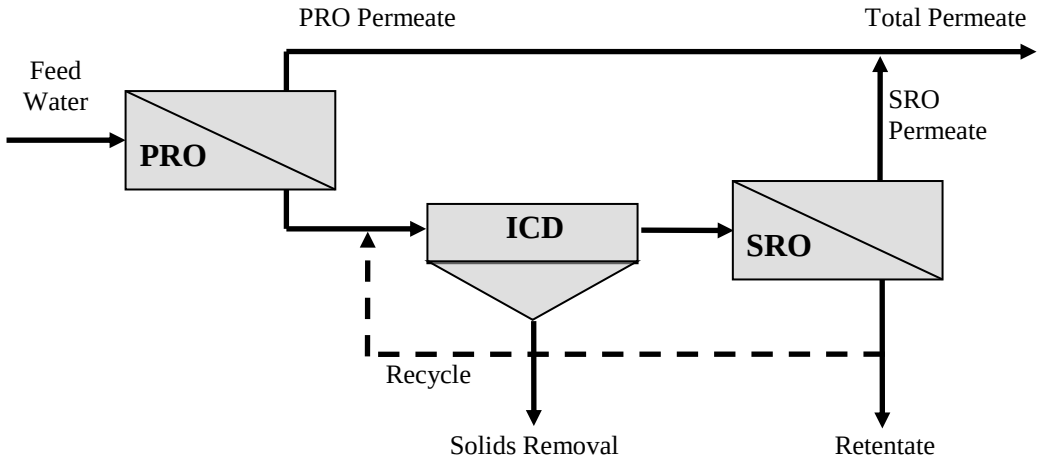

Figure 4-1. High recovery RO process utilizing intermediate concentrate demineralization (ICD) between primary RO (PRO) and secondary RO (SRO) desalination stages.

Precipitation softening has been shown in previous studies as an effective ICD method for high recovery desalination of brackish Colorado River water (~1000 mg/L TDS) [11] even in the presence of antiscalant (AS) carry-over, targeting calcium ion removal achieved via alkaline-induced $CaCO_3$ precipitation. The approach primarily reduces RO concentrate supersaturation with respect to calcium-bearing mineral scalants (e.g., gypsum and calcite), but also leads to removal of other trace constituents via co-precipitation processes [10, 11]. While effective, precipitation softening is chemically intensive as it requires at least stoichiometric amounts of an alkaline chemical (e.g. sodium hydroxide, calcium hydroxide, sodium bicarbonate, or sodium carbonate) to induce precipitation of $CaCO_3$ [10, 11, 15]. Therefore, precipitation softening of water lean in bicarbonate (e.g. San Joaquin Valley agricultural drainage water) but high in sulfate and calcium ion concentrations [5, 10, 11] requires alkaline dosing with chemicals containing carbonate (e.g. Na_2CO_3), which are generally more expensive than other alkaline sources (e.g.

$Ca(OH)_2$) [16]. Also, the presence of AS carryover that can retard $CaCO_3$ precipitation [17], may require significant overdosing of a suitable alkaline source.

In order to overcome the inhibition of calcium salt precipitation by AS carryover in the RO concentrate, electrochemical oxidation, polymeric coagulant additives, and surfactants have been investigated as methods to disrupt AS action by AS scavenging or degradation prior to ICD [17-22]. However, these treatment strategies may be detrimental to downstream processes where the presence of additional residual chemical additives may be undesirable and may lead to membrane fouling [23-26] or where the destruction of AS and other natural organic matter (NOM) present in natural waters may produce hazardous disinfection by-products [27-29]. The increased chemical and storage costs of these methods may increase the costs of integrating ICD with RO desalination.

More recently, a two-step ICD process for the treatment of RO concentrate with high gypsum scaling tendency was proposed in which AS is first removed by inducing $CaCO_3$ precipitation via partial lime softening (at a dose significantly lower than that required for conventional lime softening) [14], followed by subsequent seeded gypsum precipitation for concentrate desupersaturation—an approach referred to as chemically-enhanced seeded precipitation (CESP) [14]. Ordinarily, AS carry-over that may be present in PRO concentrate would be detrimental to the seeded precipitation process due to the stabilization of the supersaturated PRO concentrate and seed poisoning by AS. It was argued that the combination of partial lime softening and seeded precipitation sequences in the two-step CESP process can balance chemical use with favorable precipitation kinetics in the demineralization of AS-containing PRO concentrate. In the CESP approach, it was postulated that gypsum desupersaturation is enhanced by the removal of AS by alkaline pretreatment prior to gypsum

seeding. Feasibility of CESP was explored by focusing on the challenge of high recovery desalting of agricultural drainage water in California's San Joaquin Valley for a specific location (OAS) [5] nearly saturated with respect to gypsum (gypsum saturation index, *SIg* = 0.96). It was shown that effective gypsum precipitation could be sustained even when seeding with recycled precipitated gypsum solids. Although AS removal via $CaCO_3$ precipitation was not confirmed, it was postulated that lime-precipitated $CaCO_3$ particles were able to scavenge generic and commercial polycarboxylic-acid antiscalants, thereby facilitating subsequent $CaSO_4$ precipitation with minimal retardation by AS. It is interesting to note that precipitation of $CaCO_3$ at high pH has been reported to aid in the removal of natural organic matter (NOM) via adsorption onto crystal faces [30]. Also, previous studies on $CaCO_3$ crystallization in the presence of a polyacrylic acid (PAA, a polyelectrolyte often used in AS formulations) reported on the adsorption and entrapment of this polyelectrolyte into either amorphous $CaCO_3$ or vaterite solid matrices [31-34]. The above studies on the impact of NOM and polyelectrolytes on $CaCO_3$ precipitation appear to support the postulate that $CaCO_3$ precipitation can be employed to aid in AS removal, particularly when reduction in gypsum saturation is desired.

The goal of the present work is to experimentally demonstrate and quantify the feasibility of AS removal from RO concentrate via lime treatment. The efficiency of AS removal with respect to lime dosage is explored and the effectiveness of subsequent seeded gypsum precipitation to reduce the level of gypsum supersaturation was established. In addition, the filterability of the treated RO concentrate was evaluated by quantifying the size of the formed precipitate particles and measuring the turbidity of treated RO concentrate before and after microfiltration.

4.2 Experimental

4.2.1 Model solutions

Model brackish water solutions were prepared by adding NaCl, $NaHCO_3$, $MgSO_4 \cdot 7H_2O$, Na_2SO_4, and $CaCl_2 \cdot 2H_2O$ (Fisher Scientific, Pittsburg, PA) to DI water (**Table 4-1**). Solution compositions were based on those of the expected RO concentrate stream from an RO desalination process operating at the scaling recovery limit (63% recovery leading to concentrate *SIg* = 2.5) for a brackish water source in the San Joaquin Valley (OAS location) [5, 14] (see **Appendix A**). Model solution A containing polyacrylic acid (PAA) was treated with $Ca(OH)_2$ (lime) doses varying from 0.05–1.0 g/L (0.675–13.5 mM) to induce $CaCO_3$ precipitation for AS removal. Solution A contained an additional 16.6 mM $NaHCO_3$ in order to increase the carbonate level above that expected in the PRO concentrate. Thus the limitiation of $CaCO_3$ precipitation imposed by the carbonate-lean PRO concentrate was removed in solution A. Solution B was prepared for lime pretreatment experiments that where followed by seeded gypsum precipitation and contained all major ions present in the OAS field sample. The ionic strength of solution A was adjusted to match that of solution B by addition of NaCl.

Polyacrylic acid (PAA, MW = 2000 g/mol, Aldrich, St. Louis, MO) was selected as the AS for removal measurements rather than a commercial AS because its composition is known while commercial AS are generally proprietary mixtures of poly-electrolytes and precise compositions are not reported. It has been shown that commercial AS effectiveness is roughly proportional to their solids content and generally contain 13–54% solids [25] so a dose of 1 mg/L PAA is equivalent to ~2–7 mg/L of commercial AS, depending on the solids content. PAA was added to the solutions prior to alkaline treatment as it effectively retards crystal nucleation and growth and is known to be a major active ingredient in many commercial AS [25]. In the present

experiments, the initial PAA concentration was in the range of 3–12 mg/L. This range of AS dose is representative, for example, of the range expected for RO concentrate from desalting at 50–75% recovery.

4.2.2 Chemical demineralization experiments

Batch demineralization experiments (see **Appendix B**) were performed at room temperature (~23 °C) in 1-L stirred rectangular batch-reactors 20 cm tall with an 8.0 cm by 8.0 cm base (CLM 4, EC Engineering, Edmonton, Canada). Mixing was provided by a 4.0 cm by 6.0 cm rectangular paddle situated with 2.5 cm of clearance above the base of the jar. During each batch experiment, the calcium activity declined due to $CaCO_3$ precipitation and in some cases $CaSO_4$ precipitation. The degree of solution supersaturation with respect to calcite and gypsum was expressed in terms of the saturation index defined as $SIx = IAPx/Ksp,x$, (where $IAPx$ and Ksp,x are the ion activity and solubility products, respectively, of mineral salt x). Precipitation-induced changes in calcium, carbonate, and sulfate ion concentrations and gypsum and calcite saturation indices were determined based on equilibrium calculations [14] using multielectrolyte thermodynamic simulation software (Analyzer Studio 3.1) [35] based on measurements of the calcium activity and pH, along with the knowledge of the solutions' initial compositions (**Table 4-1**) (see **Appendices C** & **D**).

Table 4-1. Primary RO concentrate model solutions for San Joaquin Valley agricultural drainage water from the OAS location at 63% recovery

salt		field sample composition[(a)]	RO concentrate model solutions	
			solution A[(b)]	solution B[(c)]
$CaCl_2$	mM	11.5	30.7	30.7
Na_2SO_4	mM	54.5	--	145.4
MgSO4	mM	11.7	--	31.2
$NaHCO_3$	mM	4.3	28.0	11.4
NaCl	mM	7.6	443.7	20.3
pH		7.6	7.8	7.8
Gypsum SI		0.96	--	2.5
Calcite SI		3.9	94	20

[(a)] 11,020 mg/L TDS collected from OAS location on 4/10/2006 [5];
[(b)] Sulfate-free, bicarbonate enriched concentrate model solution at *CF* = 2.7 (63% recovery);
[(c)] concentrate model solution at *CF* = 2.7 (63% recovery)

Lime slurries were freshly prepared before each experiment by suspending 0.05–1.0 g lime powder (Sigma Aldrich, St. Louis, MO) in 10 mL of DI water. $CaCO_3$ precipitation was initiated by adding the lime slurry to the model RO concentrate solution at the start of a 2-min period of rapid mixing (shear rate $G = 1000\ s^{-1}$). Subsequently, the mixing intensity was reduced ($G = 200\ s^{-1}$) and the time evolution of calcium ion activity and pH were monitored online. The degree of AS removal as a function of lime dose was quantified by measuring the concentration of dissolved PAA in solution A samples after lime addition using the Hach Polyacrylic Acid Test Kit (Hach Company, Loveland, CO). The method involved PAA preconcentration from solution A samples via adsorption and elution using a chromatographic column, reagent addition, and subsequent colorimetric measurement via UV/VIS spectrophotometry at 482 nm [36]. Calibration was accomplished with PAA solutions over a concentration range of 0.5–10 mg/L yeilding a linear calibration with extinction coefficient $\epsilon = 10.5 \cdot 10^{-3}$ L/mg-cm.

4.2.3 Analytical measurements

Calcium ion activity was monitored with a calcium ion selective electrode (ISE25Ca-9/REF251; Radiometer Analytical, Lyon, France) interfaced with an Orion 720Aplus meter (Thermo Scientific, Waltham, MA). Solution pH also varied during the precipitation period and was monitored with a pH electrode (pHG211-8/REF201; Radiometer Analytical, Lyon, France) connected to a sensION4 meter (Hach Co., Loveland, CO). The solution temperature was recorded using a Hach temperature probe (Model 51980-00, Hach Co., Loveland, CO) connected to a sensION4 meter (Hach Co., Loveland, CO).

At various times during the experiments 1–3 mL of particle suspension samples were withdrawn from the precipitation reactors for particle size analysis. The growth of $CaCO_3$ particles (e.g., precipitative and aggregative) was evaluated by quantifying the time evolution of the particle size distribution during the alkaline treatment step of CESP. Particle size distributions were measured via an electrical zone sensing method using a Multisizer 3 Coulter Counter (Beckman Coulter, Miami, FL), operating with a 100 or 280-μm aperture tube having a particle size measurement range of 2.4–60 μm or 5.6–168 μm equivalent spherical diameter, respectively. Immediately upon withdrawal, each sample was quenched (to arrest precipitation or dissolution) by transfer to a 150 ml solution containing 5%-wt (362 mM), Na_2SO_4, 100 mg/L of Flocon 260 antiscalant (Biolab Water Additives; Lawrenceville, GA), and 12.9 and 2.3 mM $CaCl_2{\cdot}2H_2O$ and $NaHCO_3$, respectively. $CaCl_2{\cdot}2H_2O$ and $NaHCO_3$ were added to slightly supersaturate the solution (*SI*~1.1) with respect to gypsum and calcite, while the AS was added to further retard precipitation and aid in dispersion of the precipitate. It is noted that the quench solutions were vacuum filtered prior to use with 0.2-μm membrane filters (Millipore, Billerica, MA). Assessment of the filterability of the lime treated model RO concentrate (solution B) was

based on determination of the average size and turbidity of the precipitated particles, measured before and after filtration (5-µm, 0.8-µm, or 0.22-µm) via Dynamic Light Scattering (Malvern Zetasizer S90; Malvern, Westborough, MA) and a back-light scattering turbidity probe/meter (Analite 90E/160, McVan Instruments, Mulgrave, Australia), respectively.

4.3 Results and Discussion

4.3.1 Antiscalant removal by calcium carbonate precipitation via lime treatment

In order to quantify the feasibility of AS removal from RO concentrate via $CaCO_3$ precipitation, model solution A (sulfate free; **Table 4-1**) containing PAA (10 mg/L) was dosed with lime. PAA removal of 64–89% was achieved 30 min after lime dosing over the range of 0.05–1.0 g/L (0.675–13.5 mM). For example, for the single lime dose of 0.6 g/L, 84% PAA removal was achieved after 30 minutes of $CaCO_3$ precipitation, with the bulk of PAA removal occurring within the initial 10 minutes (78%). PAA removal increased linearly with the logarithm of lime dose as illustrated in **Fig. 4-2**. As expected, PAA removal increased with increased lime dose as a result of the higher initial calcite saturation index (SIc_0) and greater mass of precipitated $CaCO_3$. The above degree of PAA removal is significant and suggests that $CaCO_3$ precipitation can serve to remove dissolved AS from solution and thereby reduce the potential interference with precipitation of other major scalants of concern (e.g., gypsum). One would expect that, consistent with previous studies on polyelectrolyte adsorption onto mineral crystal surfaces [12, 17, 31, 33, 34, 37], as $CaCO_3$ crystals nucleate and grow dissolved AS would adsorb onto the available crystal surface area. Therefore, it is reasonable to postulate that AS scavenging occurs via surface adsorption of AS, followed by crystal growth from surrounding AS-free areas and via entrapment of adsorbed AS due to aggregation over the course

of the precipitation process. Accordingly, one would expect that the extent of AS scavenging should depend on the evolving total surface area (i.e., cumulative surface sites available for AS adsorption) of $CaCO_3$ particles that are generated over the course of the precipitation period, as well as the initial AS concentration in solution (i.e., the initial adsorption driving force).

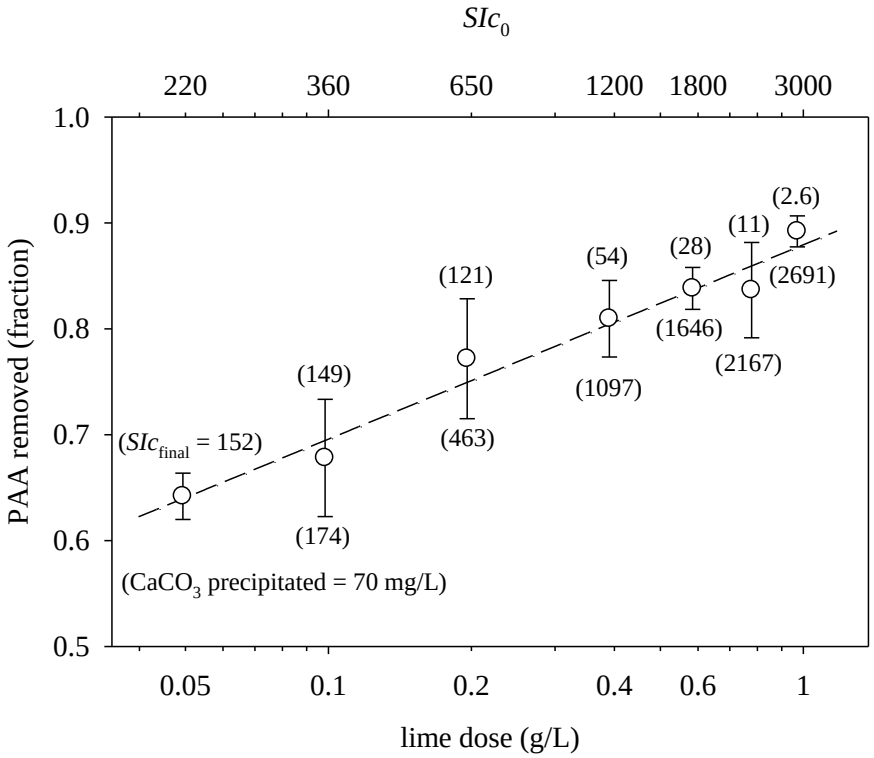

Figure 4-2. Fraction of antiscalant removed from solution A (**Table 4-1**), initially containing 10 mg/L PAA, 30 minutes after single lime doses. The values in parentheses above and below the data points correspond to the *SIc* and mass concentration (mg/L) of precipitated $CaCO_3$, respectively, 30 minutes after lime addition.

4.3.2 Calcium carbonate precipition in the presence of PAA

The impact of dissolved PAA on $CaCO_3$ precipitation in the lime treatment step of CESP was assessed by determining the calcite and gypsum saturation indices and evolution of precipitate particle size distributions during the $CaCO_3$ precipitation process. It is noted that lime addition raises *SIc* significantly with a negligible increase in *SIg*. As shown in the example of **Fig. 4-3a,** for RO-concentrate model solution B with an initial PAA concentration of 3 mg/L, a

relatively low lime dose (2.70 mM) was sufficient to raise *SIc* from 20.3 to 374 which induced rapid $CaCO_3$ precipitation and thus an associated reduction of *SIc* to 178 within the first two minutes of the precipitation period. Further decrease of *SIc* was slow reaching a value of 35 after 50 min. The solution remained supersaturated with respect to gypsum with *SIg* declining only slightly from 2.53 to 2.38. Measurements of sulfate ion concentration did not decrease during the precipitation period thus indicating that gypsum did not precipitate; therefore, the slight decline in gypsum saturation was due to calcium ion depletion resulting from $CaCO_3$ precipitation. SEM analysis of the precipitate revealed particle aggregates with raspberry-like morphology (**Fig. 4-3b**), consistent with previous studies on $CaCO_3$ crystallization in the presence of PAA in which vaterite crystals were identified [31, 33, 34, 37].

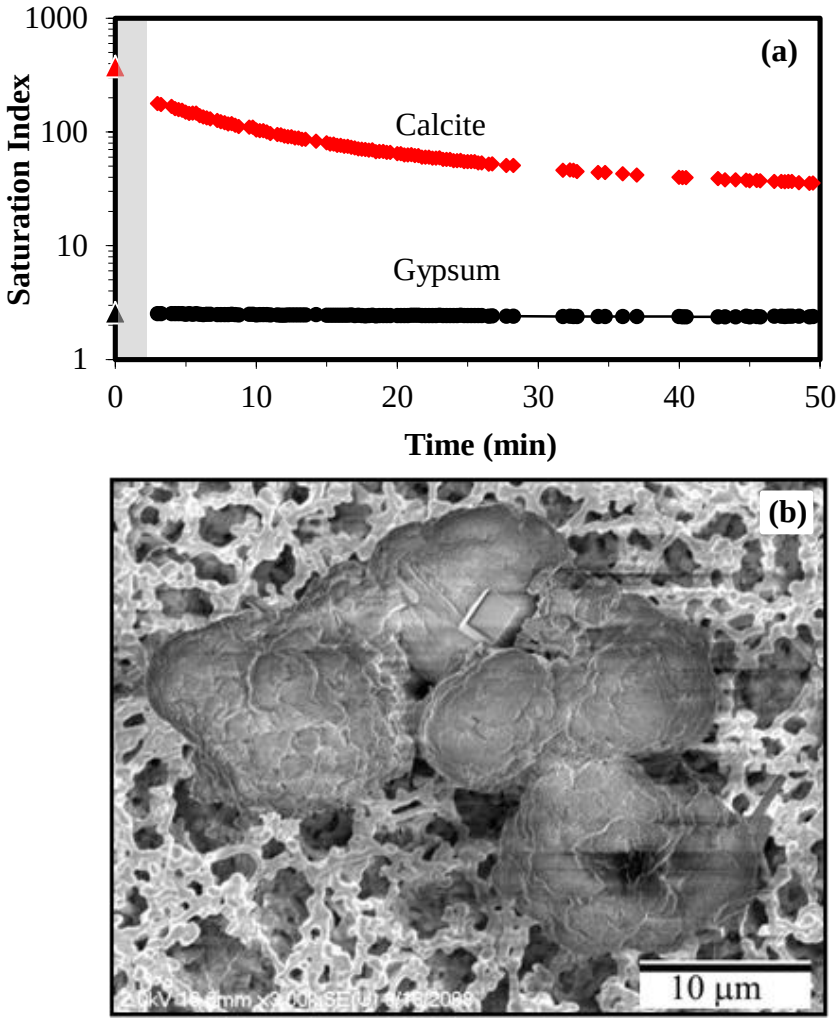

Figure 4-3. (a)Time varying saturation indices (*SIg* and *SIc*) during lime-induced (2.70 mM) precipitation of $CaCO_3$ in AS-containing (3 mg/L PAA) solution B (**Table 4-1**); (b) SEM of $CaCO_3$ precipitate. Initial conditions after alkaline dosing: SIc_0= 374, SIg_0 = 2.57. The shaded area indicates the rapid mixing period (G = 1000 s^{-1}), which was subsequently reduced (G = 200 s^{-1}).

Precipitative and aggregative growth of $CaCO_3$ particles, in the presence of PAA, was apparent from the evolution of the number and volume particle distributions during the lime treatment step. The observed shift in the number and volume modal particle diameters (d_p) to larger sizes indicated particle growth (from <5.6 to 19 µm and from 10 to 21 µm for the number and volume modal d_p, respectively) as shown in **Fig. 4-4**. This shift in the number distribution, coupled with a declining modal number concentration (from >$6 \cdot 10^5$ to $2.3 \cdot 10^5$/cm^3) is attributed

to particle aggregation (**Fig. 4-4a**). The concurrent rise in the total volume of the particles (**Fig. 4-4b**) confirmed precipitative growth of the particles in addition to aggregation. In general, the time-varying trends of the number and volume distributions were similar to those previously reported during $CaCO_3$ precipitation in AS-free solution [38]. In the present case, however, a relatively long tail of small particles is apparent in the number distribution which is indicative of AS retardation of particle growth.

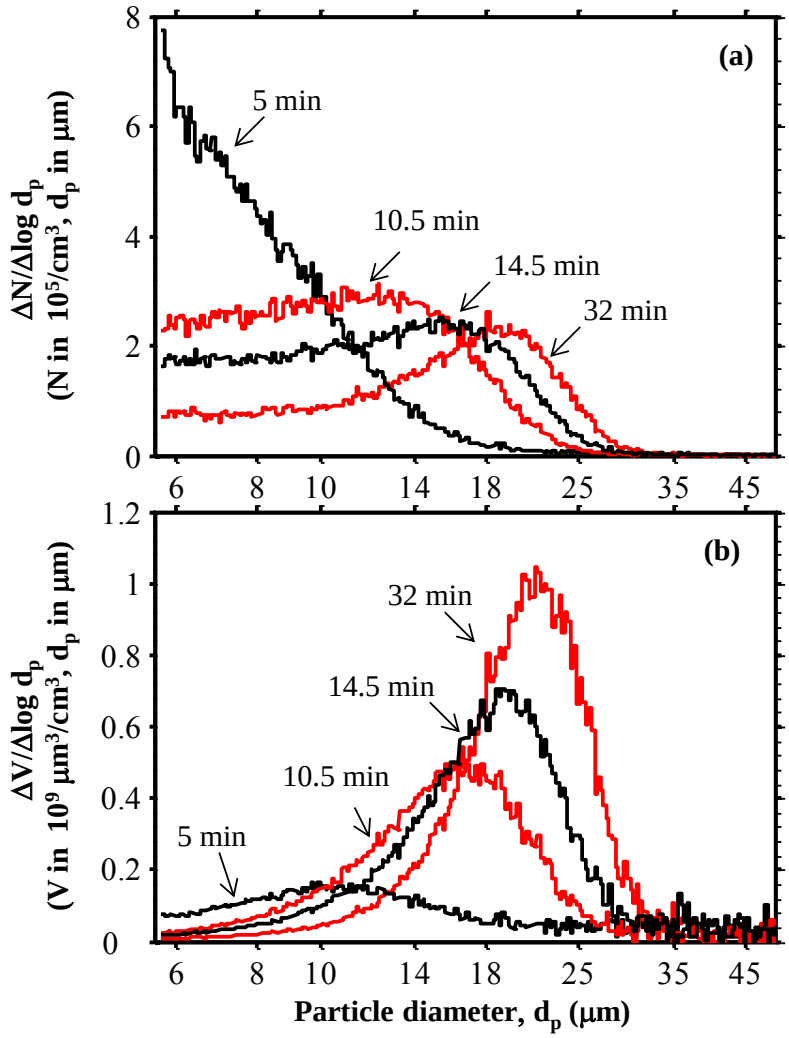

Figure 4-4. Time varying number (a) and volume (b) during lime-induced (2.70 mM) precipitation of $CaCO_3$ in AS-containing (3 mg/L PAA) solution B (**Table 4-1**). Initial conditions after alkaline dosing: SIc_0= 374, SIg_0 = 2.57.

4.3.3 Impact of antiscalant concentration on calcium carbonate precipitation

The kinetics of $CaCO_3$ and $CaSO_4$ precipitation during CESP can be quantified by the extent of reaction (α_m) as:

$$\alpha_m = \frac{[m]_0 - [m]}{[m]_0 - [m]_{eq,x}} \tag{4-1}$$

where $[m]$, $[m]_0$ and $[m]_{eq,x}$ are the concentrations of the ion m unique to the mineral salt precipitating (e.g. carbonate, sulfate) at time t, $t = 0$ (i.e., initial) and at equilibrium with respect to mineral salt x (e.g., calcite, gypsum). Following such a representation of the precipitation data it was shown for model solution B (**Table 4-1)** that, at a lime dose of 3.37 mM, the same carbonate extent of reaction of 0.56 was reached 2 min after lime addition (**Fig. 4-5**), irrespective of the initial PAA dose (for the range of 3–12 mg/L). The observed independence of the extent of reaction during the initial lime treatment period (2 min), for the above range of initial AS concentrations, suggests that the initially attained SIc_0 was sufficiently high to promote rapid nucleation/precipitation exceeding the PAA's capacity to retard precipitation. In the subsequent precipitative growth period (>2 min) the extent of reaction was clearly influenced by the initial PAA concentration indicating a significant retardation of precipitation kinetics (i.e., slower rise of the extent of reaction with time). For example, a factor of 4 increase in the initial PAA concentration (from 3 to 12 mg/L) resulted in a decrease by a factor of 5 (from 0.86 to 0.62) in the additional extent of reaction achieved after 25 min beyond the initial extent of reaction of 0.56. In all cases, the extent of reaction appeared to approach a plateau reflective of the metastable supersaturation level for the specific AS dose.

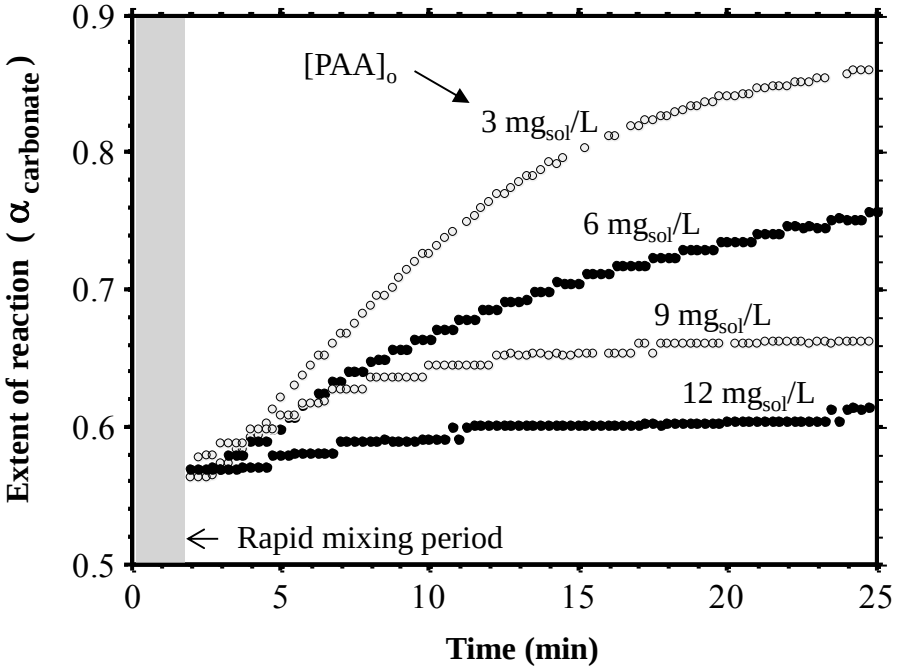

Figure 4-5. Impact of initial AS concentration (3–12 mg/L PAA) on time varying extents of reaction during lime-induced (3.37mM) precipitation of $CaCO_3$ in AS-containing solution B (**Table 4-1**). Initial conditions after alkaline dosing: SIc_0= 468, SIg_0 = 2.58. The shaded area indicates the rapid mixing period (G = 1000 s^{-1}), which was subsequently reduced (G = 200 s^{-1}).

Retardation of $CaCO_3$ precipitation by the PAA is also evident by inspecting the particle size distribution over the course of the precipitation period as shown in the example of **Fig. 4-6** after a precipitation period of 25 min (at 3.37 mM lime dose). It is apparent that, as the PAA concentration increases, the size of the precipitated particles decreases. For example, at a PAA concentration of 3 mg/L there is a significant fraction of particles in the range of ~14–30 μm, while at the highest PAA dose of 12 mg/L there is a significantly higher fraction of particles below ~10 μm. A greater particle size is expected at lower PAA concentrations since crystal growth and aggregation can proceed more freely as the retardation due to PAA is reduced. Indeed, precipitative growth and particle aggregation after the nucleation period has been observed in previous work [38]. However, AS (e.g. PAA) present in solution can adsorb onto the growing crystal surfaces [39-41] and is expected to increase the particles' negative surface

charge [41] and thus lead to greater electrostatic particle-particle repulsion. As a result, aggregation of particles is reduced in the presence of the AS. From a practical viewpoint, it is important to carry out the ICD process such that sufficiently large precipitate particles are produced to facilitate efficient sedimentation and/or filtration removal of such particles. Therefore, it may be advantageous to keep the AS dosing of the RO feed at the minimum acceptable level to avoid membrane scaling in the RO desalting process.

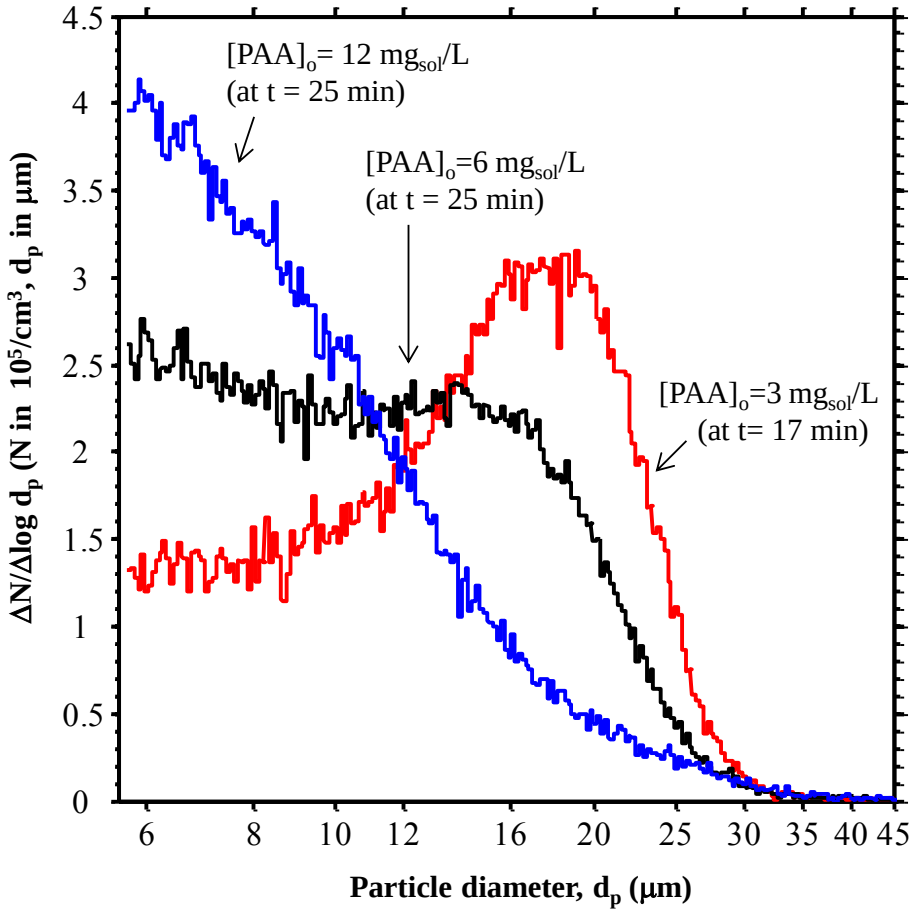

Figure 4-6. Impact of initial AS concentration (3–12 mg/L PAA) on particle number distribution during lime-induced (3.37 mM) precipitation of $CaCO_3$ in AS-containing solution B (**Table 4-1**). Initial conditions after alkaline dosing: SIc_0= 468, SIg_0 = 2.58.

4.3.4 Impact of initial supersaturation level on calcium carbonate precipitation

The kinetics of $CaCO_3$ precipitation are dictated by the initial degree of calcite supersaturation (SIc_0) that is achieved by lime addition. As shown in **Fig. 4-7**, for model solution B (**Table 4-1**) containing 3 mg/L PAA, there is a more rapid rise in the extent of reaction with increasing SIc_0. Moreover, the extent of reaction both in the initial precipitation period (<2 min) (presumably dominated by nucleation) and later precipitation period (2–25 min) was greater for higher SIc_0 (i.e., due to the higher lime dose). For example, as SIc_0 increased from 187 to 468 (by a factor of 2.5), the extent of reaction at the end of the initial 2 min rapid precipitation period increased by a factor of 2.7 (from 0.21 to 0.56). Also, the extent of reaction which increased with time reached a level of 0.86 for the highest lime dose (3.37 mM), while it remained at ~0.21 at the lowest lime dose (1.35 mM); the latter lack of additional precipitation was due to the stabilizing effect of the residual PAA in solution after the initial nucleation period. The above behavior is consistent with the observation that lower AS removal is expected at lower SIc_0 (**§4.3.1**, **Fig. 4-2**). On the other hand, at higher SIc_0 a greater fraction of the AS is removed, thereby reducing the ability of the AS to retard precipitation (**Fig. 4-7**).

It is noted that the total number and size of larger particles (>5.6 μm—the lower limit for this measurement) increased with increasing SIc_0 (i.e., higher lime dose) as illustrated in **Figs. 4-8** & **4-9** after the initial 2 min rapid growth period. This behavior was indicative of continuing growth by aggregation and surface growth of the particles in the monitored size range, as well as the growth of smaller particles [38] initially smaller than the monitored range. Clearly, the SIc_0 is a key factor affecting the rate of nucleation and growth of $CaCO_3$ particles and thus the effectiveness of AS removal. Furthermore, as is shown in **§4.3.5**, for a given total lime dose, sequential lime dosing can be more effective for AS removal than a single dose.

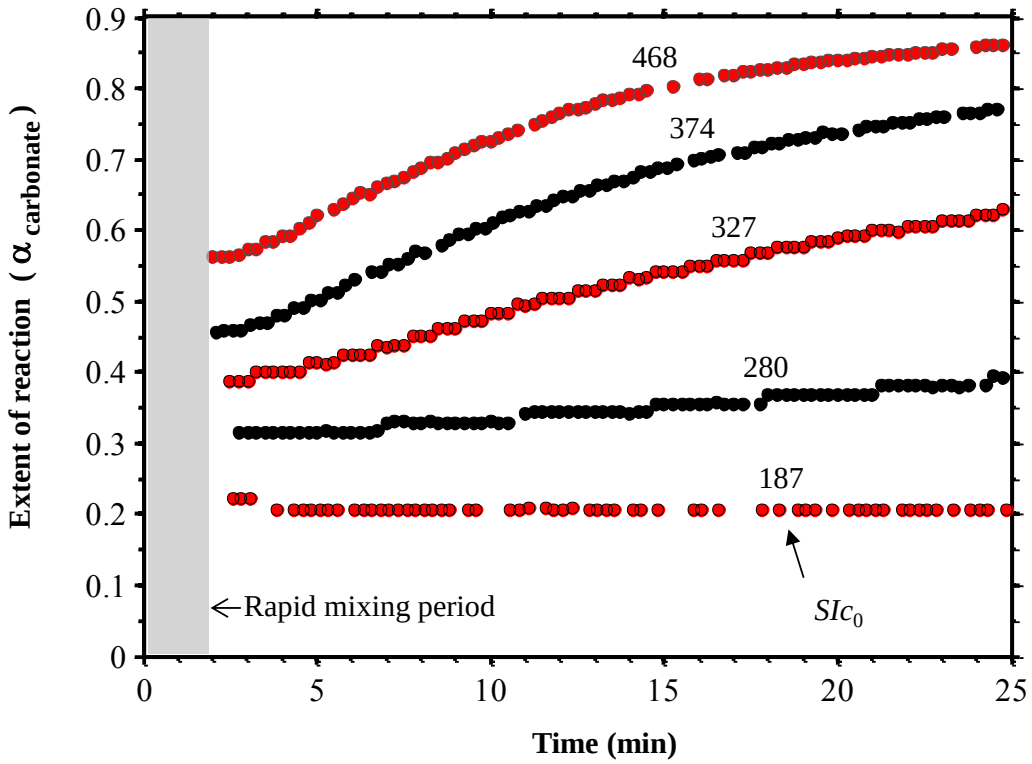

Figure 4-7. Impact of initial calcite saturation index (SIc_0) on time varying extents of reaction during lime-induced precipitation of $CaCO_3$ in AS-containing (3 mg/L PAA) solution B (**Table 4-1**) using 1.35, 2.02, 2.36, 2.70, or 3.37 mM of lime with corresponding SIc_0 of 187, 280, 327, 374, or 468 upon lime addition, respectively. There was a marginal change in SIg_0 upon lime addition (2.55→2.58).

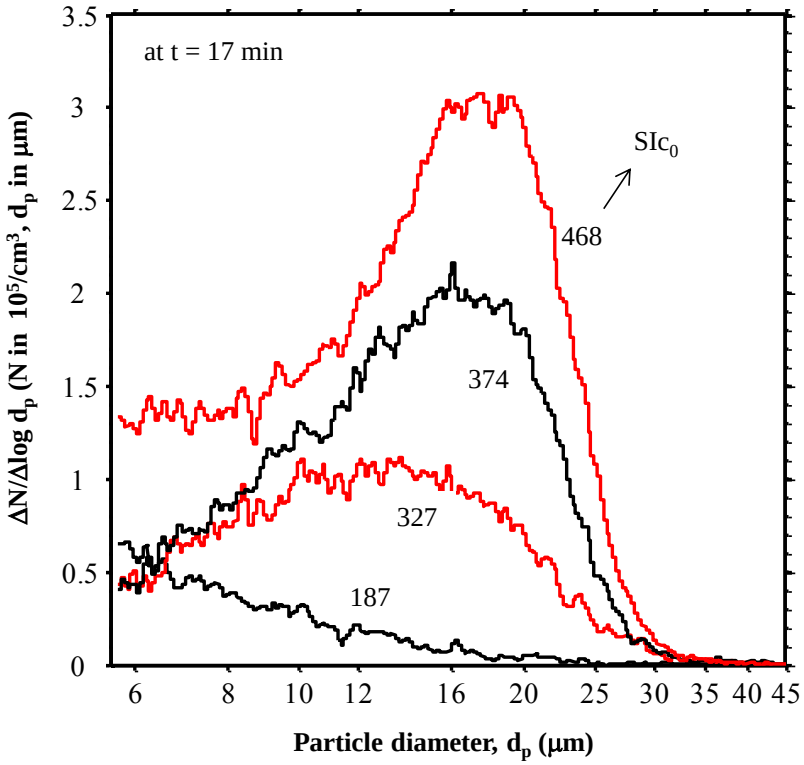

Figure 4-8. Impact of initial calcite saturation index (*SIc*$_0$) on particle number distribution during lime-induced precipitation of $CaCO_3$ in AS-containing (3 mg/L PAA) solution B (**Table 4-1**) using 1.35, 2.36, 2.70, or 3.37 mM of lime with corresponding *SIc*$_0$ of 187, 327, 374, or 468 upon lime addition, respectively. There was a marginal change in *SIg*$_0$ upon lime addition (2.55→2.58).

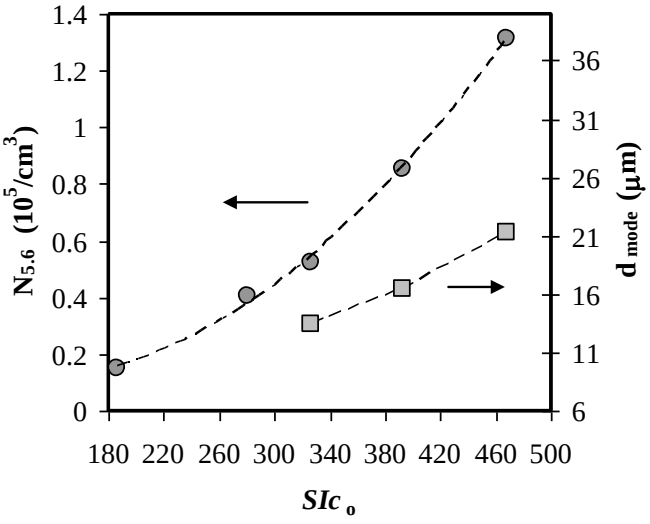

Figure 4-9. Impact of initial calcite saturation index (*SIc*$_0$) on the number concentration of particles above 5.6 μm ($N_{5.6}$) and modal number diameter (d_{mode}) during lime-induced precipitation of $CaCO_3$ in AS-containing (3 mg/L PAA) solution B (**Table 4-1**), using 1.35, 2.02, 2.36, 2.70, or 3.37 mM of lime with corresponding *SIc*$_0$ of 187, 280, 327, 374, or 468 upon lime addition, respectively. There was a marginal change in *SIg*$_0$ upon lime addition (2.55→2.58).

4.3.5 Lime dosing procedure

The effectiveness of AS removal via lime dosing increases with the initial level of solution supersaturation with respect to $CaCO_3$, SIc_0 (**Fig. 4-1**). Therefore, one may argue that raising the lime dose would be desirable in order to achieve a more rapid AS removal. However, upon lime addition the rapid initial (<2 min) nucleation and precipitation rates (**Figs. 4-5** & **4-7**) decline as nucleation and particle growth ensue. As a consequence, *SIc* also decreases resulting in a significant decline in the rate of nucleation, $J_n \propto \exp(-1/[\ln(SIc)]^2)$ [42, 43]. Since the goal of the present lime treatment is to remove the residual AS (to allow for subsequent seeded gypsum precipitation) rather than simply calcium removal, the use of staged lime addition may be a preferable approach. Such a hypothesis implies that the addition of lime in multiple doses would allow maintaining a higher *SIc* (on average) and thus greater driving force for nucleation relative to the use of an equivalent single lime dose (**Fig. 4-10)**. An evaluation of the above hypothesis was carried out, for solution A (**Table 4-1**), whereby a lime dose of 0.1 mg/L (1.35 mM) was administered both as a single dose and via three equal lime doses (totaling 0.1 mg/L) added at 5 min intervals. AS removal for the single dose was determined to be 68%, while lime dosing in three stages enabled 87% AS removal. It is interesting to note that the above staged lime dose addition was even more effective than for a significantly higher single lime dose of 0.6 mg/L that led to somewhat lower AS removal of 84%.

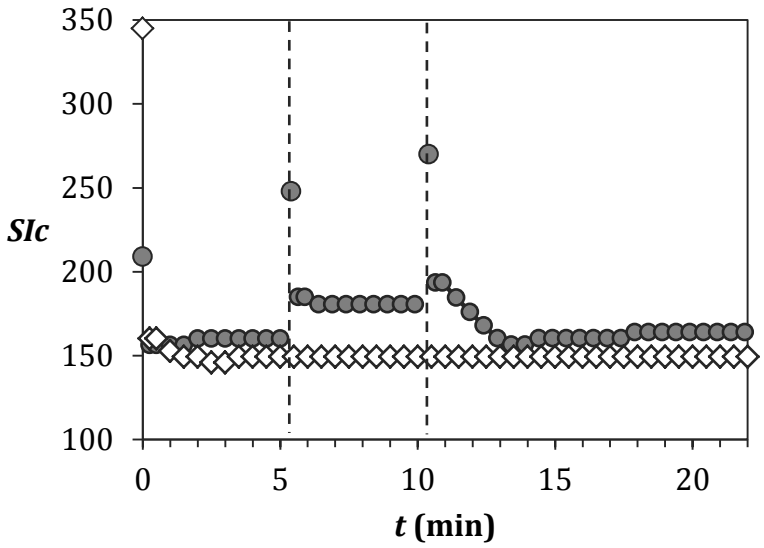

Figure 4-10. Calcite saturation index, *SIc*, after 0.10 g/L lime addition: single dose at t = 0 min (◊); staged dosing with three equal fractions added t = 0, 5.4, and 10.4 min (●).

4.3.6 Residual AS inhibition of seeded gypsum precipitation

The purpose of the initial lime treatment step in CESP is to remove a sufficient fraction of AS from the RO concentrate to accelerate the subsequent step of concentrate desupersaturation via seeded gypsum precipitation [14]. The lime dose needed to effectively achieve the required degree of desupersaturation (i.e. target *SIg* value) within a desired time frame, via the subsequent gypsum seeding stage, can be determined by evaluating the reduction in AS inhibition of gypsum precipitation with increasing lime dose. It is expected that, with increased lime dose, the extent of $CaCO_3$ precipitation increases and there is a concomitant increase of the extent of AS scavenging by $CaCO_3$ precipitate (**Fig. 4-2**). As a result, the degree of AS inhibition of gypsum precipitation is reduced during the subsequent period of seeded gypsum precipitation. The rate of gypsum precipitation can then increase toward that of the AS-free condition, with the extent of gypsum precipitation reaction approaching completion (i.e. $SIg \rightarrow 1$) within a shorter time frame.

In order to determine CESP lime dose requirements, the inhibition of gypsum precipitation due to residual AS needs to be assessed based on gypsum precipitation kinetics data (i.e., calcium concentration decline data) achieved upon gypsum seeding. Previous studies have shown that gypsum precipitation kinetics in bulk solution obey second order kinetics with respect to the limiting ion (i.e. calcium) [44, 45]:

$$r = -\frac{dC}{dt} = k \cdot S_A \cdot \left(C - C_S\right)^2 \tag{4-2}$$

where r is the rate of gypsum precipitation (mol L^{-1} min^{-1}), k is the reaction rate constant (L^2 mol^{-1} m^{-2} min^{-1}), S_A is the total active surface area (m^2 L^{-1}) available for heterogeneous gypsum crystal growth, and C and C_S are the time varying and saturation calcium ion concentrations (mol L^{-1}), respectively. It is reasonable to assume that, during the initial period of gypsum precipitation immediately after gypsum seeding, the change in total active surface area of the growing gypsum seeds (S_{A0}) is small. Thus, it is convenient to makes use of an apparent rate constant, defined as $k' = k \cdot S_{A0}$, which can be estimated from gypsum precipitation kinetics data using the integrated form of **Eq. (4-2)**:

$$\frac{\left(C_0 - C\right)}{\left(C_0 - C_S\right)\left(C - C_S\right)} = k' \cdot t \tag{4-3}$$

where C_0 is the initial calcium ion concentration. There is ample evidence that antiscalants inhibit heterogeneous crystallization by adsorbing onto crystal surfaces thus reducing the effective surface area available for surface growth (i.e. seed poisoning) [34, 41, 46, 47]. Therefore, the apparent rate constant for gypsum crystal growth in the presence of residual AS should be reduced as the available surface area for crystal growth decreases and is expected to be lower than the apparent rate constant for the AS-free case ($k'_{AS-free}$). Previous studies have suggested that AS adsorption follows a Langmuir isotherm [48, 49] given as

$\theta = K_A C_{AS} / (1 + K_A C_{AS})$, where K_A is an adsorption equilibrium constant, θ is the fraction of gypsum surface area occupied by adsorbed AS, and C_{AS} is the dissolved (i.e., free) AS concentration. If one assumes that the retardation of gypsum precipitation is primarily due to active surface area reduction, then it can be shown that the fractional area occupied by AS is related to the ratio of the apparent rate constants ($k' / k'_{AS-free}$) as $\theta = 1 - k' / k'_{AS-free}$. Therefore, the residual AS concentration in solution after lime treatment relative to that without lime treatment can be estimated from the Langmuir isotherm equation which, after rearrangement, yields the following relationship:

$$\frac{C_{AS}}{C_{AS,0}} = \frac{\theta \cdot (1-\theta_0)}{\theta_0 \cdot (1-\theta)} \tag{4-4}$$

where the subscript '0' denotes the case of gypsum seeding without prior lime treatment.

Following the above approach, the relative residual AS concentrations after lime treatment (**Fig. 4-11**) in the two step CESP process were estimated using **Eq. (4-4)** based on available gypsum precipitation kinetics data [14]. In this analysis, the apparent rate constants for gypsum precipitation were estimated from **Eq. (4-3)** based on the initial period of gypsum precipitation (~2–3 minutes). These kinetics data were generated from CESP experiments using AS-containing (3 mg/L) solution B with 25 min of lime treatment (0–3.37 mM), followed by 2.5 g/L gypsum seeding to initiate gypsum precipitation over an 85-min period. For the above specific case, a lime dose of at least 2.7 mM was needed in order to achieve ≥95% AS scavenging (i.e. to reduce $C_{AS}/C_{AS,0}$ to ≤0.05) by the end of lime treatment period, with further increases in lime dose yielding a diminishing return (**Fig. 4-11**). Such a level of residual AS was sufficiently low to prevent gypsum seed poisoning, increasing the sulfate extent of reaction to near completion (≥0.96) and thus reducing *SIg* to ≤1.1 by the end of the 85-min gypsum

precipitation period. At suboptimal lime doses (1.35–2.7 mM), a sharp transition in residual AS concentration (from $C_{AS}/C_{AS,0}$ of 0.69 to 0.05) was apparent, resulting in increased sulfate extents of reaction (from 0.65 to 0.96) and thus decreased *SIg* (from 1.63 to 1.1) at the end of the 85-min gypsum precipitation period. This sharp transition in residual AS concentration occurred once the amount of precipitated $CaCO_3$ began to increase linearly with lime dose (i.e. at >1.35 mM), suggesting that SIc_0 must be raised above a certain threshold (≥327 for the present solution) using a sufficient lime dose to overcome the AS inhibition of $CaCO_3$ precipitation. Once adequate precipitated $CaCO_3$ is available to scavenge the AS, the level of subsequent gypsum seed poisoning is significantly reduced, leading to greater extent of gypsum precipitation (as quantified by the extent of sulfate reaction). Indeed, as reported previously [14], the extent of gypsum precipitation (following lime treatment) determines the degree of concentrate desupersaturation (i.e., final *SIg*), which in turn determines the overall recovery limit of the PRO-CESP-SRO process. For the present example, application of PRO followed by CESP and then SRO would enable recoveries of up to ~85% relative to only ~63% for a single stage RO process [14].

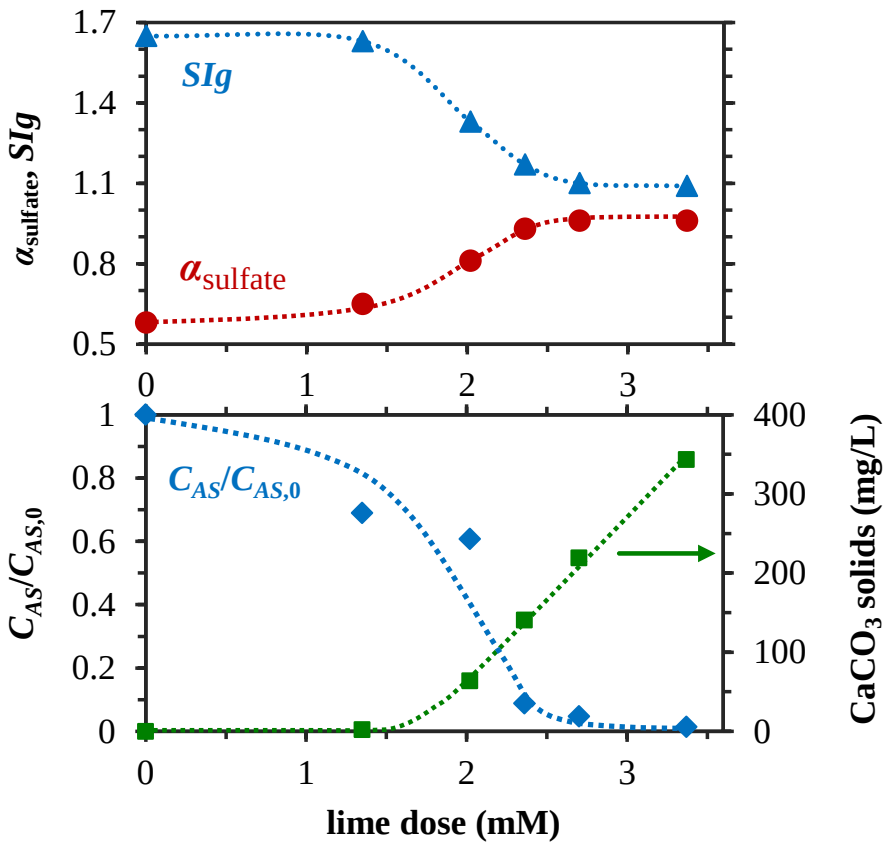

Figure 4-11. Gypsum saturation index (▲) and sulfate extent of reaction $\alpha_{sulfate}$ (●) after 85 min, ratio of AS (PAA) concentration after to before lime treatment (♦), and concentration of precipitated $CaCO_3$ solids after lime treatment (■) in solution B (**Table 4-1**) with 3 mg/L PAA, initially.

4.3.7 Filterability of CESP-treated RO concentrate

In order to allow for secondary RO desalting, the CESP treated PRO must be filtered to remove the precipitated mineral salts. This is required in order to reduce the RO feed turbidity to below the typical recommended limit of 1.0 NTU [50] and thus reduce the propensity for particulate fouling. Given that the average size of gypsum seeds in the CESP process were above 30 µm (the initial seed size), the smaller $CaCO_3$ particles formed during the initial lime treatment (**§4.3.2–4.3.4**) present the greater separation challenge. Accordingly, the lime-treated model concentrate B (without gypsum seeding), at a lime dose of 2.7 mM (for effective CESP, see **Fig.**

4-11) was micofiltered in order to determine the feasibility of attaining the required turbidity level for SRO desalting. Upon filtration with a 5-µm microfilter the turbidity of the lime treated RO concentrate decreased from 203 to 5.1 NTU (**Fig. 4-12**) with the average particle size (determined by DLS) in the filtrate being ~170 nm. It is noted that the required turbidity for RO desalting (≤1 NTU) was achieved after 0.22-µm microfiltration (**Fig. 4-12**).

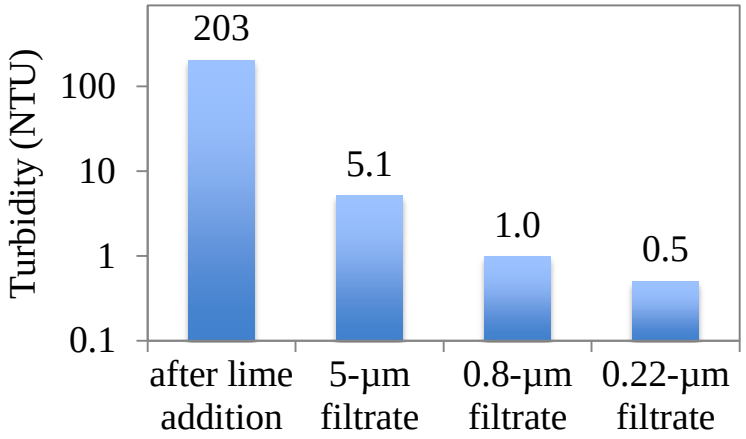

Figure 4-12. Turbidity of solution B (**Table 4-1**) after lime dose treatment (2.7 mM) and subsequent microfiltration.

4.4 Conclusions and recommendations

Removal of dissolved antiscalant from RO concentrate was shown to be feasible via initial lime treatment prior to seeded gypsum precipitation for concentrate desupersaturation, enabling enhanced product water recovery via secondary RO desalting. Microfiltration of the treated concentrate effectively reduced its turbidity to a level suitable for secondary RO desalination. This chemically-enhanced seeded precipitation process is suitable for intermediate concentrate demineralization in RO desalination of brackish water of high gypsum scaling propensity.

Analysis of gypsum precipitation and lime treatment kinetic data suggests that, after adequate $CaCO_3$ precipitation has been induced for effective AS scavenging, $CaSO_4$

desupersaturation can be achieved via seeded gypsum precipitation without retardation due to seed poisoning by AS. Also, the lime dose required to prevent seed poisoning during subsequent gypsum desupersaturation via seeded gypsum precipitation can be adequately assessed with a precipitation kinetics model that considers AS seed poisoning based on a Langmuir adsorption isotherm. The degree of AS removal after lime treatment increased linearly with the logarithm of the single lime dose additions. Antiscalant removal was attributed to adsorption onto and incorporation within precipitated $CaCO_3$ particles that increased in number and volume concentrations with increasing lime dose. It is noted that $CaCO_3$ particle size decreased with increasing antiscalant concentration due to increased adsorption of the polyelectrolyte antiscalant onto the precipitated particles which both reduced diffusional growth and enhanced particle dispersion. Staged lime dosing of 0.1 g/L lime via multiple additions was found to remove a higher fraction (87%) of residual antiscalant relative to an equivalent single lime dose addition (68% removal) since a higher average *SIc* was maintained during the lime treatment period. An approach was developed, based on available gypsum precipitation kinetics and lime treatment data, to estimate the minimum single lime dose required for sufficient antiscalant removal from the RO concentrate to prevent seed poisoning and allow effective gypsum desupersaturation via gypsum seeding.

References

1. Committee on Advancing Desalination Technology, Water Science and Technology Board, and National Research Council, *Desalination: A National Perspective*. 2008, Washington, DC: National Academies Press.
2. Bond, R. and S. Veerapaneni, *Zero Liquid Discharge for Inland Desalination*. 2007, Denver, CO: AWWA Research Foundation, AWWA, & IWA Publishing.
3. Mickley, M.C., *Membrane concentrate disposal: practice and regulation*. 2006, Mickley & Associates, US Bureau of Reclamation: Denver, CO.
4. Lee, R.-W., J. Glater, Y. Cohen, C. Martin, K. Kovac, M.N. Milobar, and D.W. Bartel, *Low-pressure RO membrane desalination of agricultural drainage water.* Desalination, 2003. **155**(2): p. 109-120.
5. McCool, B.C., A. Rahardianto, J. Faria, K. Kovac, D. Lara, and Y. Cohen, *Feasibility of reverse osmosis desalination of brackish agricultural drainage water in the San Joaquin Valley.* Desalination, 2010. **261**(3): p. 240-250.
6. Rahardianto, A., B.C. McCool, S. Rezvani, and Y. Cohen. *High recovery desalination of agricultural drainage water: integration of accelerated chemical precipitaion with RO membrane desalination*. in *Procedings of the AIChE Annual Conference*. 2005. Cincinnati, OH.
7. Zhu, A., A. Rahardianto, P.D. Christofides, and Y. Cohen, *Reverse osmosis desalination with high permeability membranes—Cost optimization and research needs.* Desalination and Water Treatment, 2010. **15** p. 256-266.
8. Almulla, A., M. Eid, P. Côté, and J. Coburn, *Developments in high recovery brackish water desalination plants as part of the solution to water quantity problems.* Desalination, 2003. **153**(1-3): p. 237-243.
9. Bremere, I., M.D. Kennedy, A. Johnson, R. van Emmerik, G.J. Witkamp, and J.C. Schippers, *Increasing conversion in membrane filtration systems using a desupersaturation unit to prevent scaling.* Desalination, 1998. **119**(1-3): p. 199-204.
10. Gabelich, C.J., M.D. Williams, A. Rahardianto, J.C. Franklin, and Y. Cohen, *High-recovery reverse osmosis desalination using intermediate chemical demineralization.* Journal of Membrane Science, 2007. **301**(1-2): p. 131-141.
11. Rahardianto, A., J. Gao, C.J. Gabelich, M.D. Williams, and Y. Cohen, *High recovery membrane desalting of low-salinity brackish water: Integration of accelerated precipitation softening with membrane RO.* Journal of Membrane Science, 2007. **289**(1-2): p. 123-137.
12. Sanciolo, P., L. Zou, S. Gray, G. Leslie, and D. Stevens, *Accelerated seeded precipitation pre-treatment of municipal wastewater to reduce scaling.* Chemosphere, 2008. **72**(2): p. 243-249.
13. Ning, R.Y., A. Tarquin, M. Trzcinski, and G. Patwardhan, *Recovery optimization of RO concentrate from desert wells.* Desalination, 2006. **201**(1-3): p. 315-322.
14. Rahardianto, A., B.C. McCool, and Y. Cohen, *Accelerated Desupersaturation of Reverse Osmosis Concentrate by Chemically-Enhanced Seeded Precipitation.* Desalination, 2010. **264**(3).
15. Kedem, O. and G. Zalmon, *Compact accelerated precipitation softening (CAPS) as a pretreatment for membrane desalination I. Softening by NaOH.* Desalination, 1997. **113**(1): p. 65-71.

16. U.S. Geological Survey, Mineral commodity summaries 2011: U.S. Geological Survey, 198 p.
17. Greenlee, L.F., F. Testa, D.F. Lawler, B.D. Freeman, and P. Moulin, *The effect of antiscalant addition on calcium carbonate precipitation for a simplified synthetic brackish water reverse osmosis concentrate.* Water Research, 2010. **44**(9): p. 2957-2969.
18. Yang, Q., Z. Ma, D. Hasson, and R. Semiat, *Destruction of anti-scalants in RO concentrates by electrochemical oxidation.* J. Chem. Ind. Eng. (China), 2004. **55**(2): p. 339-340.
19. Yang, Q.F., D. Lisitsin, Y.Q. Liu, H. David, and R. Semiat, *Desupersaturation of RO concentrates by addition of coagulant and surfactant.* J. Chem. Eng. Japan, 2007. **40**(9): p. 730-735.
20. Yang, Q., Y. Liu, D. Hasson, and R. Semiat, *Removal of CaCO3 Scaling Salt from RO Concentrates by Air-Blow and Inorganic Inducers.* Journal of Chemical Engineering of Japan, 2008. **41**(1): p. 13-20.
21. Yang, Q.F., Y.Q. Liu, H. David, and R. Semiat, *Scaling salt removal by addition of inorganic particles.* J. Chem. Eng. Japan, 2008. **41**(1): p. 6-12.
22. Yasunaga, N., S. Furukawa, Y. Kawaai, and J. Hirotsuji, *Investigation of radical reactions for efficiency improvement in ozone-hydrogen peroxide treatment.* Water Science and Technology, 2001. **43**(2): p. 205-2112.
23. Gabelich, C.J., W.R. Chen, T.I. Yun, B.M. Coffey, and I.H. Suffet, *The Role of Dissolved Aluminum in Silica Chemistry for Membrane Processes.* Desalination, 2005. **180**: p. 307-319.
24. Gabelich, C.J., K.P. Ishida, F.W. Gerringer, R. Evangelista, M. Kalyan, and I.H. Suffet, *Control of residual aluminum from conventional treatment to improve reverse osmosis performance.* Desalination, 2006. **190**(1-3): p. 147-160.
25. Kim, M.-m., J. Au, A. Rahardianto, J. Glater, Y. Cohen, F.W. Gerringer, and C.J. Gabelich, *Impact of Conventional Water Treatment Coagulants on Mineral Scaling in RO Desalting of Brackish Water.* Ind. Eng. Chem. Res., 2009. **48**(6): p. 3126-3135.
26. Shih, W.-Y., J. Gao, A. Rahardianto, J. Glater, Y. Cohen, and C.J. Gabelich, *Ranking of antiscalant performance for gypsum scale suppression in the presence of residual aluminum.* Desalination, 2006. **196**(1-3): p. 280-292.
27. Hua, G. and D.A. Reckhow, *Comparison of disinfection byproduct formation from chlorine and alternative disinfectants.* Water Research, 2007. **41**(8): p. 1667-1678.
28. Krasner, S.W., *The formation and control of emerging disinfection by-products of health concern.* Philosophical Transactions of the Royal Society a-Mathematical Physical and Engineering Sciences, 2009. **367**(1904): p. 4077-4095.
29. Wert, E.C., F.L. Rosario-Ortiz, D.D. Drury, and S.A. Snyder, *Formation of oxidation byproducts from ozonation of wastewater.* Water Research, 2007. **41**(7): p. 1481-1490.
30. Bob, M. and H.W. Walker, *Enhanced adsorption of natural organic matter on calcium carbonate particles through surface charge modification.* Colloids and Surfaces A: Physicochemical and Engineering Aspects, 2001. **191**(1-2): p. 17-25.
31. Clarkson, J.R., T.J. Price, and C.J. Adams, *Role of Metastagle Phases in the Spontaneous Precipitation of Calcium Carbonate.* J. Chem. Soc. Faraday Trans., 1992. **88**(2): p. 243-249.
32. Liao, M.Y. and S.J. Randtke, *Predicting the removal of soluble organic contaminants by lime softening.* Water Research, 1986. **20**(1): p. 27-35.

33. Meldrum, F.C. and H. CoÌˆlfen, *Controlling Mineral Morphologies and Structures in Biological and Synthetic Systems.* Chemical Reviews, 2008. **108**(11): p. 4332-4432.
34. Naka, K., S.-C. Huang, and Y. Chujo, *Formation of Stable Vaterite with Poly(acrylic acid) by the Delayed Addition Method.* Langmuir, 2006. **22**(18): p. 7760-7767.
35. OLI Systems Inc., *Stream Analyzer 3.1*. 2007: Morris Plains, NJ.
36. Shugar, G.J., D.A. Drum, S.L. Bauman, and J. Lauber, *Environmental Field Testing and Analysis Ready Reference Handbook*, ed. K. McCombs and S. Souffrance. 2000: McGraw-Hill.
37. Ouhenia, S., D. Chateigner, M.A. Belkhir, E. Guilmeau, and C. Krauss, *Synthesis of calcium carbonate polymorphs in the presence of polyacrylic acid.* Journal of Crystal Growth, 2008. **310**(11): p. 2832-2841.
38. Nason, J.A. and D.F. Lawler, *Particle size distribution dynamics during precipitative softening: Declining solution composition.* Water Research, 2009. **43**(2): p. 303-312.
39. Sawada, K., N. Abdel-Aal, H. Sekino, and K. Satoh, *Adsorption of inorganic phosphates and organic polyphosphonate on calcite.* Dalton Transactions, 2003(3).
40. Suzuki, T., S. Inomata, and K. Sawada, *Adsorption of phosphate on calcite.* Journal of the Chemical Society, Faraday Transactions 1: Physical Chemistry in Condensed Phases, 1986. **82**(6).
41. Yuan, P.-Q., N. Kong, Z.-M. Cheng, and R. Semiat, *Electrostatic potential on anti-scalants modified CaCO3 (104) surface: A molecular simulation study.* Desalination, 2009. **238**(1–3): p. 246-256.
42. Jaroslav, N., *Kinetics of nucleation in solutions.* Journal of Crystal Growth, 1968. **3–4**(0): p. 377-383.
43. Lyster, E., M.-m. Kim, J. Au, and Y. Cohen, *A method for evaluating antiscalant retardation of crystal nucleation and growth on RO membranes.* Journal of Membrane Science, 2010. **364**(1-2): p. 122-131.
44. Christoffersen, M.R., J. Christoffersen, M.P.C. Weijnen, and G.M. Van Rosmalen, *Crystal growth of calcium sulphate dihydrate at low supersaturation.* Journal of Crystal Growth, 1982. **58**(3): p. 585-595.
45. Nancollas, G.H., *The growth of crystals in solution.* Advances in Colloid and Interface Science, 1979. **10**(1): p. 215-252.
46. Ben Ahmed, S., M.M. Tlili, and N. Ben Amor, *Influence of a polyacrylate antiscalant on gypsum nucleation and growth.* Crystal Research and Technology, 2008. **43**(9): p. 935-942.
47. Gloede, M. and T. Melin, *Potentials and limitations of molecular modelling approaches for scaling and scale inhibiting mechanisms.* Desalination, 2006. **199**(1–3): p. 26-28.
48. Boels, L., T. Tervahauta, and G.J. Witkamp, *Adsorptive removal of nitrilotris(methylenephosphonic acid) antiscalant from membrane concentrates by iron-coated waste filtration sand.* Journal of Hazardous Materials, 2010. **182**(1–3): p. 855-862.
49. Rahardianto, A., B.C. McCool, and Y. Cohen, *Reverse osmosis desalting of inland brackish water of high gypsum scaling propensity: Kinetics and mitigation of membrane mineral scaling.* Environmental Science & Technology, 2008. **42**(12): p. 4292-4297.
50. Hydranautics, *Element Spec Sheet LFC3-LD*. 2011.

Chapter 5

Field validation and economic feasibility of RO concentrate demineralization via chemically-enhanced seeded precipitation

5.1 Overview

Development of new water sources is crucial in order to address the crisis of dwindling water supplies in California and around the globe. In this regard, reverse osmosis (RO) desalination is a technology that is now in common practice for developing new water sources via desalting of seawater [1-3], brackish surface water and groundwater [4-9], as well as municipal wastewater [10-13]. The growth of the RO desalination market has been spurred by advances in reverse osmosis (RO) technology that have led to significant reduction in the production cost of water desalination [14]. It is noted that RO desalination of brackish water is also viewed as a potential solution for confronting the rising salinity of agricultural drainage (AD) water, which is a major threat to the economy throughout California's agricultural heartland in the San Joaquin Valley (SJV) [9]. While RO is considered a mature technology, its application for desalination of brackish water remains challenging due to the high costs associated with residual RO concentrate disposal and membrane mineral scaling, thus preventing wide-spread use of RO technology for inland brackish water desalination [15-17]. Gypsum membrane mineral scaling in particular is a major concern for AD water and other inland water sources [9].

Previous methods attempting to partially overcome the problem of mineral scaling in brackish water RO desalting have relied on operation at low recovery levels and chemical feed conditioning (e.g., pH adjustment and use of antiscalants) both leading to high operational cost and a large volume of residual concentrate. As a consequence, traditional RO desalination approaches are limited with respect to the achievable product water recovery due to mineral

scaling that ensues once the recovery exceeds the saturation threshold of sparingly soluble mineral salts (e.g., calcium sulfate, calcium carbonate, calcium phosphate, and barium sulfate). For example, it has been reported that product water recovery is limited to ~40–60% for most brackish water sources in the SJV [18]. However, it has also been argued that high recovery operation (above ~85%–95%) is essential for inland water desalting of brackish groundwater, AD water, as well as in municipal wastewater reuse applications, in order to reduce the volume of generated residual concentrate and reduce the overall process cost.

High recovery desalination via RO with intermediate concentrate demineralization (ICD) has been proposed as a promising method to address the challenge of managing high salinity drainage water (e.g., mine drainage, AD, dumpsite leachate) with high mineral scaling propensity at inland locations [12, 19-24]. In the ICD approach to high recovery RO desalination, brackish water is first desalted in a primary RO (PRO) stage up to the PRO product water recovery limit imposed by membrane mineral scaling followed by PRO concentrate treatment (ICD) to reduce scale precursor (e.g., calcium, sulfate, carbonate, phosphate) concentrations, thus reducing the scaling propensity of the PRO concentrate. The treated PRO concentrate is filtered to remove solids and then further desalted in an SRO stage to achieve the desired overall recovery (**Fig. 5-1**). The overall PRO-ICD-SRO process can reach product water recoveries of up to 85–98%, minimizing the volume of the residual RO concentrate waste [21, 22, 25]. ICD via alkaline-induced precipitation of $CaCO_3$ from PRO concentrate (i.e., precipitation softening) has been successfully demonstrated in a number of laboratory [8, 13, 26-29] and pilot-scale studies [22, 23, 25, 30] for treating brackish water of sufficient bicabonate content to remove calcium via $CaCO_3$ precipitaiton, thereby reducing the gypsum scaling propensity. However, ICD via precipitation softening (PS) is often chemically-intensive for

bicarbonate-lean brackish waters since the addition of an alkaline chemical containing bicarbonate (e.g., soda ash) is required to sufficiently deplete calcium concentration via $CaCO_3$ precipitation [19, 21, 31].

ICD may also be carried out via seeded gypsum precipitation (SGP) [19, 21, 32, 33] in which gypsum seeds are added to the supersaturated PRO concentrate to induce gypsum precipitation in order to achieve PRO concentrate desupersaturation. In the SGP process, the rate of gypsum precipitation depends on the gypsum saturation level (i.e., *SIg*) [21]. However, gypsum precipitation kinetics are significantly reduced by AS carry-over present in PRO concentrate [21]. It has also been suggested that AS adsorbtion onto the gypsum seed surfaces inhibits heterogeneous gypsum crystal growth (i.e., seed poisoning), and thus retards PRO concentrate desupersaturation [34]. For example, previous work has demonstrated that AS (3 mg/L polyacrylic acid in the concentrate) can reduce the rate of gypsum precipitation by ~65% [21]. Clearly, in order to successfully implement an SGP process for RO concentrate desupersaturation, AS-action inhibition of gypsum precipitation must be counteracted prior to SGP treatment.

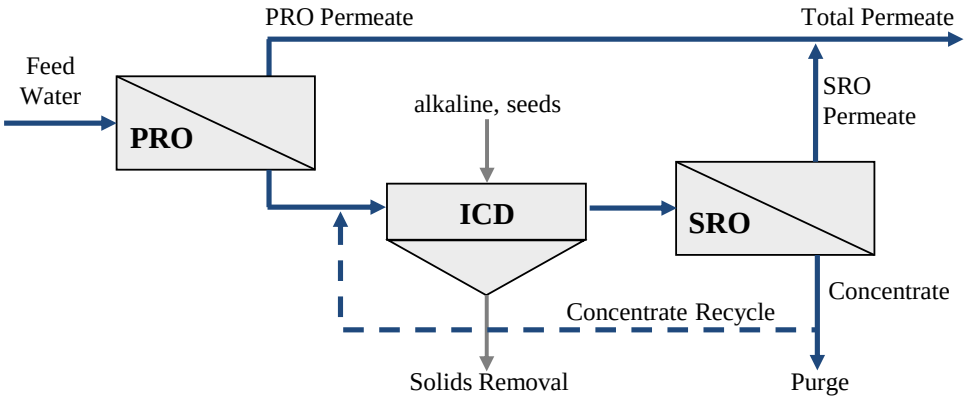

Figure 5-1. High recovery RO process utilizing intermediate concentrate demineralization (ICD) treatment of primary RO (PRO) prior to secondary RO (SRO) desalination.

Previous work [21, 34] has demonstrated that minimal alkaline use (0.25 g/L lime) during chemically-enhanced seeded precipitation (CESP) (i.e., the sequential combination of PS and SGP) can prevent gypsum seed poisoning by AS in the demineralization of AS-containing model PRO concentrate solution (*SIg* = 2.5, 3 mg/L AS). It was reported that lime-induced $CaCO_3$ precipitation removed up to ~90% of the AS in model RO concentrate solution for the case of nearly gypsum-saturated RO feed water (*SIg* = 0.96, *SIc* = 3) studied previously [34], thereby facilitating subsequent $CaSO_4$ precipitation with minimal retardation due to AS-action [21, 34]. Using the above approach it was suggested that, for the above source water, the PRO-CESP-SRO process could enhance overall water recovery to > 85%.

Whereas previous work explored the CESP process with model solutions, the goal of the present work was to: (a) demonstrate the feasibility of the CESP process in the field and, (b) to assess the economics of the process, focusing on the challenge of high recovery desalting of AD water in California's SJV [34, 35]. CESP process performance was quantified by the extent of gypsum precipitation and the degree of desupersaturation (i.e., final gypsum saturation level) achieved during gypsum-seeded precipitation with various degrees of lime pretreatment (i.e., lime dose). The attainable overall recovery level was assessed for the RO desalination process with integrated ICD based on the CESP performance demonstrated in the field study (i.e., *SIg* ≈ 1.1 after CESP). The attainable overall water recovery was based on PRO operation at a recovery corresponding to an *SIg* = 2.5 in the PRO concentrate, followed by desupersaturation during ICD to *SIg* = 1.1, and then SRO operation at a recovery corresponding to an *SIg* = 2.5 in the SRO concentrate. Additionally, the cost of RO desalination with integrated CESP (i.e., PRO-CESP-SRO) was estimated and compared to the cost of direct concentrate (i.e., brine) disposal (no treatment), stand-alone RO desalination, and high recovery desalination via PS.

5.2 Materials & methods

5.2.1 Materials

A phosphonate-based polymeric AS stock solution (PC-504T, Nalco Co., Naperville, IL) was utilized for suppressing gypsum scale formation in a pilot spiral-wound RO system during field testing. Reagent-grade lime powder (Sigma Aldrich, St. Louis, MO) was utilized for preparation of 25–35 g/L lime slurries in DI water for use in the CESP lime pretreatment step. Gypsum powder (42 μm modal spherical diameter, analytical grade) obtained from J.T. Baker (Phillipsburg, NJ) was used to seed gypsum precipitation in CESP. Calcium ion calibration solutions were prepared using reagent grade $CaCl_2 \cdot 2H_2O$ and NaCl (Fisher Scientific, Pittsburgh, PA). Cleaning solutions were composed of 5% acetic acid. Spiral-wound RO elements were 2.5 inches in diameter and 40 inches long (XLE 2540 elements, DOW FilmTec Corp., Minneapolis, MN) with an observed salt rejection of 98% and permeability of 4.57 $L \cdot m^{-2} \cdot hr^{-1} \cdot bar^{-1}$.

5.2.2 RO desalination pilot and crystallizer

RO concentrate was generated using a pilot-scale Mini-Mobile-Modular (M3) RO system [36, 37]. The system was equipped with six spiral-wound RO membrane elements each in separate pressure vessels arranged in series. The feed was supplied to the RO membranes using two high-pressure positive displacement pumps in parallel (Danfoss Model CM 3559, 3 hp, 3450 rpm, Baldor Reliance Motor, Sea Recovery Corp., Carson, California), each capable of providing up to 16 L/min (4.3 gal/min) at 68.9 bar (1000 psi) [36, 37]. Feed pretreatment consisted of media filtration (0.85-mm sand) followed by 5, 0.45, and 0.2 μm cartridge filtration (Cole Parmer Instrument Co., Vernon Hills, IL) to remove suspended solids prior to RO desalting.

RO concentrate demineralization was performed via CESP in a 20-L rectangular stirred-tank batch crystallizer at room temperature (~23 °C) with continuous monitoring of calcium ion activity, pH, and temperature. The crystallizer was 33 cm deep with a 76 cm square base (Nalgene, Thermo Fisher Scientific, Rochester, NY) and was equipped with an electric mixer (Model 71636819, 1/20 hp, 1550 rpm, Neptune Mixer Company, North Wales, PA) with a 70-cm shaft (8-mm diameter) and a 3-blade (76 mm diameter) axial flow impeller situated 5 cm above the crystallizer base. Online monitoring of pH and calcium ion activity in the crystallizer was accomplished using a calcium ion selective electrode (ISE25Ca-9/REF251) and a pH electrode (pHG211-8/REF201) from Radiometer Analytical (Lyon, France) connected, respectively, to a sensION4 meter (Hach Co., Loveland, CO) and an Orion 720Aplus meter (Thermo Scientific, Waltham, MA). Solution temperature in the crystallizer was recorded using a Hach temperature probe (Model 51980-00, Hach Co., Loveland, CO) connected to the sensION4 meter (Hach Co., Loveland, CO).

5.2.3 Field test site and generation of RO concentrate

The field study was conducted at the Panoche Drainage District DP-25 test site [38] (10 miles west of Firebaugh, CA) in the central SJV (**Fig. 5-2**) with source AD water with a salinity of 14,440 mg/L total dissolved solids (TDS) which was nearly saturated with respect to gypsum (SIg = 0.94) and carbonate lean (**Table 5-1)**. Previous field studies have indicated that membrane gypsum scaling, for this high scaling propensity AD water, was the primary challenge of RO desalting of DP-25 source water [39], making the site particularly suitable for assessing the PRO-CESP-SRO process. The recovery limit for brackish water RO desalination at DP-25 was defined as the recovery at which the RO concentrate concentration was just below the threshold

of membrane mineral scaling, following a previously developed approach [9]. The membrane scaling thresholds at the DP-25 location were based on mineral salt saturation indices (defined as $SIx = IAPx/Ksp,x$, where $IAPx$ and Ksp,x are the ion activity and solubility products, respectively, of mineral salt x) calculated using multi-electrolyte thermodynamic simulation software [40]. Taking the gypsum saturation index (SIg) of 2.5 as the gypsum scaling threshold with AS treatment [41] the RO recovery limit for desalting the nearly gypsum saturated DP-25 brackish water (SIg = 0.94) was estimated to be in the range of 62–65%, based on historical DP-25 source water quality data (**Table 5-1**) [38].

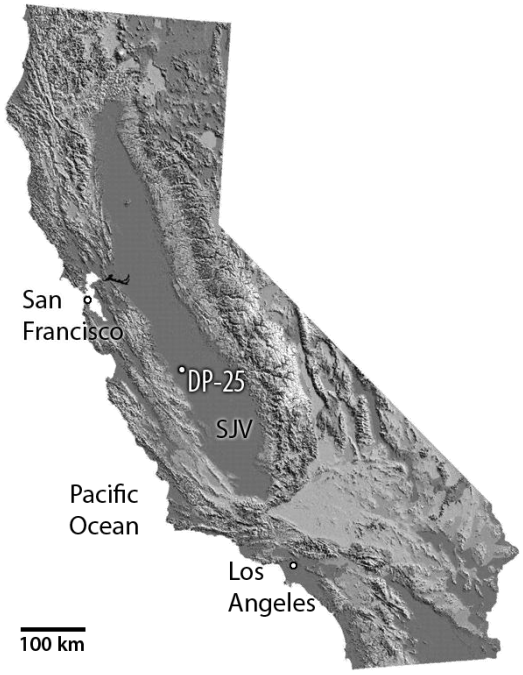

Figure 5-2. DP-25 field test site in Central California's San Joaquin Valley. Adapted from [9].

RO concentrate for CESP treatment was generated using the M3 RO pilot system, operated at a feed flow rate of 0.54 m^3/hr (3500 gal/day) and feed AS dose of 3 mg/L (PC-504T). Although operation of the M3 RO system at or near the water recovery limit (imposed by mineral scaling) of 62–65% was feasible with real-time membrane scale monitoring [42], a

conservative target water recovery range of 52–54% was adopted in the present work. At this range of conservative RO water recovery the CESP process was challenged by limiting the initial gypsum supersaturation in the primary RO concentrate to $SIg \approx 1.7$ and thus the available driving force for concentrate desupersaturation. The RO concentrate contained 6.3 mg/L AS (based on a feed dose of 3 mg/L). Field water sampling and laboratory water quality analysis of RO feed and primary RO concentrate (**Table 5-1**) were conducted by the California Department of Water Resources (Bryte Laboratory, West Sacramento, CA).

Table 5-1. Summary of water quality data from the field demonstration of CESP for high recovery desalination of AD water (DP-25 field location, see **Fig. 5-1**).

Analyte	Unit	Observed range [a]	RO Feed	RO concentrate 52.3% *Y*	CESP-treated (L) [b]	CESP-treated (H)[b]
Conductance (EC)	µS/cm		14810	21370	22320	21350
pH	pH units		7.5	7.6	8.4	8.6
Dissolved Analytes						
Boron	mg/L		38.9	47.6	45.9	46.6
Calcium	mg/L	480–590	509	897	606	595
Chloride	mg/L	960–2200	2650	4440	4430	4410
Magnesium	mg/L	190–380	455	879	831	815
Ortho-phosphate	mg/L as P		0.07	0.09	0.05	0.05
Potassium	mg/L	3–6.9	7.6	13.8	12.3	11
Selenium	mg/L		1.68	2.72	2.66	2.64
Silica (SiO_2)	mg/L	28–45	34.6	71.7	70.8	69.5
Sodium	mg/L	1400–3300	3890	6750	6630	6640
Sulfate	mg/L	3500–5900	6660	12400	11500	11500
Total Analytes						
Bicarbonate	mg/L	220–260	235	491	313	241
Barium	mg/L		0.5 [c]	1 [c]	1 [c]	1 [c]
TDS	mg/L	6700–13000	14,440	19,910	21,200	20,000
Selenium	mg/L		1.75	2.86	2.88	2.76
Strontium	mg/L		8.85	16.1	13.1	13
SI calcite		2.46–3.35 [d]	3.14	9.57	25.8	29.6
SI gypsum		0.85–0.97	0.94	1.71	1.15	1.13
SI silica		0.26–0.37	0.29	0.58	0.36	0.28

[a] Range of water quality observed at DP-25 between 2/15/2005 and 4/28/2009.
[b] CESP treated PRO concentrate samples with either low (L, 0.25 g/L) or high (H, 0.35 g/L) lime doses.
[c] Measured value is at or below detection limit.
[d] Calculated at pH = 7.5.

5.2.4 Chemically-enhanced seeded precipitation experiments

Each batch CESP run in the 20-L crystallizer commenced with a lime pretreatment period to allow for AS scavenging [21, 34], followed by SGP for concentrate desupersaturation. Lime pretreatment was initiated by adding 5–7 g lime (0.25–0.35 g/L) to 20 L of RO concentrate. At the end of the lime pretreatment period (20 min), SGP was induced by adding 5 g/L gypsum powder into the crystallizer. At the termination of CESP treatment, concentrate samples were collected and filtered using 0.2-μm filters (Millipore, Billerica, MA) prior to water quality analysis (**Table 5-1**). Online measurements of calcium activity and pH during the CESP process, along with the knowledge of the solution's initial composition (**Table 5-1**), were utilized for chemical equilibrium analysis [40] to quantify precipitation-induced changes of ion concentrations and mineral saturation indices, as described elsewhere [21, 31].

5.2.5 Estimation of AS removal

The level of AS removal after the lime treatment step of CESP was assessed using a previously proposed model [34] that describes gypsum precipitation as it is impacted by seed poisoning due to AS adsorption following a Langmuir adsorption isotherm. Briefly, in this approach, the initial rate of gypsum precipitation, upon gypsum seeding (initial ~2.5 min), was estimated based on second order reaction kinetics [43, 44] defined as $r = -dC/dt = k \cdot S_A \cdot \left(C - C_S\right)^2$, where r is the rate of gypsum precipitation (mol L^{-1} min^{-1}), k is the precipitation reaction rate constant (L^2 mol^{-1} m^{-2} min^{-1}) for heterogeneous gypsum growth, S_A is the total active surface area (m^2 L^{-1}) available for crystal growth, and C and C_S are the time varying and saturation calcium ion concentrations (mol L^{-1}), respectively. Given the reasonable assumption that the change in gypsum seed surface area, S_{A0}, is small during the initial period of

gypsum precipitation, the apparent rate constant, $k' = k \cdot S_{A0}$, can be estimated from the integrated form of the above rate equation as $k' \cdot (C_0 - C_S) \cdot t = (C_0 - C) / (C - C_S)$. In previous work [34] it was shown that the apparent precipitation rate constant decreases with increasing AS concentration due to AS adsorption onto the mineral crystal, thereby reducing the available area for surface growth (i.e., seed poisoning). The fractional crystal seed area (θ) occupied by AS was determined from: $k' / k'_{AS-free} = 1 - \theta$ where k' and $k'_{AS-free}$, are the apparent rate constants in the presence and absence of residual AS, respectively. The residual AS concentration remaining in the lime-treated concentrate (C_{AS}) relative to the untreated concentrate ($C_{AS,0}$) was then estimated based on a relationship between the fractional seed area occupied by AS before (θ_0) and after (θ) lime treatment, $C_{AS} / C_{AS,0} = \theta / \theta_0 \cdot (1 - \theta_0) / (1 - \theta)$ [34].

5.3. Economic analysis

In order to determine the economic feasibility of RO desalination of brackish AD water in the SJV (at the DP-25 location), the cost of managing (treating and/or disposing of) AD water ($/m^3-AD water feed) was estimated for a flow capacity of 10 million gallons per day (MGD). Four scenarios were considered for AD water management: (1) direct disposal (no desalination), (2) stand-alone RO desalination, (3) high recovery desalination via PS, and (4) high recovery desalination via CESP. Note that the above three scenarios utilizing RO desalination also included the cost of concentrate disposal. The 10-MGD flow capacity would represent the capacity for distributed treatment plants for handling an estimated total 67–134 MGD of brackish AD water scattered across the SJV [9, 39].

Process simulations were carried out for the economic analysis for the RO, PRO-CESP-SRO, and PRO-PS-SRO scenarios with a feed solution representative of the range of water

quality observed at the DP-25 location (**Table 5-1**). All stream properties (e.g., osmotic pressure, *SIg*) were determined using a multielectrolyte process simulator [40]. The economic analysis was thus carried out for the representative AD water as a base case with key properties (11,000 mg/L TDS, *SIc* = 3.0 and *SIg* = 0.96) within the range observed at DP-25 since 2006. The representative AD water contained calcium, magnesium, sodium, sulfate, bicarbonate, and chloride ions at concentrations of 11.5, 11.7, 121, 66.2, 4.26, and 30.7 mM (462, 284, 2780, 6360, 260, and 1087 mg/L), respectively. Costs were also estimated at the lowest and highest observed salinities to determine the impact of salinity on the cost of desalination (**Table 5-3**). The cost of the AD water desalination process included: (a) operating and maintenance (O&M) costs consisting of electrical energy use, labor, maintenance, chemicals, RO membrane replacement, and pretreatment; and (b) capital costs of the PRO, SRO, and ICD units including pumps, membranes, pressure vessels, and associated infrastructure.

The capital and O&M costs for the PRO, SRO, pretreatment (MF and ferric chloride coagulation), and chemical dosing were estimated using cost estimation software from USBR [45] and specific costs are itemized in **Table 5-2**. The capital costs of ICD were also estimated using the USBR software, however, the chemical O&M costs of ICD were calculated separately and included the required alkaline dosing (lime or soda ash), and gypsum seeding, with unit costs (in US dollars) of $112/short ton (lime), $285/short ton (soda ash), $30/metric ton (gypsum), respectively [46]. The required soda ash dose for precipitation softening was estimated, following the method developed previously [22], as the dose required to precipitate sufficient calcium to reduce the feed *SIg* and allow SRO to operate up to the required recovery level while remaining at or below a specified gypsum scaling threshold (*SIg* = 2.5) [41]. Chemical requirements considered for the CESP process covered a range of possible lime doses (0.25–0.55

g/L) and make-up gypsum seed doses (1–10 g/L). The lower lime dose (0.25 g/L) was selected as it was the lowest effective dose demonstrated in the present study (**§5.3.2**), while the higher lime dose (0.55 g/L) was selected to accommodate concentrate water that could potentially contain higher residual AS or higher natural organic matter (NOM) concentrations, thus necessitating a greater amount of $CaCO_3$ precipitation during lime treatment for AS removal. It is noted that gypsum seeding is required only as make-up for gypsum particles that would be purged from the crystallizer since gypsum seeds remain in solution for extended time periods in a continuous process. Energy cost was taken as the average industrial price for electricity in California, 0.11 $/kW-h [47]. The PS process had a single vessel (602 m^3) with a 60 min residence time while the CESP process had two vessels in series with residence times of 20 min and 60 min, respectively, for lime pretreatment and gypsum-seeded precipitation. PRO and SRO energy costs were estimated based on the assumption that the RO units would operate at a feed pressure that is equal to the osmotic pressure of the concentrate stream, representing the minimum energy required to operate cross-flow RO (i.e., at the thermodynamic restriction) [48]. All costs were adjusted to 2012 US dollar values based on the Bureau of Labor Statistics inflation calculator [49] and capital costs were annualized based on 30-year amortization with 4.25% interest. The above costs are summarized in **Table 5-2**.

Table 2. Itemized costs used in the analysis of brackish water management costs.

Consumable	Cost	Unit	
electricity	0.11	$/kWh	
AS, PC-504T	44	$/gal	
lime, $Ca(OH)_2$	112	$/short ton	
soda ash, Na_2CO_3	285	$/short ton	
gypsum	30	$/metric ton	
RO elements [a]	629	$/element	FilmTec BW30-400
MF membrane [a]	650	$/element	US Filter 90M10C

[a] RO and MF elements were assumed to have lives of 3 and 10 years, respectively.

5.4 Results and discussion

5.4.1 RO concentrate desupersaturation by CESP

The feasibility of applying the CESP process to field generated RO concentrate was demonstrated with RO concentrate generated from AD water (**Table 5-1**) via desalination by a spiral-wound RO pilot operation at 52.3% recovery with raw feed dosed with 3 ppm AS (**§5.2.3**). The lime dose during the initial lime treatment period (~20 min) was set at 0.25 g/L. This lime dose was previously reported to be effective for reducing the residual AS concentration from the RO concentrate (generated from raw feed of similar gypsum saturation level and bicarbonate level) by >95% [21, 34], thereby enabling SGP. As illustrated in **Fig. 5-3**, for a lime dose of 0.25 g/L and gypsum seeding of 5 g/L (20 min after lime addition) there is a significant initial rise in the calcite saturation index (from ~9.6 to ~206) during the lime treatment period due to initial lime addition and a subsequent decline as $CaCO_3$ precipitation ensues [21, 28, 34]. It is during the lime treatment step that the majority of residual AS is scavenged (see **§5.1**) owing to the rapid nucleation and precipitation of $CaCO_3$. AS removal in the initial lime treatment step then allows for significant reduction (~29%) in gypsum saturation index (from 1.63 to 1.15) during the subsequent SGP period (t > 20 min). Following the method described in **§5.2.4** [34], it was estimated that lime treatment prior to SGP reduced AS concentration to < 2% of its concentration in the PRO concentrate (6.3 mg/L PC-504T). This level of AS removal was consistent with the ~95% reduction in AS concentration reported previously [34] for synthetic PRO concentrate solutions of similar *SIc* and *SIg* levels, as well as concentrations of sulfate and bicarbonate ions.

While the decline in *SIg* and *SIc* is indicative of the degree of desupersaturation with respect to $CaSO_4$ and $CaCO_3$, it is convenient to describe the precipitation kinetics of these mineral salts in terms of the extent of precipitation defined as:

$$\alpha_m = \frac{[m]_0 - [m]}{[m]_0 - [m]_{eq,x}} \quad (1)$$

where $[m]$, $[m]_0$ and $[m]_{eq,x}$ are the molar concentrations of ion *m* (e.g., carbonate, sulfate) unique to the precipitating mineral salt *x* (e.g., calcite, gypsum), respectively, at time *t*, *t* = 0 (i.e., initial) and at equilibrium with respect to mineral salt *x* containing ion *m*. As shown in **Fig. 5-3c**, the carbonate extent of reaction, $\alpha_{carbonate}$, increased rapidly upon lime addition (0.25 g/L) reaching a value of ~0.5 within 2 min. The rapid initial rise of $\alpha_{carbonate}$ (upon lime addition) is attributed to $CaCO_3$ nucleation and growth [21] and substantial $CaCO_3$ precipitation continued throughout the lime treatment period with $\alpha_{carbonate}$ increasing an additional 20% (up to $\alpha_{carbonate}$ = 0.59) at the end of the lime treatment period (i.e., *t* = 20 min). It is noted that the mass of $CaCO_3$ precipitate (315 mg/L) after lime pretreatment (0.25 g/L) was consistent (within 8%) with that observed in previous work (341 mg/L) with synthetic RO concentrate (11,020 mg/L TDS, *SIg* = 0.96, *SIc* = 3.9) at the same pretreatment conditions [34]. The mass of precipitated $CaCO_3$ was calculated based on calcium ion activity measurements and solution pH (**§5.2.3**) [40]. The corresponding mass of gypsum precipitated after SGP with 5 g/L gypsum seeds was 932 mg/L and there was no detectable gypsum precipitation during lime pretreatment. The growth of $CaCO_3$ particles continued to a small degree after the initial lime treatment period (*t* > 20 min), as shown previously via detailed analysis of the particles size distribution [21, 34], with $\alpha_{carbonate}$ increasing by only about 8% (relative to the value of 0.59 at the end of the lime treatment period) by the end of the SGP period. The above results demonstrate that the bulk of the carbonate reaction (as indicated by its extent of reaction) occurs primarily during the lime treatment step, whereby the decrease in the *SIc* during the ensuing SGP period is primarily due to reduction in calcium concentration associated with gypsum precipitation. Moreover, analysis of the sulfate extent of

reaction, $\alpha_{sulfate}$, confirmed that calcium ion removal in the SGP period was primarily due to gypsum precipitation as is evidenced by the increase in $\alpha_{sulfate}$ from 0 to 0.72 over the course of the SGP period (**Fig. 5-3c**).

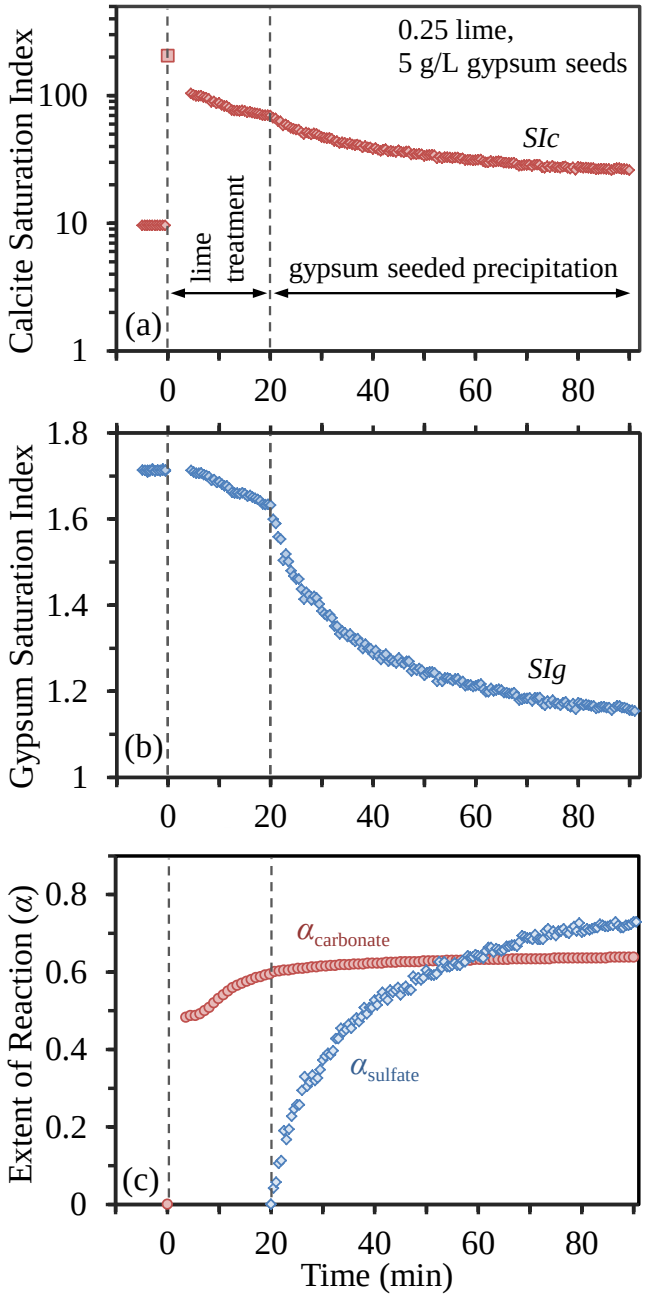

Figure 5-3. (a) Calcite saturation index, (b) gypsum saturation index, and (c) carbonate and sulfate extents of reaction during CESP treatment of DP-25 RO concentrate of initial *SIg* was ~1.7 (generated from RO desalting at recovery of 52.3% and containing 6.3 mg/L AS) in with 0.25 g/L lime addition followed by 5 g/L gypsum seeding.

5.4.2 CESP performance

Low-dose lime pretreatment of the RO concentrate was essential for removing the carry-over AS (~6.3 ppm in the PRO concentrate) in order to enable gypsum precipitation via SGP. The importance of the lime pretreatment step in the CESP process was demonstrated by comparing gypsum precipitation for three different conditions: 1) CESP with a high lime dose (0.35 g/L), 2) CESP with a low lime dose (0.25 g/L), and 3) SGP without lime pretreatment. In both of the CESP tests (1 and 2) the lime treatment period was 20 min with subsequent gypsum seeding (5.0 g/L). The lime doses for the CESP tests were in the range of the effective treatment doses reported previously based on work with synthetic RO concentrate solutions of similar level of salinity, as well as *SIg* and *SIc* [9, 21]. As expected, in the absence of lime addition (Test 3), a negligible level of gypsum precipitation was attained upon seeding, as quantified by $\alpha_{sulfate}$ and *SIg* (**Fig. 5-4**). This case (Test 3) resulted in poor SGP performance with $\alpha_{sulfate} = 0.07$ reached at the end of the SGP period (at t = 85 min). Gypsum precipitation subsequent to partial lime softening (Tests 1 and 2), however, was significant as indicated by $\alpha_{sulfate}$ values of 0.73 and 0.74 and corresponding *SIg* of 1.15 and 1.13 for the case of lime doses of 0.25 and 0.35, respectively.

The above results indicate that there is little to be gained by increasing the lime dose above the optimal dose of ~0.25 g/L and is consistent with previous work [21, 34]. The present evaluation for CESP performance, based on treatment of actual field generated RO concentrate, demonstrated that lime pretreatment for AS removal followed by gypsum seeding is a feasible method of concentrate demineralization. Admittedly, the level of *SIg* reduction for the field PRO concentrate was somewhat lower (by ~2%) for the same lime dose of 0.25 g/L used previously in evaluating the CESP process for synthetic model solutions [21]. It is plausible that the slight

decrease in desupersaturation efficiency was due to the presence of NOM present in AD water [50, 51] which is expected to inhibit mineral salt precipitation [29, 52-54]. Nonetheless, as discussed in **§5.4.1,** with the level of attained reduction in *SIg* (from ~1.7 to ~1.1) in the PRO concentrate, it should be possible to carry further desalination of the PRO concentrate via a secondary RO (SRO) desalination stage for further economical enhancement of the overall level of product water recovery.

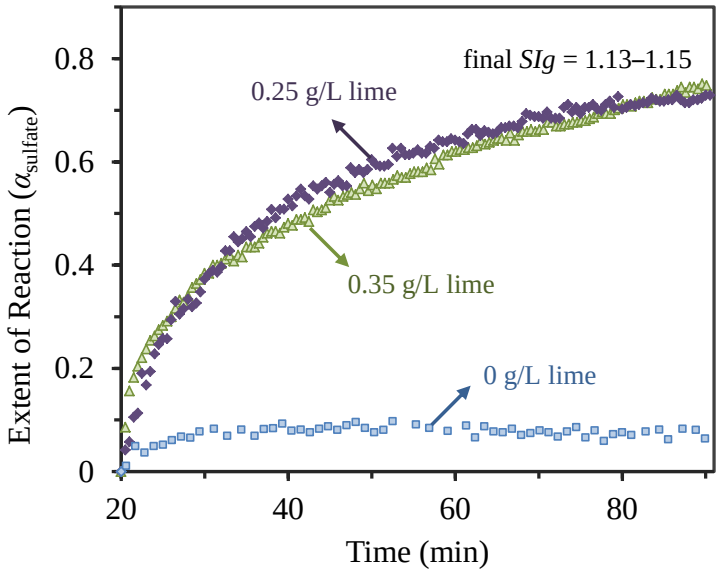

Figure 5-4. Sulfate extent of reaction during CESP treatment of DP-25 RO concentrate (Initial *SIg* was ~1.7; concentrate generated by RO desalting at 52.3% recovery and containing, 6.3 mg/L AS) with 5 g/L gypsum seeding without prior lime treatment (■), and with lime treatment of either 0.25 g/L (♦) or 0.35 g/L (▲).

Analysis of the treated PRO concentrate before and after CESP treatment (**Table 5-1**) revealed that, in addition to precipitative removal of calcium (32–34%) and phosphate ions (44%), there was measurable removal of other ions (**Fig. 5-5**) such as strontium (19%) and magnesium (6–7%) as well as silica (1–3%). Co-precipitative removal of the above ions with $CaCO_3$ and $CaSO_4$ solids could be beneficial for the added reduction in mineral scaling propensity of the PRO concentrate with respect to sparingly soluble mineral salts such as calcium phosphate, strontium sulfate as well as magnesium silicates.

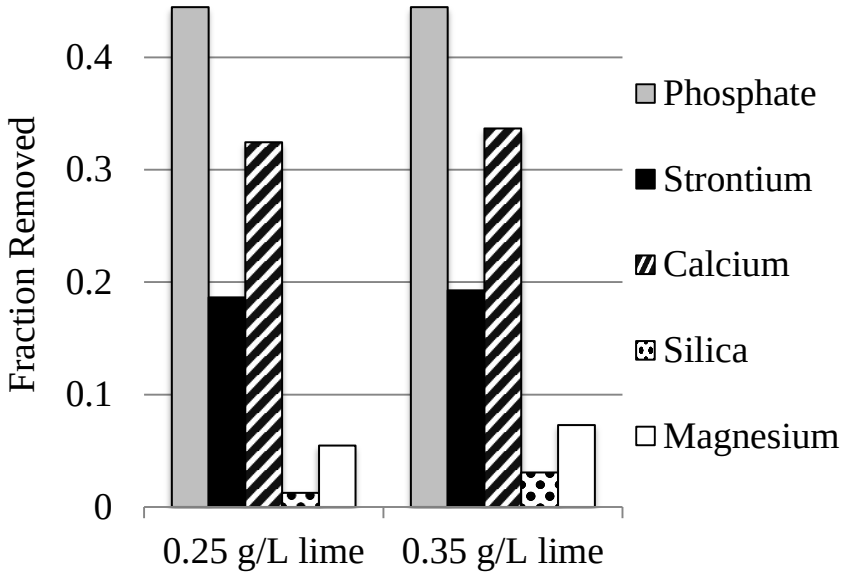

Figure 5-5. Removal fraction of major scale precursors after CESP treatment DP-25 RO concentrate (**Table 5-1**) using doses of 0.25 or 0.35 g/L lime and 5.0 g/L gypsum seeds.

5.4.3 Recovery Limit

The recovery limits for the SRO can be estimated based on the limit imposed by mineral salt and silica scaling thresholds (i.e., at the upper mineral salt SI limit recommended with AS use [41] and limit of *SI* = 1 for silica [9]). Accordingly, gypsum scaling would limit the PRO recovery for the AD source water given in **Table 5-1** to about 55%; when combined with CESP and SRO (**Fig. 5-2**) the overall recovery could be increased up to ~79%. However, with silica scaling as the recovery limiting factor, SRO recovery would be limited to ~44% (**Table 5-1**), with overall recovery for the PRO-CESP-SRO desalting process of ~73%. It is noted that that if RO operation could proceed up to silica SI of 1.8–3.4 (180–300 mg/L silica) with adequate AS use as demonstrated in previous work [55], then recovery would be limited only by gypsum scaling. It is noted that in the present field study, the PRO pilot system was operated conservatively at ~52% recovery producing a PRO concentrate with bulk *SIg* = 1.7. A more aggressive PRO desalting up to the limit of bulk *SIg* = 2.5 (i.e., the typical upper limit

recommended with the use of suitable AS [41]) attaining a recovery of 62.6%, and a CESP process enabling desupersaturation of the PRO concentrate to *SIg* ~1.13–1.15 (**Fig. 5-4**), would enable SRO desalting that would raise the overall recovery to about 83%. However, the overall recovery of the PRO-CESP-SRO process can be increased beyond the scaling imposed recovery limits in the SRO (i.e., concentrate *SIg* = 2.5) by recycling the SRO concentrate to the CESP unit (**Fig. 5-1**) as described previously [21]. Using the above approach, desalting of the DP-25 AD source water (**Table 5-1**) could be achieved up to an overall recovery limit that would be set by the maximum operating pressure rating for the deployed membrane elements and pressure vessels. As discussed in **§5.5**, based on process economic considerations, the optimal recovery for the present field water source (**Table 5-1**) was determined to be ~ 93%.

5.5. Economic analysis of high recovery RO via CESP

Economic analysis of desalting high salinity brackish SJV AD water (**Table 5-1**), via the integration of RO desalination with ICD, was conducted for the PRO-CESP-SRO process relative to PRO-PS-SRO, while considering the cost of direct and post-desalination brine disposal. An illustration of the total cost of AD water desalting (accounting for O&M and capital costs) for both ICD methods (CESP and PS), with and without brine disposal costs, is shown in **Fig. 5-6** relative to the cost of PRO desalting. There are various methods for direct brine disposal such as thermal evaporation, solar evaporators, and deep well injection with reported disposal costs in the range of 0.40–1.78 $/m^3 [17, 38, 56]; a reasonable average of 1.10 $/m^3 was utilized for the results of the analysis displayed in **Fig. 5-6**. It is also noted that the water management cost for the PRO-CESP-SRO process is provided for a lime dose range of 0.25 g/L–0.55 g/L

(**Fig. 5-6**), whereas calculations of PRO-PS-SRO process cost were based on the required stoichiometric alkaline doses [22, 25].

In enhancing the overall water recovery to a range of 70–95% from the PRO recovery limit of 62%, without accounting for residual brine disposal cost, ICD (via PS or CESP) and SRO increase the AD water desalination costs by a factor of 1.31–2.12 (on a product water basis) relative to PRO desalting (**Fig. 5-6a**). The AD water desalination cost of the PRO-PS-SRO process increases with recovery (above that of the PRO recovery level) due to the associated increased alkaline dose requirement (and thus increased chemical cost) and energy consumption (especially when the recovery in a given RO stage is above 50%). In contrast, for PRO-CESP-SRO desalting, the total water desalination cost decreased with increased recovery (above the PRO level) to a minimum that is about a factor of 1.31–1.46 above the combined cost of PRO desalting (at the maximum feasible recovery level of 62%). This cost decrease is attributed to decreasing specific chemical cost for CESP ($/m^3-product) with increasing recovery, given that the CESP chemical dose requirement (i.e., requiring only partial lime treatment for AS removal and gypsum seeding for desupersaturation) is essentially independent of the SRO recovery. Above the optimal recovery (i.e., minimum production cost) of 93% (**Fig. 5-6a**), the cost increases with recovery primarily due to increased energy consumption in the SRO stage above the optimal SRO recovery, which is 50% when operating in the absence of an energy recovery device [48]. With PRO water recovery limited at 62%, energy recovery in the PRO may be beneficial; however, following recent RO optimization work [48], it can be shown that PRO energy recovery would lead to only about 10% reduction in the overall PRO water production cost (or ~5–6% for the integrated PRO-ICD-SRO processes).

When brine disposal cost was considered, the total cost of water desalting, for both the PRO-CESP-SRO and PRO-PS-SRO processes relative to PRO, decreased with increased recovery (**Fig. 5-6b**) primarily due to the decrease in brine volume. Given an average brine disposal cost of 1.10 $/m^3, the minimum total water desalting costs are lower than the total PRO cost by factors of 0.62–0.68 and 0.88 for the PRO-CESP-SRO and PRO-PS-SRO, respectively, and occur at the corresponding recoveries of 91% and 93%. These minima occur since the brine disposal and specific capital costs for desalination ($/m^3-product) decrease, while the O&M costs increase with increasing recovery. In particular, there is a marked increase in electrical energy consumption at elevated recovery due to rapid osmotic pressure rise of the RO concentrate [48]. When considering the practical implication of the optimal recovery level, it is important to note that, if one would impose a reasonable practical upper limit for RO pressure vessels of 68.9 bar (1000 psi), this would limit the attainable maximum recovery to ~93% for the present AD water (**Table 5-1**), which is essentially the optimal recovery level (91–93%) for the PRO-ICD-SRO processes.

The advantage of RO desalination with PRO-CESP-SRO over PRO-PS-SRO is primarily due to: (a) reduced chemical dose for CESP, and (b) lower alkaline cost (by ~93–97%) for CESP, given the lower price of lime relative to soda ash (**Table 5-2**) [46]. At the lower recovery of 70%, the total water desalination cost for PRO-CESP-SRO, at the low lime dose (0.25 g/L), is only ~4% lower than PRO-PS-SRO (**Fig.5- 6b**). However, the cost advantage of PRO-CESP-SRO, relative to PRO-PS-SRO, increases significantly with increased recovery, with the water production cost for the former being 22–29% lower at the optimal recovery of 93%.

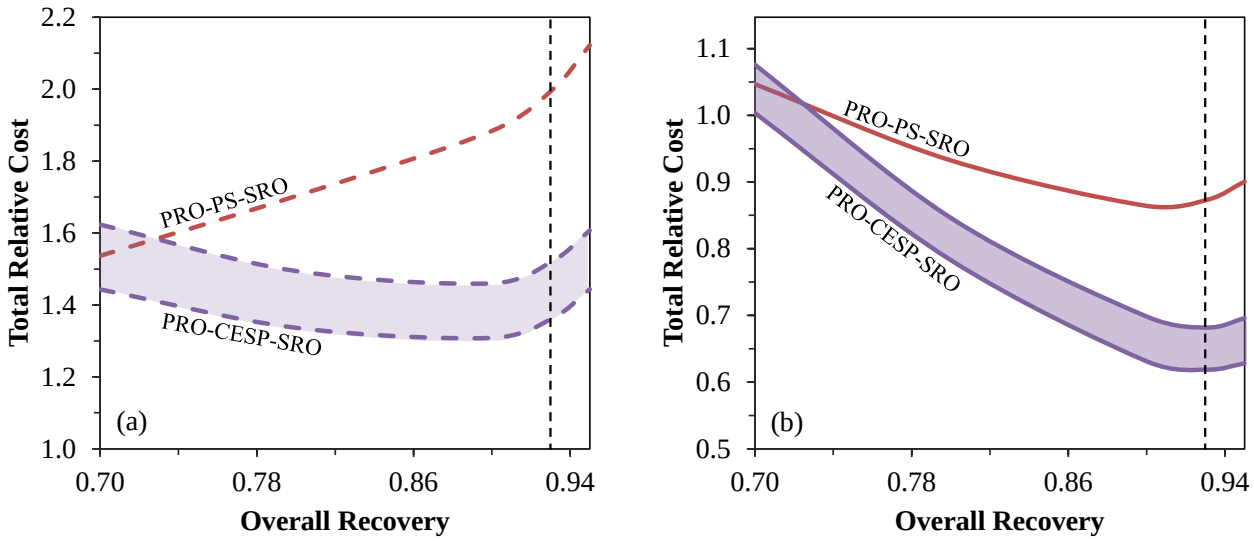

Figure 5-6. Total brackish water desalting cost for PRO-ICD-SRO relative to PRO desalting (at 62% recovery): (a) without the cost of brine disposal (PRO cost= 0.44 $/m^3–product), and (b) with brine disposal cost of 1.10 $/m^3 (PRO cost = 1.09 $/m^3–product). The vertical dashed lines indicate the recovery limit that would be imposed by RO pressure vessels at an operational limit of 68.9 bar (1000 psi).

In order to assess the cost of various AD water desalination management options on the basis of treated feed volume a comparison was undertaken of the total cost (including brine disposal for all options) [17, 38, 56] for: (a) PRO-CESP-SRO and PRO-PS-SRO at the optimal recovery limit of 93%, and (b) RO desalting up to the maximum attainable recovery of 62% (**§3**) without concentrate demineralization. As shown in **Fig. 5-7a**, water management costs for PRO-PS-SRO were higher than RO desalting by about 29%. In contrast, the total cost for the PRO-CESP-SRO desalination management option, relative to RO (including disposal cost), was lower by 8.5% at the optimal (low, 0.25 g/L) lime dose and about the same at excess (high, 0.55 g/L) lime dose. O&M costs (on the basis on desalted water volume) constitute the greatest contribution (73–80%) to total water desalination management cost for the PRO-ICD-SRO approaches. Energy costs, also on the basis of desalted product water, constitute about 26%, 37–40%, and 44% of the O&M cost (or 21%, 27–29%, and 31% of the total water production cost) for the PRO-PS-SRO, PRO-CESP-SRO and RO (same as for PRO) desalination management

options, respectively (**Fig. 5-7b**). Brine disposal costs (**Fig. 5-7a**) constitute the majority of the total cost (61%) for AD desalination management by RO desalination alone with O&M costs making the next largest contribution to the total cost (30%) of treated AD feed water. PRO-CESP-SRO desalination management (including brine disposal) is the lowest cost management option owing to the lower chemical cost and reduced brine volume generated by the process relative to PRO-PS-SRO and RO. It is noted that, the above economic analysis did not consider the potential beneficial environmental and regulatory impacts of the different water management options. However, the potential value of product water can have a beneficial impact on the overall AD water management economics as discussed later in this section.

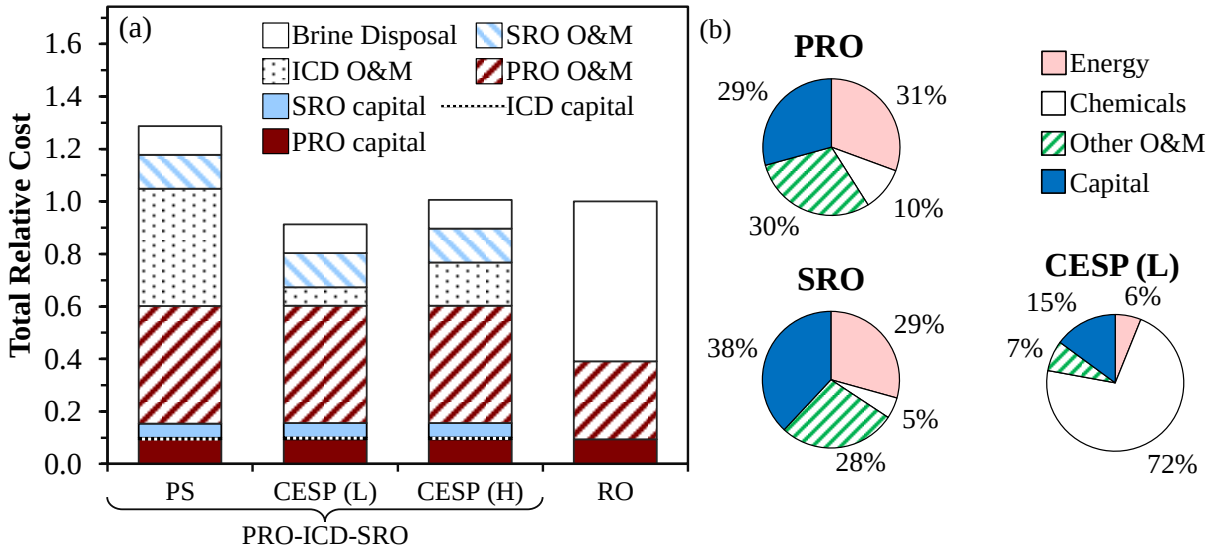

Figure 5-7. Total brackish water desalting management cost (on the treated feed volume basis) for PRO-ICD-SRO (at the optimal recovery of 93%) relative to RO desalting with brine disposal (i.e., RO cost = 0.69 \$/m^3–feed at 62% recovery and brine disposal cost of 1.10 \$/m^3). Note that CESP (L) and CESP (H) denote operation at the low (0.25 g/L) and high (0.55 g/L) lime doses.

The total cost of high recovery desalination is expected to increase with increasing salinity. Therefore, overall PRO-ICD-SRO management costs were assessed for the expected range of water quality in the present SJV field location (**§5.2.3**). The costs of total AD water management were determined, at the same recovery level (93%) as in **Figs. 5-6** and **5-7a** at the

lowest and highest reported salinities (**Table 5-3**) and compared to the base case (**§5.2.3**). As shown in **Table 5-3**, the overall cost of water management by PRO-CESP-SRO and PRO-PS-SRO increased by merely 6% and 4%, respectively, as the salinity increased from 6,700 to 14,400 mg/L TDS. Over the above salinity range, the cost of PRO-CESP-SRO was about 22–30% lower in cost relative to PRO-PS-SRO. It is noted that, at the optimal high recovery level of ~93%, the total cost of water management (i.e., desalination and brine disposal) for the above salinity range varied by only about ±1–4% relative to the base case of 11,000 mg/L TDS feed and saturation indices of *SIg* = 0.96 and *SIc* = 3 (**Table 5-3**).

Table 5-3. Impact of varying AD source water salinity on the cost of water desalination management (including brine disposal) at the optimal recovery [a].

	AD Water Quality		
	base [b]	low salinity	high salinity
salinity (mg/L TDS)	11,000	6700	14,400
SIc [c]	3.0	3.2	3.1
SIg [c]	0.96	0.87	0.94
	Relative Cost of Total Water Desalination Management [d]		
PRO-PS-SRO	1	0.98	1.02
PRO-CESP-SRO (L) [e]	1	0.96	1.01
PRO-CESP-SRO (H) [e]	1	0.97	1.03

[a] Optimal recovery was 93% (**Fig. 5-6b**) with brine disposal set at 1.10 \$/m^3 (**§5.3)**; [b] Base case for all cost estimates except where stated; [c] CESP costs include lime doses and gypsum make-up doses of either 0.25 g/L and 1 g/L (L) or 0.55 g/L and 10 g/L (H), respectively; [c] *SIc* & *SIg* associated with the periods of lowest and highest salinities [9] did not correlate with periods of the lowest and highest saturation indices (**Table 5-1**); [d] Costs are relative to the base case salinity (11,000 mg/L TDS) costs of 0.95, 0.68, and 0.74 \$/m^3-product, respectively, for ICD treatment by PS, CESP (L), and CESP (H); [e] costs are expressed on the basis of treated feed volume (including brine disposal cost) are expressed relative to the cost of RO feed desalination with brine disposal.

The overall cost of AD water desalination management would increase with increased cost of brine disposal. As illustrated in **Fig. 5-8,** for the maximum attainable desalination

recoveries for the different desalination options (62% for RO and 93% for PRO-ICD-SRO)**,** when brine disposal cost is below 0.90 $/m^3, the cost of RO desalination along with brine disposal is lower than either of the PRO-ICD-SRO options. However, the RO option is not an attractive AD water desalination management option as it is likely to present both environmental challenges and regulatory hurdles with respect to brine disposal. Moreover, this option would leave vast volumes of high salinity AD water unmanaged. For example, at the field site considered in the present work traditional RO without ICD would lead to a residual brine stream that is 38% of the feed; this is significantly higher relative to the 7% residual brine stream for the two PRO-ICD-SRO desalination methods. Therefore, AD water desalination management by low recovery RO (i.e., without ICD) is more sensitive to the brine disposal cost. Consequently, the cost of desalination by traditional RO including residual brine disposal increases with rising brine disposal cost at a rate 5.5 times greater than that of both PRO-ICD-SRO high recovery processes (**Fig. 5-8**) for the present scenario. Once brine disposal cost increases above 0.9 $/m^3, PRO-CESP-SRO becomes the most economical AD water desalination option (**Fig. 5-8**). The PRO-PS-SRO option becomes more economical than RO (with brine disposal) at brine disposal costs above 1.73 $/m^3, but remains more costly than the PRO-CESP-SRO process.

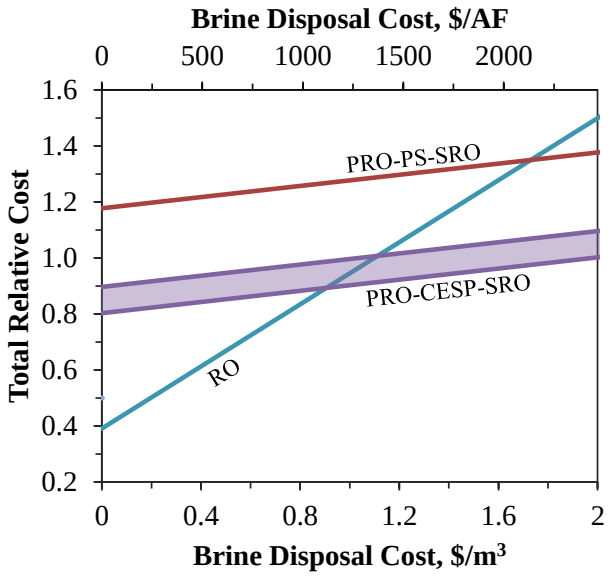

Figure 5-8. Total brackish water desalting management cost (at optimal PRO-ICD-SRO recovery of 93%) as a function of brine disposal cost for various treatment methods relative to RO desalting cost (i.e., 0.69 $/m^3–feed at 62% *Y* with brine disposal at a base cost of 1.10 $/m^3).

Considerations of the cost of brackish AD water desalination management (desalination and disposal) are clearly important elements in the selection of AD water management options. In this regard, it is also of interest to consider the possibility that desalted AD water could be a valued commodity. For example, desalted AD water in a given location could be used locally to offset purchase of imported water, exported to a neighboring needy area or a water purveyor, or even result in a subsidy for reduced saline water disposal. An illustration of the impact of product water value ($/m^3-product) on net water management cost (defined as the cost of water treatment less the product water value, both expressed on the basis of total water volume treated), is illustrated in **Fig. 5-9**. In this example, the AD desalination methods (RO and PRO-ICD-SRO), product water recovery was set at either the optimal (93% for PRO-ICD-SRO) or highest feasible recovery (62% for RO). Direct disposal of AD brackish water remains the most costly option (**Fig. 5-9**) since product water is not produced to offset brine disposal costs. Clearly, the net water management cost decreases with increased product water value. It is noted

that, at product water values < 0.63 $/m^3, the net AD water management cost by RO desalting, including brine management, would be lower than that of PRO-PS-SRO. However, due to the higher recovery in the PRO-PS-SRO process, its net water management cost decreases with product water value at a rate 1.5 times greater than for RO desalting alone; this results in the break-even water management cost (i.e., zero net treatment cost) of PRO-PS-SRO occurring at a product water value (0.95 $/m^3) which is about 14% lower than for RO desalting alone. Overall, the PRO-CESP-SRO is the most economically attractive option with a break-even water management cost at a product water value of 0.67–0.74 $/m^3 which is lower by 22–29% compared to that of the PRO-PS-SRO process (0.95 $/m^3).

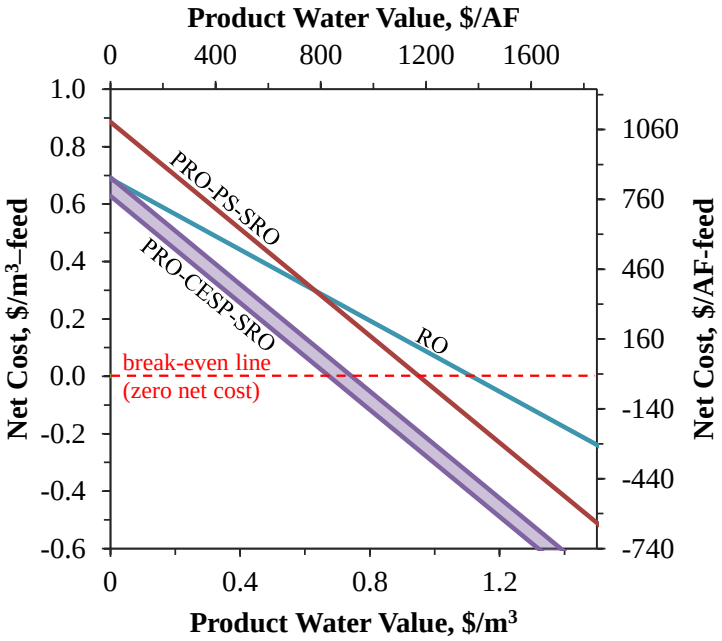

Figure 5-9. Total water management cost ($/m^3–feed) for various treatment methods as a function of product water value assuming an average brine disposal cost of 1.10 $/m^3. The costs for the RO and PRO-ICD-SRO processes are calculated at their corresponding recovery limits—62% and 93%, respectively. Note that negative net costs represent net revenue for the plant.

5.6 Conclusions

Field evaluation was undertaken to determine the feasibility of utilizing chemically-enhanced seeded precipitation (CESP) for PRO concentrate demineralization in order to enable

recovery enhancement via secondary RO desalting. The partial lime treatment step of CESP was shown to be essential for removing residual antiscalant (from the PRO concentrate) which enabled subsequent desupersaturation induced by seeded gypsum precipitation. Evaluation of CESP with brackish agricultural drainage water (~14,400 mg/L TDS), which was nearly saturated with respect to gypsum *SIg* = 0.94 and lean in bicarbonate, demonstrated significant removal of calcium (32–34%), phosphate (44%), and strontium (19%) ions, and to a lesser extent magnesium (6–7%) and silica (1–3%). CESP demineralization of PRO concentrate (generated at 52% recovery) resulted in effective reduction of its gypsum supersaturation index from about 1.7 to 1.1. This level of desupersaturation was assessed to be suitable for SRO desalting, with AS makeup, to enable enhanced overall desalination recovery in excess of 90%.

Process analysis indicated that SRO desalting of CESP-treated PRO concentrate (generated at ~52% recovery) could be carried out up to an overall recovery of about 93%. This, however, would necessitate AS makeup in the SRO and recycling of SRO concentrate to the CESP process. Economic analysis of water salinity management options for the AD water source considered suggested that, when considering the value of the desalted product water and accounting for the disposal cost of residual brine, PRO-CESP-SRO desalting is the most economically attractive option. The break-even AD water desalination management cost (i.e., zero net cost) for PRO-CESP-SRO, for the present cost estimates, was at a product water value of 0.67–0.74 $/m^3 which is lower by 22–29% compared to that of the PRO-PS-SRO process (0.95 $/m^3). Admittedly, RO desalting (along with disposal of residual brine) can be more economical when brine disposal cost is below about ~0.44 $/m^3 brine, but this is unlikely to be a feasible or acceptable water management option given the environmental challenge of disposal and loss of valuable water resource. Finally, it is noted that water salinity reduction with the

PRO-CESP-SRO approach is expected to be of lower cost for water sources that are lower in salinity and in saturation level (relative to SJV water source) with respect to mineral salt scalants. While the present work suggests PRO-CESP-SRO as a possible AD water management option for brackish AD water, field deployment would require adequate process control to handle temporal water quality variations that could be encountered with inland brackish water and management of the mineral crystal solids that would need to be continuously removed from the CESP unit.

References

1. Greenlee, L.F., et al., *Reverse osmosis desalination: Water sources, technology, and today's challenges.* Water Research, 2009. **43**(9): p. 2317-2348.
2. Malaeb, L. and G.M. Ayoub, *Reverse osmosis technology for water treatment: State of the art review.* Desalination, 2011. **267**(1): p. 1-8.
3. Technology, C.o.A.D. and N.R. Council, *Desalination: A National Perspective*. 2008: The National Academies Press.
4. Almulla, A., et al., *Developments in high recovery brackish water desalination plants as part of the solution to water quantity problems.* Desalination, 2003. **153**(1-3): p. 237-243.
5. Andi Rahardianto, et al. *High recovery desalination of agricultural drainage water: integration of accelerated chemical precipitaion with RO membrane desalination*. in *Procedings of the AIChE Annual Conference*. 2005. Cincinnati, OH.
6. Brady, P.V., et al., *Inland Desalination: Challenges and Research Needs.* Journal of Contemporary Water Research & Education, 2005. **132**: p. 46-51.
7. Gabelich, C., et al., *Pilot-scale testing of reverse osmosis using conventional treatment and microfiltration.* Desalination, 2003. **154**(3): p. 207-223.
8. Lisitsin, D., D. Hasson, and R. Semiat, *The potential of CO2 stripping for pretreating brackish and wastewater desalination feeds.* Desalination, 2008. **222**(1-3): p. 50-58.
9. McCool, B.C., et al., *Feasibility of reverse osmosis desalination of brackish agricultural drainage water in the San Joaquin Valley.* Desalination, 2010. **261**(3): p. 240-250.
10. AWWA, *Standard Methods for the Examination of Water and Wastewater*. 20th ed. 1998, Washington, DC: American Public Health Association.
11. Fritzmann, C., et al., *State-of-the-art of reverse osmosis desalination.* Desalination, 2007. **216**(1–3): p. 1-76.
12. Rautenbach, R., T. Linn, and L. Eilers, *Treatment of severely contaminated waste water by a combination of RO, high-pressure RO and NF — potential and limits of the process.* Journal of Membrane Science, 2000. **174**(2): p. 231-241.
13. Sanciolo, P., et al., *Accelerated seeded precipitation pre-treatment of municipal wastewater to reduce scaling.* Chemosphere, 2008. **72**(2): p. 243-249.
14. Zhu, A., et al., *Reverse osmosis desalination with high permeability membranes—Cost optimization and research needs.* Desalination and Water Treatment, 2010. **15** p. 256-266.
15. Bond, R. and S. Veerapaneni, *Zero Liquid Discharge for Inland Desalination*. 2007, Denver, CO: AWWA Research Foundation, AWWA, & IWA Publishing.
16. Committee on Advancing Desalination Technology, Water Science and Technology Board, and National Research Council, *Desalination: A National Perspective*. 2008, Washington, DC: National Academies Press.
17. Mickley, M.C., *Membrane concentrate disposal: practice and regulation*. 2006, Mickley & Associates, US Bureau of Reclamation: Denver, CO.
18. McCool, B.C., et al. *Technical and Economic Feasibility of Reverse Osmosis Reclamation of Agricultural Drainage Water in the San Joaquin Valley*. in *Procedings of the AIChE Annual Conference*. 2006. San Francisco, CA.

19. Gray, S., et al., *Treatise on Water Science*, ed. P. Wilderer. Vol. 4, Ch. 77. 2011: Elselvier.
20. Juby, G.J.G. and C.F. Schutte, *Membrane life in a seeded-slurry reverse osmosis system.* Water Sa, 2000. **26**(2): p. 239-248.
21. Rahardianto, A., B.C. McCool, and Y. Cohen, *Accelerated Desupersaturation of Reverse Osmosis Concentrate by Chemically-Enhanced Seeded Precipitation.* Desalination, 2010. **264**(3).
22. Rahardianto, A., et al., *High recovery membrane desalting of low-salinity brackish water: Integration of accelerated precipitation softening with membrane RO.* Journal of Membrane Science, 2007. **289**(1-2): p. 123-137.
23. Gabelich, C.J., et al., *Process evaluation of intermediate chemical demineralization for water recovery enhancement in production-scale brackish water desalting.* Desalination, 2011. **272**(1–3): p. 36-45.
24. Sanciolo, P., et al., *Enhancement of Reverse Osmosis Water Recovery Using Interstage Calcium Precipitation.* Desalination, 2012. **495**: p. 43-52.
25. Gabelich, C.J., et al., *High-recovery reverse osmosis desalination using intermediate chemical demineralization.* Journal of Membrane Science, 2007. **301**(1-2): p. 131-141.
26. Gilron, J., et al., *Comparison between compact accelerated precipitation softening (CAPS) and conventional pretreatment in operation of brackish water reverse osmosis (BWRO).* Industrial & Engineering Chemistry Research, 2005. **44**(15): p. 5465-5471.
27. Greenlee, L.F., et al., *The effect of antiscalant addition on calcium carbonate precipitation for a simplified synthetic brackish water reverse osmosis concentrate.* Water Research, 2010. **44**(9): p. 2957-2969.
28. Nason, J.A. and D.F. Lawler, *Particle size distribution dynamics during precipitative softening: Declining solution composition.* Water Research, 2009. **43**(2): p. 303-312.
29. Yang, Q., et al., *Removal of CaCO3 Scaling Salt from RO Concentrates by Air-Blow and Inorganic Inducers.* Journal of Chemical Engineering of Japan, 2008. **41**(1): p. 13-20.
30. Ning, R.Y., et al., *Recovery optimization of RO concentrate from desert wells.* Desalination, 2006. **201**(1-3): p. 315-322.
31. Rahardianto, A., *High recovery desalting of brackish water, doctoral dissertation*. 2009, University of California Los Angeles.
32. Seewoo, S., R. Van Hille, and A. Lewis, *Aspects of gypsum precipitation in scaling waters.* Hydrometallurgy, 2004. **75**(1-4): p. 135-146.
33. Yang, Q., et al., *Desupersaturation of RO Concentrates by Addition of Coagulant and Surfactant.* Journal of Chemical Engineering of Japan, 2007. **40**(9): p. 730-735.
34. McCool, B.C., A. Rahardianto, and Y. Cohen, *Antiscalant removal in accelerated desupersaturation of RO concentrate via chemically-enhanced seeded precipitation (CESP).* Water Research, 2012(0).
35. Rahardianto, A., B.C. McCool, and Y. Cohen, *Reverse osmosis desalting of inland brackish water of high gypsum scaling propensity: Kinetics and mitigation of membrane mineral scaling.* Environmental Science & Technology, 2008. **42**(12): p. 4292-4297.
36. Bartman, A.R., P.D. Christofides, and Y. Cohen, *Nonlinear Model-Based Control of an Experimental Reverse-Osmosis Water Desalination System.* Industrial & Engineering Chemistry Research, 2009. **48**(13): p. 6126-6136.

37. Bartman, A.R., et al., *Minimizing energy consumption in reverse osmosis membrane desalination using optimization-based control.* Journal of Process Control, 2010. **20**(10): p. 1261-1269.
38. Faria, J., *Disposal of Brine and Solids in the Westside of the San Joaquin Valley (personal communication)*. 2012.
39. *US Bureau of Reclamation, San Luis Drainage District Feature Re-evaluation - Feasibility Report, Appendix D: Reverse Osmosis Analysis Reports, US Department of the Interior, Mid-Pacific Region, Sacramento, CA.* 2008.
40. OLI Systems Inc., *Stream Analyzer 3.1*. 2007: Morris Plains, NJ.
41. Hydranautics, *Chemical Pretreatment of RO and NF, Technical Application Bulletin No. 111 Rev. C*. 2008, Nitto Denko: Oceanside, CA. p. 10.
42. Bartman, A.R., et al., *Mineral scale monitoring for reverse osmosis desalination via real-time membrane surface image analysis.* Desalination, 2010.
43. Christoffersen, M.R., et al., *Crystal-growth of calcium-sulfate dihydrate at low supersaturation.* Journal of Crystal Growth, 1982. **58**(3): p. 585-595.
44. Nancollas, G.H., *Growth of crystals in solution.* Advances in Colloid and Interface Science, 1979. **10**(JAN): p. 215-252.
45. USBR, *WaTER Cost Estimation Software*, M. Chapman, Editor. 2011: Denver.
46. U.S. Geological Survey, Mineral commodity summaries 2012: U.S. Geological Survey, 198 p.
47. OLI, *OLI Analyzer 2.0*. 2005, OLI Systems, Morris Plains, NJ.
48. Zhu, A.Z., P.D. Christofides, and Y. Cohen, *Effect of Thermodynamic Restriction on Energy Cost Optimization of RO Membrane Water Desalination.* Industrial & Engineering Chemistry Research, 2009. **48**(13): p. 6010-6021.
49. Bureau of Labor Statistics, U.D.o.L. *Inflation calculator*. 2012 [cited 2012 June 2012]; Available from: http://www.bls.gov/data/inflation_calculator.htm.
50. Byrne, C.M.P., et al., *Compositional changes in the hydrophobic acids fraction of drainage water from different land management practices.* Water Research, 2010. **44**(15): p. 4379-4390.
51. Hayes, T.M., M.H.B. Hayes, and R.S. Swift, *Detailed investigation of organic matter components in extracts and drainage waters from a soil under long term cultivation.* Organic Geochemistry, 2012 (in press).
52. Bob, M. and H.W. Walker, *Enhanced adsorption of natural organic matter on calcium carbonate particles through surface charge modification.* Colloids and Surfaces A: Physicochemical and Engineering Aspects, 2001. **191**(1-2): p. 17-25.
53. Bremere, I., et al., *Controlling scaling in membrane filtration systems using a desupersaturation unit.* Desalination, 1999. **124**(1-3): p. 51-62.
54. Bremere, I., et al., *Increasing conversion in membrane filtration systems using a desupersaturation unit to prevent scaling.* Desalination, 1998. **119**(1-3): p. 199-204.
55. Darton, E.G., *RO plant experiences with high silica waters in the Canary Islands.* Desalination, 1999. **124**(1–3): p. 33-41.
56. W. R. Johnson, K. K. Tanji, and R.T. Burns, *Drainage water disposal*. Management of agricultural drainage water quality, ed. C. A. Madramootoo, W. R. Johnston, and S. Lyman. 1997, Rome, Italy: Food and Agricultural Organization of the United Nations.

Chapter 6

Process requirements for continuous chemically-enhanced seeded precipitation: gypsum precipitation kinetics and reactor sizing

6.1 Overview

The potential of the chemically-enhanced seeded precipitation (CESP) process to enable high recovery desalination (i.e., PRO-CESP-SRO, see **Ch. 4** & **5**) of brackish water of high gypsum scaling propensity has been demonstrated in batch laboratory and field studies utilizing both model PRO concentrate (**Ch. 4**) and PRO concentrate generated in the field (**Ch. 5**). Large-scale deployment, however, requires continuous CESP operation to demineralize the continuous production of concentrate generated by RO desalination.

The major components of a proposed continuous CESP process are illustrated in **Fig. 6-1**. First, the PRO concentrate undergoes lime treatment to induce $CaCO_3$ precipitation and the associated AS removal (see **Ch. 4**). Next, $CaCO_3$ solids are separated from the lime-treated PRO concentrate (i.e., centrifugal separation) prior to gypsum seeded precipitation (GSP) to desupersaturated the PRO concentrate with respect to gypsum thereby enabling SRO. The GSP step is performed in a vertical plug flow reactor (PFR) to maximize the driving force for gypsum precipitation and minimize the reactor volume required to achieve a given extent of reaction (**§4.3.3, Eq. 4-1**). The GSP reactor contains a specified volume fraction of gypsum particles which provide the reactive surface area for heterogeneous gypsum precipitation and, thus, desupersaturation of the lime-treated PRO concentrate. As gypsum particles grow they are gradually purged from the reactor and replaced with fresh gypsum seeds in order to maintain a steady-state particle size distribution and total specific surface area (m^2/L) within the reactor. In order to maintain a constant level of performance (i.e., final gypsum saturation level or sulfate

extent of reaction) in the GSP step of CESP, the available active surface area must be preserved. Insufficient AS removal during lime pretreatment may lead to a reduction in the active surface area due to poisoning of gypsum solids caused by AS adsorption onto the gypsum solids. Previous CESP batch studies have demonstrated that seed poisoning by residual AS can be prevented with adequate lime treatment (e.g. 0.25 g/L 20–25 min prior to gypsum seeding—see **Ch. 4** & **5**). However, the ability to maintain the gypsum precipitation rate constant during reuse of gypsum solids over a long time period (i.e., multiple cycles of batch CESP) has not been successfully demonstrated. Solids reuse was demonstrated previously [1] during multiple cycles of batch CESP, but a decrease in the rate of gypsum precipitation was observed after multiple CESP cycles. It was not shown whether this decrease was due to poisoning of the gypsum seed surfaces by residual AS or due to the aggregation of gypsum seed particles reducing the effective surface area available for heterogeneous precipitation. When two or more particles aggregate the resulting available surface area exposed to the solution is reduced where the particle surfaces overlap. Thus, particle aggregation results in a decrease in the rate of precipitation.

The results of the study described in this chapter demonstrate the potential of a continuous CESP process via a series of multi-cycle seeded gypsum precipitation batch experiments with solids reuse in model RO concentrate solution (OAS solution B, 63% *Y*, see **§4.2.2** & **Table 4-1**). This water source was selected for the study as its high gypsum scaling propensity present a challenge for traditional RO desalination and high recovery desalination via softening is unattractive economically due to the low bicarbonate content (see **§3.3**). Additionally, the requirements (e.g., residence time, seed makeup rate) are assessed for the continuous GSP step based on the observed kinetics of gypsum precipitation during the batch CESP experiments and direct model simulation of the GSP process. It is hypothesized that the

observed rate of precipitation over multiple cycles, and therefore a continuous process, can be sustained by minimizing particle aggregation and the accompanying loss of crystal surface area (m^2/L) during solids recycling. After the GSP reactor requirements have been determined from simulations of the process, the reactor size (i.e., height, diameter) can be calculated following the procedure developed in **§6.3.4**.

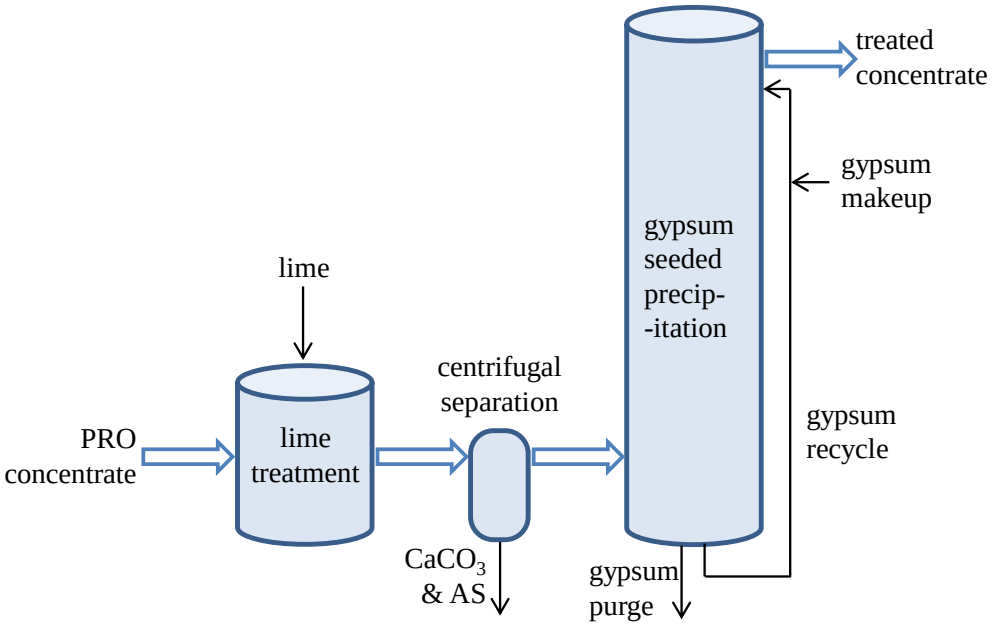

Figure 6-1. Schematic of a proposed continuous CESP process illustrating pretreatment via lime-induced $CaCO_3$ precipitation for AS removal prior to gypsum desupersaturation via gypsum seeded precipitation with recycling of gypsum solids.

6.2 Experimental

6.2.1 Model solutions and chemicals

Model brackish water solution was prepared using reagent grade salts in DI water as detailed in **§4.2.1** and **Table 4.1** (solution B). Briefly, solution compositions were based on those of the expected RO concentrate stream from an RO desalination process operating at the scaling recovery limit (63% recovery leading to concentrate *SIg* = 2.5) for a brackish water source in the San Joaquin Valley (OAS location) [1, 2] (see **Appendix A**). Solution B contained all major ions

present in the OAS field sample and had the same gypsum saturation level, *SIg* = 2.5. Polyacrylic acid (PAA, MW = 2000 g/mol, Aldrich, St. Louis, MO) was selected as the antiscalant (AS) because its composition is known while commercial AS are generally proprietary mixtures of polyelectrolytes for which precise compositions are not generally reported by AS suppliers. Solutions containing PAA (3 mg/L) were dosed prior to lime treatment (0.15 or 0.25 g/L) and gypsum seeding. Gypsum seeds (J.T. Baker, Phillipsburg, NJ) had an average particle size diamter, d_p, of 45 μm with a standard deviation, σ_p, of ~10 μm.

6.2.2 CESP experiments

Concentrate demineralization was performed via CESP in a 1-L lab-scale crystallizer at room temperature (~23 ± 1 °C) with continuous monitoring of calcium ion activity, pH, and temperature. The 1-L crystallizer was 20 cm tall with an 8.0 cm square base (CLM 4, EC Engineering, Edmonton, Canada) with a 4.0 cm by 6.0 cm radial flow paddle mixer situated with 2.5 cm of clearance above the base (See **Appendix B**). All experiments were carried out at paddle mixing rates of 200 rpm (G = 560 s^{-1}) as it was found to minimize gypsum particle aggregation which would lead to loss of particle surface area (see **Appendix E.1**). The pH and the calcium ion activity were measured using a pH electrode (Cole Parmer Instrument Company, Vernon Hill, IL) and a calcium ion selective electrode (Orion 97-20, Thermo Electron Corporation, Somerset, NJ), respectively. Calcium, sulfate, and bicarbonate ion concentrations were estimated based on the pH and calcium activity data using OLI Stream Analyzer 3.1 (Morris Plains, NJ) to model the complex, multi-electrolyte aqueous system in liquid phase equilibrium, but not in solid-liquid equilibrium as the model solutions in the present study are metastable (i.e., supersaturated) (see **Appendix D**). Particle size analyses were performed via the

Multisizer 3 Coulter Counter (Beckman Coulter, Miami, FL) for 1–3 mL samples withdrawn from the 1-L crystallizers at various times throughout the experiments as detailed in **§4.3.6**.

GSP was carried out over five cycles for each of four different cases: 1) GSP without AS addition, 2) GSP with 3 mg/L AS, 3) CESP with 3 mg/L AS and 0.15 g/L lime treatment prior to gypsum seeding, and 4) CESP with 3 mg/L AS and 0.25 g/L lime treatment prior to gypsum seeding. Gypsum seeding without AS addition was performed to demonstrate the ideal case of gypsum precipitation with no seed poisoning. Additionally, gypsum seeding in the presence of AS without lime pretreatment for AS removal was performed to illustrate the impact of seed poisoning on gypsum precipitation. The lime doses used in the present CESP experiments were selected based on precious work (see **Ch. 4**). Both high (0.25 g/L) and low (0.15 g/L) lime doses were selected for the present work to demonstrate the effect of sufficient and insufficient lime doses, respectively, during lime pretreatment. The lime dose of 0.25 g/L was determined to be sufficient for preventing subsequent gypsum seed poisoning by reducing residual AS concentration by >95% based on previous results shown in **§4.3.6** and **Fig. 4-11**. The lime dose of 0.15 g/L, however, was expected to only partially prevent seed poisoning by reducing residual AS concentration by only ~40% (**Fig 4-11**). For each of the four cases, gypsum precipitation was induced by addition of 5 g/L of gypsum seeds in the first cycle and the remaining cycles were seeded with the solids collected at the end of the preceding cycle.

6.3 Results and Discussion

6.3.1 CESP with multiple cycles of solids recycling

The rate of gypsum precipitation was found to increase with each cycle (**Fig. 6-2a**) for all four cases tested as measured by the sulfate extent of reaction, $\alpha_{sulfate}$ (defined in **§4.3.3, Eq. 4-1**),

during multi-cycle CESP with solids recycling. For example, in the case of CESP with 0.25 mg/L lime the sulfate extent of reaction in the first cycle reached 0.9 after 85 min, yet in the fifth cycle the sulfate extent of reaction reached 0.9 after only 45 min, a decrease of 47% in the time required (**Fig. 6-2a**). The increase in the rate of precipitation with each cycle was due to the increased mass of solids (and corresponding increased surface area) added with each cycle (**Fig. 6-2b**). The first cycle was dosed with 5 g/L gypsum while each subsequent cycle was dosed with all precipitated solids collected at the end of the preceding cycle. The gypsum solids mass (g/L) at the end of each cycle is shown in **Fig. 6-2b**.

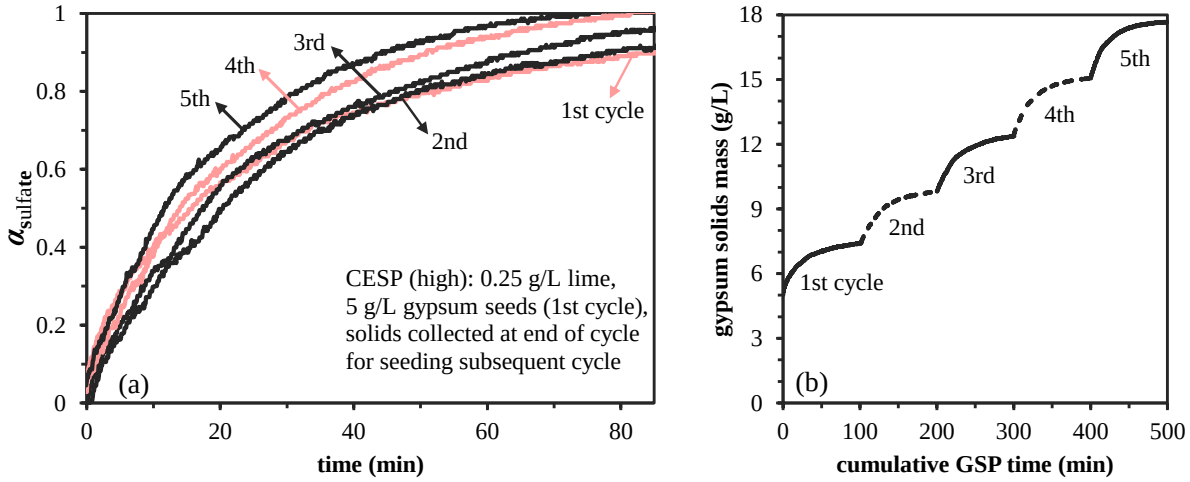

Figure 6-2. Sulfate extent of reaction (a) and gypsum solids mass (b) in model PRO concentrate (*SIg* = 2.5) subsequent to 0.25 g/L lime treatment (not shown) during five cycles of CESP with 5 g/L gypsum seeds to induce gypsum precipitation in the 1st cycle followed by recycled solids in the remaining cycles.

The rate of gypsum precipitation during GSP increased with each cycle in all four cases tested (i.e., GSP without AS addition, GSP with 3 mg/L AS, CESP with 3 mg/L AS and 0.15 g/L lime treatment, and CESP with 3 mg/L AS and 0.25 g/L lime treatment). The observed increase in precipitation with each cycle was due to the increased mass of gypsum solids present at the start of each cycle. When CESP was conducted with the high lime dose (0.25 g/L) the rate of precipitation during the first cycle was nearly equal to (within 5%) that of GSP without AS

addition with $\alpha_{sulfate}$ reaching 0.90 and 0.94, respectively, after 85 min. During the fifth cycle $\alpha_{sulfate}$ reached 1.0 after 80 minutes for both the case with no AS and the case with CESP with 0.25 g/L (**Fig. 6-3**). That these two cases had the same performance with respect to the sulfate extent of reaction after 80 minutes indicates that lime treatment (0.25 g/L) was sufficient to prevent AS seed poisoning over five cycles. However, the case of CESP with the lower lime dose (0.15 g/L) exhibited significantly worse performance (i.e., lower $\alpha_{sulfate}$) than that with the higher lime dose (0.25 g/L). In the first cycle of CESP with 0.15 g/L lime, $\alpha_{sulfate}$ reached only 0.69 after 85 minutes, whereas at the higher lime dose (0.25 g/L) $\alpha_{sulfate}$ reached the same value (0.69) in less than have the time (32 min) than that required at the lower lime dose. The sulfate extents of reaction for the first and fifth cycles for each of the four GSP cases tested are shown in **Fig. 6-3**. These results provide evidence that the rate of gypsum precipitation could be sustained in a continuous CESP process provided there is sufficient lime pretreatment to remove AS.

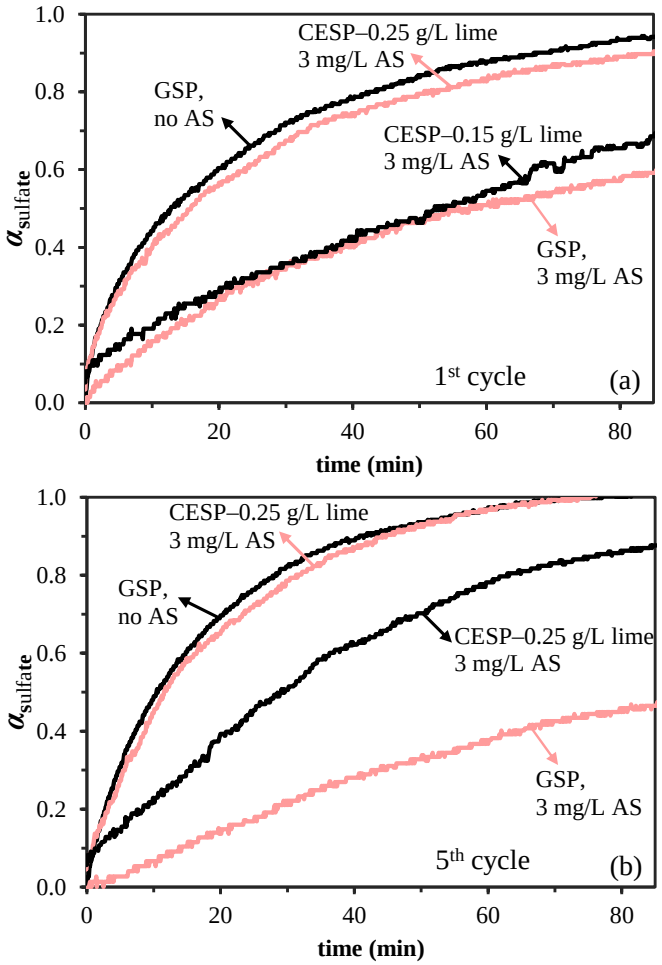

Figure 6-3. Sulfate extent of reaction, $\alpha_{sulfate}$, during the 1st (a) and 5th (b) cycles of seeded precipitation using 5 g/L gypsum seeds to induce gypsum precipitation for the 1st cycle followed by recycled solids in the remaining cycles. Gypsum seeding was tested in model PRO concentrate (*SIg* = 2.5) with and without the presence of 3 mg/L AS and at two different lime pretreatment doses (0.25 or 0.15 g/L) for AS removal.

6.3.2 Gypsum precipitation rate constant during multi-cycle CESP

The rate constants for gypsum precipitation (**Eq. 6-1**) and residual AS concentrations after lime treatment were determined using the previously developed initial rate method (see **§4.3.6**) and **Eq. 6-1:**

$$R = kA\left(C - C_S\right)^2 \tag{6-1}$$

where R is the rate of gypsum precipitation (mol/L-min), k is the observed rate constant (L^2/m^2-mol-min), A is the total active surface area of the gypsum particles (m^2/L), C is the time-varying

sulfate concentration (M), and C_S is the sulfate concentration (M) at gypsum saturation. Gypsum precipitation was modeled with assuming second order reaction kinetics as described in **§4.3.6** where the initial rate was based on a second order rate law (**Eq. 4-2**). Furthermore, previous studies [3-5] have shown that gypsum precipitation kinetics in bulk solutions obey second order kinetics.

The observed rate constants for GSP without AS addition and for CESP with 0.25 g/L lime were found to decrease after the first cycle before reaching constant values of 12.9 and 13.5 (±15%) L^2/m^2-mol-min, respectively, averaged over the remaining cycles (**Fig. 6-4a**). The decrease in the observed rate constant between cycles one and two may be a result of the fresh seeds' initial surfaces having a different surface energy [6, 7] compared to that of the seeds after undergoing heterogeneous growth and, therefore, the first cycle was excluded from further comparisons in the present work as it was not significant in a continuous process. The observed rate constant for CESP with 0.25 g/L lime (12.9 L^2/m^2-mol-min) was only slightly lower (4%) than that observed for GSP without AS (13.5 L^2/m^2-mol-min) indicating that gypsum seed poisoning by AS was prevented (**Fig. 6-4a**). In fact, based on the indirect measurements of AS concentration (see **§4.3.6**), the AS concentration was reduced by 95% via the $CaCO_3$ precipitation induced with 0.25 g/L lime (**Fig. 6-4b**). This level of AS removal was consistent with previous results (**§4.3.6**, **Fig 4-11**) using the same model solution (solution B, **Table 4.1**) for which the AS concentration was found to have been reduced by ~99% after 0.25 g/L lime treatment. The above results indicate that a continuous CESP process could be sustained if gypsum seed poisoning by AS was prevented via sufficient lime pretreatment.

The observed rate constants for gypsum precipitation during CESP with only 0.15 g/L lime pretreatment, however, were reduced significantly (~46–67%) compared to the case of GSP

without AS addition (**Fig. 6-4a**). The large reduction in the observed gypsum precipitation rate constants indicate that the lower lime dose (0.15 g/L) was insufficient to prevent subsequent gypsum seed poisoning. Furthermore, in the case of CESP with 0.15 g/L lime, the observed gypsum precipitation rate constant decreased with each cycle of CESP because solids that were already poisoned from the previous cycles were added to the model solutions for which insufficient AS was removed by the low lime treatment dose. The 63% reduction in AS concentration, based on indirect measurements of the AS concentration (see **§4.3.6**), after lime treatment at the lower lime dose (0.15 g/L) also qualitatively agrees with previous results from **§4.3.6** where there was a 41% reduction in AS concentration as shown in **Fig. 6-4b**. Additionally, the gypsum precipitation rate constants were found, in general, to decrease with each cycle in the cases with significant seed poisoning (i.e., GSP with AS and CESP with 0.15 g/L lime) (**Fig. 6-4a**). The absence of a large decrease in the observed gypsum precipitation rate constant after the first cycle (as observed during GSP without AS and CESP with 0.25 g/L lime) was likely due to AS seed-poisoning. As a result any differences in surface properties of fresh gypsum seeds (in the first cycle) were masked relative to gypsum particles that have undergone heterogeneous growth throughout later cycles. Nonetheless, after sufficient lime pretreatment (0.25 g/L), further reduction in the gypsum precipitation rate constant was not observed after the second cycle. Therefore, it is argued that the average rate constants for the second through fifth cycles, can serve as a reasonable estimate of the values for gypsum precipitation in a continuous CESP process.

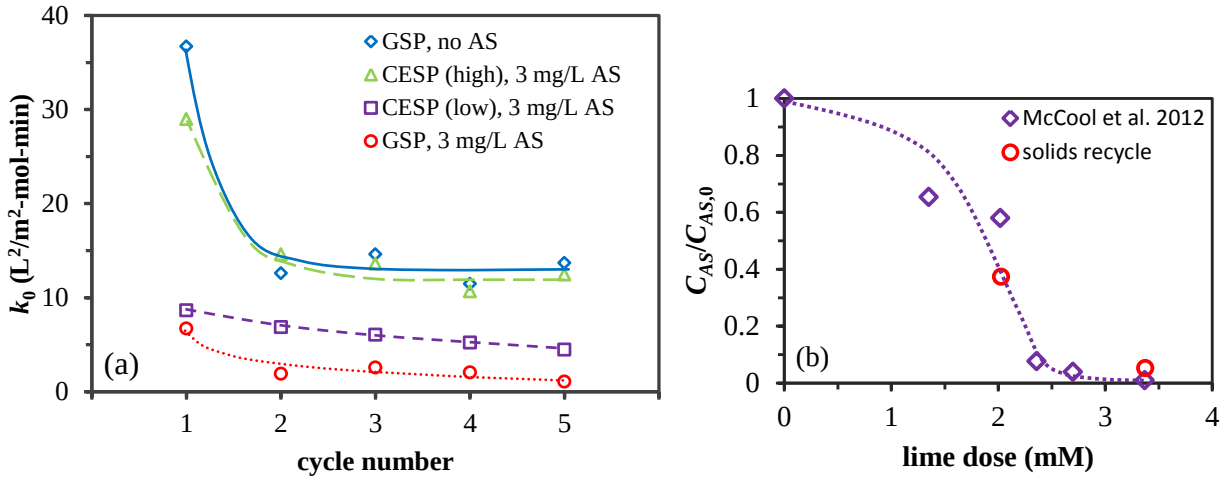

Figure 6-4. Initial gypsum precipitation rate constants (a) and average residual AS concentration (b) for five cycles of seeded precipitation using 5 g/L gypsum seeds to induce gypsum precipitation for the 1st cycle followed by recycled solids in the remaining cycles. Gypsum seeding was tested in model PRO concentrate (*SIg* = 2.5) with and without the presence of 3 mg/L AS and at two different lime pretreatment doses (0.25 or 0.15 g/L) for AS removal.

6.3.3 Reactor simulation model

In order to determine the requirements for a continuous CESP process, gypsum seeded precipitation was simulated for a crystallizer modeled as a vertical cylindrical plug-flow reactor (PFR, see **Appendix E.2**) with volume, V_R (L). The differential equation relating the sulfate concentration, *C*, to axial position, *x*, in an ideal PFR at steady-state is shown in **Eq. E-1**:

$$u_w \frac{dC}{dx} = -R = -kA\left(C_0 - C_{sat}\right)^2 \tag{6-2}$$

where u_w is the axial liquid velocity (m/s), *R* is the reaction rate for gypsum precipitation (mol/L-min), *k* is the rate constant (m^2/L^2-mol-min), *A* is the gypsum particle surface area (m^2/L), C_0 is the initial sulfate concentration (mol/L), and C_{sat} is the sulfate concentration (mol/L) at gypsum saturation (i.e., *SIg* = 1).

The lime-treated PRO concentrate, which was fed through the bottom of the PFR and exited at the top of the PFR, contained a specified volume fraction, ϕ_S, of suspended gypsum particles (see **Fig. 6-5**). The solids volume fraction was defined as: $\phi_S = V_S/V_R$, where V_S is the

total volume of gypsum particles. The gypsum seed particles, initially of diameter d_p (m) and standard deviation σ_p (m), were assumed to be evenly distributed throughout the reactor. The number of simulated particles, N, was determined based on the specified initial volume fraction, $\phi_{S,i}$. It was assumed that the seed particles did not aggregate or disaggregate, thereby preserving the number of particles in the reactor at steady-state. It is noted that if aggregation were to occur the surface area available for gypsum precipitation would decrease leading to a decreased overall rate of gypsum precipitation. Therefore, the occurrence of aggregation would necessitate a larger reactor. A flowchart of the simulation procedure is provided in **Fig. 6-6**.

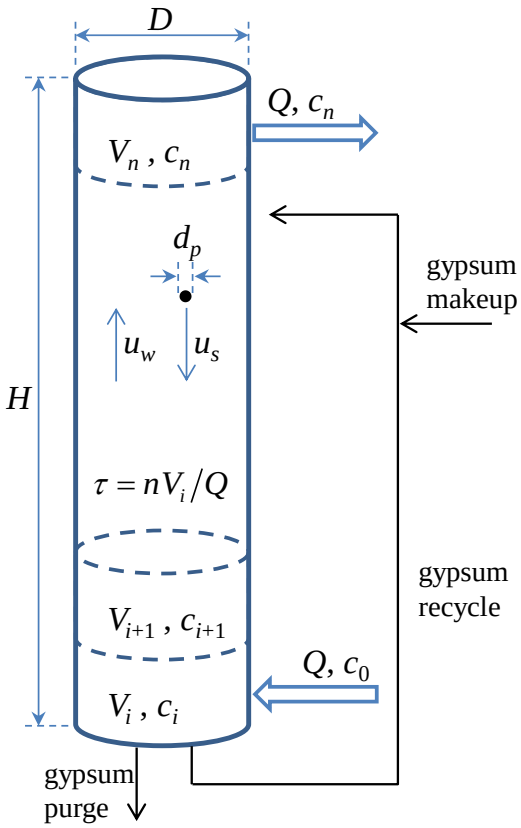

Figure 6-5. Detail of the GSP step of the continuous CESP process indicating gypsum recycle and simulation parameters.

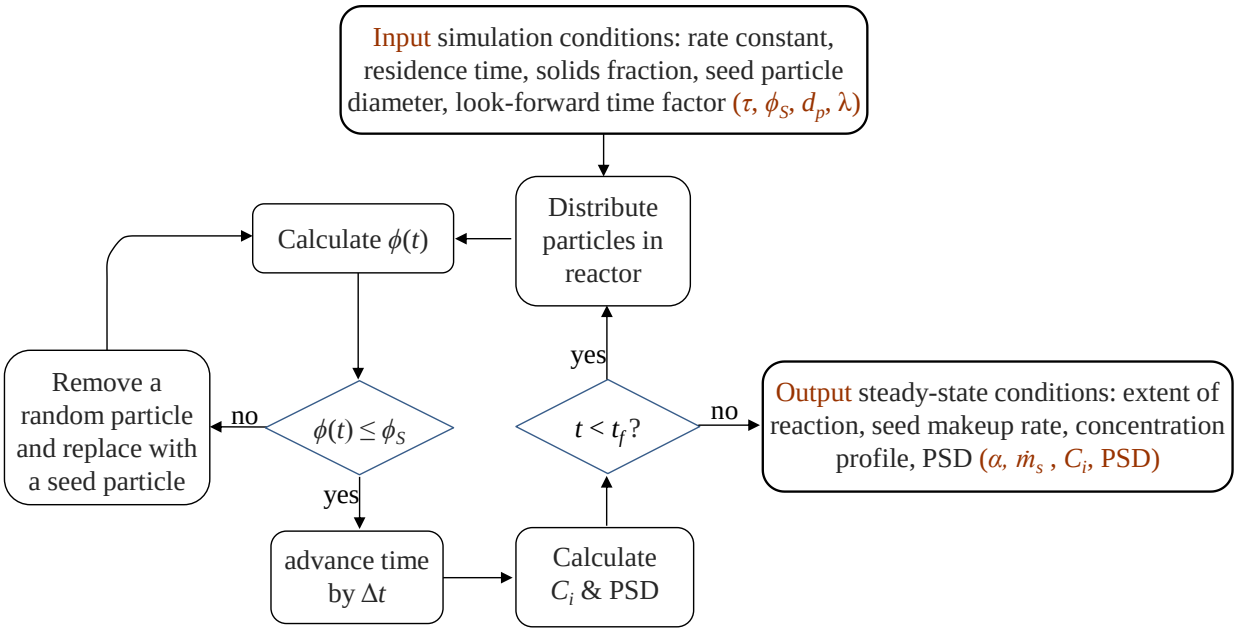

Figure 6-6. Reactor simulation flowchart

The concentration profile in the simulated reactor was determined as a function of position (i.e., reactor bin no.) and time, *t*, because the model did not assume steady-state conditions. In order to calculate the concentration profile and seed particle size at time *t*, the PFR was divided vertically into *n* equal-sized reactor bins of volume $V_i = V_R / n$ with uniform concentration and velocity profiles (i.e., plug flow). A sulfate mass balance on a differential reactor control volume leads to the following equation:

$$\frac{dC}{dt} = u_w \frac{dC}{dx} - R \tag{6-3}$$

where *C* is the sulfate concentration (mol/L), u_w is the average plug-flow velocity (m/s) along the reactor (*x*-direction), and *R* is the rate of gypsum precipitation (mol/L-min) given by **Eqn. (6-1)**. **Equation (6-3)** can be solved by a finite difference approach, whereby the reactor is divided vertically into *n* bins (see **Fig. 6-5**). Accordingly, the finite difference model can be expressed as:

$$C_i(t+\Delta t) = C_i(t) + \left(C_{i-1}(t) - C_i(t)\right)\frac{\Delta t}{\tau/n} - R_i(t)\Delta t \tag{6-4a}$$

$$R_i(t) = kA_i\left(C_i(t) - C_S\right)^2 \tag{6-4b}$$

where C_i is the sulfate concentration in the i^{th} bin, τ is the reactor convective residence time (min) and R_i is the rate of gypsum precipitation (mol/L-min) in the i^{th} bin, k is the rate constant (L^2/m^2-mol-min) for heterogeneous gypsum precipitation, A_i is the total specific surface area (m^2/L) of gypsum particles in the i^{th} bin at time t, and C_S is the sulfate concentration (M) at saturation (i.e., *SIg* =1). The gypsum precipitation rate constant, k, used in the simulation for the present work was set conservatively at 12 L^2/m^2-mol-min—slightly lower (7%) than the empirical value of 12.9 (L^2/m^2-mol-min) determined in **§6.3.2** for CESP with 0.25 g/L lime treatment—in order to model the continuous CESP process under a more challenging condition. The specific surface area in each bin, A_i, was calculated from **Eq. (6-5)**:

$$A_i(t) = \frac{\pi}{V_i}\sum_{j=1}^{N_i} d_{p,j}^2(t) \tag{6-5}$$

where $N_i = N/n$ is the number of particles in the i^{th} bin and $d_{p,j}$ is the size of the j^{th} particle. The particle sizes were determined at each time step based on their precipitative growth rates, assuming a spherical geometry, as shown in **Eqs. (6-6)** & **(6-7)**:

$$d_{p,j}(t+\Delta t) = d_{p,j}(t) + \frac{d}{dt}\left(d_{p,j}\right)\Delta t \tag{6-6}$$

$$\frac{d}{dt}\left(d_{p,j}\right) = \frac{2kF}{\rho_g}\left(C_i(t) - C_S\right)^2 \tag{6-7}$$

where F is the formula weight of gypsum (172.17 g/mol) and ρ_g is the density of gypsum (2.32 g/cm^3) [8]. At the end of each time step the seed particles in the reactor were randomly redistributed among the reactor bins to simulate the gypsum solids recycling (**Fig. 6-5**).

The model equations were solved subject to a concentration boundary condition set as $C(x = 0) = C_0$ at the reactor bottom (i.e., $x = 0$), as determined by the PRO concentrate to be

treated. The initial concentration throughout the reactor (i.e., at $t = 0$) was set to $C(t = 0) = 0$. The simulation was initiated with a seed dose of 5 g/L (and corresponding initial volume fraction); a specified volume fraction, ϕ_S, was used to determine if particles were removed or if makeup seeds were needed. If the volume fraction calculated after each time step, $\phi(t)$, was greater than the specified value, ϕ_S, random particles were removed from the reactor one at a time and replaced with an equal number of makeup seed particles until $\phi(t) < \phi_S$ prior to the next time step. While $\phi(t) < \phi_S$, the particles currently in the reactor grow until $\phi(t) > \phi_S$, at which time the cycle of particle removal and replacement continues until the specified final time, t_f. For example, in the present work, t_f was set as a multiple, $\lambda = 1.5$, of the time required to reach steady-state, t_{ss}, with respect to the concentration profile and particle size distribution. This multiple of the steady-state time ($\lambda = 1.5$) allowed the simulation to continue after reaching steady-state for a time period equal to 50% of the time required to reach steady-state. The resulting reactor conditions (e.g., α_{sulfate}, seed makeup rate) were calculated as averages over the steady-state time period (i.e., from t_{ss} to $t_f = 1.5 \cdot t_{ss}$) and used for subsequent reactor sizing as described in **§6.3.4**.

6.3.4 Reactor sizing

The continuous GSP process was sized based on a vertical cylindrical PFR. The height, H (m), of the PFR desupersaturation unit was expressed as the product of the maximum axial fluid velocity, u_w (m/s), and the residence time, τ (s), required to achieve the desired sulfate extent of reaction as shown in **Eq. (6-8)**. This relationship was based on the assumption of plug flow where the distance traveled (i.e., total height traversed, H) for any given fluid element is simply

equal to the product of the velocity of the fluid element, u_w, and the length of time, τ, the fluid element spends in the reactor.

$$H = u_w \cdot \tau \tag{6-8}$$

The maximum fluid velocity was set equal to the Stokes' settling velocity of the seed particle diameter, d_p, such that the crystallizer operation would avoid particle overflow:

$$u_w = \frac{\left(\rho_g - \rho_w\right)}{18\mu_w} g \cdot d_p^2 \tag{6-9}$$

where ρ_g and ρ_w are densities (kg/m^3) of the gypsum particles and water, respectively, g is the gravitational acceleration (m/s^2), and μ_w is the viscosity (kg/m-s^2) of the water. The Stokes' settling velocity calculation assumes that the settling particles do not affect each other, i.e., the settling velocity of each particle is independent of the other settling particles. Thus, the Stokes' settling velocity provides a lower limit on the actual particle settling velocities as any induced convective flow trailing a particle may increase the settling velocity of neighboring particles. It is noted that a seed particle may overflow from the top of the reactor if its size is much smaller than the average seed particle size as the maximum fluid velocity in the column is based on the average seed particle size (see **Eq. 6-9**). However, in the present case of seed particles with a standard deviation equal to 22% of the average size (based on the gypsum seeds used in the present study, see **§6.2.1**), particle overflow would be negligible since the steady-state particle size distributions (see **Appendix E.2**, **Fig. E-5**) indicate that 98% of the particles (containing >99.9% of the total surface area) would be larger than the average seed particle diameter. Thus, at steady-state, the gypsum precipitation rate in the reactor would be maintained (with negligible loss of solids surface area) with a fluid velocity equal to the settling velocity of the average seed

particle size over the range of reactor conditions simulated in the present work (see **Appendix E.3**).

The minimum column diameter, D (m), for a cylindrical PFR is determined by the total fluid flow rate, Q (m^3/s), from the PRO concentrate stream, the reactor solids fraction ϕ, and the maximum fluid velocity in the column, u_w, as shown in **Eq. (6-10)**, derived from the fundamental relationship between cross-sectional area (Ac), fluid velocity (u_w), and volumetric flow rate (Q): $Q = Ac \cdot u_w$.

$$D = \left(\frac{4Q}{\pi (1-\phi) u_w} \right)^{1/2} \tag{6-10}$$

If the minimum column diameter calculated from **Eq. (6-10)** is undesirably or impractically large, the crystallizer may be scaled down while maintaining the same residence time. The crystallizer may be implemented as a number, n_c, of smaller diameter columns in parallel to reduce the diameter of each column while still being able to accommodate the same PRO concentrate flow rate, Q, as shown in **Eq. (6-11)**. The diameter of the scaled down columns, D_n, operating in parallel is calculated by maintaining a constant total cross sectional area. As the cross sectional area is proportional to the square of the diameter, the following relationship can be derived to obtain D_n as a function of the number of columns in parallel, n_c.

$$D_n = D \cdot n_c^{-1/2} \tag{6-11}$$

The general approach to reactor sizing based on simulation results is summarized in **Fig. 6-7**.

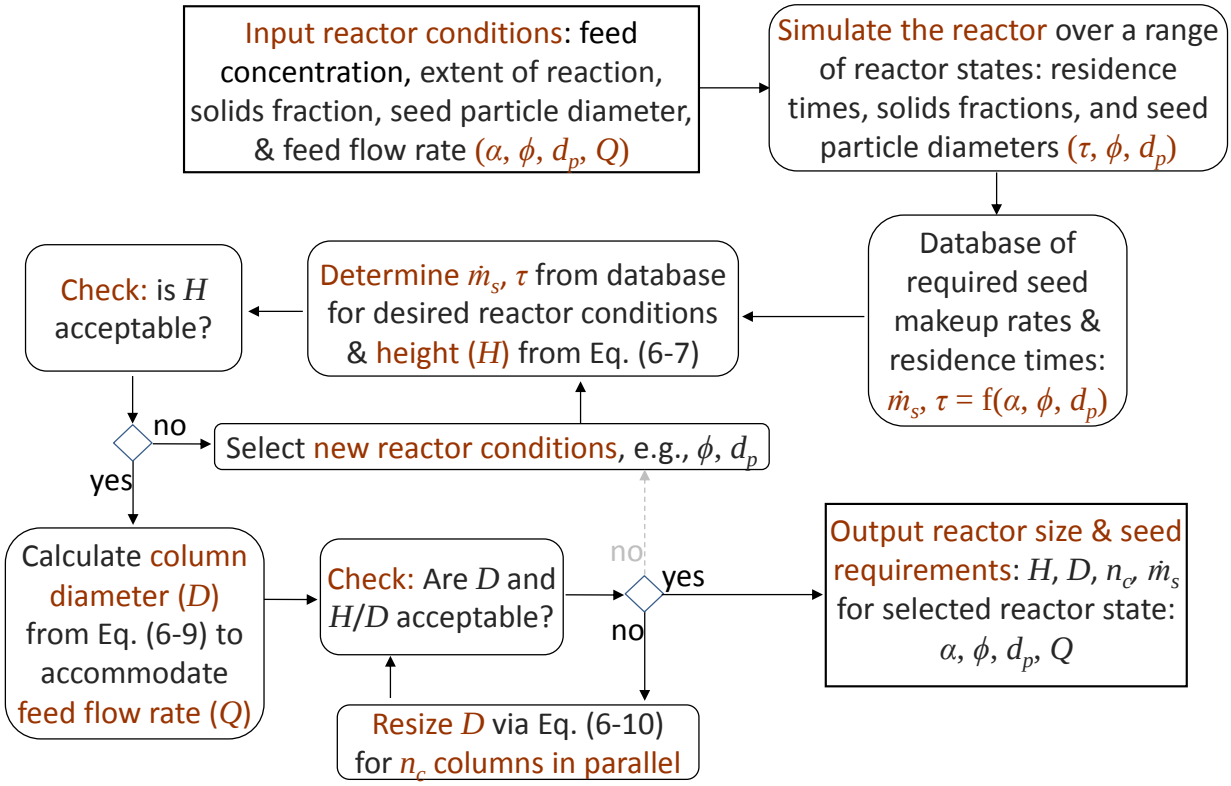

Figure 6-7. Gypsum seeded precipitation PFR reactor (crystallizer) sizing flowchart. The desired reactor state (α, ϕ, d_p) is the input and the reactor size (H, D, n) and seed makeup requirement ($\dot{m}_s$) are the outputs.

6.3.5 Reactor simulation results

A representative example of the reactor sizing approach is illustrated in **Fig. 6-7**. The analysis was performed for PRO concentrate with *SIg* = 2.5 (OAS location in SJV, 63% *Y*, see **Tables 3-4, 4-1** & **Appendix A**). The reactor was modeled over a range of reactor states (i.e., combinations of residence times, solids fractions, and seed particle diameters) to generate a database of residence times required to achieve the desired extent of reaction for various solid fractions and seed particle diameters (**Appendix E.3**). Illustrative model results are provided in **Fig. 6-8** for the simulation of a reactor with 65-μm gypsum seeds. The required residence time

and corresponding reactor height (see **Eq. 6-8**) increased with sulfate extent of reaction with the residence time increasing rapidly as the extent of reaction and *SIg* approach unity (**Fig. 6-8a**) as would be expected for a PFR (see **Appendix E**, **Eq. E-3**). The required residence times also decreased with increasing solids fraction as the amount of surface area and hence the rate of reaction (**Eq. 6-4**) increased with increasing solids fraction in the reactor (**Fig. 6-8a**). Both the seed makeup rate and solids purge rate (g/L-min) decreased with increasing extent of reaction (**Figs. 6-8b** & **6-8c**) because higher residence times and larger reactor volumes are required at higher extents of reaction. Therefore, the specific seed makeup rate and solids purge rates (g/L-min) decrease with increasing reactor volume.

The solids purge rate, $\dot{m}_p$, increased with increasing solids fraction (**Fig. 6-8b**) because the shorter required residence times, occurring at larger solids fractions, resulted in a larger average particle growth rate (i.e., volume average $d(d_p)/dt$, see **§6.3.3**) and consequently, larger average particle volume growth rate (i.e., $d(V_p)/dt = \pi d_p^2/2 \cdot d(d_p)/dt$). Therefore, at higher solids fractions the reactor must be purged more frequently to maintain the solids fraction set point, ϕ_S. The required seed makeup rate, $\dot{m}_s$, was calculated from the solids purge rate, $\dot{m}_p$, according to the steady-state mass balance expressed by **Eq. 6-12**:

$$\dot{m}_S = \dot{m}_P - \dot{m}_{ppt} = \dot{m}_P - F\alpha_{sulfate}\left(C_0 - C_S\right)/\tau \tag{6-12}$$

where $\dot{m}_{ppt}$ is the gypsum precipitation rate in the reactor and is specified by the sulfate extent of reaction and the residence time (as indicated in **Eq. 6-12**) and F is the formula weight of gypsum. The seed makeup rate was independent of the solids fraction (**Fig. 6-8c**) because the increase in the solids purge rate that occurs increasing solids fraction was offset by the corresponding decrease in residence time as shown in **Eq. 6-12**. In other words, both the solids purge rate, $\dot{m}_p$, and gypsum precipitation rate, $\dot{m}_{ppt}$, increase equally with increasing solids

fraction resulting in their difference, $\dot{m}_s$, remaining constant. The above simulation results revealed that there is a trade-off between reactor height and sulfate extent of reaction, with required reactor heights increasing rapidly for sulfate extents of reaction greater than ~0.9. The trends observed in **Fig. 6-8** were representative of those observed for all seed particle sizes (45–200 μm) used in simulations for the present work. These results also indicate that the reactor should be designed to operate with the highest feasible solids fraction in order to minimize the required reactor height for a given sulfate extent of reaction.

The simulation results for the specific case of a reactor with τ = 10 min, ϕ = 0.5, d_p = 65 μm, and Q = 1 gal/min (0.063 L/s) resulting in a final α_{sulfate} = 0.914, are presented here as a representative example for reactor sizing. The detailed concentration profile and particle size distribution are described in **Appendix E.2** (**Figs. E-4** & **E-5)**. The corresponding reactor size requirements were determined to be: H = 1.78 m, D = 0.233 m, n_c = 1, $\dot{m}_p$ = 0.2998 g/L-min, and $\dot{m}_s$ = 0.0024 g/L-min based on the flowchart illustrated in **Fig. 6-7**. It is noted that in the present work aggregation was neglected, however, if aggregation were to occur the overall rate of gypsum precipitation would decrease. Thus, larger residence times and reactor heights would be required in the presence of gypsum particle aggregation.

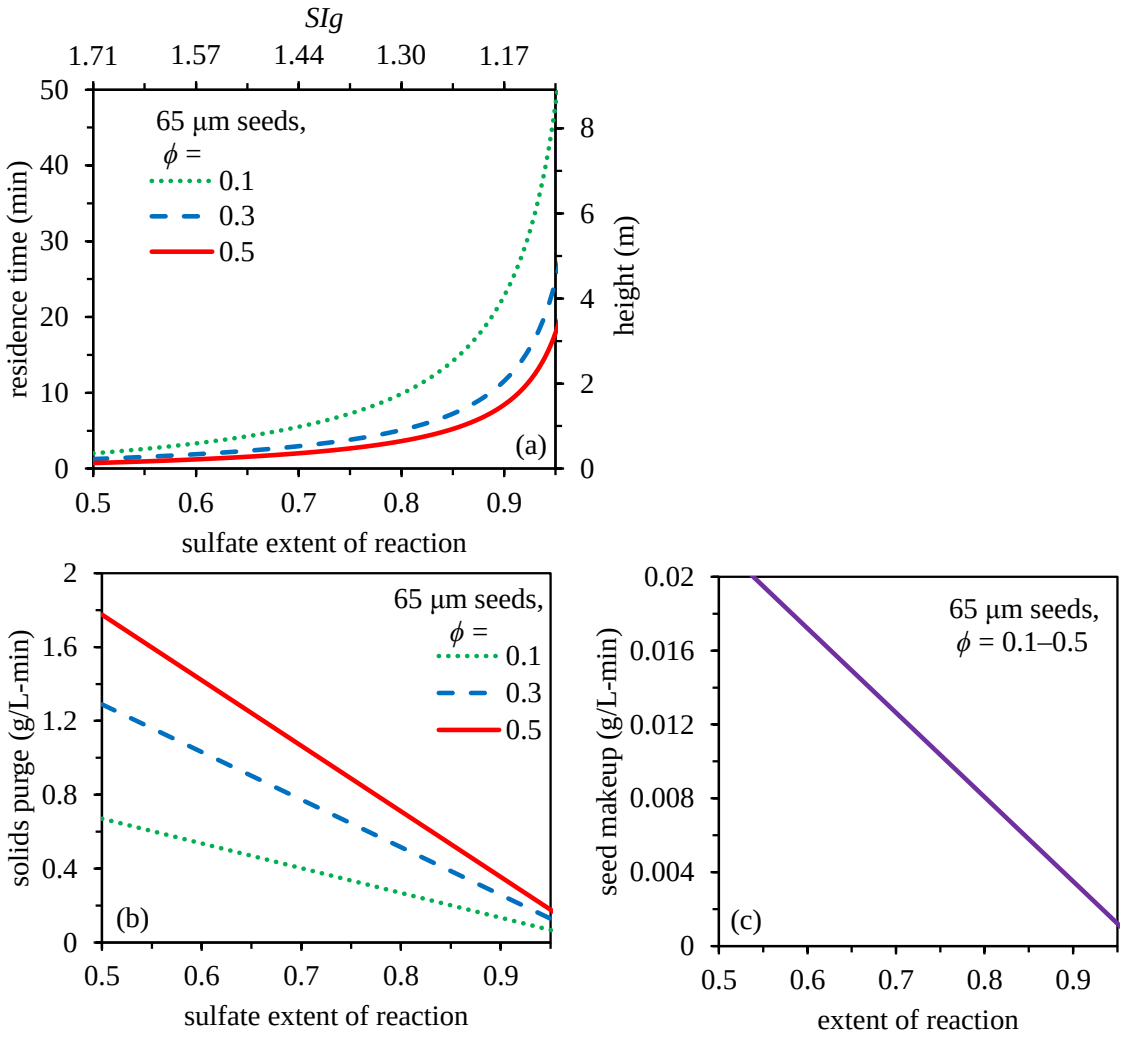

Figure 6-8. Crystallizer residence time, τ, and height, H (a), solids purge rate, $\dot{m}_p$ (b), and seed makeup rate, $\dot{m}_s$ (c) as a function of extent of reaction, $\alpha_{sulfate}$, and *SIg* for solids fraction, ϕ = 0.1–0.5, all using 65-µm seeds.

6.4 Conclusions

An experimental study was performed to demonstrate the feasibility of a continuous CESP reactor with gypsum solids recycling and quantify the gypsum precipitation kinetics during chemically-enhanced seeded precipitation of brackish water RO concentrate of high gypsum scaling propensity. A series of batch multi-cycle seeded gypsum precipitation experiments with solids recycling were performed to assess the feasibility of a continuous CESP process. The removal of AS carry-over via lime-induced $CaCO_3$ precipitation (see **Ch. 4**) prior to

gypsum seeding was found to prevent poisoning of the gypsum seeds during CESP over multiple cycles. The observed kinetic rate constant for gypsum precipitation subsequent to adequate lime pretreatment (0.25 g/L lime) for AS removal (see **Ch. 4**) was found to reach a constant value of 12.9 L^2/m^2-mol-min after the first cycle of CESP; the rate of precipitation was maintained over multiple subsequent cycles with solids recycling. The observed rate constant for CESP with 0.25 g/L lime (12.9 L^2/m^2-mol-min) was only slightly lower (4%) than that observed for GSP without AS dosing (13.5 L^2/m^2-mol-min) indicating that gypsum seed poisoning by AS was prevented. Furthermore, indirect measurements of AS concentration based on the observed gypsum precipitation rate constants showed that the AS concentration was reduced by 95% via lime-induced $CaCO_3$ precipitation prior to gypsum seeding.

Additionally, a general model was developed to simulate the crystallization reactor as a cylindrical PFR in order to determine the operating requirements for the continuous GSP process. The empirically determined rate constant from the batch CESP studies was used in the GSP crystallizer simulations to generate a database of feasible reactor conditions (e.g., residence time, seed particle size, feed flow rate, extent of reaction, and seed makeup rate). Finally, a general process was developed to size the GSP crystallizer (e.g., height, diameter) based on the desired reactor operating conditions selected from the previously generated database. The simulation results revealed that there is a trade-off between sulfate extent of reaction (i.e., final *SIg*) and reactor height, with the required reactor height increasing rapidly for sulfate extents of reaction above ~ 0.9. Furthermore, the required reactor height can be reduced by operating the reactor at the highest feasible gypsum solids fraction.

References

1. Rahardianto, A., B.C. McCool, and Y. Cohen, *Accelerated Desupersaturation of Reverse Osmosis Concentrate by Chemically-Enhanced Seeded Precipitation.* Desalination, 2010. **264**(3).
2. McCool, B.C., et al., *Feasibility of reverse osmosis desalination of brackish agricultural drainage water in the San Joaquin Valley.* Desalination, 2010. **261**(3): p. 240-250.
3. Christoffersen, M.R., et al., *Crystal-growth of calcium-sulfate dihydrate at low supersaturation.* Journal of Crystal Growth, 1982. **58**(3): p. 585-595.
4. McCool, B.C., A. Rahardianto, and Y. Cohen, *Antiscalant removal in accelerated desupersaturation of RO concentrate via chemically-enhanced seeded precipitation (CESP).* Water Research, 2012(0).
5. Nancollas, G.H., *Growth of crystals in solution.* Advances in Colloid and Interface Science, 1979. **10**(JAN): p. 215-252.
6. Hina, A. and G.H. Nancollas, *Precipitation and dissolution of alkaline earth sulfates: Kinetics and surface energy.* Sulfate Minerals - Crystallography, Geochemistry and Environmental Significance, 2000. **40**: p. 277-301.
7. Rahardianto, A., *High recovery desalting of brackish water, doctoral dissertation*. 2009, University of California Los Angeles.
8. Deer, W., R. Howie, and J. Zussman, *Rock Forming Minerals, Vol. 5: Non-Silicates*. 1962, New York.

Appendix A. Water quality analytical reports

The detailed water quality analyses for all water samples utilized in the reported studies (see **§3.3.1 §4.2.1, §5.2, §6.2**) are provided in this appendix. Water quality analyses were performed by the California Department of Water Resources (DWR) Bryte Laboratory (West Sacramento, CA). Historical water quality data from the CNR (CNR0801), ERR (ERR8429), LNW (LNW6467), OAS (OAS2548), and VGD (VGD4406) locations (see **Fig. 3-1**) were obtained from the DWR *San Joaquin Valley Drainage Monitoring Program 2000* (2003) report (see **§3.3.1**).

A.1 CNR, 7/31/06

Monday, August 21, 2006 *Submittal ID FWA0706B0110*

DWR Bryte Laboratory
1450 Riverbank Road, West Sacramento, CA 95605

Inorganic Analyses

Including Misc Physical Measurements

Report of Analytical Results

Sample Number	Station:	Cost Code:	Collection Date	Sample Purpose
FWA0706B0436	CNR0801 T.D. CNR0801	100681	7/31/2006 10:30:00 AM	Normal Sample 0

Matrix: Water, Natural *Description:* Tile Drain Water

Customer Instructions Tile Drain Water for Scale Potential Study *SampleCondition:*

Method	Analyte	Result	Units	Reprting Limit	Footnotes:	Chemist	Analysis Date
Std Method 2510-B	Conductance (EC)	7111	µS/cm	1		Chan, Elaine	8/4/2006
Std Method 4500-CO2	Dissolved Bicarbonate (HCO3-)	229	mg/L as CaCO3	1		Chan, Elaine	8/4/2006
EPA 200.7 (D)	Dissolved Boron	13.5	mg/L	0.5	R4	Quiambao, Josie	8/8/2006
EPA 200.7 (D)	Dissolved Calcium	350	mg/L	5	R4	Quiambao, Josie	8/8/2006
Std Method 4500-CO2	Dissolved Carbonate (CO3--)	1	mg/L as CaCO3	1		Chan, Elaine	8/4/2006
EPA 300.0 28d Hold	Dissolved Chloride	324	mg/L	50		Pineda, Maritza	8/2/2006
EPA 300.0 28d Hold	Dissolved Fluoride	< 5.	mg/L	5	R5	Pineda, Maritza	8/2/2006
Std Method 4500-CO2	Dissolved Hydroxide (OH-)	< 1.	mg/L as CaCO3	1		Chan, Elaine	8/4/2006
EPA 200.7 (D)	Dissolved Magnesium	236	mg/L	5	R4	Quiambao, Josie	8/8/2006
EPA 300.0 28d Hold	Dissolved Nitrate	344	mg/L	5		Pineda, Maritza	8/2/2006
EPA 415.1 (D) Ox	Dissolved Organic Carbon	4.2	mg/L as C	0.5		Fong, Sid	8/3/2006
EPA 200.7 (D)	Dissolved Potassium	46.7	mg/L	2.5	R4	Quiambao, Josie	8/8/2006
EPA 200.8 (D)	Dissolved Selenium	0.032	mg/L	0.01		Thind, Pritam	8/10/200
EPA 200.7 (D)	Dissolved Silica (SiO2)	23.5	mg/L	0.5	R4	Quiambao, Josie	8/8/2006
EPA 200.7 (D)	Dissolved Sodium	1250	mg/L	5	R4	Quiambao, Josie	8/8/2006
EPA 300.0 28d Hold	Dissolved Sulfate	3700	mg/L	50		Pineda, Maritza	8/2/2006
Std Method 2320 B	pH	7.5	pH Units	0.1		Chan, Elaine	8/4/2006
EPA 150.1	pH	7.5	pH Units	0.1	H2	Chan, Elaine	8/4/2006
Std Method 2320 B	Total Alkalinity	230	mg/L as CaCO3	1		Chan, Elaine	8/4/2006
EPA 200.8 (T)	Total Aluminum	< .1	mg/L	0.1		Thind, Pritam	8/11/200
EPA 200.8 (T)	Total Arsenic	< .01	mg/L	0.01		Thind, Pritam	8/11/200
EPA 200.8 (T)	Total Barium	< .5	mg/L	0.5		Thind, Pritam	8/11/200
Std Method 2540 C	Total Dissolved Solids	6372	mg/L	1		Chan, Elaine	8/2/2006
EPA 200.8 (T)	Total Iron	0.174	mg/L	0.05		Thind, Pritam	8/11/200
EPA 200.8 (T)	Total Manganese	< .05	mg/L	0.05		Thind, Pritam	8/11/200
EPA 415.1 (T) Ox	Total Organic Carbon	4.5	mg/L as C	0.5		Fong, Sid	8/3/2006
EPA 365.4	Total Phosphorus	0.01	mg/L	0.01		Hernandez, Rich	8/7/2006
EPA 200.8 (T)	Total Selenium	0.034	mg/L	0.01		Thind, Pritam	8/11/200
EPA 200.8 (T)	Total Strontium	17.2	mg/L	0.05		Thind, Pritam	8/11/200
EPA 160.2	Total Suspended Solids	< 1.	mg/L	1		Chan, Elaine	8/4/2006
Std Method 5910B	UV Absorbance @254nm	0.126	absorbance/cm	0.001		Toomey, Marilyn	8/10/200

N.A.=Not Analyzed *Reporting Limits Adjusted For Dilution*

A.2 ERR, 1/29/07

Tuesday, February 27, 2007 *Submittal ID FWA0107B0001*

DWR Bryte Laboratory
1450 Riverbank Road, West Sacramento, CA 95605

Inorganic Analyses

Including Misc Physical Measurements

Report of Analytical Results

Sample Number	Station:	Cost Code:	Collection Date	Sample Purpose
FWA0107B0001	ERR8429 T.D. ERR8429	100681	1/29/2007 8:15:00 AM	Normal Sample 0

Matrix: Water, Natural Description: Tile Drain Water

Customer Instructions: Tile Drain Water for Scale Potential Study SampleCondition:

Method	Analyte	Result	Units	Reprting Limit	Footnotes:	Chemist	Analysis Date
Std Method 2510-B	Conductance (EC)	5580	µS/cm	1		Chan, Elaine	2/2/2007
Std Method 4500-CO2	Dissolved Bicarbonate (HCO3-)	699	mg/L as CaCO3	1		Chan, Elaine	2/2/2007
EPA 200.7 (D)	Dissolved Boron	2.6	mg/L	0.1		Quiambao, Josie	2/2/2007
EPA 200.7 (D)	Dissolved Calcium	88	mg/L	1		Quiambao, Josie	2/2/2007
Std Method 4500-CO2	Dissolved Carbonate (CO3--)	7	mg/L as CaCO3	1		Chan, Elaine	2/2/2007
EPA 300.0 28d Hold	Dissolved Chloride	632	mg/L	50		Pineda, Maritza	2/2/2007
EPA 300.0 28d Hold	Dissolved Fluoride	< 5.	mg/L	5	R5	Pineda, Maritza	2/2/2007
Std Method 4500-CO2	Dissolved Hydroxide (OH-)	< 1.	mg/L as CaCO3	1		Chan, Elaine	2/2/2007
EPA 200.7 (D)	Dissolved Magnesium	59	mg/L	1		Quiambao, Josie	2/2/2007
EPA 300.0 28d Hold	Dissolved Nitrate	51.3	mg/L	5		Pineda, Maritza	2/2/2007
EPA 415.1 (D) Ox	Dissolved Organic Carbon	15.8	mg/L as C	0.5		Wong, Allan	2/14/200
EPA 200.7 (D)	Dissolved Potassium	3.5	mg/L	0.5		Quiambao, Josie	2/2/2007
EPA 200.8 (D)	Dissolved Selenium	0.011	mg/L	0.01		Thind, Pritam	2/5/2007
EPA 200.7 (D)	Dissolved Silica (SiO2)	38	mg/L	0.5	R4	Quiambao, Josie	2/2/2007
EPA 200.7 (D)	Dissolved Sodium	1250	mg/L	5	R4	Quiambao, Josie	2/2/2007
EPA 300.0 28d Hold	Dissolved Sulfate	1570	mg/L	50		Pineda, Maritza	2/2/2007
Std Method 2320 B	pH	8	pH Units	0.1		Chan, Elaine	2/2/2007
Std Method 2320 B	Total Alkalinity	706	mg/L as CaCO3	1		Chan, Elaine	2/2/2007
EPA 200.8 (T)	Total Aluminum	0.102	mg/L	0.1		Thind, Pritam	2/5/2007
EPA 200.8 (T)	Total Arsenic	0.089	mg/L	0.01		Thind, Pritam	2/5/2007
EPA 200.8 (T)	Total Barium	< .5	mg/L	0.5		Thind, Pritam	2/5/2007
Std Method 2540 C	Total Dissolved Solids	4116	mg/L	1		Chan, Elaine	2/2/2007
Std Method 2540 C	Total Dissolved Solids	4114	mg/L	1		Chan, Elaine	2/2/2007
EPA 200.8 (T)	Total Iron	0.279	mg/L	0.05		Thind, Pritam	2/5/2007
EPA 200.8 (T)	Total Manganese	0.595	mg/L	0.05		Thind, Pritam	2/5/2007
EPA 415.1 (T) Ox	Total Organic Carbon	16.7	mg/L as C	0.5		Wong, Allan	2/14/200
EPA 365.4	Total Phosphorus	1.96	mg/L	0.01		Nickels, Bill	2/6/2007
EPA 200.8 (T)	Total Selenium	0.013	mg/L	0.01		Thind, Pritam	2/5/2007
EPA 200.8 (T)	Total Strontium	0.898	mg/L	0.05		Thind, Pritam	2/5/2007
EPA 160.2	Total Suspended Solids	4	mg/L	1		Chan, Elaine	2/2/2007
EPA 160.2	Total Suspended Solids	4	mg/L	1		Chan, Elaine	2/2/2007
Std Method 5910B	UV Absorbance @254nm	0.587	absorbance/cm	0.001		Toomey, Marilyn	2/2/2007

N.A.=Not Analyzed *Reporting Limits Adjusted For Dilution*

A.3 LNW, 2/15/06

Thursday, March 02, 2006 *Submittal ID FWA0206B0034*

DWR Bryte Laboratory
1450 Riverbank Road, West Sacramento, CA 95605

Inorganic Analyses

Including Misc Physical Measurements

Report of Analytical Results

Sample Number	Station:	Cost Code:	Collection Date	Sample Purpose
FWA0206B0118	LNW6467 T.D. LNW6467	100681	2/15/2006 10:15:00 AM	Normal Sample 0

Matrix: Water, Natural Description: Tile Drain Water

Customer Instructions Tile Drain Water for Scale Potential Study SampleCondition:

Method	Analyte	Result	Units	Reprting Limit	Footnotes:	Chemist	Analysis Date
Std Method 2510-B	Conductance (EC)	14430	µS/cm	1		Chan, Elaine	2/17/200
Std Method 4500-CO2	Dissolved Bicarbonate (HCO3-)	128	mg/L as CaCO3	1		Chan, Elaine	2/17/200
EPA 200.7 (D)	Dissolved Boron	17.5	mg/L	1	R4	Quiambao, Josie	2/23/200
EPA 200.7 (D)	Dissolved Calcium	625	mg/L	10	R4	Quiambao, Josie	2/23/200
Std Method 4500-CO2	Dissolved Carbonate (CO3--)	1	mg/L as CaCO3	1		Chan, Elaine	2/17/200
EPA 300.0 28d Hold	Dissolved Chloride	3020	mg/L	100		Pineda, Maritza	2/17/200
EPA 300.0 28d Hold	Dissolved Fluoride	< 10.	mg/L	10	R5	Pineda, Maritza	2/17/200
Std Method 4500-CO2	Dissolved Hydroxide (OH-)	< 1.	mg/L as CaCO3	1		Chan, Elaine	2/17/200
EPA 200.7 (D)	Dissolved Magnesium	198	mg/L	10	R4	Quiambao, Josie	2/23/200
EPA 300.0 28d Hold	Dissolved Nitrate	155	mg/L	10		Pineda, Maritza	2/17/200
EPA 415.1 (D) Ox	Dissolved Organic Carbon	4.6	mg/L as C	0.5		Aylesworth, Stac	2/24/200
					Ran twice. DOC higher than TOC both times.		
EPA 200.7 (D)	Dissolved Potassium	< 5.	mg/L	5	R4	Quiambao, Josie	2/23/200
EPA 200.8 (D)	Dissolved Selenium	0.223	mg/L	0.01		Thind, Pritam	2/16/200
EPA 200.7 (D)	Dissolved Silica (SiO2)	37.9	mg/L	1	R4	Quiambao, Josie	2/23/200
EPA 200.7 (D)	Dissolved Sodium	2820	mg/L	20	R4	Quiambao, Josie	2/23/200
EPA 300.0 28d Hold	Dissolved Sulfate	4520	mg/L	100		Pineda, Maritza	2/17/200
EPA 150.1	pH	7.6	pH Units	0.1	H2	Chan, Elaine	2/17/200
Std Method 2320 B	pH	7.6	pH Units	0.1		Chan, Elaine	2/17/200
Std Method 2320 B	Total Alkalinity	128	mg/L as CaCO3	1		Chan, Elaine	2/17/200
EPA 200.8 (T)	Total Aluminum	< .1	mg/L	0.1		Thind, Pritam	2/24/200
EPA 200.8 (T)	Total Arsenic	0.014	mg/L	0.01		Thind, Pritam	2/24/200
EPA 200.8 (T)	Total Barium	< .5	mg/L	0.5		Thind, Pritam	2/24/200
Std Method 2540 C	Total Dissolved Solids	11270	mg/L	1		Chan, Elaine	2/17/200
EPA 200.8 (T)	Total Iron	0.152	mg/L	0.05		Thind, Pritam	2/24/200
EPA 200.8 (T)	Total Manganese	< .05	mg/L	0.05		Thind, Pritam	2/24/200
EPA 415.1 (T) Ox	Total Organic Carbon	3.4	mg/L as C	0.5		Aylesworth, Stac	2/23/200
					Ran twice. DOC higher than TOC both times.		
EPA 365.4	Total Phosphorus	0.03	mg/L	0.01		Hernandez, Rich	2/17/200
EPA 200.8 (T)	Total Selenium	0.235	mg/L	0.01		Thind, Pritam	2/24/200
EPA 200.8 (T)	Total Strontium	9.96	mg/L	0.05		Thind, Pritam	2/24/200
EPA 160.2	Total Suspended Solids	4	mg/L	1		Aylesworth, Stac	2/17/200
Std Method 5910B	UV Absorbance @254nm	0.094	absorbance/cm	0.001		Toomey, Marilyn	2/17/200

N.A.=Not Analyzed *Reporting Limits Adjusted For Dilution*

A.4 OAS, 4/10/06

Tuesday, May 02, 2006 *Submittal ID FWA0406B0065*

DWR Bryte Laboratory
1450 Riverbank Road, West Sacramento, CA 95605

Inorganic Analyses

Including Misc Physical Measurements

Report of Analytical Results

Sample Number FWA0406B0246

Station: T.D. OAS2548
T.D. OAS2548

Cost Code: 100681

Collection Date 4/10/2006 11:30:00 AM

Sample Purpose Normal Sample 0

Matrix: Water, Natural **Description:** Tile Drain Water

Customer Instructions Tile Drain Water for Scale Potential Study **SampleCondition:**

Method	Analyte	Result	Units	Reprting Limit	Footnotes:	Chemist	Analysis Date
Std Method 2510-B	Conductance (EC)	12620	µS/cm	1		Chan, Elaine	4/13/200
Std Method 4500-CO2	Dissolved Bicarbonate (HCO3-)	212	mg/L as CaCO3	1		Chan, Elaine	4/13/200
EPA 200.7 (D)	Dissolved Boron	23.5	mg/L	1	R4	Quiambao, Josie	4/19/200
EPA 200.7 (D)	Dissolved Calcium	462	mg/L	10	R4	Quiambao, Josie	4/19/200
Std Method 4500-CO2	Dissolved Carbonate (CO3--)	1	mg/L as CaCO3	1		Chan, Elaine	4/13/200
EPA 300.0 28d Hold	Dissolved Chloride	1060	mg/L	100		Pineda, Maritza	4/14/200
EPA 300.0 28d Hold	Dissolved Fluoride	< 10.	mg/L	10	R5	Pineda, Maritza	4/14/200
Std Method 4500-CO2	Dissolved Hydroxide (OH-)	< 1.	mg/L as CaCO3	1		Chan, Elaine	4/13/200
EPA 200.7 (D)	Dissolved Magnesium	284	mg/L	10	R4	Quiambao, Josie	4/19/200
EPA 300.0 28d Hold	Dissolved Nitrate	46.7	mg/L	10		Pineda, Maritza	4/14/200
EPA 415.1 (D) Ox	Dissolved Organic Carbon	5.1	mg/L as C	0.5		Aylesworth, Stac	4/22/200
EPA 200.7 (D)	Dissolved Potassium	< 5.	mg/L	5	R4	Quiambao, Josie	4/19/200
EPA 200.8 (D)	Dissolved Selenium	0.184	mg/L	0.01		Thind, Pritam	4/19/200
EPA 200.7 (D)	Dissolved Silica (SiO2)	31.4	mg/L	1	R4	Quiambao, Josie	4/19/200
EPA 200.7 (D)	Dissolved Sodium	2780	mg/L	10	R4	Quiambao, Josie	4/19/200
EPA 300.0 28d Hold	Dissolved Sulfate	6360	mg/L	100		Pineda, Maritza	4/14/200
Std Method 2320 B	pH	7.6	pH Units	0.1		Chan, Elaine	4/13/200
EPA 150.1	pH	7.6	pH Units	0.1	H2	Chan, Elaine	4/13/200
Std Method 2320 B	Total Alkalinity	213	mg/L as CaCO3	1		Chan, Elaine	4/13/200
EPA 200.8 (T)	Total Aluminum	< .05	mg/L	0.05		Thind, Pritam	4/18/200
EPA 200.8 (T)	Total Arsenic	0.006	mg/L	0.005		Thind, Pritam	4/18/200
EPA 200.8 (T)	Total Barium	< .25	mg/L	0.25		Thind, Pritam	4/18/200
Std Method 2540 C	Total Dissolved Solids	11020	mg/L	1		Chan, Elaine	4/12/200
EPA 200.8 (T)	Total Iron	0.045	mg/L	0.025		Thind, Pritam	4/18/200
EPA 200.8 (T)	Total Manganese	< .025	mg/L	0.025		Thind, Pritam	4/18/200
EPA 415.1 (T) Ox	Total Organic Carbon	5.1	mg/L as C	0.5		Aylesworth, Stac	4/21/200
EPA 365.4	Total Phosphorus	0.08	mg/L	0.01		Hernandez, Rich	4/12/200
EPA 200.8 (T)	Total Selenium	0.195	mg/L	0.005		Thind, Pritam	4/18/200
EPA 200.8 (T)	Total Strontium	5.5	mg/L	0.025		Thind, Pritam	4/18/200
EPA 160.2	Total Suspended Solids	4	mg/L	1		Aylesworth, Stac	4/12/200
Std Method 5910B	UV Absorbance @254nm	0.13	absorbance/cm	0.001		Bettencourt, Mar	4/24/200

N.A.=Not Analyzed *Reporting Limits Adjusted For Dilution*

A.5 VGD, 11/13/06

Friday, December 08, 2006 *Submittal ID FWA1106B0131*

DWR Bryte Laboratory
1450 Riverbank Road, West Sacramento, CA 95605

Inorganic Analyses

Including Misc Physical Measurements

Report of Analytical Results

Sample Number	Station:	Cost Code:	Collection Date	Sample Purpose
FWA1106B0568	VGD4406 T.D. VGD4406	100681	11/13/2006 8:17:00 AM	Normal Sample 0

Matrix: Water, Natural *Description:* Tile Drain Water

Customer Instructions Tile Drain Water for Scale Potential Study *SampleCondition:*

Method	Analyte	Result	Units	Reprting Limit	Footnotes:	Chemist	Analysis Date
Std Method 2510-B	Conductance (EC)	26070	µS/cm	1		Chan, Elaine	11/15/20
Std Method 4500-CO2	Dissolved Bicarbonate (HCO3-)	367	mg/L as CaCO3	1		Chan, Elaine	11/15/20
EPA 200.7 (D)	Dissolved Boron	43.4	mg/L	0.5	R4	Quiambao, Josie	11/28/20
EPA 200.7 (D)	Dissolved Calcium	422	mg/L	5	R4	Quiambao, Josie	11/28/20
Std Method 4500-CO2	Dissolved Carbonate (CO3--)	1	mg/L as CaCO3	1		Chan, Elaine	11/15/20
EPA 300.0 28d Hold	Dissolved Chloride	1910	mg/L	200		Pineda, Maritza	11/21/20
EPA 300.0 28d Hold	Dissolved Fluoride	< 5.	mg/L	5		Pineda, Maritza	11/21/20
Std Method 4500-CO2	Dissolved Hydroxide (OH-)	< 1.	mg/L as CaCO3	1		Chan, Elaine	11/15/20
EPA 200.7 (D)	Dissolved Magnesium	962	mg/L	5	R4	Quiambao, Josie	11/28/20
EPA 300.0 28d Hold	Dissolved Nitrate	51.9	mg/L	20		Pineda, Maritza	11/21/20
EPA 415.1 (D) Ox	Dissolved Organic Carbon	6.2	mg/L as C	0.5		Wong, Allan	11/19/20
EPA 200.7 (D)	Dissolved Potassium	7.8	mg/L	2.5	R4	Quiambao, Josie	11/28/20
EPA 200.8 (D)	Dissolved Selenium	< .05	mg/L	0.05		Thind, Pritam	11/28/20
EPA 200.7 (D)	Dissolved Silica (SiO2)	43.2	mg/L	2	R4	Quiambao, Josie	11/28/20
EPA 200.7 (D)	Dissolved Sodium	9270	mg/L	20	R4	Quiambao, Josie	11/28/20
EPA 300.0 28d Hold	Dissolved Sulfate	21400	mg/L	200		Pineda, Maritza	11/21/20
Std Method 2320 B	pH	7.6	pH Units	0.1		Chan, Elaine	11/15/20
EPA 150.1	pH	7.6	pH Units	0.1	H2	Chan, Elaine	11/15/20
Std Method 2320 B	Total Alkalinity	368	mg/L as CaCO3	1		Chan, Elaine	11/15/20
EPA 200.8 (T)	Total Aluminum	< .5	mg/L	0.5		Thind, Pritam	11/28/20
EPA 200.8 (T)	Total Arsenic	< .05	mg/L	0.05		Thind, Pritam	11/28/20
EPA 200.8 (T)	Total Barium	< 2.5	mg/L	2.5		Thind, Pritam	11/28/20
Std Method 2540 C	Total Dissolved Solids	28780	mg/L	1		Chan, Elaine	11/15/20
EPA 200.8 (T)	Total Iron	1.41	mg/L	0.25		Thind, Pritam	11/28/20
EPA 200.8 (T)	Total Manganese	1.55	mg/L	0.25		Thind, Pritam	11/28/20
EPA 415.1 (T) Ox	Total Organic Carbon	6.2	mg/L as C	0.5		Wong, Allan	11/19/20
EPA 365.4	Total Phosphorus	0.12	mg/L	0.01		Hernandez, Rich	11/15/20
EPA 200.8 (T)	Total Selenium	< .05	mg/L	0.05		Thind, Pritam	11/28/20
EPA 200.8 (T)	Total Strontium	9.6	mg/L	0.25		Thind, Pritam	11/28/20
EPA 160.2	Total Suspended Solids	2	mg/L	1		Chan, Elaine	11/16/20
Std Method 5910B	UV Absorbance @254nm	0.178	absorbance/cm	0.001		Toomey, Marilyn	11/16/20

N.A.=Not Analyzed *Reporting Limits Adjusted For Dilution*

A.6 DP-25, 4/28/09

Sample Number	Station:	Cost Code:	Collection Date	Sample Purpose
FWA0409B0971	HMH8054	L10068100000	4/28/2009 12:05:00 PM	Normal Sample 0

Matrix: Water, Natural Description: RO Feed - Panoche DP25

Customer Instructions: RO Feed - Panoche DP25 SampleCondition: 8.0 °C when received.

The aliquot for cations and silica was not acidified. There was no separate, filtered/acidified 1/2 pint received for Cation analysis, only one 1/2 pint received not acidified, labeled for silica analysis.

Method	Analyte	Result	Units	Reporting Limit	Footnotes:	Chemist	Analysis Date
Std Method 2510-B	Conductance (EC)	9397	µS/cm	1	T1	Chan, Elaine	4/29/200
EPA 200.7 (D)	Dissolved Boron	23.5	mg/L	0.5	R4	Quiambao, Josie	4/29/200
EPA 200.7 (D)	Dissolved Calcium	492	mg/L	1		Quiambao, Josie	4/29/200
EPA 300.0 28d Hold	Dissolved Chloride	1190	mg/L	1	T1	Nickels, Bill	4/28/200
Std Method 2340 B	Dissolved Hardness	2279	mg/L as CaCO3	1		Quiambao, Josie	4/29/200
EPA 200.7 (D)	Dissolved Magnesium	255	mg/L	1		Quiambao, Josie	4/29/200
EPA 300.0 28d Hold	Dissolved Nitrate	337	mg/L	0.1	T1	Nickels, Bill	4/28/200
EPA 200.7 (D)	Dissolved Potassium	4.3	mg/L	0.5		Quiambao, Josie	4/29/200
EPA 200.8 (D)	Dissolved Selenium	0.465	mg/L	0.01		Thind, Pritam	4/30/200
EPA 200.7 (D)	Dissolved Silica (SiO2)	31.4	mg/L	0.1		Quiambao, Josie	4/29/200
EPA 200.7 (D)	Dissolved Sodium	1810	mg/L	5	R4	Quiambao, Josie	4/29/200
EPA 300.0 28d Hold	Dissolved Sulfate	4080	mg/L	1	T1	Nickels, Bill	4/28/200
Std Method 2320 B	pH	7.6	pH Units	0.1	T1	Chan, Elaine	4/29/200
Std Method 2320 B	Total Alkalinity	225	mg/L as CaCO3	1	T1	Chan, Elaine	4/29/200
EPA 200.8 (T)	Total Arsenic	< .01	mg/L	0.01		Thind, Pritam	4/30/200
EPA 200.8 (T)	Total Barium	< .5	mg/L	0.5		Thind, Pritam	4/30/200
Std Method 2540 C	Total Dissolved Solids	8500	mg/L	1	T1	Chan, Elaine	4/29/200
EPA 200.8 (T)	Total Selenium	0.472	mg/L	0.01		Thind, Pritam	4/30/200
EPA 200.8 (T)	Total Strontium	7.83	mg/L	0.05		Thind, Pritam	4/30/200

A.7 DP-25 5/19/2009: RO feed

Friday, May 29, 2009 *Submittal ID FWA0509B0238*

DWR Bryte Laboratory
1450 Riverbank Road, West Sacramento, CA 95605

Inorganic Analyses

Including Misc Physical Measurements

Report of Analytical Results

Sample Number	Station:	Cost Code:	Collection Date	Sample Purpose
FWA0509B1071	DP25-RO Feed	L10068100000	5/19/2009 11:12:00 AM	Normal Sample 0

Matrix: Water, Natural Description: RO Feed

Customer Instructions: Pre-filtered RO Feed SampleCondition: 2.0 °C when received.

Method	Analyte	Result	Units	Reprting Limit	Footnotes:	Chemist	Analysis Date
Std Method 2510-B	Conductance (EC)	14810	µS/cm	1		Chan, Elaine	5/21/200
EPA 200.7 (D)	Dissolved Boron	38.9	mg/L	0.5	R4	Quiambao, Josie	5/22/200
EPA 200.7 (D)	Dissolved Calcium	509	mg/L	5	R4	Quiambao, Josie	5/22/200
EPA 300.0 28d Hold	Dissolved Chloride	2650	mg/L	100		Pineda, Maritza	5/22/200
Std Method 2340 B	Dissolved Hardness	3145	mg/L as CaCO3	1		Quiambao, Josie	5/21/200
EPA 200.7 (D)	Dissolved Magnesium	455	mg/L	5	R4	Quiambao, Josie	5/22/200
EPA 300.0 28d Hold	Dissolved Nitrate	597	mg/L	10		Pineda, Maritza	5/22/200
EPA 365.1 (DWR Mod	Dissolved Ortho-phosphate	0.07	mg/L as P	0.01		Hernandez, Rich	5/20/200
EPA 200.7 (D)	Dissolved Potassium	7.6	mg/L	0.5		Quiambao, Josie	5/22/200
EPA 200.8 (D)	Dissolved Selenium	1.68	mg/L	0.01		Thind, Pritam	5/21/200
EPA 200.7 (D)	Dissolved Silica (SiO2)	34.6	mg/L	0.5	R4	Quiambao, Josie	5/22/200
EPA 200.7 (D)	Dissolved Sodium	3890	mg/L	10	R4	Quiambao, Josie	5/22/200
EPA 300.0 28d Hold	Dissolved Sulfate	6660	mg/L	100		Pineda, Maritza	5/22/200
Std Method 2320 B	pH	7.5	pH Units	0.1		Chan, Elaine	5/21/200
Std Method 2320 B	Total Alkalinity	235	mg/L as CaCO3	1		Chan, Elaine	5/21/200
EPA 200.8 (T)	Total Arsenic	0.013	mg/L	0.01		Thind, Pritam	5/27/200
EPA 200.8 (T)	Total Barium	< .5	mg/L	0.5		Thind, Pritam	5/27/200
Std Method 2540 C	Total Dissolved Solids	14440	mg/L	1		Chan, Elaine	5/22/200
EPA 200.8 (T)	Total Selenium	1.75	mg/L	0.01		Thind, Pritam	5/27/200
EPA 200.8 (T)	Total Strontium	8.85	mg/L	0.05		Thind, Pritam	5/27/200

A.8 DP-25 5/19/2009: RO concentrate (52.3% recovery)

Friday, May 29, 2009 *Submittal ID FWA0509B0238*

DWR Bryte Laboratory
1450 Riverbank Road, West Sacramento, CA 95605

Inorganic Analyses

Including Misc Physical Measurements

Report of Analytical Results

Sample Number	Station:	Cost Code:	Collection Date	Sample Purpose
FWA0509B1072	DP25-Concentrate Panoche Concentrate	L10068100000	5/19/2009 2:00:00 AM	Normal Sample 0

Matrix: Water, Natural *Description:* RO Concentrate - Panoche DP25

Customer Instructions RO Concentrate *SampleCondition:* 2.0 °C when received.

Method	Analyte	Result	Units	Reprting Limit	Footnotes:	Chemist	Analysis Date
Std Method 2510-B	Conductance (EC)	21370	µS/cm	1		Chan, Elaine	5/21/200
EPA 200.7 (D)	Dissolved Boron	47.6	mg/L	0.5	R4	Quiambao, Josie	5/22/200
EPA 200.7 (D)	Dissolved Calcium	897	mg/L	5	R4	Quiambao, Josie	5/22/200
EPA 300.0 28d Hold	Dissolved Chloride	4440	mg/L	200		Pineda, Maritza	5/22/200
Std Method 2340 B	Dissolved Hardness	5861	mg/L as CaCO3	1		Quiambao, Josie	5/21/200
EPA 200.7 (D)	Dissolved Magnesium	879	mg/L	5	R4	Quiambao, Josie	5/22/200
EPA 300.0 28d Hold	Dissolved Nitrate	951	mg/L	20		Pineda, Maritza	5/22/200
EPA 365.1 (DWR Mod	Dissolved Ortho-phosphate	0.09	mg/L as P	0.01		Hernandez, Rich	5/20/200
EPA 200.7 (D)	Dissolved Potassium	13.8	mg/L	2.5	R4	Quiambao, Josie	5/22/200
EPA 200.8 (D)	Dissolved Selenium	2.72	mg/L	0.02		Thind, Pritam	5/21/200
EPA 200.7 (D)	Dissolved Silica (SiO2)	71.7	mg/L	0.5	R4	Quiambao, Josie	5/22/200
EPA 200.7 (D)	Dissolved Sodium	6750	mg/L	20	R4	Quiambao, Josie	5/22/200
EPA 300.0 28d Hold	Dissolved Sulfate	12400	mg/L	200		Pineda, Maritza	5/22/200
Std Method 2320 B	pH	7.6	pH Units	0.1		Chan, Elaine	5/21/200
Std Method 2320 B	Total Alkalinity	491	mg/L as CaCO3	1		Chan, Elaine	5/21/200
EPA 200.8 (T)	Total Arsenic	0.022	mg/L	0.02		Thind, Pritam	5/27/200
EPA 200.8 (T)	Total Barium	< 1.	mg/L	1		Thind, Pritam	5/27/200
Std Method 2540 C	Total Dissolved Solids	19910	mg/L	1		Chan, Elaine	5/22/200
EPA 200.8 (T)	Total Selenium	2.86	mg/L	0.02		Thind, Pritam	5/27/200
EPA 200.8 (T)	Total Strontium	16.1	mg/L	0.1		Thind, Pritam	5/27/200

N.A.=Not Analyzed *Reporting Limits Adjusted For Dilution*

A.9 DP-25 5/19/2009: Treated RO concentrate 1

Friday, May 29, 2009 *Submittal ID FWA0509B0239*

DWR Bryte Laboratory
1450 Riverbank Road, West Sacramento, CA 95605

Inorganic Analyses

Including Misc Physical Measurements

Report of Analytical Results

Sample Number	Station:	Cost Code:	Collection Date	Sample Purpose
FWA0509B1076	DP25-TrConc1 TrConc1	L10068100000	5/19/2009 2:00:00 AM	Normal Sample 0

Matrix: Water, Natural *Description:* Treated Concentrate 1

Customer Instructions Treated Concentrate 1 *SampleCondition:* 2.0 °C when received.

Method	Analyte	Result	Units	Reprting Limit	Footnotes:	Chemist	Analysis Date
Std Method 2510-B	Conductance (EC)	22320	µS/cm	1		Chan, Elaine	5/21/200
EPA 200.7 (D)	Dissolved Boron	45.9	mg/L	0.5	R4	Quiambao, Josie	5/22/200
EPA 200.7 (D)	Dissolved Calcium	606	mg/L	5	R4	Quiambao, Josie	5/22/200
EPA 300.0 28d Hold	Dissolved Chloride	4430	mg/L	200		Pineda, Maritza	5/22/200
Std Method 2340 B	Dissolved Hardness	4936	mg/L as CaCO3	1		Quiambao, Josie	5/21/200
EPA 200.7 (D)	Dissolved Magnesium	831	mg/L	5	R4	Quiambao, Josie	5/22/200
EPA 300.0 28d Hold	Dissolved Nitrate	950	mg/L	20		Pineda, Maritza	5/22/200
EPA 365.1 (DWR Mod	Dissolved Ortho-phosphate	0.05	mg/L as P	0.01		Hernandez, Rich	5/20/200
EPA 200.7 (D)	Dissolved Potassium	12.3	mg/L	2.5	R4	Quiambao, Josie	5/22/200
EPA 200.8 (D)	Dissolved Selenium	2.66	mg/L	0.02		Thind, Pritam	5/21/200
EPA 200.7 (D)	Dissolved Silica (SiO2)	70.8	mg/L	0.5	R4	Quiambao, Josie	5/22/200
EPA 200.7 (D)	Dissolved Sodium	6630	mg/L	20	R4	Quiambao, Josie	5/22/200
EPA 300.0 28d Hold	Dissolved Sulfate	11500	mg/L	200		Pineda, Maritza	5/22/200
Std Method 2320 B	pH	8.4	pH Units	0.1		Chan, Elaine	5/21/200
Std Method 2320 B	Total Alkalinity	313	mg/L as CaCO3	1		Chan, Elaine	5/21/200
EPA 200.8 (T)	Total Arsenic	0.02	mg/L	0.02		Thind, Pritam	5/27/200
EPA 200.8 (T)	Total Barium	< 1.	mg/L	1		Thind, Pritam	5/27/200
Std Method 2540 C	Total Dissolved Solids	21200	mg/L	1		Chan, Elaine	5/22/200
EPA 200.8 (T)	Total Selenium	2.88	mg/L	0.02		Thind, Pritam	5/27/200
EPA 200.8 (T)	Total Strontium	13.1	mg/L	0.1		Thind, Pritam	5/27/200

A.10 DP-25 5/19/2009: Treated RO concentrate 2

Friday, May 29, 2009 *Submittal ID FWA0509B0239*

DWR Bryte Laboratory
1450 Riverbank Road, West Sacramento, CA 95605

Inorganic Analyses

Including Misc Physical Measurements

Report of Analytical Results

Sample Number	Station:	Cost Code:	Collection Date	Sample Purpose
FWA0509B1077	DP25-TrConc2 TrConc2	L10068100000	5/19/2009 2:00:00 AM	Normal Sample 0

Matrix: Water, Natural Description: Treated Concentrate 2

Customer Instructions: Treated Concentrate 2 SampleCondition: 2.0 °C when received.

Method	Analyte	Result	Units	Reprting Limit	Footnotes:	Chemist	Analysis Date
Std Method 2510-B	Conductance (EC)	21350	µS/cm	1		Chan, Elaine	5/21/200
EPA 200.7 (D)	Dissolved Boron	46.6	mg/L	0.5	R4	Quiambao, Josie	5/22/200
EPA 200.7 (D)	Dissolved Calcium	595	mg/L	5	R4	Quiambao, Josie	5/22/200
EPA 300.0 28d Hold	Dissolved Chloride	4410	mg/L	200		Pineda, Maritza	5/22/200
Std Method 2340 B	Dissolved Hardness	4843	mg/L as CaCO3	1		Quiambao, Josie	5/21/200
EPA 200.7 (D)	Dissolved Magnesium	815	mg/L	5	R4	Quiambao, Josie	5/22/200
EPA 300.0 28d Hold	Dissolved Nitrate	946	mg/L	20		Pineda, Maritza	5/22/200
EPA 365.1 (DWR Mod	Dissolved Ortho-phosphate	0.05	mg/L as P	0.01		Hernandez, Rich	5/20/200
EPA 200.7 (D)	Dissolved Potassium	11	mg/L	2.5	R4	Quiambao, Josie	5/22/200
EPA 200.8 (D)	Dissolved Selenium	2.64	mg/L	0.02		Thind, Pritam	5/21/200
EPA 200.7 (D)	Dissolved Silica (SiO2)	69.5	mg/L	0.1		Quiambao, Josie	5/22/200
EPA 200.7 (D)	Dissolved Sodium	6640	mg/L	5		Quiambao, Josie	5/22/200
EPA 300.0 28d Hold	Dissolved Sulfate	11500	mg/L	200		Pineda, Maritza	5/22/200
Std Method 2320 B	pH	8.6	pH Units	0.1		Chan, Elaine	5/21/200
Std Method 2320 B	Total Alkalinity	241	mg/L as CaCO3	1		Chan, Elaine	5/21/200
EPA 200.8 (T)	Total Arsenic	0.02	mg/L	0.02		Thind, Pritam	5/27/200
EPA 200.8 (T)	Total Barium	< 1.	mg/L	1		Thind, Pritam	5/27/200
Std Method 2540 C	Total Dissolved Solids	20000	mg/L	1		Chan, Elaine	5/22/200
EPA 200.8 (T)	Total Selenium	2.76	mg/L	0.02		Thind, Pritam	5/27/200
EPA 200.8 (T)	Total Strontium	13	mg/L	0.1		Thind, Pritam	5/27/200

N.A.=Not Analyzed *Reporting Limits Adjusted For Dilution*

A.11 San Joaquin Valley Historic water quality

This appendix provides a summary of the latest year of historical water quality data from the CNR, ERR, LNW, OAS, and VGD locations obtained from the DWR *San Joaquin Valley Drainage Monitoring Program 2000* (2003) report (see **§3.3.1**).

Summary of San Joaquin Valley water quality measurements for the latest year of historical data

Station	Date	pH	T	TDS	Total Alk. (mg/L as $CaCO_3$)	EC	$[Na^+]$	$[SO_4^{2-}]$	$[Cl^-]$	$[NO_3^-]$	$[Ca^{2+}]$	$[Mg^{2+}]$	$[K^+]$	$[Ba^{2+}]$	$[B]_T$	$[As]_T$	$[Se]_T$
			(°C)	(mg/L)		(µS/cm)	(mg/L)	(mg/L)	(mg/L)	(mg/L)	(mg/L)	(mg/L)	(mg/L)	(mg/L)	(mg/L)	(mg/L)	(mg/L)
OAS 2548	5/5/2003	7.3	16	3460	136	5150	751	2910	219	7.8	463	128	2.5	0.25	10.8	0.005	0.04
OAS 2548	7/14/2003	7.6	22	5864	271	9030	1810	3990	779	72.6	283	159	3.4	0.5	18.4	0.01	0.099
OAS 2548	9/9/2003	7.1	21	3828	239	5610	1080	2340	468	26.0	224	104	2.7	0.25	9.3	0.005	0.061
OAS 2548	11/12/2003	7.9	18	9344	160	10760	2320	5550	952	73.4	385	202	5	0.5	19.4	0.01	0.144
OAS 2548	1/12/2004	7.9	14	11100	173	13160	2830	6460	1120	56.0	430	249	5	0.5	23.0	0.01	0.171
OAS 2548	3/22/2004	7.9	15	9576	146	11010	2310	5630	847	45.4	454	223	10	0.5	19.8	0.01	0.149
OAS 2548	5/10/2004	7.9	17	8284	217	9756	2060	4890	783	49.0	358	192	3.6	0.5	18.0	0.01	0.15
VGD 4406	7/29/2003	7.8	21	14,110	359	21,880	5,270	13,900	1,020	--	346	492	5.4	1.0	32	0.020	0.020
VGD 4406	9/10/2003	7.7	21	24,500	393	25,100	6,620	15,700	1,240	67.5	372	632	8.1	1.0	33	0.020	0.020
VGD 4406	11/13/2003	7.9	20	28,960	442	28,000	7,550	18,700	1,630	71.6	318	725	10	1.0	33	0.020	0.020
VGD 4406	1/13/2004	8.1	18	29,760	446	29,920	8,240	18,900	1,560	43.7	387	844	25	1.0	35	0.020	0.020
VGD 4406	3/11/2004	7.8	18	19,330	342	20,920	5,280	12,700	783	52.4	391	466	10	1.0	30	0.020	0.020
VGD 4406	5/12/2004	8.1	18	24,220	379	26,060	6,730	16,470	1,390	50.9	387	674	5	1.0	34	0.020	0.020
LNW 6467	5/5/2003	7.6	19	11,720	139	17,710	3,680	5,050	4,050	213	642	303	2.5	0.5	24.0	0.013	0.270
LNW 6467	7/28/2003	7.1	22	11,030	135	17,170	3,280	5,160	3,730	--	589	246	5	0.5	23.0	0.010	0.314
LNW 6467	9/9/2003	7.1	23	13,400	132	17,820	3,590	5,070	3,740	212	629	256	5	1	22.0	0.020	0.262
LNW 6467	11/12/2003	7.7	21	12,140	130	15,690	3,030	4,710	3,550	181	561	220	10	0.5	18.0	0.010	0.263
LNW 6467	1/12/2004	7.8	20	11,430	128	15,580	2,930	4,410	3,280	154	608	218	10	0.5	17.6	0.015	0.251
CNR 0801	7/28/2003	7.2	22	4,660	225	7,490	1,230	4,040	288	--	367	276	48	0.25	14.2	0.006	0.050
CNR 0801	9/9/2003	7.3	23	6,260	210	7,170	1,250	3,670	271	316	387	269	45	0.25	12	0.005	0.043
CNR 0801	11/12/2003	8	22	9,136	351	9,660	2,020	5,760	545	132	333	312	80	0.50	23.3	0.010	0.022
CNR 0801	1/12/2004	7.9	20	6,736	221	7,940	1,310	4,030	279	295	362	262	46	0.25	14	0.006	0.047
CNR 0801	3/10/2004	7.7	18	7,828	284	8,830	1,730	4,640	294	204	358	294	54	0.25	18	0.006	0.038
CNR 0801	5/11/2004	7.9	20	7,304	249	8,203	1,490	4,430	318	256	340	252	45	0.25	15	0.005	0.040

A.12 DP-25: Historic water quality data collected by CA DWR

PANOCHE DRAINAGE DISTRICT

DP-25

Analyte	Method	Units	2/15/2005 Results	6/21/2005 Results	11/15/2005 Results	1/16/2006 Results	4/7/2006 Results	Average
Alkalinity as CaCO3	SM 2320B	mg/L	250	260	250	220	220	240.0
Aluminum	EPA 200.7	mg/L	ND	ND	ND	0.42	1.4	
Antimony	EPA 200.8	ug/L	ND	ND	ND	ND	ND	
Arsenic	EPA 200.8	ug/L	11	14.0	33	ND	33	22.8
Barium	EPA 200.7	mg/L	ND	ND	ND	ND	ND	
Beryllium	EPA 200.8	ug/L	ND	ND	ND	ND	ND	
Bicarbonate CaCO3	SM 2320B	mg/L	250	260.0	250	220	220	240.0
BOD 1/	SM 5210-B	mg/L	ND	ND	ND	ND	ND	
Boron	EPA 200.7	mg/L	16	18.0	35	18	32	23.8
Cadmium	EPA 200.8	ug/L	ND	ND	ND	ND	ND	
Calcium	EPA 200.7	mg/L	480	500.0	510	520	590	520.0
Carbonate	SM 2320B	mg/L	ND	ND	ND	ND	ND	
COD	SM 5220-D	mg/L	26	21.0	41	5.1	36	25.8
Chloride	EPA 300.0	mg/L	960	1200.0	2200	1100	1300	1352.0
Chromium Total	EPA 200.8	ug/L	60	63.0	120	80	130	90.6
Color	SM 2120 B	units	10	15.0	20	60	10	23.0
EC	SM 2510 B	umho/cm	6800	8400.0	15000	8000	9200	9480.0
Copper	EPA 200.8	ug/L	ND	ND	ND	ND	52	
Fluoride	EPA 300.0	mg/L	ND	ND	ND	ND	ND	
Hardness CaCO3	SM 2340 B	mg/L	2000	2200.0	2800	2100	2900	2400.0
Hydroxide CaCO3	SM 2320B	mg/L	ND	ND	ND	ND	ND	
Iron	EPA 200.7	mg/L	ND	ND	ND	0.65	2.4	
LISI 2/			13	19.0	52	21	20	25.0
Lead	EPA 200.8	ug/L	ND	ND	ND	ND	ND	
Magnesium	EPA 200.7	mg/L	190	220.0	380	200	350	268.0
Manganese	EPA 200.7	mg/L	0.020	ND	ND	0.25	0.82	0.4
MBAS	SM 5540 C	mg/L	ND	ND	0.6	ND	ND	
Mercury	EPA 200.8	ug/L	0.80	0.5	0.9	ND	3.2	1.4
Nickel	EPA 200.8	ug/L	ND	ND	ND	ND	21	
Nitrate	EPA 300.0	mg/L	240	300.0	420	260	280	300.0
Nitrite	EPA 300.0	mg/L	ND	ND	ND	ND	ND	
Odor	SM 2150 B	TON	1.0	1.0	1	1	1	1.0
pH	SM 4500-H+B		7.7	7.7	7.7	7.8	7.9	7.8
Potassium	EPA 200.7	mg/L	3.0	ND	6.9	4.1	6.7	5.2
Selenium	EPA 200.8	ug/L	310	440.0	1400	250	1600	800.0
Silica	EPA 200.7	mg/L	28.0	31.0	35	29	45	33.6
Silver	EPA 200.7	mg/L	ND	ND	ND	ND	ND	
Sodium	EPA 200.7	mg/L	1700	1800.0	3300	1400	2800	2200.0
Sulfate	EPA 300.0	mg/L	3500	3600.0	5900	3500	3700	4040.0
Thallium	EPA 200.8	ug/L	ND	ND	ND	ND	ND	
TDS	SM 2540 C	mg/L	6700	8000.0	13000	8400	8100	8840.0
Turbidity	SM 2130 B	NTU	0.90	0.7	0.9	30	2.9	7.1
Zinc	EPA 200.7	mg/L	ND	ND	ND	ND	ND	

1/ Biochemical Oxygen Demand
2/ Langlier index saturation index
3/ Chemical Oxygen Demand

A.12 (continued)

PANOCHE DRAINAGE DISTRICT

DP-25

Analyte	Method	Units	7/17/2006 Results	10/3/2006 Results	Results	Results	Results	Average
Alkalinity as CaCO3	SM 2320B	mg/L	220	250				235.0
Aluminum	EPA 200.7	mg/L	0.12	ND				
Antimony	EPA 200.8	ug/L	ND	ND				
Arsenic	EPA 200.8	ug/L	26	32.0				29.0
Barium	EPA 200.7	mg/L	ND	ND				
Beryllium	EPA 200.8	ug/L	ND	ND				
Bicarbonate CaCO3	SM 2320B	mg/L	220	250.0				235.0
BOD 1/	SM 5210-B	mg/L	ND	ND				
Boron	EPA 200.7	mg/L	23	24.0				23.5
Cadmium	EPA 200.8	ug/L	ND	ND				
Calcium	EPA 200.7	mg/L	530	490.0				510.0
Carbonate	SM 2320B	mg/L	ND	ND				
COD	SM 5220-D	mg/L	27	25.0				26.0
Chloride	EPA 300.0	mg/L	1400	1300.0				1350.0
Chromium Total	EPA 200.8	ug/L	79	79.0				79.0
Color	SM 2120 B	units	15	20.0				17.5
EC	SM 2510 B	umho/cm	9800	9700.0				9750.0
Copper	EPA 200.8	ug/L	ND	ND				
Fluoride	EPA 300.0	mg/L	ND	ND				
Hardness CaCO3	SM 2340 B	mg/L	2400	2300.0				2350.0
Hydroxide CaCO3	SM 2320B	mg/L	ND	ND				
Iron	EPA 200.7	mg/L	0.1	ND				
LISI 2/			24	23.0				23.5
Lead	EPA 200.8	ug/L	ND	ND				
Magnesium	EPA 200.7	mg/L	250	260.0				255.0
Manganese	EPA 200.7	mg/L	ND	ND				
MBAS	SM 5540 C	mg/L	ND	ND				
Mercury	EPA 200.8	ug/L	0.52	0.7				0.6
Nickel	EPA 200.8	ug/L	10	ND				
Nitrate	EPA 300.0	mg/L	320	320.0				320.0
Nitrite	EPA 300.0	mg/L	ND	ND				
Odor	SM 2150 B	TON	1.0	1.0				1.0
pH	SM 4500-H+B		7.9	7.9				7.9
Potassium	EPA 200.7	mg/L	4.4	4.6				4.5
Selenium	EPA 200.8	ug/L	690	620.0				655.0
Silica	EPA 200.7	mg/L	39.0	38.0				38.5
Silver	EPA 200.7	mg/L	ND	ND				
Sodium	EPA 200.7	mg/L	2000	2100.0				2050.0
Sulfate	EPA 300.0	mg/L	4000	4200.0				4100.0
Thallium	EPA 200.8	ug/L	ND	ND				
TDS	SM 2540 C	mg/L	9000	8700.0				8850.0
Total Organic Carbon	SM5310-c	mg/L	6.90	7.2				7.1
Turbidity	SM 2130 B	NTU	1.3	0.4				0.8
Zinc	EPA 200.7	mg/L	ND	ND				

1/ Biochemical Oxygen Demand
2/ Langlier index saturation index
3/ Chemical Oxygen Demand

Appendix B. Detailed experimental procedures

SDI Measurement:

The silt density index (SDI) is a measure of the particulates present in natural waters that are rejected by a 0.45 μm filter (see **§2.1.4**). The SDI is calculated by comparing the length of time required to collect a designated volume of permeate initially and after a certain length of time in dead-end filtration. The SDI is defined by the ASTM Standard Test Method D4189-95:

$$SDI_T = \frac{\%P_{30}}{T} = \frac{\left[1 - t_i / t_f\right] 100}{T} \quad \text{(B-1)}$$

where $\%P_{30}$ is the plugging factor at a trans-membrane pressure of 30 psi, T is the time between sample collections (min), and t_i and t_f are the elapsed times (min) to collect initial and final permeate samples, respectively. Prefiltration is generally recommended for water having an SDI_{15} greater than 5.0 to prevent particulates from plugging the RO membrane. Follow *ASTM: D 4189-95 (Reapproved 2002)* using the Simple SDI Portable Auto SDI Tester (Applied Membranes, Inc.). Collect the water sample after passing through the SDI Analyzer for later use.

Figure B-1. Simple SDI test kit (Applied Membranes, Inc) [1] .

Alkalinity Measurement:

Alkalinity measurements in **§3.4.1** were verified by following the procedure as provided with the HACH model AL-DT alkalinity test kit as summarized below.

1. Choose the titration cartridge corresponding to the expected alkalinity range for a given water sample, attach the delivery tube, and lock the cartridge into the hand-held titrator.
2. Press the plunger release button and advance the plunger into the titration cartridge to fill the delivery tube with the titration solution. Rinse the tip of the deliver tube to remove any excess solution and reset the digital counter.
3. Add the reagents from the provided foil packets to the Erlenmeyer flask and swirl to dissolve. Hold the flask in one hand and insert the tip of the deliver tube into the sample with the other hand. Swirl the flask while titrating the solution until the endpoint has been reached.
4. Note the number of digits indicated on the hand-held titrator and calculate the alkalinity of the sample by multiplying the number of digits by the appropriate multiplier as indicated in the table provided in the HACH alkalinity test kit operating manual.
5. Rinse the tip of the delivery tube, reset the counter and repeat **steps 3** & **4** for any remaining samples.

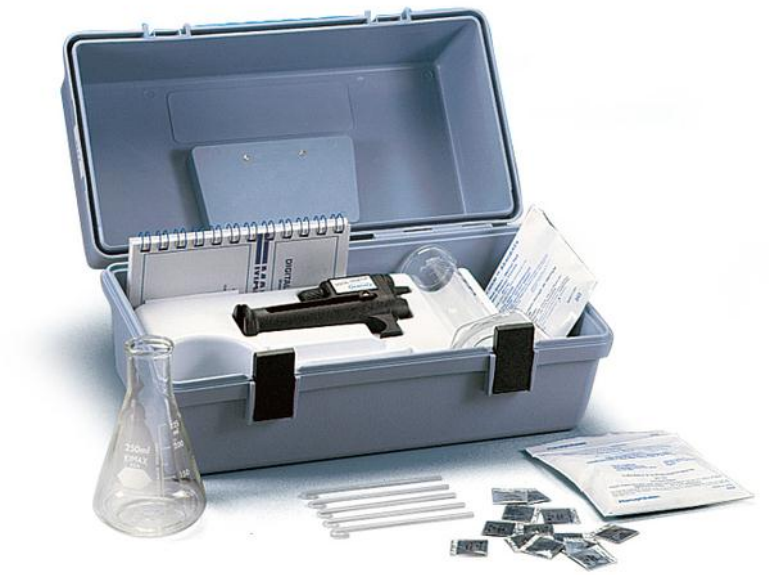

Figure B-2. HACH model AL-DT alkalinity test kit [2].

Plate-and-frame (PFRO) system:

RO flux decline tests (**§3.3.2**) were performed in a plate-and-frame (PFRO) system (**Fig. B-3**) with a range of water compositions to develop and assess the diagnostic approach to evaluating mineral scaling propensity. Scaling tests were carried out over a range of pH conditions (pH ~5-8). Prior to each RO test, the feed water was filtered using a 5 μm gradient density polypropylene filter cartridge and a 0.2 μm filter cartridge to remove suspended particles. In order to reduce pH drift during the experiments, air was bubbled through the water feed reservoir during pH adjustment to reduce the time required to reach equilibrium with respect to carbon dioxide. Some of the RO tests included antiscalant addition to observe the impact on reduction in mineral scaling. Flux decline was expressed as either a ratio of the flux at time *t* relative to the initial flux (i.e., at *t=0*) or as percent flux decline.

Membranes used in the flat-sheet PFRO cells were cut from a commercial stock membrane roll. The membrane coupons were first rinsed with DI water and subsequently soaked in DI water for at least two hours prior to placement in the RO cells. Prior to commencing with a

desalting run, the membrane coupons were placed in the RO cells and conditioned by flowing through the RO system a sodium sulfate solution having approximately the same osmotic pressure as the scaling solution field. Membrane compaction was carried out at a retentate flow rate of about 4.5 L/min for a period of about 1 hour and then for 3 hours at retentate and permeate flow rates equal to the rates desired for the subsequent flux decline run. After membrane conditioning, each flux decline test was initiated at the desired operating conditions for the specific feed water. All runs were carried out at the same initial flux and cross flow velocity in order to ensure that the all flux experiments were compared at the same level of initial concentration polarization. At the end of the 24 hour flux decline the system was cleaned with DI water, followed by pH adjustment to 10 and using 0.1% v/v Micro-90, a concentrated detergent (International Products Corporation, Burlington, NJ), and also EDTA solution (0.07M EDTA) to remove traces of mineral scale, followed by rinsing with DI water.

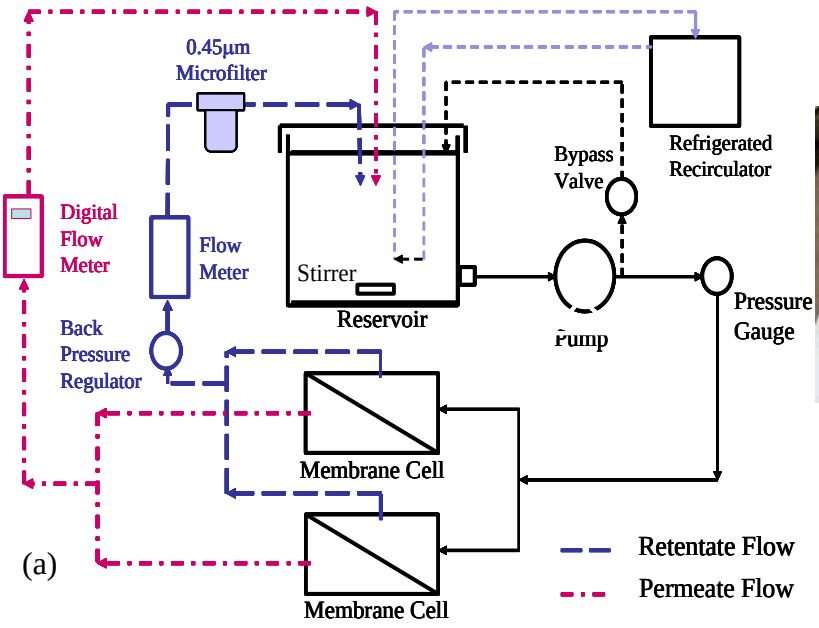

(b)

Fig. B-3. (a) PFRO system diagram, (b) picture of two PFRO cells in parallel.

Microfiltration for the PFRO system:

Prior to RO experiments (**§3.3.2**), field water samples are successively passed through 5-µm gradient density and a 0.2-µm pleated MF cartridges (Filter Klear 08PT Series, Keystone Filter, Hatfield, PA). Samples first filtered in a single-pass mode and then in a continuous mode.

1. Place the 5 µm MF cartridge in the filter housing and secure all tubing. Place the MF cartridge effluent tube so that it empties into a 5-gallon container (single-pass mode).
2. Fill the reservoir (about 5 gallons) with field water from the selected sampling location.
3. Maintain the sample water at 4 ºC with a refrigeration coil for the duration of the pretreatment procedure.
4. Fully open the back-pressure and bypass valves and turn on the pump. The end of the bypass tube must empty into the sample reservoir.
5. Close the bypass valve so that all of the water must pass through the MF cartridge. The backpressure valve may be adjusted to increase the flow rate, but the operating pressure does not need to be very high (<50 psi).
6. When the sample reservoir is nearly empty (when the liquid level drops below pump intake nozzle) turn off the pump, but do not open the valves.
7. Move the MF cartridge effluent tube so that it empties into the sample reservoir (continuous recycle mode).
8. Turn the pump on and continue to filter the sample water with the 5 µm MF cartridge for 20 minutes. Then turn off the pump and open both valves so all of the sample water can drain into the reservoir.
9. Switch to 0.2 µm MF cartridge and repeat steps 1 through 8.
10. Transfer the sample water into a five gallon container and return it to the refrigerator.

pH adjustment for the PFRO system (**§3.3.2**)*:*

1. Attach plastic tubing to the regulator of a compressed air tank. Insert a stainless steel diffuser at the end of the tubing and place in a 3-gallon bucket.
2. Place 10 L of filtered field water in a bucket with the refrigeration coil and magnetic stir bar. Place the bucket on a stir plate and maintain the temperature at 4 ºC.
3. Adjust the regulator pressure such that there are visible air bubbles in the water, but be sure no to set the pressure too high in order to avoid splashing (~10 psi).
4. Adjust to the desired pH by drop-wise addition of 2 N HCl while stirring and bubbling air through the water. Let the system equilibrate to a new pH. Add more HCl until the desired pH is reached again and then allow the water to equilibrate. The pH equilibration process may take several iterations before the water equilibrates at the desired pH. With each iteration the equilibration time will increase. The final equilibration periods may take several hours each. The total amount of 2.0 N HCl should not be more than a few milliliters.
5. If too much HCl is added 0.10N NaOH to re-adjust to the target pH and store the treated sample water in the refrigerator until use.

Compaction for the PFRO system (**§3.3.2**)*:*

1. Prepare 10 L of synthetic solution using Na_2SO_4 and DI water such that it has an electrical conductivity (EC) that is about 20% greater than the field water sample being used for the flux decline run.
2. Secure all tubing connections and fully open the backpressure and bypass valves. Note that the end of the bypass tube must empty into the sample reservoir.

3. Pour the model solution into the reservoir and maintain it at 20 ºC with a refrigeration coil for the duration of the compaction period.
4. Fully open the backpressure and bypass valves; turn on the pump; and adjust the valves for a few minutes to remove most of the trapped air from the pump.
5. With the backpressure valve fully opened close the bypass valve. The flow rate should be around 4.5 L/min. If the flow rate is below 4.5 L/min continue adjusting the valves to remove any remaining entrapped air.
6. After running for 1 hour, open the bypass valve and adjust the backpressure valve such that the retentate and permeate flow rates are at their desired levels (in most cases they are 0.76 L/min and 2.9 mL/min, respectively).
7. Throughout the next 3 hours periodically adjust both valves to maintain the desired flow rates.
8. After 3 hours drain the model solution from the system.

Pilot RO system:

Field RO concentrate for CESP experiments was produced by the UCLA M3 RO pilot system (**Fig. B-4**) at 52.3% recovery producing concentrate of *SIg* = 1.71 (see **§2.2**) at the DP-25 test site (10 miles west of Firebaugh, CA) in the central San Joaquin Valley. After pretreatment (1-mm sand media filtration followed by 5, 0.45, and 0.2 μm cartridge filtration), 3500 gal/day (0.54 m^3/hr) of RO feed water was desalted by six RO membrane elements arranged in series (2.5 inch diameter, 40 inch long XLE 2540 elements, DOW FilmTec Corp., Minneapolis, MN), with an observed salt rejection 98% and permeability of 4.57 $L \cdot m^{-2} \cdot hr^{-1} \cdot bar^{-1}$ [3, 4]. The feed was supplied to the RO membranes using two high-pressure positive displacement pumps (Danfoss

Model CM 3559, 3 hp, 3450 rpm, Baldor Reliance Motor, Sea Recovery Corp. Carson, California) in parallel, each capable of providing feed flow of up to 4.3 gal/min at 1000 psi [5, 6].

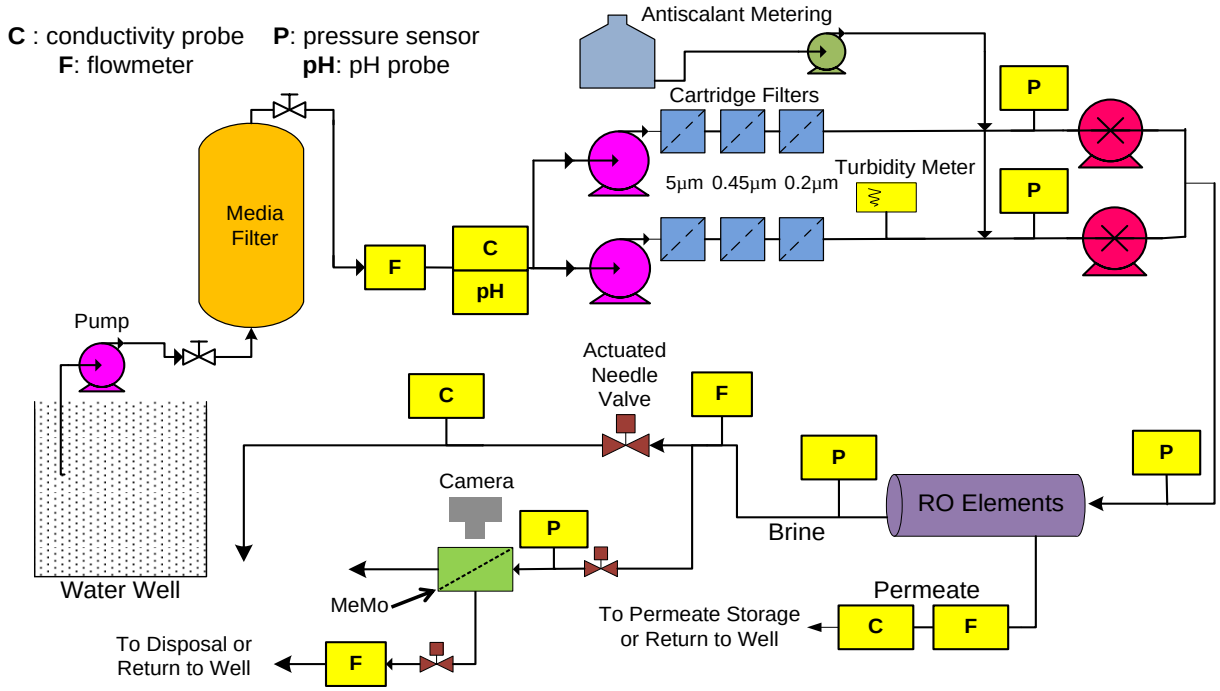

Figure B-4. Diagram of field-deployed M3 pilot RO system providing RO concentrate for CESP precipitation studies (**§2.2**). Adapted from [4].

Flux Decline Run for the PFRO system (**§3.3.2**)*:*

1. Secure all tubing connections and fully open back-pressure and by-pass valves. Note that the end of the by-pass tube should empty into the sample reservoir.
2. Pour 10 L of pretreated real water into the reservoir and maintain the sample at 20 ºC with a refrigeration coil for the duration of flux decline run. Add antiscalant if applicable.
3. Fully opern the back-pressure and by-pass valves, turn on the pump and adjust the valves for a few minutes to remove most of the entrapped air from the pump.
4. With the back-pressure valve fully opened close the by-pass valve. The flow rate should be around 4.5 L/min. If the flow rate is below 4.5 L/min continue adjusting the valves to remove any remaining entrapped air.

5. Adjust backpressure and bypass valves such that retentate and permeate flow rates are at their desired levels (in most cases they are 0.76 L/min and 2.9 mL/min, respectively).
6. Monitor the flow rates for 30 minutes while adjusting both valves to maintain the desired flow rates. While monitoring the flow rates, remove a small sample of water from the system for alkalinity measurements.
7. Periodically monitor the experiment over the entire 24 period checking for leaks or any other malfunctions. The pressure may need to be adjusted back to the initial levels after several hours of running.
8. After 24 hours drain the water from the system and turn off the pump.
9. Fully open both valves and carefully remove the membranes and replace them with cleaning membranes.
10. Fill the reservoir with DI water and turn the pump on.
11. Flush the system several times with DI water and then drain the system.

CESP Experiments

Concentrate demineralization (**§4.2.2, §5.2, §6.2**) was performed via CESP in either a 1-L lab-scale crystallizer (**Fig. B-5**) or a 20-liter bench-scale stirred-tank batch crystallizer (**Fig. B-6**) at room temperature (~23 °C) with continuous monitoring of calcium ion activity, pH, and temperature. The 1-L crystallizer was 20 cm tall with an 8.0 cm square base (CLM 4, EC Engineering, Edmonton, Canada). Mixing was provided by a 4.0 cm by 6.0 cm radial flow paddle mixer situated 2.5 cm above the base. The larger 20-L rectangular batch-reactor was 13 in. tall with a 30 in. square base (Nalgene, Thermo Fisher Scientific, Rochester, NY) utilizing an electric mixer (Model 71636819, 1/20 hp, 1550 rpm, Neptune Mixer Company, North Wales, PA)

and a 30 inch long 5/16 inch diameter shaft with a 3 inch diameter 3-blade axial flow impeller situated 5 cm above the base of the 20-L crystallizer (**Fig. B-6**). The pH and the calcium ion activity were measured using a pH electrode (Cole Parmer Instrument Company, Vernon Hill, IL) and a calcium ion selective electrode (Orion 97-20, Thermo Electron Corporation, Somerset, NJ), respectively. A diagram of the general CESP procedure is shown in **Fig. B-4**.

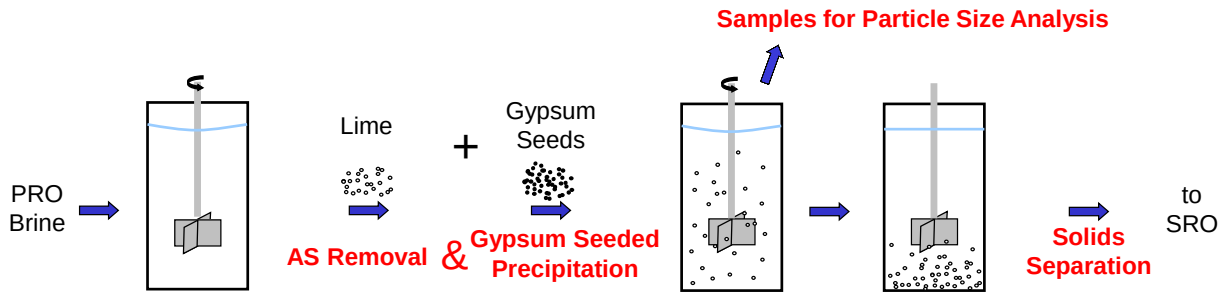

Figure B-4. General procedure for CESP demineralization experiments.

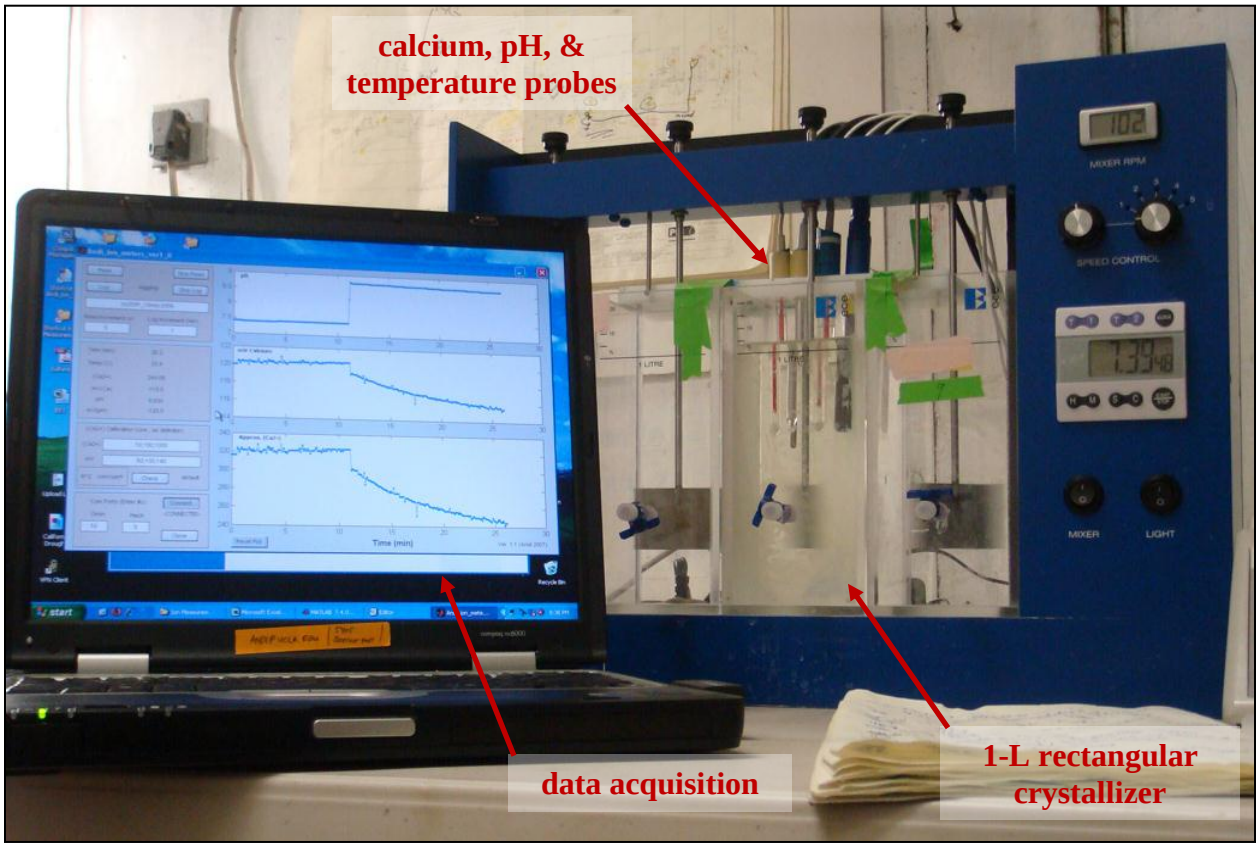

Figure B-5. Lab-scale 1-L crystallizer with 4 rectangular jar testers.

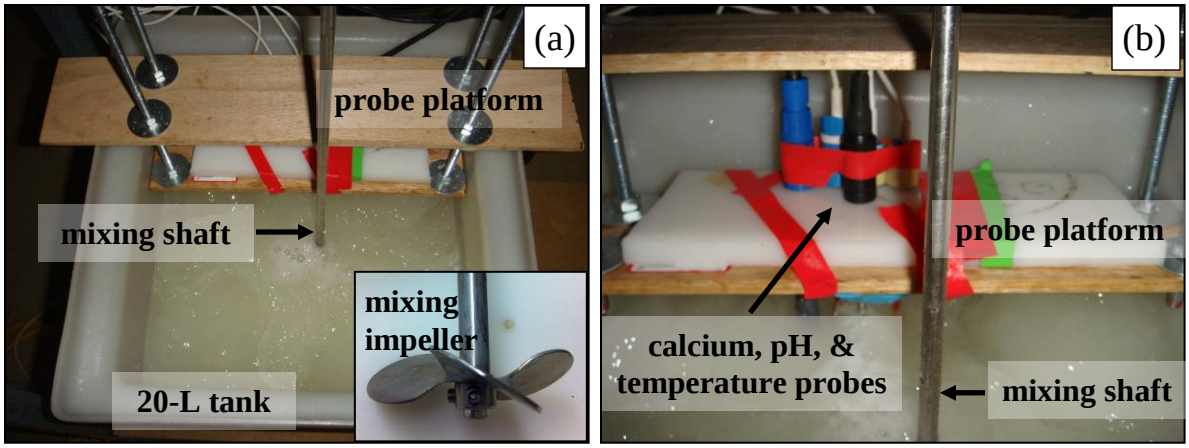

Figure B-6. Bench-scale 20-L brine demineralization crystallizer: (a) overhead view during brine demineralization with inset close-up view of radial-flow mixing impeller and (b) close-up of calcium ion, pH, and temperature probes and support platform with the stirring impeller shaft in the foreground.

1. If using actual RO concentrate proceed to **Step 3**, otherwise prepare the four 2-L OAS model solutions: 1) 18.08 g/L $CaCl_2 \cdot H_2O$, 2) 82.62 g Na2SO4 and 30.73 g $MgSO_4 \cdot 7H_2O$, 3) 4.75 g NaCl and 3.81 g $NaHCO_3$., 4) DI water with no salt. When the above four solutions are mixed in equal proportions, the desired working solution composition will be attained.
2. Prior to each batch CESP run in the 1-L stirred tank rectangular jar tester pour 250 mL of each stock solution from Step 1 into four separate 250 mL volumetric flasks. If using the larger 20-L crystallizer with actual RO concentrate, pour 20 liters of RO concentrate sample into the crystallizer.
3. Weigh the desired mass of alkaline material (e.g., lime) and gypsum powder into separate 20-mL cuvettes for later use.
3. Add ~10-15 mL of DI water to the cuvette containing the alkaline material (e.g., lime) to form a slurry.
4. The cuvette containing the gypsum powder should remain dry prior to seeding. Do **not** form a slurry!

5. Slowly and individually pour each of the 250-mL portions of stock solution into the jar tester, **except** for the calcium containing solution (solution 1). If using actual RO concentrate fill entire volume of sample into the crystallizer.
6. Place the supporting platform for the calcium, pH, and temperature probes on top of the jar tester and then insert each probe into its corresponding slot. The tip of each probe should be ~0.5 cm below the surface of the water.
7. Begin data acquisition, turn on the mixing paddle to the desired rate (RPM), and then immediately pour in the remaining calcium containing model solution (solution 1).
8. Allow at least 10 minutes of calcium ISE and pH probe conditioning and make sure that the calcium activity is stable prior to any alkaline slurry or seed additions.
9. At the appropriate time add alkaline slurry in a single motion as quickly as possible. It may help to stir the slurry immediately prior to addition.
10. At the end of the alkaline pretreatment period, add the gypsum powder (from step 3) to the solution in the crystallizer in a single motion as quickly as possible.
11. At the end of the CESP run, turn off the data acquisition and mixing paddle and allow the solids to settle out of solution if the solids are to be used as seeds for the next CESP cycle.
12. Remove the Calcium ISE and pH probes and probe support platform and remove the jar tester from its platform. Place the probes temporarily into a small beaker of OAS model solution to prevent drying of the probes between runs.
13. Once the solids have settled out of solution, slowly remove the liquid without disturbing the solids and then collect the remaining solids in a separate container for later use as seeds for the next cycle.
14. Rinse out the jar tester with DI water and then dry.

Particle Size Measurements

During precipitation experiments (**§4.2.2, §5.2, §6.2**), slurry samples were withdrawn from the precipitation reactor using a micropipette (1-3 mL) and transferred into quench solution (150 mL). The quench solution was prepared such that it was saturated with respect to gypsum and calcium carbonate and contained a high concentration of antiscalant (100 mg/L Flocon 260; Biolab Water Additives, Lawrenceville, GA); therefore, nucleation and growth of crystals were retarded in the quench solutions. By transferring small amounts of slurry samples (1-3 mL) from the precipitation reactor into quench solutions at different times during the precipitation experiment and subsequently measuring the crystal size distributions (CSDs), the time evolution of CSD in the precipitation reactor could be deduced.

CSDs in the quench solutions were determined using the Multisizer 3 Coulter Counter (Beckman Coulter Inc., Miami, FL). This particle size analyzer employs the Coulter principle by measuring the impedance of a standard electrolyte solution between two electrodes separated by an interchangeable non-conducting tube with a small aperture. As suspended particles pass through the aperture, the impedance increases in proportion to the volume of the particle. The Coulter Counter can measure the size of hundreds of particles per second to produce the particle size distribution for the sample. However, the appropriate electrolyte and aperture size must be selected based on the type of sample for which the PSD is being measured. The aperture is selected such that the average expected particle size falls near the center of the measureable range (2-60% of aperture size) for the given aperture and an electrolyte solution is chosen that will not react with or affect the properties of the suspended particles. The particle size analyzer also must be calibrated using NIST standard particle suspensions of known modal size when

apertures and/or electrolyte solutions are changed. A diagram of the apparatus and photograph of the Multisizer M3 are shown in **Figs. B-7** & **B-8**.

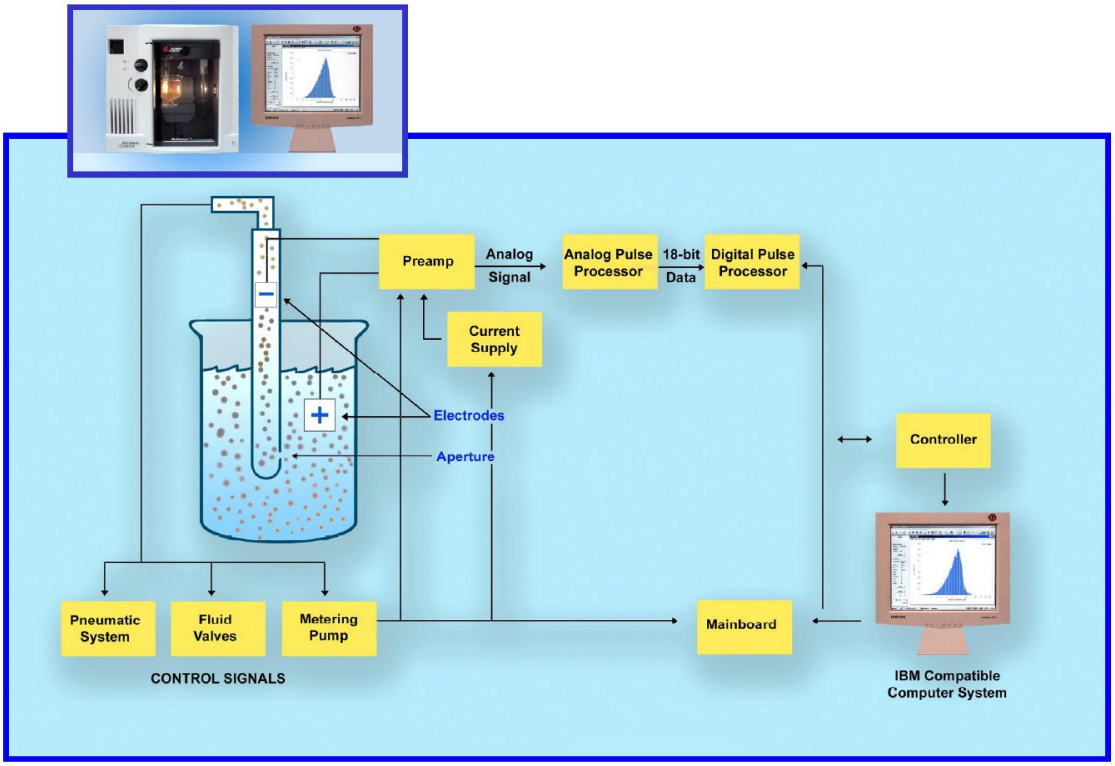

Figure B-7. Beckman Coulter Multisizer 3 particle size analyzer and data acquisition computer**.**

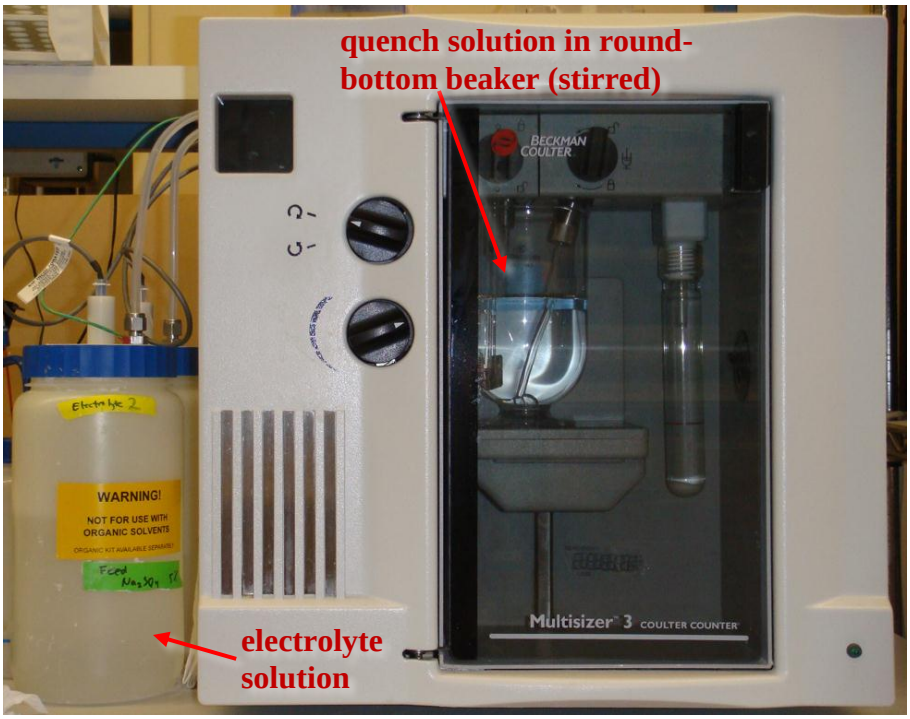

Figure B-8. Beckman coulter Multisizer 3 particle size analyzer [7].

Particle size analysis procedure:

1. Prepare 10 L of electrolyte solution for the Coulter Counter containing 50 g/L sodium sulfate (5 wt%) and 0.1 g/L sodium azide. Vacuum filter the solution prior to use with 0.22 μm filters.
2. Prepare ~20 L of quench solution for particle size samples containing 5 wt% sodium sulfate plus appropriate amounts of calcium chloride and sodium bicarbonate to saturate the solution with respect to calcite and gypsum. Also add 1 g/L Flocon 260 antiscalant and 0.1 g/L sodium azide. Vacuum filter the solution prior to use with 0.22 μm filters.
3. Collect small samples (1–3 mL) of solution with a micropipette during CESP experiments and immediately dispense into 150 mL of quench solution. Gently swirl the quench solution prior to pouring into the coulter counter round-bottom beaker and place the beaker on the platform inside the coulter counter.

4. The stirring impeller should be set to a speed high enough to keep all particles suspended without causing splashing.
5. Begin collecting particle size data and stop collecting data when the solution level is ~0.5 cm above the aperture to prevent entrainment of air in the system.

References

1. *Applied Membranes Simple SDI Portable Auto SDI Tester*. 2012; Available from: http://www.simplesdi.com/.
2. *Hach Alkalinity Test Kit Model AL-DT*. 2012; Available from: http://www.hach.com/alkalinity-test-kit-model-al-dt/product?id=7640219547.
3. Gu, H., et al., *Demonstration of automated feed flow reversal mode of RO operation without chemical additives in a RO pilot system with real-time gypsum scale monitoring.* Desalination, 2012. **(Sumbitted)**.
4. Thompson, J., et al., *Rapid Field Optimization of RO Desalination Operating Conditions for High Scaling Propensity Brackish Water.* Desalination, 2012. **(Submitted)**.
5. Bartman, A.R., P.D. Christofides, and Y. Cohen, *Nonlinear Model-Based Control of an Experimental Reverse-Osmosis Water Desalination System.* Industrial & Engineering Chemistry Research, 2009. **48**(13): p. 6126-6136.
6. Bartman, A.R., et al., *Minimizing energy consumption in reverse osmosis membrane desalination using optimization-based control.* Journal of Process Control, 2010. **20**(10): p. 1261-1269.
7. *Beckman Coulter Multisizer 3 Coulter Counter.* 2012.

Appendix C. Calcium ion selective electrode (ISE) calibration

Six standards of known calcium concentration and activity were prepared for calibration of the calcium ISE prior to each use (see **§4.2, §5.2, §6.2**). A master calibration curve was created for the calcium ISE which was used to correct the calibration obtained during each daily calibration. The details of the calibration method are provided below (A. Rahardianto, UCLA 2009).

1. Make six calibration standard solutions mimicking the composition of the RO concentrate model solution excluding sodium bicarbonate and with additional sodium chloride to maintain the ionic strength.
2. The six calibration standards should mimic the compositions expected throughout the CESP experiments covering the range of *SIg* (e.g., ~2.5–1.0) expected over the course of the demineralization process as shown in **Table C-1**.
3. The master calibration curve for the calcium ISE is found by plotting the measured potential difference (ΔE) versus the logarithm of the known calcium activities (mol/kg-water) as in **Fig. C-1**. This curve will yield the gain (α) and offset (β) unique to the Ca ISE which had values of -31.1 mV/p(Ca^{2+}) and 196.5 mV as shown in **Fig. C-1**.
4. Perform a daily calibration prior to CESP runs using standards 2, 3, and 5 to calculate the daily gain and offset values (α_{daily} and β_{daily}).
5. The daily gain and offset values are used to correct the measured potential (ΔE_{daily}) using a linear transformation: $\Delta E = \frac{\alpha}{\alpha_{daily}} \cdot \Delta E_{daily} + \beta\text{-}\beta_{daily}\left(\frac{\alpha}{\alpha_{daily}}\right)$.

Table C-1. Calcium calibration standard solution compositions

	std 1 (g/L)	**std 2** (g/L)	**std 3** (g/L)	**std 4** (g/L)	**std 5** (g/L)	**std 6** (g/L)
$CaCl_2 \cdot 2H_2O$	5.3601	4.5201	3.2602	2.4202	1.7202	1.2722
Na_2SO_4	20.6557	20.6557	19.4384	18.6268	17.9505	17.5176
$MgSO_4 \cdot 7H_2O$	7.6816	7.6816	7.6816	7.6816	7.6816	7.6816
NaCl	1.1863	1.8497	2.8515	3.5193	4.0758	4.4320
$NaHCO_3$	0	0	0	0	0	0
SIg	2.954	2.525	1.852	1.390	0.998	0.742
$p(Ca^{2+})$, (Ca^{2+}) in (mol/kg-water)	2.30	2.37	2.49	2.61	2.75	2.88

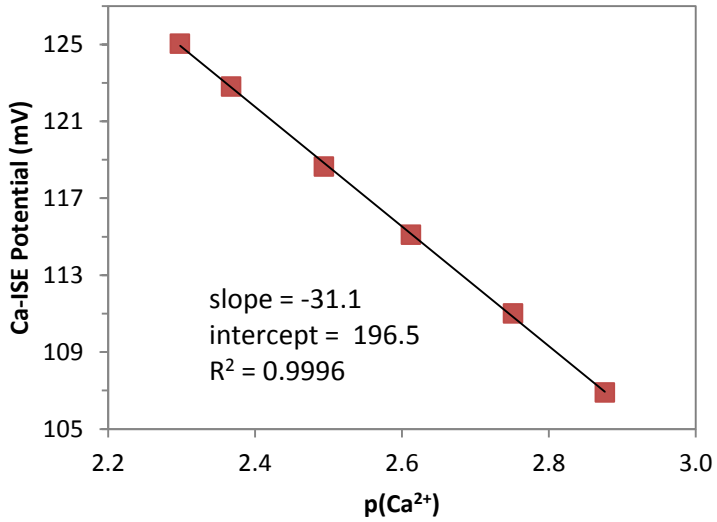

Figure C-1. Calcium ISE master calibration curve of potential difference as a function of $p(Ca^{2+})$, i.e., the negative logarithm of calcium ion activity (mol/kg-water).

Appendix D.

Estimation of ion concentrations from calcium activity and pH data

During each batch CESP experiment (see **§4.2, §5.2, §6.2**), $CaCO_3$ and $CaSO_4$ precipitation caused a decline in calcium activity and pH. pH and calcium ion activity were monitored during CESP experiments with a calcium ion selective electrode (ISE25Ca-9/REF251) and a pH electrode (pHG211-8/REF201) from Radiometer Analytical (Lyon, France) connected, respectively, to a sensION4 meter (Hach Co., Loveland, CO) and an Orion 720Aplus (Thermo Scientific, Waltham, MA) meter. The solution temperature was recorded using a Hach temperature probe (Model 51980-00, Hach Co., Loveland, CO) connected to the sensION4 meter (Hach Co., Loveland, CO). Details of the concentration calculations are available elsewhere (A. Rahardianto, UCLA 2009). Briefly, ion concentrations were estimated using OLI Stream Analyzer 3.1 (Morris Plains, NJ) to model the complex, multi-electrolyte aqueous system in liquid phase equilibrium, but not in solid-liquid equilibrium for the supersaturated metastable solutions.

1. Calculate the initial calcium ion activity, $(Ca^{2+})_i$, and pH, pH_i, for the model solution including considerations of any alkaline addition.
2. Compare the calculated calcium ion activity, $(Ca^{2+})_i$ to the measured calcium activity, $(Ca^{2+})_m$. at each time step for the given data sampling rate. The differences in calcium activity are due to the precipitation of $CaCO_3$ and $CaSO_4$, and the differences in pH are due to deprotonation of bicarbonate during precipitation of $CaCO_3$.
3. Adjust the relative amounts of precipitated $CaCO_3$ and $CaSO_4$ until the calculated and measured calcium activity and pH are equal.

4. Repeat steps 2 and 3 for each time step to generate a database of thermodynamic properties of the solution throughout the CESP run.
5. Extract the desired concentrations, saturation indices, and mass of solids precipitated from the database generated in step 4 as needed.

Appendix E

Gypsum solids recycling and GSP reactor simulation validation

E.1 Gypsum seeded precipitation mixing rate optimization

Prior to performing the multi-cycle CESP experiments presented in **Ch. 6**, the mixing rate was optimized with respect to particle aggregation in order to minimize aggregation and, thus, maximize the sulfate extent of reaction. The rate of gypsum precipitation as quantified by the sulfate extent of reaction, $\alpha_{sulfate}$, increased with mixing rate from between 75 and 150 rpm (**Fig. E-1**). When the mixing rate was increased from between 150 and 275 rpm the rate of gypsum precipitation did not improve any further (**Fig. E-1**). This increase in the rate of gypsum precipitation was hypothesized to be due to the reduced aggregation (see **Fig. E-2**) that occurred at higher mixing rates [1, 2] resulting in a larger available surface area.

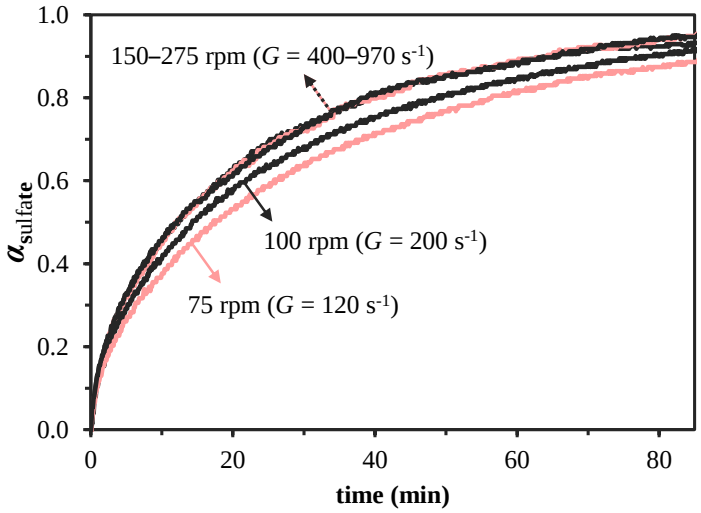

Figure E-1. Calcium removal as a function of time during seeded precipitation of PRO concentrate model solution (*SIg* = 2.5) with 5.0 g/L gypsum seed dose (45–µm diameter) and mixing rates ranging from 75 to 275 rpm in a 1-L rectangular crystallizer with a radial-flow impeller (see **§4.2.2**).

The postulate that particle aggregation is reduced with increasing mixing rate was verified via particle size measurements (i.e., PSD, see **§4.2.3**). The modal particle number (i.e., peak height) was found to decrease with time at the lowest mixing rate (75 rpm) indicating that

significant particle aggregation occurred (**Fig. E-2**). However, at 200 rpm and above, the modal particle number remained constant (within ±5%) with time indicating particle aggregation was prevented at mixing rates ≥ 200 rpm (**Fig. E-2**). Furthermore, at mixing rates < 200 rpm, the total number concentrations decreased by 30–72% indicating significant aggregation, while at a mixing rate of 200 rpm, the total number concentration decreased by only 12% (**Fig. E-3**). At the maximum mixing rate (275 rpm) there was no significant difference (< 4–5%) in the modal diameter and number concentration compared to those observed at 200 rpm. Thus, a mixing rate of 200 rpm was selected as the optimal mixing rate for the work presented in **Ch. 6**. The modal particle number and total number concentration as a function of time are shown in **Fig. E-3** for all mixing rates tested: 75, 100, 150, 200, and 275 rpm.

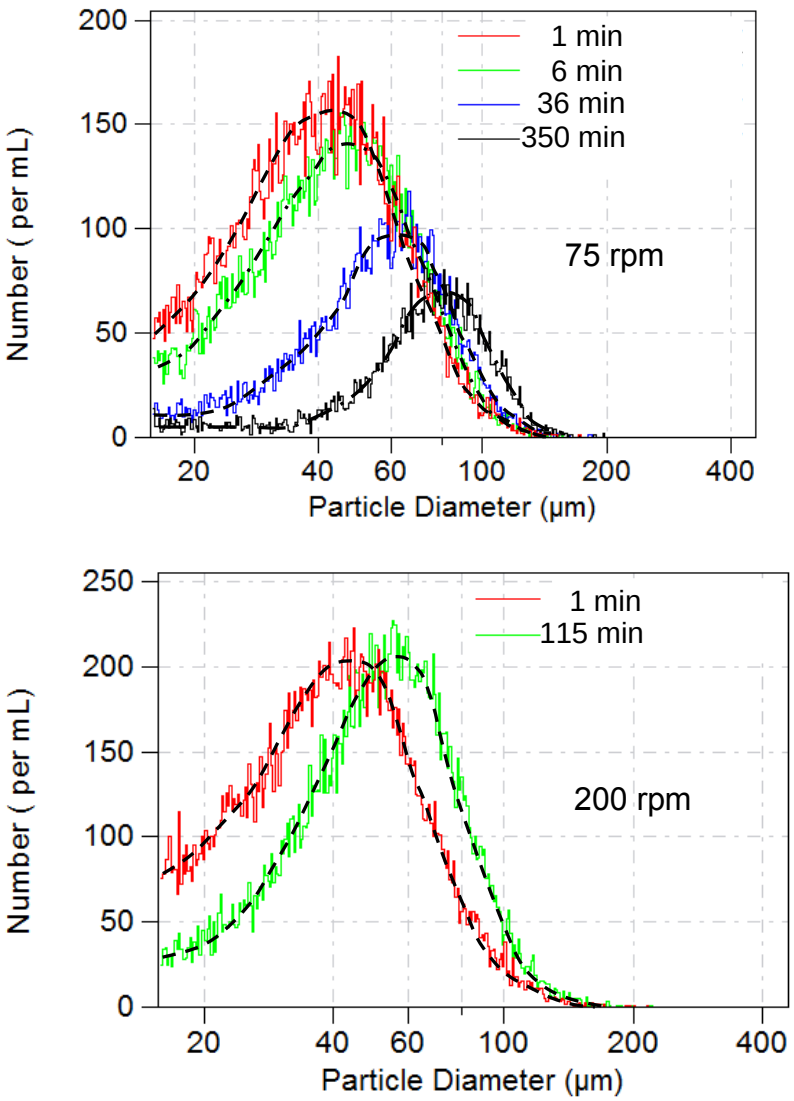

Figure E-2. Particle size distribution during seeded precipitation of PRO concentrate model solution (*SIg* = 2.5, see **§4.2.2**) with 5.0 g/L gypsum at mixing rates of 75 rpm and 200 rpm, respectively.

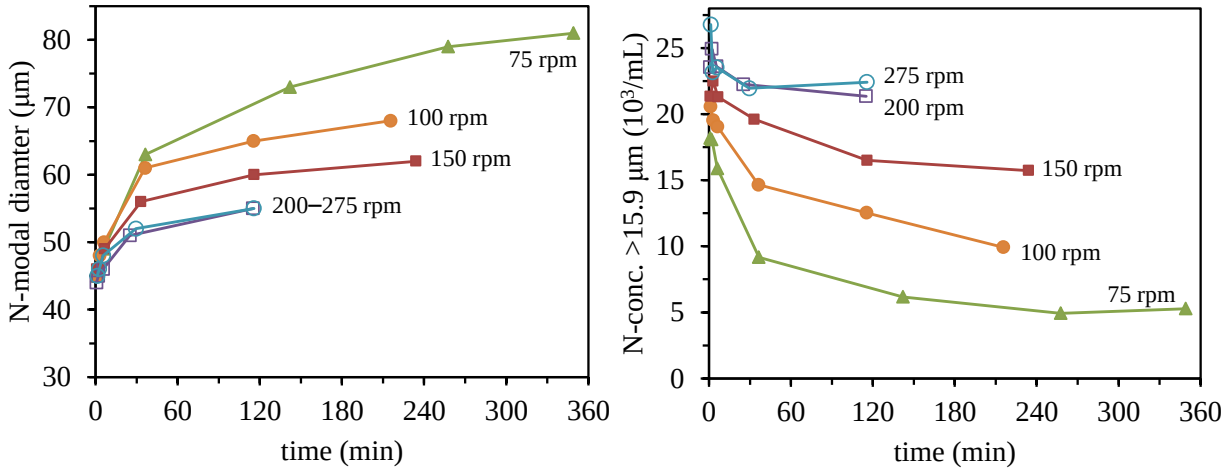

Figure E-3. Particle number concentration and modal diameter during seeded precipitation of PRO concentrate model solution (*SIg* = 2.5, see **§4.2.2**) with 5.0 g/L gypsum seed dose and mixing rates ranging from 75 to 275 rpm.

E.2 Validation of reactor simulation

The continuous gypsum seeded precipitation step of CESP was modeled via simulation of the crystallizer as a vertical cylindrical plug-flow reactor (see **§6.3.3**). The simulation results were compared to the ideal PFR in order to confirm that the performance of the simulated reactor was close to the ideal PFR. It is noted that the simulation provided solids particle size distributions, whereas the ideal PFR provides no details on the PSD in the reactor. The differential equation relating the concentration, C, to axial position, x, in an ideal PFR at steady-state is given by **Eq. E-1**:

$$u_w \frac{dC}{dx} = -R = -kA\left(C_0 - C_{sat}\right)^2 \qquad \text{(E-1)}$$

where u_w is the axial liquid velocity (m/s), R is the reaction rate for gypsum precipitation (mol/L-min), k is the rate constant (m^2/L^2-mol-min), A is the gypsum particle surface area (m^2/L), C_0 is the initial sulfate concentration (mol/L), and C_{sat} is the sulfate concentration (mol/L) at gypsum saturation (i.e., *SIg* = 1). The concentration profile (**Eq. E-3**) as a function of residence time for an ideal PFR is found by rearrangement and integration of **Eq. E-1**, and by noting that $\tau = H/u_w$.

$$\int_{C_0}^{C} \frac{dC}{\left(C - C_{sat}\right)^2} = -\frac{kA}{u_w}\int_0^H dx \tag{E-2}$$

$$C = \frac{C_0 + \beta C_{sat}}{1+\beta}, \quad \beta = kA\tau\left(C_0 - C_{sat}\right) \tag{E-3}$$

The concentration profile and final particle size distributions (number and surface area) for a representative simulation (ID# 1372, see **Table E-1**) with a residence time, τ = 10 min, solids fraction, ϕ = 0.5, and a seed particle diameter, d_p = 65 μm is shown in **Figs. E-4** & **E-5**. The resulting final total solids surface area A = 5.27 m^2/L was then used to calculate the concentration profile of the ideal PFR plotted in **Fig. E-4**. The simulation was found to agree with the ideal PFR to within < 1%; the sulfate extents of reaction, $\alpha_{sulfate}$, for the simulation and the ideal PFR were 0.914 and 0.923, respectively.

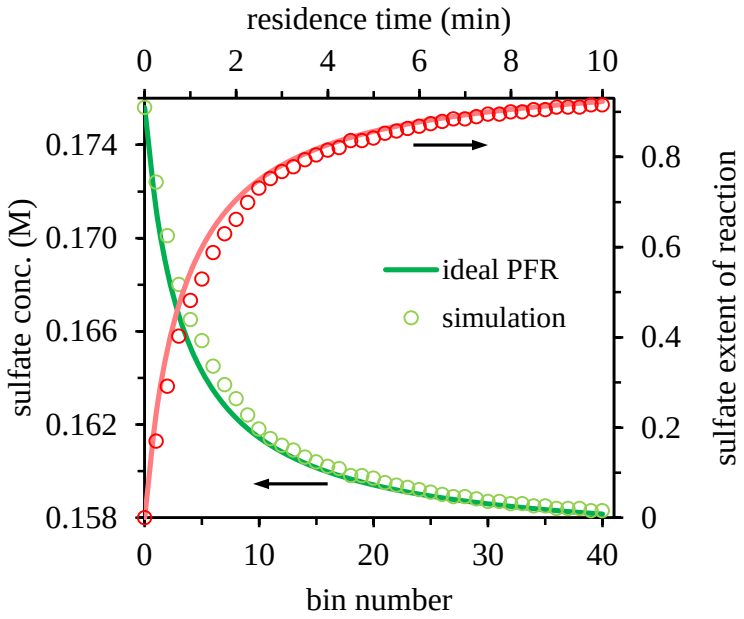

Figure E-4. Representative concentration profile and sulfate extent of reaction for an ideal PFR (solid lines) and for the simulated GSP crystallizer with 40 bins (circles) at the following conditions: τ = 10 min, ϕ = 0.5, d_p = 65 μm, A = 5.27 m^2/L, and $\alpha_{sulfate}$ = 0.914. The feed was PRO concentrate model solution (*SIg* = 2.5, see **§4.2.2**).

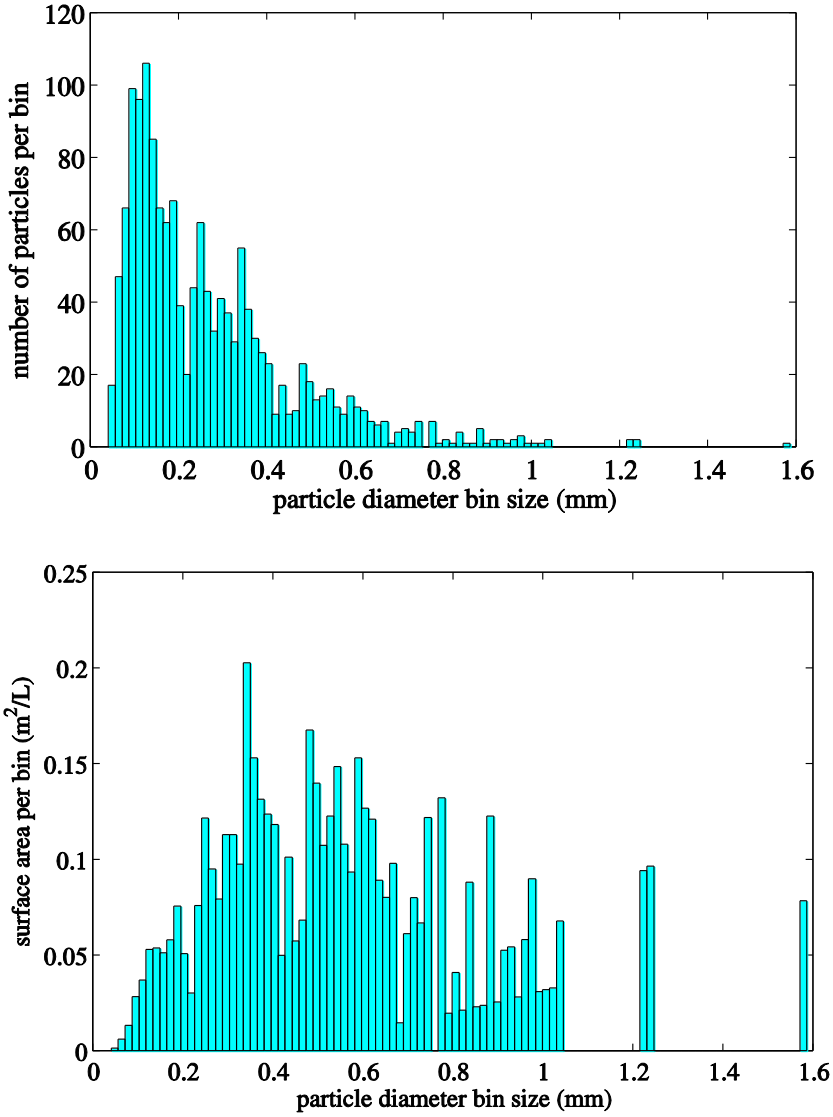

Figure E-5. Representative steady-state particle size distribution and surface area distribution from the simulation of the GSP crystallizer at the following conditions: τ = 10 min, ϕ = 0.5, d_p = 65 μm, $\alpha_{sulfate}$ = 0.914. The feed was PRO concentrate model solution (*SIg* = 2.5, see **§4.2.2**).

The independence of the model results with respect to number of bins was confirmed by varying the number of reactor bins, *n*, simulated from 10 to 360 for a residence time, τ = 30 min, solids fraction, ϕ = 0.1, and a seed particle diameter, d_p = 45 μm. The steady-state sulfate extents of reaction for these simulations (ID# 1101–1136, see **Table E-1**) are plotted versus 1/*n* in **Fig. E-6**. The sulfate extent of reaction changed by < 0.2% for n > 40, with the $\alpha_{sulfate}$ = 0.945, 0.946

and 0.946 for n = 40, 80, and 360, respectively. Therefore, to minimize the computation time while still producing reliable data, the simulation results presented in **Ch. 6** were obtained with n = 40 unless otherwise stated. Simulations were performed on a cluster of 20 Intel Xeon Quad-Core processors at 2.2–3.0 GHz with 176 GB of total RAM. The length of computational time required to complete a typical simulation varied from between a few minutes to several days.

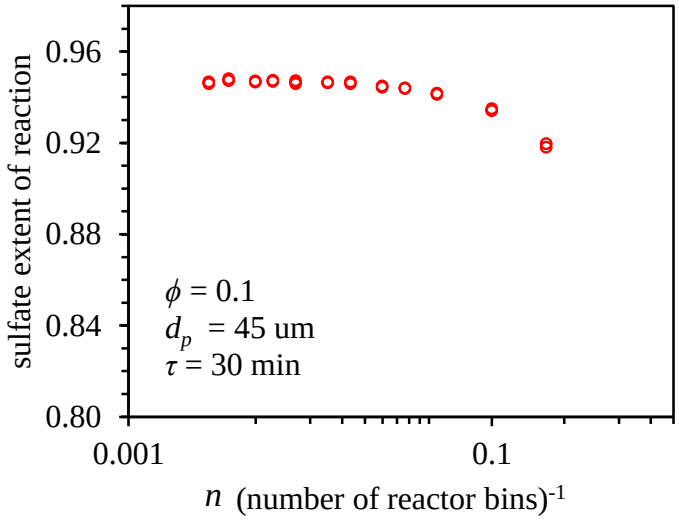

Figure E-6. Independence of model results with respect to the number of reactor bins. The sulfate extent of reaction, $\alpha_{sulfate}$, was calculated over a range of number of reactor bins simulated, n (10–360).

E.3 Summary of reactor simulation results

The continuous CESP process simulation (see **§6.3.5** & **App. E.2**) input parameters and results (output) are summarized in **Table E-1**. *Input parameters*: "ID" is a unique identifier for a single simulation, ϕ_S is the desired solids fraction, "seed d_p" is the average gypsum seed particle diameter, λ is the steady-state time multiplier ($t_f = \lambda \cdot t_{ss}$), n is the number of reactor bins, k is the gypsum precipitation rate constant. *Steady-state output*: $\alpha_{sulfate}$ is the sulfate extent of reaction, "mean d_p" is the average particle size in the reactor, A is the total particle surface area, R is the overall rate of gypsum precipitation, ϕ_S is the solids fraction in the reactor, "particle conc." is the

total mass concentration of gypsum particles in the reactor, “solids purge” is the rate of solids removal, “seed makeup” is the rate of seed addition.

Table E-1. Continuous reactor simulation inputs and outputs

ID	simulation inputs						simulaiton outputs [a]							
	t_res	ϕ_S	seed d_p	λ	n	k	$\alpha_{sulfate}$	mean d_p	A	R	ϕ_S	particle conc.	solids purge	seed makeup
	min	--	m	--	--	L^2/m^2-mol-min	--	m	m^2/L	mol/L-m^2-min	--	g/L	g/L-min	g/L-min
1084	30	0.1	4.5E-05	1.5	60	12	0.94525	1.16E-04	2.666	3.43E-05	0.09989	231.7	0.1057	0.0032
1085	30	0.1	4.5E-05	1.5	120	12	0.94726	1.18E-04	2.740	3.28E-05	0.09990	231.8	0.1064	0.0037
1086	30	0.1	4.5E-05	1.5	200	12	0.94714	1.18E-04	2.734	3.29E-05	0.09997	231.9	0.1068	0.0041
1087	30	0.1	4.5E-05	1.5	280	12	0.94726	1.17E-04	2.685	3.21E-05	0.09992	231.8	0.1056	0.0028
1088	30	0.1	4.5E-05	1.5	360	12	0.94639	1.18E-04	2.730	3.37E-05	0.09992	231.8	0.1048	0.0022
1089	30	0.1	4.5E-05	1.5	60	12	0.94525	1.16E-04	2.666	3.43E-05	0.09989	231.7	0.1057	0.0032
1090	30	0.1	4.5E-05	1.5	120	12	0.94726	1.18E-04	2.740	3.28E-05	0.09990	231.8	0.1064	0.0037
1091	30	0.1	4.5E-05	1.5	200	12	0.94714	1.18E-04	2.734	3.29E-05	0.09997	231.9	0.1068	0.0041
1092	30	0.1	4.5E-05	1.5	280	12	0.94726	1.17E-04	2.685	3.21E-05	0.09992	231.8	0.1056	0.0028
1093	30	0.1	4.5E-05	1.5	360	12	0.94639	1.18E-04	2.730	3.37E-05	0.09992	231.8	0.1048	0.0022
1094	30	0.1	4.5E-05	1.5	60	12	0.94525	1.16E-04	2.666	3.43E-05	0.09989	231.7	0.1057	0.0032
1095	30	0.1	4.5E-05	1.5	120	12	0.94726	1.18E-04	2.740	3.28E-05	0.09990	231.8	0.1064	0.0037
1096	30	0.1	4.5E-05	1.5	200	12	0.94714	1.18E-04	2.734	3.29E-05	0.09997	231.9	0.1068	0.0041
1097	30	0.1	4.5E-05	1.5	280	12	0.94726	1.17E-04	2.685	3.21E-05	0.09992	231.8	0.1056	0.0028
1098	30	0.1	4.5E-05	1.5	360	12	0.94639	1.18E-04	2.730	3.37E-05	0.09992	231.8	0.1048	0.0022
1101	30	0.1	4.5E-05	1.5	5	12	0.91949	1.17E-04	2.708	7.52E-05	0.09995	231.9	0.1063	0.0066
1100	30	0.1	4.5E-05	1.5	5	12	0.91796	1.15E-04	2.645	7.63E-05	0.09988	231.7	0.1055	0.0059
1099	30	0.1	4.5E-05	1.5	5	12	0.91962	1.17E-04	2.714	7.51E-05	0.09991	231.8	0.1052	0.0055
1103	30	0.1	4.5E-05	1.5	10	12	0.93392	1.17E-04	2.692	5.04E-05	0.09991	231.8	0.1043	0.0030
1102	30	0.1	4.5E-05	1.5	10	12	0.93426	1.17E-04	2.708	5.02E-05	0.09991	231.8	0.1041	0.0028
1106	30	0.1	4.5E-05	1.5	20	12	0.94164	1.18E-04	2.723	3.98E-05	0.09991	231.8	0.1058	0.0037
1108	30	0.1	4.5E-05	1.5	30	12	0.94366	1.17E-04	2.707	3.69E-05	0.09991	231.8	0.1046	0.0022
1104	30	0.1	4.5E-05	1.5	10	12	0.93399	1.17E-04	2.695	5.04E-05	0.09991	231.8	0.1034	0.0021
1109	30	0.1	4.5E-05	1.5	30	12	0.9438	1.18E-04	2.714	3.68E-05	0.09993	231.9	0.1050	0.0026
1110	30	0.1	4.5E-05	1.5	30	12	0.94386	1.18E-04	2.717	3.68E-05	0.09990	231.8	0.1033	0.0009
1107	30	0.1	4.5E-05	1.5	20	12	0.94109	1.17E-04	2.695	4.02E-05	0.09988	231.7	0.1036	0.0015
1112	30	0.1	4.5E-05	1.5	40	12	0.9449	1.18E-04	2.716	3.55E-05	0.09990	231.8	0.1065	0.0040
1105	30	0.1	4.5E-05	1.5	20	12	0.94168	1.18E-04	2.726	3.98E-05	0.09990	231.8	0.1039	0.0017
1111	30	0.1	4.5E-05	1.5	40	12	0.94438	1.17E-04	2.689	3.58E-05	0.09993	231.8	0.1042	0.0017
1113	30	0.1	4.5E-05	1.5	40	12	0.94423	1.16E-04	2.681	3.59E-05	0.09993	231.8	0.1045	0.0021
1114	30	0.1	4.5E-05	1.5	60	12	0.94639	1.18E-04	2.727	3.37E-05	0.09992	231.8	0.1048	0.0021
1116	30	0.1	4.5E-05	1.5	60	12	0.94665	1.18E-04	2.741	3.35E-05	0.09991	231.8	0.1074	0.0047
1115	30	0.1	4.5E-05	1.5	60	12	0.94566	1.17E-04	2.688	3.41E-05	0.09994	231.9	0.1045	0.0019
1119	30	0.1	4.5E-05	1.5	80	12	0.94607	1.17E-04	2.686	3.36E-05	0.09992	231.8	0.1056	0.0030
1118	30	0.1	4.5E-05	1.5	80	12	0.94621	1.17E-04	2.693	3.35E-05	0.09992	231.8	0.1064	0.0038
1120	30	0.1	4.5E-05	1.5	120	12	0.94661	1.17E-04	2.705	3.32E-05	0.09990	231.8	0.1050	0.0023
1117	30	0.1	4.5E-05	1.5	80	12	0.94623	1.17E-04	2.695	3.35E-05	0.09992	231.8	0.1049	0.0023
1124	30	0.1	4.5E-05	1.5	160	12	0.94732	1.17E-04	2.708	3.23E-05	0.09992	231.8	0.1050	0.0022
1123	30	0.1	4.5E-05	1.5	160	12	0.94668	1.17E-04	2.673	3.26E-05	0.09992	231.8	0.1073	0.0046
1125	30	0.1	4.5E-05	1.5	160	12	0.94712	1.17E-04	2.696	3.24E-05	0.09991	231.8	0.1064	0.0036
1127	30	0.1	4.5E-05	1.5	200	12	0.94688	1.18E-04	2.720	3.30E-05	0.09995	231.9	0.1043	0.0016
1121	30	0.1	4.5E-05	1.5	120	12	0.94641	1.17E-04	2.694	3.33E-05	0.09991	231.8	0.1065	0.0039
1122	30	0.1	4.5E-05	1.5	120	12	0.94577	1.16E-04	2.659	3.37E-05	0.09996	231.9	0.1054	0.0028
1128	30	0.1	4.5E-05	1.5	200	12	0.94675	1.18E-04	2.713	3.31E-05	0.09991	231.8	0.1063	0.0036
1130	30	0.1	4.5E-05	1.5	280	12	0.94812	1.18E-04	2.732	3.16E-05	0.09994	231.9	0.1045	0.0017
1129	30	0.1	4.5E-05	1.5	280	12	0.94728	1.17E-04	2.687	3.21E-05	0.09993	231.9	0.1035	0.0007
1126	30	0.1	4.5E-05	1.5	200	12	0.94645	1.17E-04	2.696	3.33E-05	0.09993	231.8	0.1070	0.0043
1132	30	0.1	4.5E-05	1.5	360	12	0.94616	1.18E-04	2.718	3.38E-05	0.09989	231.7	0.1058	0.0032
1134	30	0.1	4.5E-05	1.5	360	12	0.9457	1.17E-04	2.693	3.41E-05	0.09991	231.8	0.1037	0.0011
1133	30	0.1	4.5E-05	1.5	360	12	0.94673	1.19E-04	2.748	3.35E-05	0.09993	231.8	0.1046	0.0019
1131	30	0.1	4.5E-05	1.5	280	12	0.94718	1.17E-04	2.681	3.21E-05	0.09992	231.8	0.1063	0.0036
1183	30	0.1	4.5E-05	1.5	40	12	0.9449	1.18E-04	2.714	3.55E-05	0.09989	231.7	0.1050	0.0025
1184	30	0.1	4.5E-05	1.5	40	12	0.94443	1.17E-04	2.689	3.58E-05	0.09989	231.8	0.1053	0.0029
1185	30	0.1	4.5E-05	1.5	40	12	0.94442	1.17E-04	2.689	3.58E-05	0.09989	231.7	0.1055	0.0031
1186	20	0.1	4.5E-05	1.5	40	12	0.92028	1.18E-04	2.718	7.44E-05	0.09989	231.7	0.1539	0.0041
1187	20	0.1	4.5E-05	1.5	40	12	0.9199	1.17E-04	2.703	7.47E-05	0.09988	231.7	0.1539	0.0042
1188	20	0.1	4.5E-05	1.5	40	12	0.92043	1.18E-04	2.723	7.42E-05	0.09989	231.7	0.1539	0.0041
1189	15	0.1	4.5E-05	1.5	40	12	0.89665	1.17E-04	2.707	1.24E-04	0.09988	231.7	0.2000	0.0055
1190	15	0.1	4.5E-05	1.5	40	12	0.89584	1.16E-04	2.683	1.25E-04	0.09988	231.7	0.2001	0.0057
1191	15	0.1	4.5E-05	1.5	40	12	0.89698	1.18E-04	2.717	1.24E-04	0.09989	231.8	0.2002	0.0056

[a] simulation outputs are averages calculated over the steady-state time period, i.e., from t_{ss} to t_f, where $t_f = \lambda * t_{ss}$

Table E-1. Continuous reactor simulation inputs and outputs (cont.)

ID	simulation inputs						simulaiton outputs [a]							
	t_res	ϕ_S	seed d_p	λ	n	k	$\alpha_{sulfate}$	mean d_p	A	R	ϕ_S	particle conc.	solids purge	seed makeup
	min	--	m	--	--	L^2/m^2-mol-min	--	m	m^2/L	mol/L-m^2-min	--	g/L	g/L-min	g/L-min
1192	15	0.3	4.5E-05	1.5	40	12	0.94345	1.57E-04	5.278	7.27E-05	0.29951	694.9	0.2067	0.0021
1194	15	0.3	4.5E-05	1.5	40	12	0.94302	1.55E-04	5.236	7.32E-05	0.29949	694.8	0.2067	0.0021
1195	10	0.3	4.5E-05	1.5	40	12	0.91801	1.56E-04	5.269	1.52E-04	0.29960	695.1	0.3023	0.0036
1196	10	0.3	4.5E-05	1.5	40	12	0.91836	1.58E-04	5.296	1.52E-04	0.29951	694.9	0.3030	0.0042
1197	10	0.3	4.5E-05	1.5	40	12	0.91862	1.57E-04	5.313	1.51E-04	0.29957	695.0	0.3022	0.0033
1198	8	0.3	4.5E-05	1.5	40	12	0.90122	1.58E-04	5.343	2.24E-04	0.29957	695.0	0.3707	0.0041
1199	8	0.3	4.5E-05	1.5	40	12	0.90063	1.57E-04	5.308	2.26E-04	0.29952	694.9	0.3706	0.0042
1200	8	0.3	4.5E-05	1.5	40	12	0.90138	1.58E-04	5.354	2.24E-04	0.29954	694.9	0.3707	0.0041
1201	8	0.5	4.5E-05	1.5	40	12	0.92588	1.82E-04	7.364	1.74E-04	0.49922	1158.2	0.3788	0.0022
1202	8	0.5	4.5E-05	1.5	40	12	0.92493	1.81E-04	7.263	1.76E-04	0.49922	1158.2	0.3790	0.0028
1203	8	0.5	4.5E-05	1.5	40	12	0.9254	1.82E-04	7.313	1.75E-04	0.49923	1158.2	0.3791	0.0027
1204	6	0.5	4.5E-05	1.5	40	12	0.90377	1.82E-04	7.340	2.92E-04	0.49918	1158.1	0.4942	0.0040
1205	6	0.5	4.5E-05	1.5	40	12	0.90401	1.83E-04	7.359	2.92E-04	0.49920	1158.1	0.4941	0.0039
1206	6	0.5	4.5E-05	1.5	40	12	0.90321	1.81E-04	7.292	2.94E-04	0.49913	1158.0	0.4939	0.0040
1207	4	0.5	4.5E-05	1.5	40	12	0.8625	1.81E-04	7.291	5.93E-04	0.49915	1158.0	0.7081	0.0064
1208	4	0.5	4.5E-05	1.5	40	12	0.86178	1.80E-04	7.246	5.96E-04	0.49920	1158.1	0.7077	0.0066
1209	4	0.5	4.5E-05	1.5	40	12	0.86337	1.82E-04	7.346	5.90E-04	0.49924	1158.2	0.7088	0.0064
1210	60	0.1	1.0E-04	1.5	40	12	0.93804	2.62E-04	1.223	2.04E-05	0.09946	230.8	0.0523	0.0015
1211	60	0.1	1.0E-04	1.5	40	12	0.93753	2.61E-04	1.213	2.05E-05	0.09940	230.6	0.0523	0.0015
1212	60	0.1	1.0E-04	1.5	40	12	0.9378	2.61E-04	1.218	2.04E-05	0.09947	230.8	0.0523	0.0015
1213	30	0.1	1.0E-04	1.5	40	12	0.88456	2.61E-04	1.220	7.05E-05	0.09948	230.8	0.0990	0.0030
1214	30	0.1	1.0E-04	1.5	40	12	0.88433	2.61E-04	1.218	7.06E-05	0.09944	230.7	0.0990	0.0031
1215	30	0.1	1.0E-04	1.5	40	12	0.88287	2.58E-04	1.200	7.14E-05	0.09942	230.7	0.0992	0.0035
1216	20	0.1	1.0E-04	1.5	40	12	0.83689	2.62E-04	1.216	1.40E-04	0.09926	230.3	0.1406	0.0044
1217	20	0.1	1.0E-04	1.5	40	12	0.83849	2.63E-04	1.230	1.39E-04	0.09938	230.6	0.1410	0.0046
1218	20	0.1	1.0E-04	1.5	40	12	0.83713	2.61E-04	1.218	1.40E-04	0.09940	230.6	0.1408	0.0046
1219	30	0.3	1.0E-04	1.5	40	12	0.93662	3.50E-04	2.386	4.16E-05	0.29809	691.6	0.1029	0.0013
1220	30	0.3	1.0E-04	1.5	40	12	0.93681	3.51E-04	2.395	4.15E-05	0.29800	691.4	0.1028	0.0012
1221	30	0.3	1.0E-04	1.5	40	12	0.93712	3.52E-04	2.406	4.13E-05	0.29785	691.0	0.1028	0.0012
1222	20	0.3	1.0E-04	1.5	40	12	0.90718	3.46E-04	2.353	8.77E-05	0.29743	690.0	0.1497	0.0021
1223	20	0.3	1.0E-04	1.5	40	12	0.90742	3.47E-04	2.359	8.75E-05	0.29741	690.0	0.1497	0.0020
1224	20	0.3	1.0E-04	1.5	40	12	0.90756	3.47E-04	2.359	8.74E-05	0.29718	689.5	0.1498	0.0021
1227	15	0.3	1.0E-04	1.5	40	12	0.881	3.47E-04	2.357	1.45E-04	0.29769	690.6	0.1940	0.0029
1234	8	0.5	1.0E-04	1.5	40	12	0.84756	4.05E-04	3.298	3.32E-04	0.49580	1150.3	0.3493	0.0046
1237	120	0.1	2.0E-04	1.5	40	12	0.93926	5.23E-04	0.611	9.70E-06	0.09949	230.8	0.0262	0.0007
1238	120	0.1	2.0E-04	1.5	40	12	0.93941	5.25E-04	0.613	9.68E-06	0.09942	230.7	0.0260	0.0005
1240	60	0.1	2.0E-04	1.5	40	12	0.8858	5.19E-04	0.604	3.39E-05	0.09945	230.7	0.0495	0.0014
1241	60	0.1	2.0E-04	1.5	40	12	0.88673	5.24E-04	0.610	3.37E-05	0.09940	230.6	0.0495	0.0014
1242	60	0.1	2.0E-04	1.5	40	12	0.88603	5.20E-04	0.605	3.38E-05	0.09940	230.6	0.0495	0.0014
1243	40	0.1	2.0E-04	1.5	40	12	0.83902	5.20E-04	0.605	6.73E-05	0.09936	230.5	0.0703	0.0021
1244	40	0.1	2.0E-04	1.5	40	12	0.83726	5.16E-04	0.596	6.79E-05	0.09919	230.1	0.0703	0.0022
1245	40	0.1	2.0E-04	1.5	40	12	0.84025	5.22E-04	0.609	6.69E-05	0.09946	230.7	0.0704	0.0020
1247	60	0.3	2.0E-04	1.5	40	12	0.93883	7.08E-04	1.213	1.95E-05	0.29822	691.9	0.0514	0.0005
1254	30	0.3	2.0E-04	1.5	40	12	0.88286	6.92E-04	1.176	6.92E-05	0.29751	690.2	0.0969	0.0012
1264	240	0.1	4.0E-04	1.5	40	12	0.93687	1.03E-03	0.297	5.13E-06	0.09941	230.6	0.0131	0.0004
1265	240	0.1	4.0E-04	1.5	40	12	0.93764	1.04E-03	0.301	5.07E-06	0.09942	230.7	0.0131	0.0004
1266	240	0.1	4.0E-04	1.5	40	12	0.93838	1.05E-03	0.305	5.02E-06	0.09952	230.9	0.0131	0.0004
1267	120	0.1	4.0E-04	1.5	40	12	0.88581	1.05E-03	0.306	1.73E-05	0.09951	230.9	0.0248	0.0007
1268	120	0.1	4.0E-04	1.5	40	12	0.88526	1.05E-03	0.305	1.74E-05	0.09945	230.7	0.0248	0.0008
1269	120	0.1	4.0E-04	1.5	40	12	0.88461	1.04E-03	0.303	1.75E-05	0.09944	230.7	0.0247	0.0007
1270	80	0.1	4.0E-04	1.5	40	12	0.83824	1.04E-03	0.305	3.45E-05	0.09949	230.8	0.0352	0.0011
1271	80	0.1	4.0E-04	1.5	40	12	0.8396	1.05E-03	0.308	3.43E-05	0.09951	230.9	0.0353	0.0012
1272	80	0.1	4.0E-04	1.5	40	12	0.83863	1.05E-03	0.305	3.44E-05	0.09951	230.9	0.0352	0.0011
1273	120	0.3	4.0E-04	1.5	40	12	0.93363	1.36E-03	0.567	1.07E-05	0.29566	685.9	0.0256	0.0003
1274	120	0.3	4.0E-04	1.5	40	12	0.93715	1.40E-03	0.598	1.02E-05	0.29811	691.6	0.0257	0.0003
1275	120	0.3	4.0E-04	1.5	40	12	0.93828	1.42E-03	0.609	1.01E-05	0.29829	692.0	0.0257	0.0003
1276	80	0.3	4.0E-04	1.5	40	12	0.90885	1.39E-03	0.594	2.14E-05	0.29807	691.5	0.0374	0.0005
1277	80	0.3	4.0E-04	1.5	40	12	0.90889	1.39E-03	0.595	2.14E-05	0.29830	692.1	0.0375	0.0005
1278	80	0.3	4.0E-04	1.5	40	12	0.9087	1.39E-03	0.593	2.14E-05	0.29784	691.0	0.0374	0.0005
1279	60	0.3	4.0E-04	1.5	40	12	0.88334	1.40E-03	0.598	3.52E-05	0.29814	691.7	0.0486	0.0007

[a] simulation outputs are averages calculated over the steady-state time period, i.e., from t_{ss} to t_f, where $t_f = \lambda * t_{ss}$

Table E-1. Continuous reactor simulation inputs and outputs (cont.)

ID	simulation inputs						simulaiton outputs [a]							
	t_res	ϕ_S	seed d_p	λ	n	k	$\alpha_{sulfate}$	mean d_p	A	R	ϕ_S	particle conc.	solids purge	seed makeup
	min	--	m	--	--	L^2/m^2-mol-min	--	m	m^2/L	mol/L-m^2-min	--	g/L	g/L-min	g/L-min
1280	60	0.3	4.0E-04	1.5	40	12	0.87975	1.38E-03	0.579	3.61E-05	0.29657	688.1	0.0484	0.0007
1281	60	0.3	4.0E-04	1.5	40	12	0.88427	1.41E-03	0.604	3.50E-05	0.29817	691.8	0.0486	0.0006
1285	40	0.5	4.0E-04	1.5	40	12	0.87383	1.62E-03	0.820	5.64E-05	0.49566	1149.9	0.0719	0.0008
1287	40	0.5	4.0E-04	1.5	40	12	0.87488	1.63E-03	0.828	5.60E-05	0.49641	1151.7	0.0719	0.0008
1289	30	0.5	4.0E-04	1.5	40	12	0.83743	1.60E-03	0.808	9.23E-05	0.49560	1149.8	0.0920	0.0012
1290	30	0.5	4.0E-04	1.5	40	12	0.83918	1.61E-03	0.820	9.15E-05	0.49585	1150.4	0.0922	0.0011
1291	8	0.1	4.5E-05	1.5	40	12	0.82302	1.17E-04	2.685	3.62E-04	0.09989	231.7	0.3453	0.0105
1292	8	0.1	4.5E-05	1.5	40	12	0.82333	1.17E-04	2.691	3.61E-04	0.09988	231.7	0.3453	0.0104
1293	8	0.1	4.5E-05	1.5	40	12	0.82324	1.17E-04	2.690	3.62E-04	0.09988	231.7	0.3456	0.0107
1294	4	0.3	4.5E-05	1.5	40	12	0.82109	1.58E-04	5.299	7.30E-04	0.29954	694.9	0.6773	0.0093
1295	4	0.3	4.5E-05	1.5	40	12	0.82359	1.59E-04	5.393	7.22E-04	0.29957	695.0	0.6788	0.0088
1296	4	0.3	4.5E-05	1.5	40	12	0.82115	1.57E-04	5.303	7.30E-04	0.29948	694.8	0.6779	0.0099
1297	2	0.5	4.5E-05	1.5	40	12	0.76268	1.83E-04	7.371	1.79E-03	0.49927	1158.3	1.2561	0.0152
1298	2	0.5	4.5E-05	1.5	40	12	0.7636	1.83E-04	7.409	1.78E-03	0.49930	1158.4	1.2571	0.0147
1299	2	0.5	4.5E-05	1.5	40	12	0.76133	1.81E-04	7.315	1.79E-03	0.49922	1158.2	1.2536	0.0149
1300	10	0.1	1.0E-04	1.5	40	12	0.72278	2.61E-04	1.220	4.05E-04	0.09947	230.8	0.2447	0.0095
1301	10	0.1	1.0E-04	1.5	40	12	0.72234	2.61E-04	1.217	4.06E-04	0.09946	230.8	0.2446	0.0095
1302	10	0.1	1.0E-04	1.5	40	12	0.72311	2.61E-04	1.222	4.05E-04	0.09947	230.8	0.2453	0.0100
1305	8	0.3	1.0E-04	1.5	40	12	0.80414	3.54E-04	2.422	4.02E-04	0.29758	690.4	0.3334	0.0064
1306	4	0.5	1.0E-04	1.5	40	12	0.74018	4.09E-04	3.339	9.75E-04	0.49629	1151.4	0.6135	0.0114
1308	4	0.5	1.0E-04	1.5	40	12	0.73678	4.04E-04	3.278	9.82E-04	0.49580	1150.3	0.6152	0.0158
1309	20	0.1	2.0E-04	1.5	40	12	0.72529	5.19E-04	0.604	1.96E-04	0.09943	230.7	0.1221	0.0041
1310	20	0.1	2.0E-04	1.5	40	12	0.72603	5.20E-04	0.606	1.96E-04	0.09944	230.7	0.1221	0.0040
1311	20	0.1	2.0E-04	1.5	40	12	0.72698	5.22E-04	0.609	1.95E-04	0.09948	230.8	0.1223	0.0040
1314	15	0.3	2.0E-04	1.5	40	12	0.79816	7.10E-04	1.216	2.13E-04	0.29769	690.6	0.1756	0.0024
1318	40	0.1	4.0E-04	1.5	40	12	0.72787	1.06E-03	0.310	9.93E-05	0.09948	230.8	0.0614	0.0022
1319	40	0.1	4.0E-04	1.5	40	12	0.71984	1.03E-03	0.298	1.01E-04	0.09942	230.6	0.0609	0.0024
1320	40	0.1	4.0E-04	1.5	40	12	0.72434	1.05E-03	0.305	1.00E-04	0.09950	230.9	0.0612	0.0022
1321	30	0.3	4.0E-04	1.5	40	12	0.79424	1.41E-03	0.602	1.10E-04	0.29823	691.9	0.0877	0.0015
1322	30	0.3	4.0E-04	1.5	40	12	0.79426	1.41E-03	0.602	1.10E-04	0.29818	691.8	0.0877	0.0015
1323	30	0.3	4.0E-04	1.5	40	12	0.79224	1.39E-03	0.594	1.11E-04	0.29810	691.6	0.0875	0.0015
1324	15	0.5	4.0E-04	1.5	40	12	0.72743	1.62E-03	0.827	2.65E-04	0.49647	1151.8	0.1605	0.0027
1325	15	0.5	4.0E-04	1.5	40	12	0.72574	1.61E-03	0.819	2.66E-04	0.49599	1150.7	0.1605	0.0030
1329	16	0.5	1.0E-04	1.5	40	12	0.91658	4.06E-04	3.308	9.98E-05	0.49594	1150.6	0.1883	0.0019
1339	45	0.5	2.0E-04	1.5	40	12	0.93984	8.08E-04	1.646	2.56E-05	0.49633	1151.5	0.0685	0.0005
1340	45	0.5	2.0E-04	1.5	40	12	0.93932	8.03E-04	1.633	2.58E-05	0.49630	1151.4	0.0684	0.0005
1342	10	0.1	6.5E-05	1.5	40	12	0.80039	1.68E-04	1.853	3.18E-04	0.09953	230.9	0.2690	0.0086
1343	10	0.1	6.5E-05	1.5	40	12	0.8018	1.69E-04	1.869	3.16E-04	0.09964	231.2	0.2693	0.0084
1344	10	0.1	6.5E-05	1.5	40	12	0.80295	1.70E-04	1.883	3.15E-04	0.09966	231.2	0.2695	0.0082
1345	20	0.1	6.5E-05	1.5	40	12	0.88858	1.69E-04	1.868	9.99E-05	0.09964	231.2	0.1488	0.0043
1346	20	0.1	6.5E-05	1.5	40	12	0.88861	1.70E-04	1.869	9.99E-05	0.09958	231.0	0.1487	0.0041
1347	20	0.1	6.5E-05	1.5	40	12	0.88709	1.67E-04	1.840	1.01E-04	0.09963	231.1	0.1489	0.0045
1348	30	0.1	6.5E-05	1.5	40	12	0.92255	1.70E-04	1.876	4.85E-05	0.09965	231.2	0.1029	0.0028
1349	30	0.1	6.5E-05	1.5	40	12	0.92189	1.69E-04	1.858	4.89E-05	0.09959	231.0	0.1028	0.0028
1350	30	0.1	6.5E-05	1.5	40	12	0.92104	1.67E-04	1.836	4.94E-05	0.09955	231.0	0.1029	0.0030
1351	40	0.1	6.5E-05	1.5	40	12	0.94026	1.69E-04	1.870	2.88E-05	0.09963	231.1	0.0787	0.0022
1352	40	0.1	6.5E-05	1.5	40	12	0.94068	1.70E-04	1.884	2.86E-05	0.09967	231.2	0.0787	0.0022
1353	40	0.1	6.5E-05	1.5	40	12	0.9402	1.69E-04	1.868	2.88E-05	0.09964	231.2	0.0786	0.0021
1354	6	0.3	6.5E-05	1.5	40	12	0.82603	2.27E-04	3.671	4.78E-04	0.29853	692.6	0.4550	0.0070
1355	6	0.3	6.5E-05	1.5	40	12	0.8249	2.26E-04	3.639	4.81E-04	0.29849	692.5	0.4537	0.0063
1356	6	0.3	6.5E-05	1.5	40	12	0.82435	2.25E-04	3.625	4.82E-04	0.29854	692.6	0.4538	0.0068
1357	10	0.3	6.5E-05	1.5	40	12	0.88732	2.28E-04	3.689	2.02E-04	0.29873	693.1	0.2922	0.0035
1358	10	0.3	6.5E-05	1.5	40	12	0.88658	2.27E-04	3.661	2.03E-04	0.29849	692.5	0.2920	0.0035
1359	10	0.3	6.5E-05	1.5	40	12	0.88721	2.28E-04	3.685	2.02E-04	0.29871	693.0	0.2922	0.0035
1360	16	0.3	6.5E-05	1.5	40	12	0.92571	2.28E-04	3.683	8.76E-05	0.29858	692.7	0.1905	0.0023
1361	16	0.3	6.5E-05	1.5	40	12	0.92552	2.27E-04	3.673	8.78E-05	0.29862	692.8	0.1903	0.0021
1362	16	0.3	6.5E-05	1.5	40	12	0.92464	2.25E-04	3.625	8.88E-05	0.29855	692.6	0.1903	0.0023
1363	22	0.3	6.5E-05	1.5	40	12	0.94406	2.26E-04	3.653	4.93E-05	0.29859	692.7	0.1411	0.0014
1364	22	0.3	6.5E-05	1.5	40	12	0.9443	2.27E-04	3.669	4.91E-05	0.29867	692.9	0.1411	0.0014
1365	22	0.3	6.5E-05	1.5	40	12	0.94498	2.29E-04	3.717	4.85E-05	0.29879	693.2	0.1412	0.0014

[a] simulation outputs are averages calculated over the steady-state time period, i.e., from t_{ss} to t_f, where $t_f = \lambda * t_{ss}$

Table E-1. Continuous reactor simulation inputs and outputs (cont.)

ID	simulation inputs						simulaiton outputs [a]							
	t_res	ϕ_S	seed d_p	λ	n	k	$\alpha_{sulfate}$	mean d_p	A	R	ϕ_S	particle conc.	solids purge	seed makeup
	min	--	m	--	--	L^2/m^2-mol-min	--	m	m^2/L	mol/L-m^2-min	--	g/L	g/L-min	g/L-min
1366	4	0.5	6.5E-05	1.5	40	12	0.81417	2.63E-04	5.070	7.54E-04	0.49759	1154.4	0.6697	0.0074
1367	4	0.5	6.5E-05	1.5	40	12	0.81353	2.62E-04	5.048	7.56E-04	0.49760	1154.4	0.6692	0.0074
1368	4	0.5	6.5E-05	1.5	40	12	0.81408	2.63E-04	5.070	7.54E-04	0.49730	1153.7	0.6696	0.0073
1370	6	0.5	6.5E-05	1.5	40	12	0.86652	2.62E-04	5.048	3.87E-04	0.49731	1153.8	0.4751	0.0052
1372	10	0.5	6.5E-05	1.5	40	12	0.915	2.63E-04	5.077	1.58E-04	0.49756	1154.3	0.3001	0.0023
1374	10	0.5	6.5E-05	1.5	40	12	0.91398	2.60E-04	5.009	1.60E-04	0.49734	1153.8	0.2998	0.0024
1375	12	0.5	6.5E-05	1.5	40	12	0.92707	2.60E-04	5.013	1.15E-04	0.49742	1154.0	0.2533	0.0019
1376	12	0.5	6.5E-05	1.5	40	12	0.92754	2.61E-04	5.049	1.14E-04	0.49751	1154.2	0.2542	0.0027
1377	12	0.5	6.5E-05	1.5	40	12	0.92701	2.61E-04	5.015	1.15E-04	0.49651	1151.9	0.2533	0.0019

[a] simulation outputs are averages calculated over the steady-state time period, i.e., from t_{ss} to t_f where $t_f = \lambda * t_{ss}$

E.4 Simulation code

The reactor model was written in MATLAB and the code is provided below.

```
function
crystal_recycle(t_res,VAF,Vf_mean,dp,std_multiplier,N_min,look_forward,dt_multiplier,N_reactor_bi
n,Q,k)

%INSTRUCTIONS %

% Change Input Parameters and Simulation Parameters to suit your simulation
% Simulation will output mass removed and added during each cycle. To
% disable this, comment out the line starting with "disp(sprintf('Time is %0.5g min...".

% Simulation will also output cycle_X.mat, where X is the cycle number.
% This file contains a single variable "particles", which is an array of
% diameters [m] of all particles at the end of cycle X. Use
% hist(particles,100) to graph the particle size distribution

% To plot other results, do "plot(result(:,1),result(:,Y))", where Y is:
% 2 - mean particle size
% 3 - specific surface area [m^2 L^-1]
% 4 - reaction rate [mol L^-1 m^-2]
% 5 - volume fraction
% 6 - particle concentration [g L^-1]
% 7 - specific removed mass [g L^-1]
% 8 - overall removed mass [g]
% 9 - specific makeup mass[g L^-1]
% 10 - overall makeup mass [g]
%%%%%%%%%%%%%%%%%%%%%%%%%%%%%%%%
clc;close all;
%%%%%%%%%%%%%%%%%%%%%%%%%%%%%%%%
% Input Parameters
% t_res = 30; %residence time of water [min]
% Q = 3.2; %flow rate of water [mgd]
% k=12; %reaction rate constant [L m^-2 mol^-1 min^-1]
% dC=0.0135; %delta C [mol L^-1]
C0 = 0.1756; %Initial Concentration [mol L^-1] corresponding to SIg = 2.5
%Cf = 0.1586; %final concentration [mol L^-1] correspondign to SIg = 1.15
Cs = 0.1567; %saturation concentration [mol L^-1] correspondign to SIg = 1
% dC=0.0135; % average driving force assuming driving force at end of PFR is 0, delta C [mol L^-
1]
% assume_uniform_dC = false; % whether dC is uniform throughout the reactor or not. If not
uniform, growth of each particle is calculaed based on a random driving force between dC_min and
dC;
% dC_min = 0; %minimum driving force [mol L^-1]
% A_min = 1.88; %min specific area [m^2 L^-1]
% VAF = 1.1; %volume allowance factor between 1.01 and 1.5...maximum increase in solids volume
relative to min volume
% A_max = 1.88*(VAF)^(2/3); %max specific area [m^2 L^-1]... larger by VAF compared to min by
volume
% VAF = 0.1; %volume allowance factor, fraction of Vf_mean to oscillate between
% Vf_mean=0.1;
% dp = 45; %initial particle diameter [um]
% std_multiplier = 10;
std = std_multiplier*dp/45; %initial particle size standard deviation [um]
Cp = 5; %particle concentration [g L^-1]
rhop = 2.32;% particle density [g mL^-1]
M = 172.17; %molecular weight [g mol^-1]
%%%%%%%%%%%%%%%%%%%%%%%%%%%%%%%%
% Unit Conversions
Q = (Q*1e6*3.785)/(24*60);%[L min^-1]
rhop = rhop*1e6; % [g m^-3]
dp = dp/1e6; % [m]
std = std/1e6; % [m]
%%%%%%%%%%%%%%%%%%%%%%%%%%%%%%%%
% Simulation Parameters
```

```
V_sim = 0.0001;%0.00004 % Simulated reactor size [L] Use a smaller number to speed up simulation.
Absolute mass are scaled w.r.t. real V (V=Q*t_res).
% N_min=1000;
% N_reactor_bin=20; %number of reactor bins, 1 = entrance, 20 = exit;
sim_complete_condition='steady_state_by_peak'; %criteria used to decide when to stop simulation.
Options are 'time', 'cycle', 'steady_state', or steady_state_by_peak. If using 'time' or 'cycle'
need to specify 't_final' or 'N_c_final', respectively. If using 'steady-state', specify
para_test, tol_test, look_forward.
t_final = 2000; %time to simulate [min]
N_c_final = 100;%ceil(13.375*(VAF-1)^-0.901);% Cycles to simulate. Valid for 1.01<VAF<1.5. Number
of cycles required to reach 2000 min elapsed time to remove 2nd peak, i.e., "steady-state."

%if using steady state, please specify the following parameters. Steady
%state is calculated based on moving average, where the lag of the moving
%average is equal to the steps between the last two cycles. Steady state is
%assumed to have occured if the relative difference between the current
%moving average and moving average from a cycle ago is less than tol_test
%based on the "para_test" parameter. (See plot portion
%of Instruction for definition of these parameters.) It probably does not
%
%make sense to use para_test = 1, 3, 4, 7, 8, 9,or 10.
%Optionally,
para_test=2; %the parameter for which the last points were tested
tol_test=0.001; %tolerance
% look_forward=0.5; %fraction of time to look forward past the "steady state" mark. Use 0 for
disable.

%for steady_state_by_peak
N_hist=100;% number of bins used for histogram in finding peak;
min_peak_height=round(0.01*N_min); %minimum histogram peak height to register as a peak
%%%%%%%%%%%%%%%%%%%%%%%%%%%%%%%%
N = round(Cp/(dp^3*pi/6*rhop)*V_sim);% Number of particles in simulated reactor size
if N<N_min
   V_sim=V_sim*N_min/N;
   N=round(Cp/(dp^3*pi/6*rhop)*V_sim);
end
t = 0; % time [min]

dt = dt_multiplier*t_res/(N_reactor_bin+1); % time step [min]
N_c = 0; % Cycle #
resultCounter=0;
C_bin=zeros(N_reactor_bin+1,1); %concentration in each bin
N_bin=floor(N/N_reactor_bin); %Number of particle in each reactor bin. Last reactor contains upto
2x the particles than previous bin.
specific_removed_mass = 0; %specific removed mass [g L^-1]
overall_removed_mass = 0; %overall removed mass [g]
specific_makeup_mass = 0; %specific makeup mass [g L^-1]
overall_makeup_mass = 0; %overall makeup mass [g]
result=zeros(1e6,12+N_reactor_bin);
%%%%%%%%%%%%%%%%%%%%%%%%%%%%%%%%
% Main
V = Q*t_res; %Volume of reactor [L]
C_bin(1)=C0;
Vf_min=Vf_mean*(1-VAF/2);
Vf_max=Vf_mean*(1+VAF/2);
% dC_min=Cf-Cs; %minimum concentration driving force.
particles=abs(normrnd(dp,std,round(N),1)); %initial particle diameter of N particles [m]
% disp(sprintf('*Assuming V = resident time (%d min) * flow rate (%0.5g L/min) = %0.5g
L.\n\n',t_res,Q,V));
sim_incomplete=true;
while sim_incomplete
    resultCounter=resultCounter+1;
    for i = 1:N_reactor_bin
        dC=max(C_bin(i+1)-Cs,0);
        dd_dt=2*k*abs(dC)^2*M/(rhop); %particle growth rate [m/s]
        previous_mole = sum(particles((i-1)*N_bin+1:(i-1)*N_bin+N_bin).^3)*pi/6*rhop/M; %mol of
particles in bin i
        particles((i-1)*N_bin+1:(i-1)*N_bin+N_bin) = particles((i-1)*N_bin+1:(i-
1)*N_bin+N_bin)+dt*dd_dt;
        dM = sum(particles((i-1)*N_bin+1:(i-1)*N_bin+N_bin).^3)*pi/6*rhop/M - previous_mole;
        C_bin(i+1)=C_bin(i+1)-dM/(V_sim*N_bin/N)+(C_bin(i)-C_bin(i+1))*dt/(t_res*N_bin/N);
```

```
%         C_bin(i+1)=C_bin(i+1)+(C_bin(i)-C_bin(i+1))*dt/(t_res*N_bin/N);

    end
    dC=max(C_bin(N_reactor_bin+1)-Cs,0);
    dd_dt=2*k*abs(dC)^2*M/(rhop); %particle growth rate [m/s]
    previous_mole = sum(particles((N_reactor_bin-1)*N_bin+1:N).^3)*pi/6*rhop/M; %mol of particles
in bin i
    particles((N_reactor_bin-1)*N_bin+1:N) = particles((N_reactor_bin-1)*N_bin+1:N)+dt*dd_dt;

    dM = sum(particles((N_reactor_bin-1)*N_bin+1:N).^3)*pi/6*rhop/M - previous_mole;
    C_bin(i+1)=C_bin(i+1)-dM/(V_sim*(N-(N_reactor_bin-1)*N_bin)/N)+(C_bin(i)-
C_bin(i+1))*dt/(t_res*(N-(N_reactor_bin-1)*N_bin)/N);
%     C_bin(i+1)=C_bin(i+1)+(C_bin(i)-C_bin(i+1))*dt/(t_res*(N-(N_reactor_bin-1)*N_bin)/N);
    t=t+dt; %time advance by dt
    particles=particles(randperm(N));
%     disp(sprintf('Time is %0.5g min. V_frac is %0.5g, A_dot is %0.5g, dd_dt is
%0.5g.\n',t,sum(pi/6*particles.^3)/(V_sim/1000),sum(pi*particles.^2)/V_sim,dd_dt));


    if sum(pi/6*particles.^3)/(V_sim/1000)>=Vf_max %if overall specific area exceed A_max
        p_replaced=[]; %replaced particles "collection" reset to empty
        d_replaced=[];
        while sum(pi/6*particles.^3)/(V_sim/1000)>Vf_min %while overall specific area is greater
than A_min
            p_replace=ceil(rand*length(particles)); %pick a particle from existing distribution
to replace
            if any(p_replace==p_replaced)==0 %if the previously picked particle hasn't already
picked in this cycle
                p_replaced=[p_replaced p_replace]; %picked particle is added to replaced particle
"collection"
                d_replaced=[d_replaced particles(p_replace)];
                particles(p_replace)=normrnd(dp,std); %picked particle is replaced from normal
distribution based on intial particle diameter and std.
            end
        end
        specific_removed_mass = sum(d_replaced.^3*pi/6*rhop)/V_sim; %specific removed mass [g L^-
1]
        overall_removed_mass = specific_removed_mass*V; %overall removed mass [g]
        specific_makeup_mass = length(p_replaced)*dp.^3*pi/6*rhop/V_sim; %specific makeup mass [g
L^-1]
        overall_makeup_mass = specific_makeup_mass; %overall makeup mass [g]
        disp(sprintf('Time is %0.5g min. Removed mass is %0.5g g/L (%0.5g g*). Makeup mass is
%0.5g g/L (%0.5g
g*).\n\n',t,specific_removed_mass,overall_removed_mass,specific_makeup_mass,overall_makeup_mass))
;
        N_c = N_c+1; %cycle count advance
%         psd_filename=sprintf('cycle_%d.mat',N_c);
%         save(psd_filename,'particles');
    end
    result(resultCounter,:)=[t mean(particles) sum(pi*particles.^2)/V_sim
k*sum(pi*particles.^2)/V_sim*dC^2 sum(pi/6*particles.^3)/(V_sim/1000)
sum(pi/6*particles.^3*rhop)/V_sim specific_removed_mass overall_removed_mass specific_makeup_mass
overall_makeup_mass C_bin' (C0-C_bin(N_reactor_bin+1))/(C0-Cs)];
    specific_removed_mass = 0; %specific removed mass [g L^-1]
    overall_removed_mass = 0; %overall removed mass [g]
    specific_makeup_mass = 0; %specific makeup mass [g L^-1]
    overall_makeup_mass = 0; %overall makeup mass [g]
    switch sim_complete_condition
        case 'time'
            sim_incomplete=(t<=t_final);
        case 'cycle'
            sim_incomplete=(N_c<=N_c_final);
        case 'steady_state'
            if N_c>2
                step=diff(find(result(:,7),2,'last'));
                coef=zeros(step,1)+1/step;
                result_size=length(find(result(:,para_test)));
                isodd=bitand(step,1);
                step_even=floor(step/2);
                movavg=filter(coef,1,find(result(:,para_test)));
```

```
                movavg=movavg([zeros(1,step_even-
1+isodd)+step,step:result_size,zeros(1,step_even)+result_size]);

                last_ma=movavg(length(movavg));
                prev_cycle_ma=movavg(length(movavg)-step);

                if abs(last_ma-prev_cycle_ma)/last_ma<=tol_test;
                    disp(sprintf('Steady state is reached at t=%0.5g min.',t));
                    t_ss=t;
                    ind_ss=resultCounter;
                    %sim_incomplete=false;
                    sim_complete_condition='time';
                    t_final=t*(1+look_forward);
                end
            end
        case 'steady_state_by_peak'
            [n,xout]=hist(particles,N_hist);
            ns=smooth(n);
            [pks,~]=findpeaks(ns);%,'MINPEAKHEIGHT',min_peak_height);
            [pks,loc]=findpeaks(ns,'MINPEAKHEIGHT',max(pks)/50);

            if length(loc)==1 && loc(1)<=N_hist*2/5;
                plot(xout,n,'r');hold on; plot(xout,ns,'g');
plot(xout(loc),pks,'k^','markerfacecolor',[1 0 0]);hold off;
                disp(sprintf('Steady state is reached at t=%0.5g min.',t));
                t_ss=t;
                ind_ss=resultCounter;
                %sim_incomplete=false;
                sim_complete_condition='time';
                t_final=t*(1+look_forward);
            end
    end
end
filename=sprintf('reactor_%0.5g_%0.5g_%0.5g.mat',VAF,N_reactor_bin,t_final);
result=result(1:resultCounter,:);
save(filename)
%%%results
fun=@(a) sum(result(ind_ss:resultCounter,a))/(t-t_ss); %requires R2009a or later.
fun2=@(a) sum(result(ind_ss:resultCounter,a))/(length(result(ind_ss:resultCounter,a)));
%
plot(result(round(length(result)*0.04):length(result),1),result(round(length(result)*0.04):length
(result),N_reactor_bin+12))
% disp(sprintf('Final alfa = %0.5g, average removal mass per cycle is %0.5g [g L^-1 min^-
1].',result(length(result),N_reactor_bin+12),fun(7))); %requires R2009a or later.
% disp(sprintf('Final alfa = %0.5g, avg alfa =%0.5g, avg removal and added per cycle = %0.5g and
%0.5g [g L^-1 min^-1].',result(resultCounter,N_reactor_bin+12),fun(N_reactor_bin+12),fun(7),
fun(9))); %requires R2009a or later.


fid=fopen('results.txt','a');
fprintf(fid,'%d\t%0.5s\t%0.5s\t%d\t%d\t%d\t%0.5s\t%0.5g\t%d\t%0.5g\t%0.5g\t%0.5g\t%0.5g\t%0.5g\t%
0.5g\t%0.5g\t%0.5g\t%0.5g\t%0.5g\n',t_res,VAF,Vf_mean,dp,std_multiplier,N_min,look_forward,dt,N_r
eactor_bin,Q,k,fun2(N_reactor_bin+12),fun2(2),fun2(3),fun2(4),fun2(5),fun2(6),fun(7),fun(9));
fclose(fid);
```

References

1. Nason, J.A. and D.F. Lawler, *Particle size distribution dynamics during precipitative softening: Constant solution composition.* Water Research, 2008. **42**(14): p. 3667-3676.
2. Nason, J.A. and D.F. Lawler, *Particle size distribution dynamics during precipitative softening: Declining solution composition.* Water Research, 2009. **43**(2): p. 303-312.